September 2021

Cellular And Molecular Alterations Associated with Ovarian and Renal Cancer Pathophysiology

Ravneet Kaur Chhabra
University of South Florida

Cellular And Molecular Alterations Associated with Ovarian and Renal Cancer Pathophysiology

by

Ravneet Kaur Chhabra

A dissertation submitted in partial fulfillment
of the requirements for the degree of
Doctor of Philosophy
Department of Cell Biology, Microbiology and Molecular Biology
College of Arts and Science
University of South Florida

Major Professor: Meera Nanjundan, Ph.D.
Brant Burkhardt, Ph.D.
Sandy Westerheide, Ph.D.
Yu Chen, Ph.D.

Date of Approval:
September 8, 2021

Keywords: Lysophosphatidic Acid, Iron, miRNA, Fallopian Tube Secretory Epithelial Cells

Dedication

I dedicate this dissertation to my beloved mother. Her unconditional love, care, and sacrifices made it possible for me to reach at this juncture of life. Although my mom was my inspiration to pursue my doctoral degree, she was unable to see my graduation. This is dedicated to her beautiful memories, which will always be cherished.

I also dedicate this work to my father for his immense care, my husband Kanwal who is my constant source of support and encouragement, my brother and dearest friend Manmeet, who has been there for me at every step of life, my precious nephews Hardit and Sanvir for being my joy and source of smile whenever I feel low, and my sister-in-law Dimple for all her affection and prayers.

Acknowledgement

I would like to express my sincerest gratitude to my mentor, Dr. Meera Nanjundan, for her insightful advice, understanding, and support. Her conscientious dedication and unwavering enthusiasm for science and research are inspiring. I will be forever grateful to her for teaching me all the research methodology and for providing me with the opportunity to learn and grow professionally throughout my Ph.D. program. Her generous guidance and persistent help have significantly contributed to making this dissertation possible.

I would like to sincerely acknowledge all my committee members Dr. Brant Burkhardt, Dr. Sandy Westerheide, Dr. Yu Chen, and prior committee member Dr. Younghoon Kee for their valuable inputs and scientific discussions. I would especially like to thank Dr. Burkhardt and Dr. Westerheide for being extremely understanding and supportive in difficult situations during this journey. I also thank Dr. Stanley Stevens for his collaboration with the proteomics project.

I wish to thank all the current and former lab members for their assistance and discussions during our time together. I am very grateful to all my friends and family for motivating me and uplifting my spirit. I would also like to acknowledge all my prior teachers who paved stepping stones throughout my life to help me achieve my goals.

Table of Contents

List of Tables

List of Figures

List of Abbreviations

ACAT	Acetyl-CoA Cholesterol Acetyl Transferase
ACC	Acetyl-CoA Carboxylase
ACLY	ATP citrate lyase
AGPAT	1-acylglycerol-3-phosphate-O-acyltransferase
AJCC	American Joint Committee on Cancer
ALDH1A2	Aldehyde dehydrogenase 1 family, member A2
ATGL	Adipose triglyceride lipase
ATX	Autotaxin
AZA	5′-Azacytidine
BAP1	BRCA1 Associated Protein 1
BRIP1	BRCA1 Interacting Protein 1
ccRCC	Clear cell renal cell carcinoma
CIDEC	Cell death inducing DFFA like effector C
CM	Complete media
CV	Control Virus Infected
DAG	Diacylglycerol
DAPI	4′,6-diamidino-2-phenylindole
DDA	Data-Dependent Acquisition
DGAT2	Diacylglycerol O-aceyltransferase 2
DMEM/F12	Dulbecco’s Modified Eagle Medium Nutrient Mixture F-12
DMRs	Differentially Methylated Regions
DMSO	Dimethylsulfoxide
DNA	Deoxyribonucleic acid
DNMT1	DNA (Cytosine-5-)-Methyltransferase 1
DRP1	Dynamin-related protein 1
ENPP2	Ectonucleotide pyrophosphatase
EVI1	Ecotropic Viral Integration Site-1
F	Iron-Treated
FABP	Fatty Acid Binding Protein
FAC	Ferric Ammonium Citrate
FAF-BSA	Fatty-acid free bovine serum albumin
FASN	Fatty Acid Synthase
FBP1	Fructose Bisphosphate-1
FBS	Fetal Bovine Serum
FH	Fumarate dehydrogenase
FTSECs	Fallopian Tube Secretory Epithelial Cells
G6PD	Glucose-6-phosphate dehydrogenase
Glut1	Glucose Transporter 1
GNB2L1	Guanine Nucleotide Binding Protein subunit beta 2 like 1

GSK3	Glycogen synthase kinase 3
HCQ	Hydroxychloroquine
HDL	High Density Lipoprotein
HGSOC	High-grade Serous Ovarian Carcinoma
HIF	Hypoxia Inducible Factor
HK	Hexokinase
HMGCR	3-hydroxy-3-methylglutaryl-CoA reductase
HMGCS	Hydroxymethylglutaryl-CoA synthase
H-Ras	Harvey Rat Sarcoma Viral Oncogene Homology
hTERT	Human Telomerase Reverse Transcriptase
IDH	isocitrate dehydrogenase
IPA	Ingenuity Pathway Analyses
LC3B	Microtubule associated protein 1 light chain 3 beta
LC–MS/MS	Liquid Chromatography with Tandem Mass Spectrometry
LDH	Lactate dehydrogenase
LDL	Low Density Lipoprotein
LDs	Lipid droplets
LFQ	Label-Free Quantification
LGSOC	Low grade serous ovarian carcinoma
LPA	Lysophosphatidic acid
LPC	Lysophosphatidylcholine
MAP1S	Member of the Microtubule-Associated Protein family 1
MAPK	Mitogen-activated protein kinase 1
MAPK	Mitogen-Activated Protein Kinase 1
miR	MicroRNA
MS	Mass spectrometry
mTOR	mammalian target of rapamycin
mTOR	Mechanistic target of rapamycin kinase
NTBI	Non-Transferrin Bound Iron
OCV	Oncogene Cocktail Virus Infected
OVCA	Ovarian Cancer
PA	Phosphatidic acid
PARP1	Poly (ADP-ribose) polymerase 1
PAX8	Paired Box 8
PBRM1	Polybromo 1
PC	Phopshotidyl Choline
PCR	Polymerase Chain Reaction
PDGF	Platelet-Derived Growth Factor
PDH	Pyruvate Dehydrogenase
PDK1	Pyruvate dehydrogenase Kinase
PIP3	Phosphatidylinositol-3,4,5-triphosphate
PLIN1	Perilipin 1
PLPP1	Phospholipid phosphatase 1
PNPLA2	Patatin like phospholipase domain containing 2
PPP	Pentose Phosphate Pathway

PR	Phenol-Red
PTEN	Phosphatase And Tensin Homolog
RNU6B	RNA U6B Small Nuclear
RPPA	Reverse Phase Protein Array
SAHA	Suberoylanilide Hydroxamic Acid
SDH	Succinate dehydrogenase
SDS-PAGE	Sodium Dodecyl Sulfate Polyacrylamide Gel Electrophoresis
SETD2	SET Domain Containing 2, Histone Lysine Methyltransferase
SFM	Serum free media
SQSTM1/p62	Sequestosome 1
S-Trap	Suspension-Trap
SV40 LTAg	Simian Virus 40 Large T Antigen
TAG	Triacylglycerol
TBI	Transferrin bound iron
TCGA	The Cancer Genome Atlas
TEMS	Temsirolimus
TOM	Translocase of outer mitochondrial membrane
U	Untreated
UPLC	Ultra-Performance Liquid Chromatography
VEGF	Vascular Endothelial Growth Factor
VHL	Von Hippel-Lindau tumor suppressor
VLDL	Very Low-Density Lipoprotein

Abstract

Elucidating molecular alterations underlying tumor development and chemoresistance are critical to expand our understanding of the disease pathophysiology. This dissertation is focused on analyzing the cellular and molecular alterations associated with LPA-induced chemoresistance in clear cell renal cell carcinoma (ccRCC) cells and chronic iron-induced deregulation of miRNA expression in fallopian tube secretory epithelial cells (FTSECs).

Kidney cancer is one of the ten most common cancers worldwide with <15% survival rate at advanced stage (American Cancer Society). ccRCC is the most common type of kidney cancer and is described as a metabolic disease characterized by deregulated lipid metabolism leading to increased intracellular lipid droplets [9, 10]. The current molecular-targeted treatment strategies involve VEGF/VEGFR and mTOR inhibition [9, 12]. However, there are limitations to these approaches leading to the reduced efficacy and/or increased resistance in ccRCC cells [13, 14]. Therefore, it is important to decipher the factors involved in compromising the chemosensitivity in these cells.

Lysophosphatidic acid (LPA), a bioactive phospholipid, was previously reported to increase resistance against Sunitinib (VEGFR/PDGFR inhibitor) in ccRCC cells and to increase migration and invasion in various tumors [15-17]. In Chapter 3 of this dissertation, we analyzed the role of LPA in mediating chemotherapeutic resistance in ccRCC cells by reversing the effects of an mTOR inhibitor Temsirolimus (TEMS). We further identified that LPA reverses the TEMS-induced changes in cellular viability, lipid droplets and mitochondrial networks, autophagy and PI3K/mTOR pathway markers *in vitro* [19]. We also observed that LPA increases lipid droplets partially in a MAPK-dependent manner [19]. Overall, these results indicate the role of LPA in inducing potential

chemoresistance in ccRCC cells, which can be further explored for pre-clinical research applications in future.

Since epithelial ovarian cancer (EOC) is commonly diagnosed at advanced stage, it is imperative to investigate the molecular alterations associated with initiation of the disease [34-36]. HGSOC initiation from transformed fallopian tube stem cells was reported to be associated with iron addiction and deregulated iron homeostasis markers [40]. The contribution of chronic iron exposure in mediating oncogenic transformative events in FTSECs was previously studied in our lab [22]. We have extended these studies in Chapter 4 of this dissertation using a multi-omics approach to determine the global protein and miRNA alterations in chronic iron exposed FTSECs. Interestingly, ~57% of the altered miRNAs were located at chromosome 14q32 [43]. Chromosome 14q32 harbors a cluster of 54 miRNAs, which are deregulated in various tumor types, including ovarian cancer [25, 26, 422]. However, the role of iron-induced deregulation of 14q32 miRNAs in FTSECs had not been previously studied. We focused on the two most downregulated (~100-fold) 14q32 miRNAs – miR-432-5p and miR-127-3p and their common protein targets. We identified that overexpression of miR-432-5p reduced cell numbers induced by long-term iron exposure in FTSECs. We also identified that combinatorial treatment with methyltransferase and deacetylation inhibitors reversed the expression of miR-432-5p and miR-127-3p, suggesting that chronic iron treatment downregulates miRNA expression via epigenetic alterations.

Additionally, miR-138-5p was also downregulated in chronic iron exposed FTSECs. This miRNA is located at chromosome 3 (which also harbors EVI1, a common transcriptional activator in EOC). We identified a potential EVI1 binding site in miR-138 promoter region and therefore analyzed whether miR-138 transcription is regulated by EVI1. Although our studies indicated that miR-138-5p is regulated independently of EVI1, TERT RNA was found to be partially regulated by miR-138-5p [43]. Overall, this study reveals global molecular alterations induced by iron, potentially associated with transformation of FTSECs.

Collectively, these studies suggest the involvement of LPA in reversing ccRCC chemosensitivity and highlight the potential role of iron-induced 14q32 miRNA downregulation in FTSEC transformation. In future, a detailed study of the mechanism involved in LPA-mediated chemoresistance, and the role and regulation of miRNAs at 14q32 will expand our understanding of their functional consequences, which will also prove useful to design clinically improved therapeutic strategies.

Chapter 1

Introduction

Note to reader

One sub-section of this chapter has been adopted from “Iron Pathways and Iron Chelation Approaches in Viral, Microbial, and Fungal Infections (MDPI: Pharmaceuticals) Doi: 10.3390/ph13100275 with the copyright permission as included in Appendix A.

Renal Cancer

Renal Cancer is one of the top ten causes of cancer-related deaths worldwide, as per the data reported by the American Cancer Society. The heterogeneous group of cancers arising from renal epithelium is known as Renal Cell Carcinoma [6], comprising >90% kidney cancers [7]. In 2021, the National Cancer Institute [9] statistical prediction estimated 76,080 new RCC cases (4% of total cancer cases), and 13,780 deaths in the United States. Within the last four decades, there has been an increase in RCC incidence by 5-fold and increase in RCC-caused mortality by 2-fold [12, 13].

RCC incidence is higher for men than for women and increases with age. The gender ratio is approximately 2:1 for males and females. The exact reason behind this gender bias is not known, though these variations were reported to be due to alterations of androgen receptors in one study, which may play distinct roles in stage/tissue- or gender-specific manner [14]. The major established risk factors for RCC include excess body weight, hypertension, and cigarette smoking [16]. Individuals with chronic kidney disease on dialysis for a long-term are also at greater risk of developing RCC [26]. As per the American Joint Committee on Cancer (AJCC), RCC is staged

clinically and pathologically using the TNM (Tumor origin site, lymph Node involvement and Metastasis to distant organs) staging classification, as shown in figure 1.

The five major histological sub-types of RCC include: clear cell RCC (70-80% patient cases), papillary (10%), chromophobe (5%), oncocytoma (~3-7%) and collecting duct (>1%) [28]. Three to five percent of RCC tumors remain unclassified, with no clear distinction between different sub-types [13].

Stage	*TNM classification*	*Localization and Description*
STAGE I 	Diameter <7cm N_0M_0	Localized tumor found only within kidney
STAGE II 	Diameter >7cm N_0M_0	Localized tumor found only within kidney
STAGE III 	Diameter >7cm (Any size) N_0 or N_1 M_0	Regional tumor found within kidney parenchyma or blood vessels and spread to surrounding kidney tissues
STAGE IV 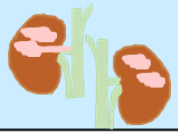	Diameter >7cm (Any size) N_0 or N_1 M_0 or M_1	Metastatic tumor spread beyond the kidney into adrenal gland and other surrounding organs

Figure 1: Different stages of RCC representing increase in disease aggressiveness with TNM classification (T: primary tumor site, N: regional lymph node and M: metastasis)

At stage I, RCC tumors are 7cm or less, with no involvement of lymph node and no metastasis. At stage II, the RCC tumors are larger than 7cm, without involving lymph node or metastasis, confined only to kidney. At stage III, the large RCC tumors may or may not involve lymph node, but these have metastasized to the surrounding kidney tissues, growing into renal vein/vena cava. At stage IV, the large RCC tumors most commonly involve lymph nodes, and are metastasized outside the kidney into adrenal glands and other surrounding tissues [7].

Clear cell RCC (ccRCC) cells contain glycogen-, lipid- and mitochondria- rich cytoplasm, with a clear histological appearance [31, 32]. Sub-classification of ccRCC has revealed two sub-groups with differentiating biological features: (i) ccA, associated with changes in genes involved in angiogenesis, fatty acid metabolism, and pyruvate metabolism; (ii) ccB, associated with genes involved in TGFβ signaling and cell cycle changes [34]. ccRCC has a worse survival rate than localized papillary RCC and chromophobe RCC [35, 36].

Molecular characterization of clear cell Renal Cell Carcinoma (ccRCC)

Genetic and Signaling Pathway alterations

Somatic copy number alterations (SCNAs) in ccRCC are characterized with higher percentage of deletions involving entire chromosomes or chromosomal arms (17%) as compared to focal alterations (0.4%) [37]. Most commonly, arm-level mutations encompass loss of chromosome 3p (including four commonly mutated genes: *VHL, PBRM1, BAP1* and *SETD2*). Biallelic inactivation of VHL tumor suppressor gene has been reported to be caused by Loss of heterozygosity [35], homozygous deletion and chromosomal rearrangement at this locus in ~90% of ccRCC patients [38, 39]. *VHL* mutation is an “obligate” event in ccRCC, leading to stabilization and accumulation of hypoxia inducible factors (HIF-1α and HIF-2α). These transcription factors then activate the genes responsible for hypoxic response, angiogenesis and other signaling pathways, including vascular endothelial growth factors (VEGF), platelet-derived growth factors (PDGF) and glucose transporter 1 (Glut1), leading to increased tumor cell survival and metastasis [38, 40-42]. Arm level loss at chromosome 14q, harboring *HIF1A* gene and *DLK1-DIO3* gene locus, is reported to be associated with ~45% of patients and is associated with increased disease aggressiveness and poor survival outcome [37, 43, 44]

PI3K/AKT/mTOR pathway alterations are actively involved in increased ccRCC progression [37]. Mutations at chromosome 5q35.3 harboring *GNB2L1* (Guanine Nucleotide

Binding Protein (G Protein), Beta Polypeptide 2-Like 1 or RACK1) and *SQSTM1* (Sequestosome 1 or p62) genes are associated with PI3K signaling activation [45, 46]. Additionally, VEGF and PDGF bind to their receptor tyrosine kinases (VEGFR, PDGFR) on RCC tumor cells activating PI3K, and promoting phosphatidylinositol-3,4,5-triphosphate (PIP3) formation, which recruits AKT to the cell membrane. AKT is phosphorylated and activated, leading to apoptosis inhibition, inactivation of GSK-3β, activation of transcription factors such as c-Myc, β-catenin, c-Jun and Notch, as well as mTOR activation [47, 48]. PTEN tumor suppressor gene is also negatively regulated leading to Akt activation in RCC [49] and mutations in TSC1/2 lead to further aggressiveness of the disease [50]. mTOR pathway is further activated by Wnt/β-catenin pathway via inhibition of GSK3 [51].

The role of autophagic pathway dysregulation has been well studied in various cancer types, including ccRCC [52-55]. Autophagy is a lysosome-dependent intracellular degradation process, which is activated under cellular stress conditions, such as nutrient deficiency and starvation [56-59]. Maintenance of cell survival and homeostasis is majorly regulated by autophagy in normal cells [60, 61]. This process can perform tumor suppressive function by degrading mutated DNA and damaged proteins [59, 62]. Cancer cells can exploit this process by deregulating autophagic markers for increased cell survival and tumorigenicity and/or by protein aggregation [63, 64]. Low levels of LC3-II and Beclin 1 autophagic markers have been shown to be associated with poor prognosis of ccRCC [65]. Additionally, p62 (SQSTM1, overexpressed via gain at chromosome 5 in RCC) is an autophagic marker and an agonist of NRF2 (Nuclear factor-erythroid factor 2-related factor 2) [54, 66]. p62 links the autophagy pathway and the ubiquitin–proteasome system upon ubiquitinated protein degradation [67]. NRF2 is released from KEAP1 (Kelch-like ECH-associated protein 1) by competitive binding of p62 and activates downstream genes for RCC tumor cell survival [68]. Additionally, increased promoter methylation of KEAP1 gene has been shown to be associated with increased progression of ccRCC [69].

Current Treatment Strategies for ccRCC

Based on ccRCC staging and risk assessment, patients with small cortical tumors (originated in renal tubules) [70] of <3cm can be subjected to radiofrequency ablation [71], microwave ablation [72] or cryoablation treatments, although the preferred option is partial nephrectomy of tumors <7cm diameter, confined within the kidney [73]. In advanced RCC cases, immunotherapeutic cytokine treatments, such as use of interferon-α and high-dose IL-2 are used alone or in combination, though these can be associated with significant toxicity and low response rates [74]. More recently, inhibitors of T-cell immune checkpoint markers and monoclonal antibodies programmed cell death protein 1, such as Nivolumab, are being used to exploit intrinsic anti-tumor immune response in patients [1].

Management of advanced and metastatic ccRCC requires alternative strategies. Since signaling pathway alterations play a key role in ccRCC pathogenesis, molecular systemic strategies are commonly used alone or as adjuvant to the above-mentioned treatments. ccRCC is commonly targeted using tyrosine kinase inhibitors targeting VEGF, PDGF, fibroblast growth factors and their respective receptors, using drugs such as sunitinib, pazopanib, sorafenib, bevacizumab [6, 47, 48, 75, 76], as well as drugs targeting Glut1 and Warburg effect, such as STF 31 (Selective inhibitor of Glucose Transporter 1) [77], as shown in figure 2. Everolimus and temsirolimus (TEMS) are FDA-approved allosteric inhibitors of mTOR (as shown in figure 1). These are used clinically for RCC treatment and are being studied for combinational regimens as well as sequential therapy with VEGF pathway in various clinical trials [78-81].

Chemoresistance in ccRCC

Majority of ccRCC tumors are prone to resistance towards chemotherapeutics [82]. The resistance can be “intrinsic” leading to immediate inefficacy of treatment, or “acquired” leading to tumor re-growth after an initial disease regression [83, 84]. The sub-optimal efficacy of

chemoresistance has been reported to be due to lysosomal sequestration of tyrosine kinase inhibitors [85], mutation in mTOR inhibitor binding site such as FKBP-12 [86, 87], activation of angiogenic factors [4, 88-90], increase in cholesterol levels [91] and/or intratumoral heterogeneity [92].

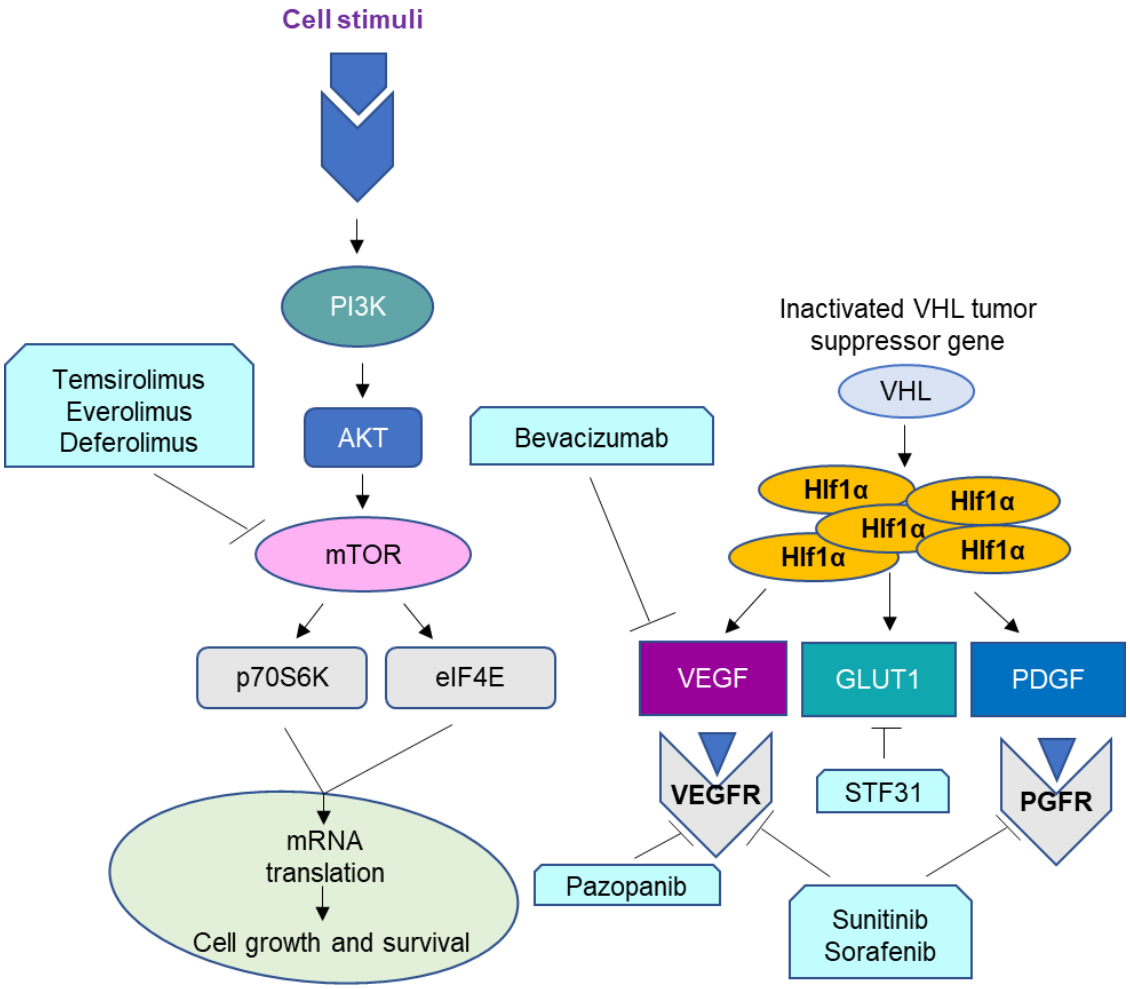

Figure 2: Commonly altered signaling pathways and chemotherapeutic approach in ccRCC PI3K/AKT/mTOR pathway is hyperactivated leading to increased tumor growth and survival. Loss of VHL tumor suppressor gene leads to accumulation of HIF1α, which in turn activates markers involved in angiogenesis such as VEGF and PDGF and altered cellular metabolism such as Glut1, ultimately leading to increase in metastatic potential of the ccRCC tumor. Parts of this figure adapted from [4, 5].

Drugs targeting PI3K/AKT/mTOR pathway can also activate autophagy, which could be another key mechanism of chemoresistance in ccRCC cells [93]. To overcome this resistance, autophagic flux inhibitors chloroquine and hydroxychloroquine (HCQ) have been reported to be used in combination with chemotherapeutic drugs for ccRCC treatment [94, 95], though more in-depth research would be required for clinical applications.

Metabolic Reprogramming in ccRCC

Clear cell renal cancer is known as a metabolic disease, with alterations in various pathway mediators involved in glycolysis, TCA cycle, protein biosynthetic pathways, nucleotide biosynthesis, as well as lipid metabolism [96-100], which are directly associated with increased RCC development as shown in Figure 3. Kidney epithelial cells are associated with high numbers of glucose transporters, which are further upregulated in VHL mutated ccRCC cells [101] leading to enhanced glycolysis [102]. Further, loss of rate-limiting gluconeogenetic enzyme fructose-1-bisphophatase (FBP1) expression was reported in 100% of the 600 RCC tumors analyzed [103]. The hyperactivated mTOR pathway also regulates HIF-mediated gene expression by inducing hypoxia response elements to activate the genes involved in enhanced metabolism (such as PDK1, Glut1) and in angiogenesis (such as VEGF) [104], as shown in Figure 3. Well-known HIF-mediated ccRCC effects also include increased expression of LDH (lactate dehydrogenase), PDK1 (pyruvate dehydrogenase kinase), and HK (hexokinase) [105-108].

Activated oxidative and non-oxidative glucose metabolism via pentose phosphate pathway (PPP) is also reported to be activated in RCC cells [109], along with increased expression of glucose-6-phosphate dehydrogenase (G6PD) augmenting RCC progression [110]. Furthermore, altered expression of TCA cycle genes, such as reduction in succinate dehydrogenase (SDH), Fumarate dehydrogenase (FH) and isocitrate dehydrogenase (IDH) are shown to be associated with ccRCC tumors [99, 111-113].

As the “clear cell” phenotype in ccRCC tumors can be histologically attributed to its lipid and glycogen rich cytoplasmic deposits [98, 114], it is well established that alterations in lipid metabolic pathways are hallmarks of this disease. Increased metabolic demands of proliferating ccRCC tumor cells are met by either enhanced uptake of exogenous lipids or by hyper-activating the endogenous lipid synthesis (i.e., lipogenesis and cholesterol synthesis) [114-116] (as shown in figure 3). Increased expression of lipogenic enzymes, such as acetyl-CoA carboxylase (ACC) and fatty acid synthase (FASN), and ATP citrate lyase (ACLY) that promote cholesterol synthesis have been reported in ccRCC [115, 117-119].

Excessive lipids and cholesterol in ccRCC are stored in the form of lipid droplets [77, 120]. LDs are often found in close vicinity with the endoplasmic reticulum, mitochondria, endosomes, peroxisomes, and the plasma membrane [121]. These organelle associations assist in the lipid exchange, either for LD growth (anabolic) or for their catabolic breakdown [122]. Alternatively, LDs provide a means of transporting lipids between organelles within the cell [123] and may protect mitochondria during autophagy by acting as an energy source by supplying fatty acids for mitochondrial β-oxidation and by sequestering excessively accumulated lipids that arise during autophagic degradation of membranous organelles [124].

High LDs and stored-cholesteryl ester content in tumors have are also associated with ccRCC aggressiveness [125]. ccRCC is characterized by increased cellular esterified cholesterol, very low density lipoprotein (VLDL), Low density lipoprotein (LDL) and ACAT activity (acetyl-coA cholesterol acetyl transferase) as well as reduced high density lipoprotein (HDL), which lead to increased lipid accumulation or diminished efflux [96, 126-128].

Lipid droplet accumulation in ccRCC can also be attributed to defects in autophagic LD turnover, via lipophagy [129]. MAP1S (member of the microtubule-associated protein family 1), a positive regulator of autophagic flux, is downregulated in ccRCC tissues and cell lines, as compared to the normal renal cells which consequently reduces lipophagy of LDs, contributing to

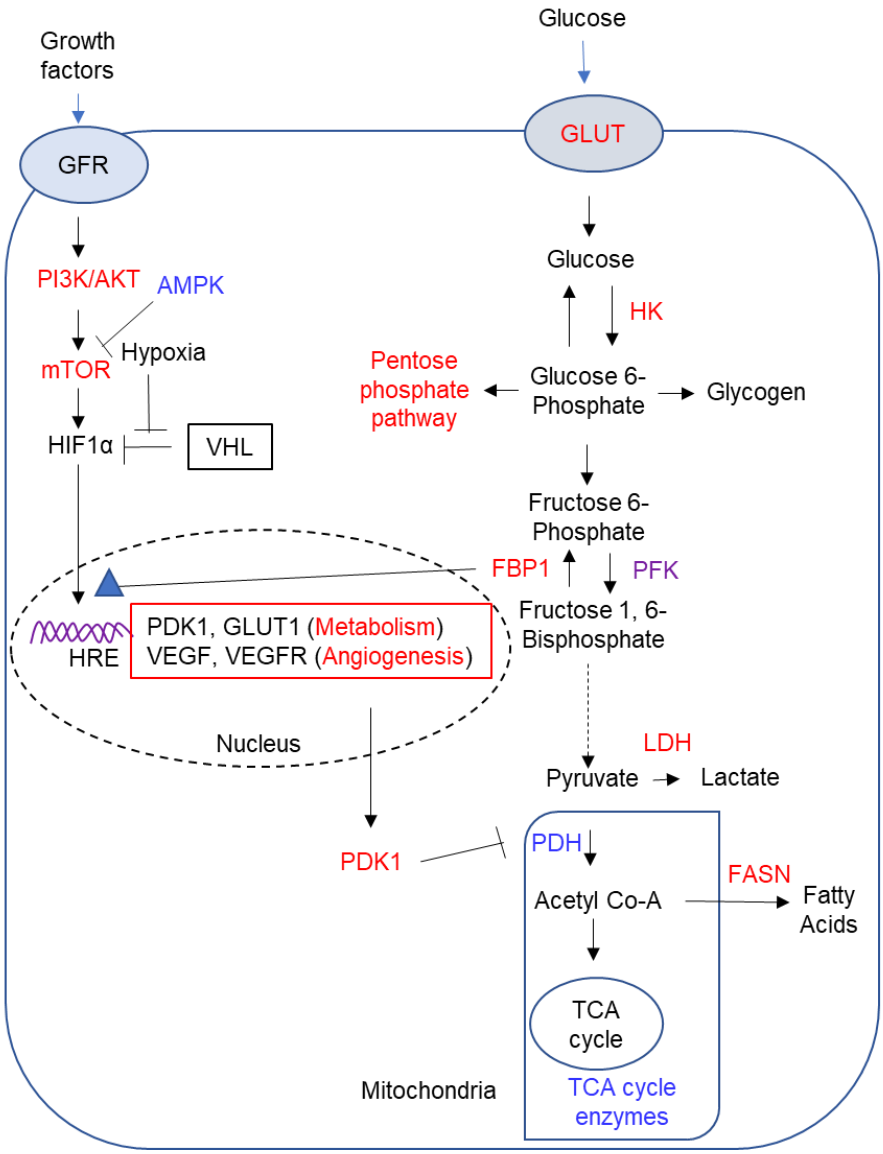

Figure 3: Metabolic Reprogramming in Renal Cell Carcinoma

Glycolysis and Pentose phosphate pathway are upregulated in ccRCC. GLUT transporters mediate Glucose transport, which generates pyruvate via glycolysis. Pyruvate goes through TCA cycle to generate ATP. Flux of pyruvate into TCA cycle decreases in ccRCC and consequently pyruvate undergoes lactic acid fermentation for the increased production of ATP. Activated PI3K/AKT/mTOR pathway and VHL mutation lead to HIF1α stabilization, leading to increase in hypoxia response elements to aid cancer cells with increased bioenergetic needs and angiogenesis. These cells are also characterized by upregulation of fatty acid biosynthesis. Enzymes in Blue are downregulated, and Red are upregulated. Partially adapted from [8].

increase in lipid droplet accumulation, potentially enhancing ccRCC development [130]. Interestingly, mTOR targeting chemotherapeutic agents (such as TEMS) is shown to reduce LD formation [131]. Further studies based on targeting lipid pathway alterations can provide novel direction to ccRCC treatment.

Role of Lysophosphatidic acid in ccRCC

Signaling pathways regulated by phospholipids contribute to pathophysiology of cancer [132]. Overall phospholipid content is reported to be higher in renal tumors as compared to normal kidney cells and is increased with cellular transformation [133]. Lysophosphatidic acid (LPA) is a glycerophospholipid, that acts via G-protein coupled receptors and occurs naturally in nearly every organ of human body, including the kidneys [134]. LPA can be produced extracellularly by Autotaxin (ATX) that functions as a lysophospholipase D enzyme to hydrolyze phosphodiester bonds in lysophospholipids [10], as shown in Figure 5. ATX mRNA levels are significantly increased in RCC tumors [135]. LPA is reported to be associated with RCC progression by activating Arf6 to promote mesenchymal malignancy and LPA-ATX axis is shown to promote acquired resistance against sunitinib (VEGFR inhibitor) to mediate tumorigenesis [136]. Intracellularly, LPA can be formed by phospholipase A1 and A2 enzymes from phosphatidic acid (PA). PA is shown to form supersized lipid droplets in yeast [137], but the involvement of LPA in LD biology, role of LPA-LD relation in RCC and the mechanism by which LPA mediates these effects needs further investigation in renal tumor biology.

Ovarian Cancer

Often known as “silent killer” or “whispering disease” [138], ovarian cancer (OVCA) is the fifth leading cause of cancer deaths in women, usually diagnosed at an advanced stage leading to poor disease outcome [139]. The American Cancer Society data predicted diagnosis of ovarian

cancer in 21,410 women and 13,770 deaths in 2021, accounting for highest number of gynecological cancer-related deaths in women.

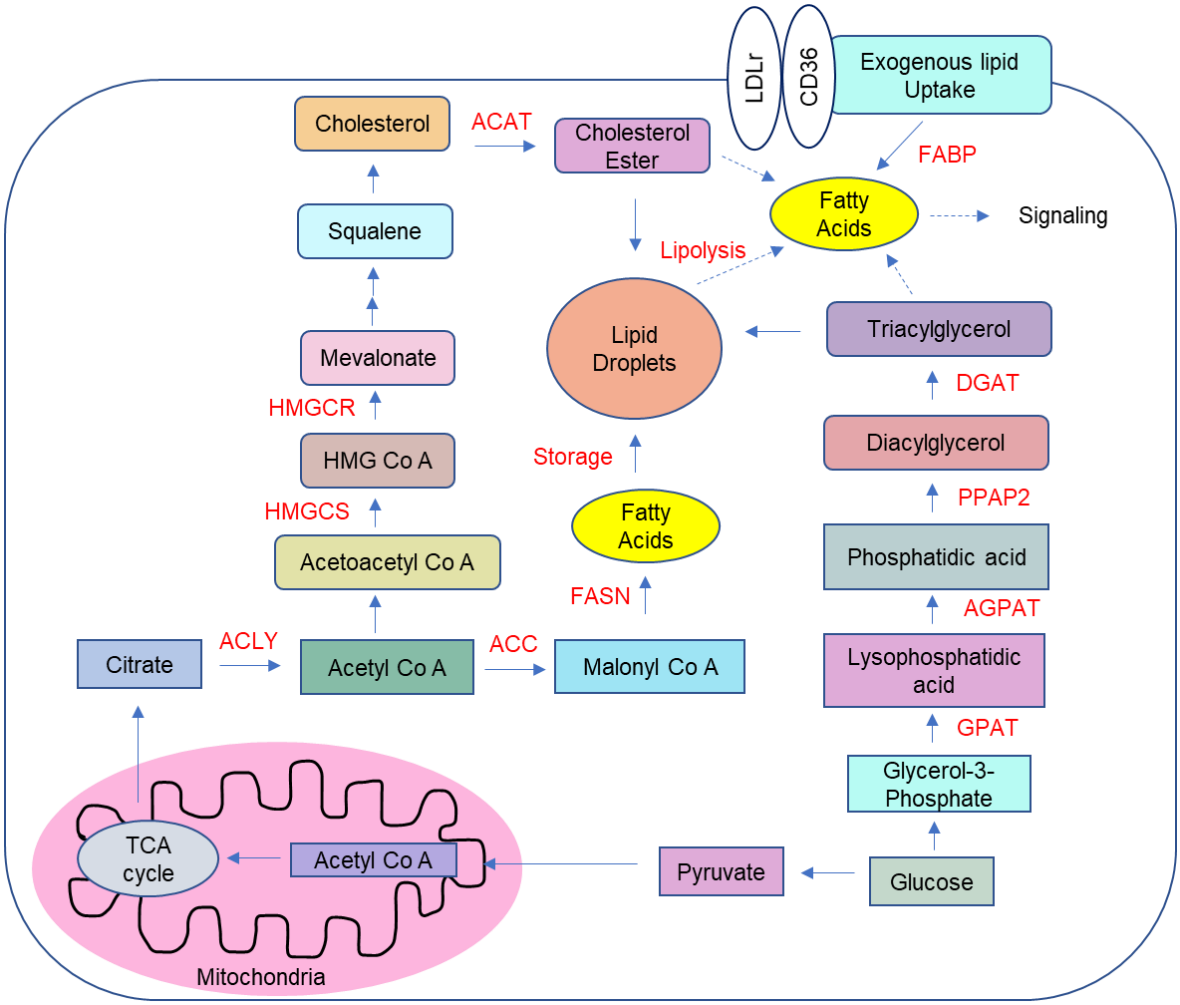

Figure 4: Lipid and Cholesterol metabolic pathways commonly altered in ccRCC

Lipid biogenesis, increased uptake and decrease in lipolysis are utilized to maintain increased proliferation of cancer cells and excessive lipids are stored in the form of lipid droplets. Excessive fatty acids in ccRCC cells provide membrane biosynthetic substrates and work in conjunction with mitochondria through β-oxidation to increase cellular growth and proliferation [2, 3].

Risk factors associated with OVCA development can be genetic (such as hereditary mutations in genes including, BRCA1/BRCA2, MMR, BRIP1, MSH6 [140, 141]) and non-genetic

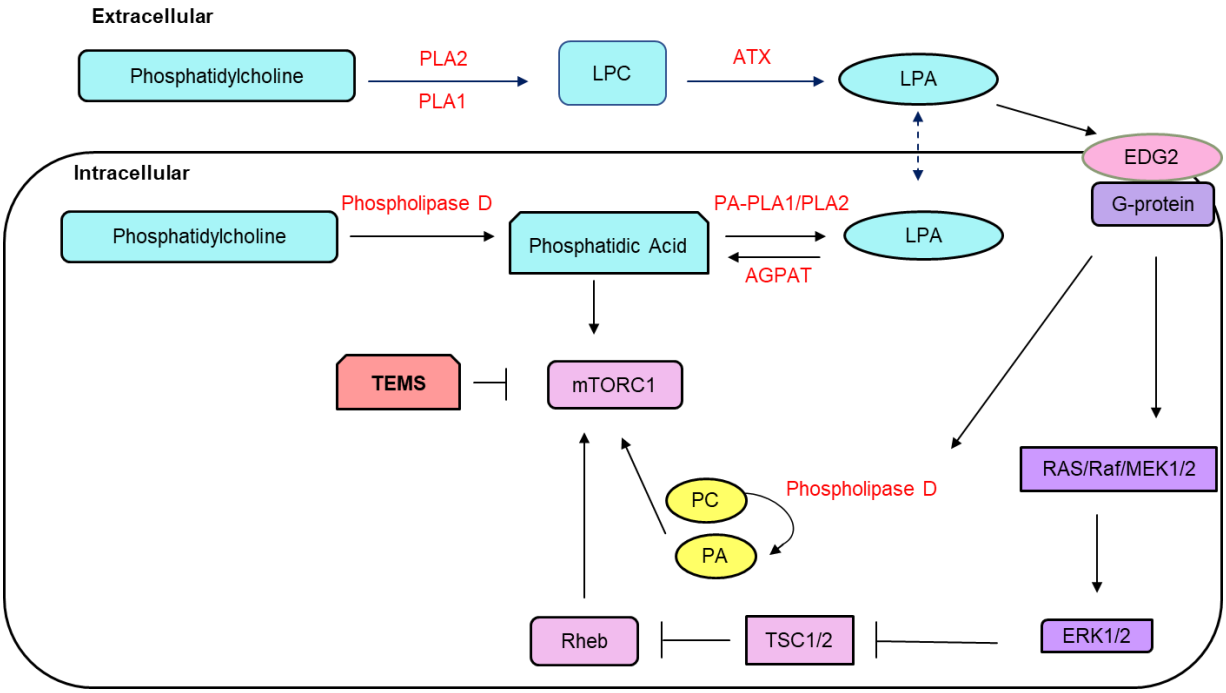

Figure 5: Model for crosstalk between Lysophosphatidic acid and mTOR pathway
Phosphatidylcholine is commonly found in the exoplasmic or outer leaflet of a cell membrane. Autotaxin (ATX) generates LPA from plasma membrane phospholipids and from circulating lysophosphatidylcholine (LPC) bound to albumin. This is followed by subsequent binding of LPA to endothelial differentiation gene receptors. Activation of EDG receptors lead to increased signaling through the Ras/Raf/MEK/ERK pathway, which represses TSC1/2 to inhibit Rheb, releasing mTOR for activation. LPA can also be generated intracellularly from phosphatidylcholine (PC) and phosphatidic acid. Alternatively, LPA can also potentially migrate into and out of the cytosol, though the mechanism involved is not known. Intracellular LPA can form PA via 1-acylglycerol-3-phosphate-O-acyltransferase (AGPAT) enzyme. PA can directly bind to mTOR leading to its activation [10] [11].

such as smoking, obesity and hormonal replacement therapy [142]. Treatment strategies are employed based on the OVCA tumor staging; these are divided into stages I to IV, according to the FIGO (International Federation of Gynecology and Obstetrics) system. In stage I, tumor is found in one or both ovaries; in stage II, OVCA cells are spread to other pelvic organs such as

fallopian tubes or uterus; in stage III, cells have metastasized to nearby organs outside of pelvis such as lymph nodes, diaphragm, intestine, or liver; in stage IV cells spread beyond the abdominal region into lungs and spleen [143]. Most common treatment in early stages is surgical removal of tumor or affected ovary and in advanced stages, these tumors are treated by cytoreductive surgery (or debulking of tumor), followed by chemotherapy [144]. Chemotherapeutic strategies include carboplatin/ paclitaxel combination, bevacizumab, poly (ADP-ribose) polymerase inhibitors and platinum-based therapies amongst others [144, 145]. However, chemoresistance and mortality rate are high because most OVCA cases are diagnosed are advanced stages [146, 147]. Further understanding of OVCA pathophysiology and determination of significant early-stage markers are required to combat the disease.

There are three main types of ovarian cancer: epithelial ovarian cancer (EOC) is the most common type which occurs in ~95% of OVCA cases; germ-cell and sex-cord stromal comprise of ~5% of the cases and are less common [148]. Epithelial ovarian cancers have four common histological sub-types: endometrioid, mucinous, clear cell and serous [149]. Endometrioid, mucinous, and clear cell contribute to 10%, 3% and 10% of EOC, respectively. Serous OVCA is further classified into high grade serous ovarian carcinoma (HGSOC) contributing to ~70-80% of EOCs and low grade serous ovarian carcinoma (LGSOC) accounting for <5% of the cases [150].

Origin of High Grade Serous Ovarian Carcinoma: Existing theories and Proof of Concept

Due to early metastasis and lack of distinct anatomical barriers in peritoneal cavity, HGSOC cells are transported via physiological peritoneal fluid and disseminates within the abdominal cavity [151]. However, this contributes to increased tumor heterogeneity, along with the distinct clinicopathological features in HGSOC cells which has led to the challenges in identifying the cell of origin [152].

Historically, ovarian surface epithelium (OSE) was believed to be the precursor due to “incessant evolution hypothesis” suggesting that repetitive ovulation events lead to pro-

inflammatory microenvironment by causing trauma, hormonal changes, and oxidative stress induced DNA damage, followed by subsequent and/or inadequate repair [153, 154]. This concept is further supported by reports suggesting that patients harboring mutations in BRCA1/2 (responsible for homologous recombination-mediated repair of double strand breaks) are at higher risk of developing HGSOC [154]. Since this theory co-related HGSOC development with high number of ovulatory cycles, it was reinforced by studies suggesting that pregnancy, breastfeeding, and oral-contraceptive hormonal pills, which suppress ovulation, can reduce the risk of developing this disease [155, 156]. Ovulatory repair can also result in invagination of sections of OSE to get entrapped beneath cortical inclusion cysts (CICs), which have been proposed to possess oncogenic potential to differentiate into Mullerian phenotype, prior to malignant transformation into HGSOC [157]. However, there is lack of convincing mechanistic evidence for this theory and due to absence of any precursor lesions identified from OSE within the ovary, this concept was challenged with alternative hypotheses [158].

The tubal origin of high-grade serous carcinoma was proposed with the discovery of small dysplastic lesions similar to HGSOC within the fallopian tubes [159]. The severely dysplastic lesions also have highly proliferating cells and accumulation of p53 gene mutation, characteristic of HGSOC [160]. These lesions are known as serous tubular intra-epithelial carcinomas (STICs) and are reported to overexpress DNA-double strand break marker γH2AX [161] and shortened telomeres [162], which are hallmarks of early-stage cancer. STICs are reported as precursor lesions in both BRCA 1/2-mutation carrier women [163] as well as in non-BRCA1/2 mutation carriers [164, 165]; more specifically fallopian tube secretory epithelial cells (FTSECs) were reported to be cells of origin for HGSOC [166].

Fallopian tube precursor concept was reinforced by literature evidence, such as the study of fallopian tube stem cell transformation *in vitro* recapitulating the molecular and histological alterations characteristic of HGSOC [167], generation of novel mouse model with induced mutations in same genes commonly affected in human patients (*BRCA, Tp53*, and *PTEN* genes)

used to demonstrate transformation of STIC to HGSOC, mimicking the underlying molecular alterations [168]; transcriptomic analysis of OSE cells, FTSECs and HGSOC cells showed highest similarities between FTSECs and a cohort of ~400 HGSOC samples [169].

To directly compare between the two cells of origin, a study was conducted to generate genetically engineered mouse models from organoids targeting the same genetic aberrations as found in OSE and in fallopian tube epithelia (FTE) [170]. Despite the identical driver mutations, tumor development was affected by the cell of origin, increased p53 signaling in FTE-derived tumors, and enhanced DNA repair pathways in OSE tumors [170]. In comparison with the TCGA human data, it was found that OSE-derived tumors resembled HGSOC of the proliferative sub-type, while FTE-derived tumors showed mesenchymal subtype features of HGSOC [170]. Their response to chemotherapeutic drugs was also variable in vitro [170]. This suggests that both OSE and FTE can possibly serve as precursors to development of HGSOC. However, the factors that contribute to development of HGSOC from either of these cells of origin remain understudied and thus require further investigation.

Iron metabolism and Role of Iron in Ovarian Cancer

Excessive iron is reported to be associated with development and progression various cancer types including breast, ovarian, prostate, colon, renal cancer, melanoma, osteosarcoma [171-173]. Fenton reaction-induced reactive oxygen species (ROS) generation has also been reported to increase cell migration, angiogenesis, and aggressiveness in cancer stem cells [174]. Transformed fallopian tube epithelial stem cells (described as tumor initiating cells) are also reported to be addicted to iron, promoting tumor initiation and growth by accumulating excessive iron content [175]. Iron overload caused by hemochromatosis is associated with increased risk of OVCA [176, 177]. In normal cells, iron homeostasis is tightly regulated. Cells require iron to maintain balance between the level required for metabolic needs, such as functioning as co-factor for DNA polymerases and helicases, mitochondrial respiration, citric acid cycle enzymes [178]

and iron homeostasis deregulation leading to excessive iron, which can contribute to tumor initiation and progression [179]. Iron can be detrimental to the cells due to its ability to generate reactive oxygen species contributing to free radical formation, inducing oxidative stress and DNA damage [179, 180]. Iron accumulation can also lead lipid alterations in cancer cells, leading to ferroptosis [27]. However, cancer cells can reprogram iron metabolism by deregulating the iron regulatory proteins, such as increase in TFR1 and TFR2 [181, 182], downregulation of FPN [183], decrease in ferritin [184], increase in hepcidin [185] and overexpression of DMT1 [186], as shown in figure 6. Some of the possible causes of iron induced OVCA development include oxidative stress [187], retrograde menstruation [188] and iron deposition in endometriotic cysts of fallopian tubes [189], in pelvic cavity [190] as well as in follicular fluid [191].

Long-term iron exposure of FTSECs with a NTBI form (Ferric Ammonium Citrate (FAC)) was shown to increase cell numbers and migration potential, DNA damage response protein (FANCD2), hTERT mRNA and EVI1 transcriptional regulator [19], providing preliminary evidence regarding role of iron in initiating transformative events in FTSECs. However, a detailed mechanism of alterations caused by iron to induce transformative or tumorigenic effects needs further investigation.

Micro-RNAs

Role in Cancer

Mature micro-RNAs (miRNAs) are short non-coding RNAs (20-23 nucleotides in length) and function by repressing the target mRNA to play major role in various biological processes [192]. miRNA biogenesis involves transcription of primary miRNA (pri-miRNA) by RNA polymerase II, followed by processing into precursor miRNA (pre-miRNA) by DGCR8/Drosha. Pre-miRNA is ~85

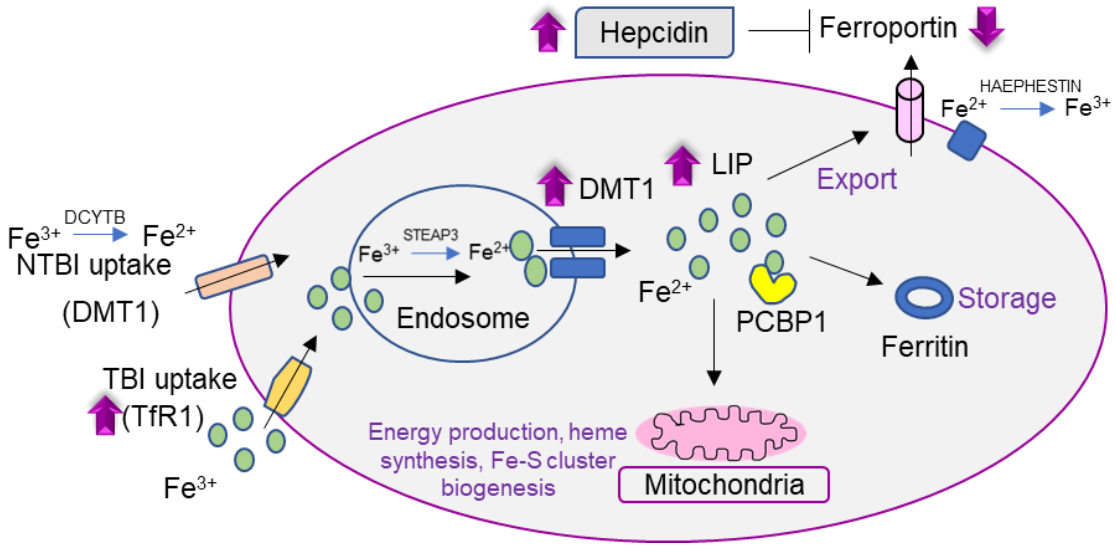

Figure 6: Iron Homeostasis in normal and cancer cells

Transferrin, a carrier glycoprotein which binds to iron (TBI), facilitates the transport of iron into cells via the transferrin receptor (CD71) [17]. Cellular entry of TBI occurs via an endocytic process which is followed by the release of iron from transferrin. STEAP3 (Six Transmembrane Epithelial Antigen of Prostate 3) mediates reduction of the Fe3+ (ferric) to the Fe2+ (ferrous) [20]. Once reduced, the iron is released from the endosomal compartment to the cytosol via endosomal DMT1 (Divalent Metal Transporter 1). The divalent metal transporter ZIP8 (Solute carrier family 39 member 8 (SLC39A8)) is one way through which NTBI can enter cells [21]. Another mechanism underlying NTBI uptake, specifically into small intestinal cells, involves the reduction of ferric iron via duodenal cytochrome b (DCYTB) [22], followed by its transport via cell surface localized DMT1 [23-25]. The imported iron (from either NTBI or TBI) can either (1) be stored in a complex with ferritin (FTN), (2) be added to the labile iron pool, (3) be exported extracellularly via ferroportin (FPN), or (4) be integrated within key enzymes involved in regulating cellular metabolic processes [29]. Extracellular export involving FPN is the only means of exporting iron out of cells and its levels are regulated by HAMP [30]. Excess iron can also be stored in the form of labile iron pool. PCBP1 binds to ferritin and facilitates the loading of iron into ferritin [33]. The mediators of iron altered in cancer are denoted with arrows showing upregulation or downregulation in different cancer types.

nucleotide stem-loop structure which is transported from nucleus to cytoplasm by Exportin 5/Ran-GTP complex. In the cytoplasm, pre-miRNAs are further processed by Dicer to a miRNA/miRNA* duplex (* indicates the passenger strand and the strand complementary to it is the mature or guide strand). The duplex is unwound, and mature miRNA is incorporated into RNA-induced silencing complex (RISC), which is targeted to the respective mRNA for translational repression or mRNA degradation [15], as shown in figure 7. Target recognition by miRNAs is determined by nucleotides 2 to 7 at the 5' end of the miRNA, known as "seed sequence" [193]. Mismatched target recognition without the seed sequence is known as non-canonical targeting and is associated with lower repression levels [194]. miRNAs also possess tumor suppressive or oncogenic properties in various cancer types, including cancer of breast, liver, lung, ovaries, colon, prostate, pancreatic, cervical, kidney and blood, which not only serve to alter tumorigenic properties of cells, but also confer chemoresistance by directly altering molecular mechanisms involved in cell cycle, DNA damage repair, cell death, disease progression, among others [195].

miRNA – Genomic Organization and miRNA cluster at 14q32

Non-protein coding RNA transcripts encode for approximately 50% miRNAs, and the rest can be encoded from introns or exons [196, 197]. Based on their genomic location, the miRNA genes can be categorized as: a). Intergenic miRNAs, which have their own promoter region and can be monocistronic (encoded as a single miRNA) or polycistronic (encoded as miRNA cluster); b). Exonic miRNAs, which are rare and are often transcribed by their own promoter overlapping between intron and exon of a coding region; c). Intronic miRNAs, which are located within introns, can have their own promoter or can use host promoter and can be monocistronic or polycistronic [198].

Many clustered miRNAs are transcribed as a polycistronic unit [196]. It is reported that clustered miRNAs are generated via gene duplication events or de novo miRNA-like hairpin

formation in the existing miRNA transcripts [199], are evolutionarily conserved [200] and can exert cooperative repressive effects to target functionally related genes [201]. Interestingly, miRNAs from the same cluster can belong to different miRNA families (derived from different precursor miRNAs) and can target multiple mRNAs. These mRNAs translate into proteins that can either interact with each other or belong to the same signaling pathway, suggesting an intricately regulated miRNA network for carefully nuanced functional consequences [202].

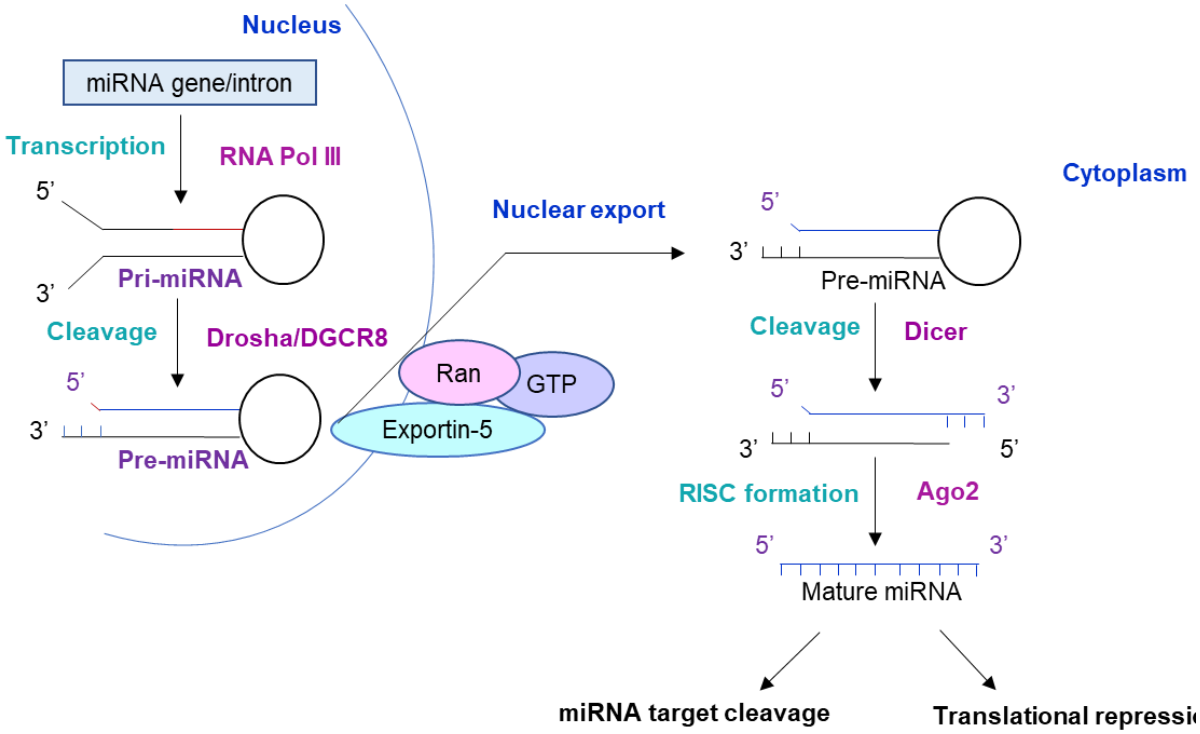

Figure 7: miRNA biogenesis pathway

miRNA gene transcription generated primary miRNA (pri-miRNA) via RNA polymerase III. Precursor miRNA (pre-miRNA) is generated from pri-miRNA via Drsoha/DGCR8, which is transported outside the nucleus into the cytoplasm via exportin5/Ran-GTP. In cytoplasm, Dicer cleaves pre-miRNA to generate two miRNA strands, which are loaded onto RNA-induced silencing complex (RISC) via Argonaute 2 (Ago2). This leads to formation of mature miRNA, which targets specific miRNAs [15].

Approximately 25% of human miRNA genes are organized to be transcribed as miRNA clusters, including chromosome X with 18 clusters, chromosomes 1 and 17 with 13 clusters each and chromosome 19 harboring a large miRNA cluster [203]. One of the largest miRNA clusters on human genome exists on chromosome 14q32 (C14MC) containing 54 mature miRNAs and is genomically imprinted [204]. Imprinted genes are expressed in parent-of-origin specific manner, where one allele (from one parent) is transcriptionally active, while the other is silent [205]. The 14q32 miRNA cluster (also known as DLK1-DIO3 cluster) is expressed from the maternal allele [204, 206, 207]. The miRNAs at 14q32 are reported to induce aortic valve disease [208], are differentially expressed, acting as potential biomarkers in Non-alcoholic fatty acid liver disease [209] and can increase neovascularization [210]. Either individually, or in form of cluster/sub-clusters, these miRNAs have oncogenic or tumor suppressive functions in a tissue-specific or disease progression-specific manner [211, 212]. Existing literature evidence suggests their role in various cancer types, including lung adenocarcinoma [206], osteosarcoma [213], breast cancer [214], thyroid cancer [215] and Hepatoblastoma [216]. However, its functional significance and role in renal cancer and initiation of ovarian cancer had not been well studied, which was the focus of part of our study.

miRNA Regulation: Epigenetic control of 14q32 miRNAs

miRNAs can be regulated via (1) transcription factors such as Myc, E2F, FOXO1, β-catenin [203, 217]; (2) genetic alterations such as chromosomal translocation and miRNA localization to fragile sites [218]; [27] altered expression of miRNA processing genes such as Drosha, Dicer or Argonaute 2 [203] and (4) epigenetic mechanisms such as methylation or acetylation [203, 219, 220].

Gene transcription occurs when chromatin is in “open” configuration. Epigenetic modifications like methylation and acetylation can affect this state [25]. As shown in Figure 7, hypermethylation of DNA (with more CpG islands located near the transcription start site), recruit

methyl-binding proteins triggering a silencing cascade by sequentially deacetylating and methylating histones, which results in a compact “silent” chromatin [25]. On the other hand, DNA demethylation does not allow recruitment of histone deacetylating enzymes but rather increases affinity for histone acetyltransferases, which leads to acetylated state of histones, whereby promoting transcription [221].

The chromosomal locus at 14q32 possess differentially methylated regions: Intergenic (IG-DMR), MEG3-DMR and MEG8-DMR, located within the DLK1-DIO3 gene locus [222]. These DMRs has been reported to be epigenetically silenced in various cancer types, including melanoma, lung cancer, liver cancer and hepatoblastoma [5, 216, 223, 224]. However, whether the epigenetic regulation of 14q32 locus is responsible for aberrant miRNA expression in ovarian cancer initiation had not yet been investigated, which we have analyzed and explained in Chapter 4. Additionally, there is contrasting literature evidence regarding 14q32 miRNA transcription as a polycistronic unit via epigenetic mechanisms [204] or via independent regulation at unique miRNA promoters by nuclear receptors including Estrogen related receptor (ERRγ)/small heterodimer partner [225] [226]. Further investigation would be required to understand the regulation of this miRNA cluster in detail.

Role of Iron in regulating miRNAs

Micro-RNA induced post-transcriptional gene expression targeting iron homeostasis pathway has been extensively studied, including expression of genes involved in iron acquisition (transferrin receptor and divalent metal transporter), iron export (ferroportin), iron storage (ferritin) and iron utilization (ISCU), amongst others [227-230]. However, the role of iron in regulating miRNAs is understudied. One literature evidence supporting the contribution of iron-induced reactive oxygen species (ROS) in miRNA expression suggests that upregulating or downregulating ROS by iron

treatment or antioxidants, respectively, can synergistically alter the expression of miRNAs-125b and miR-146b in astroglial primary cells [231].

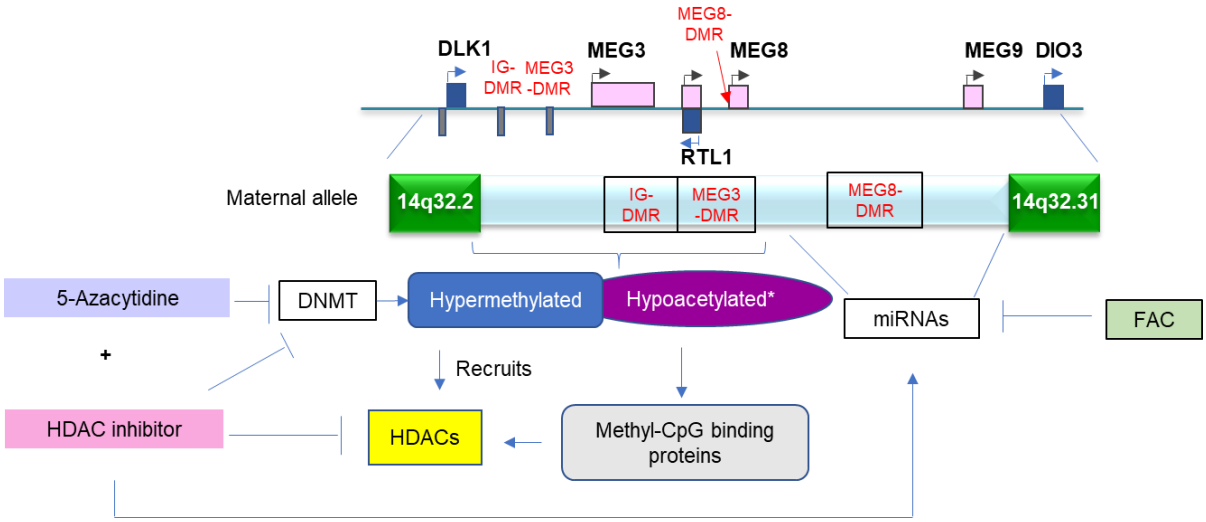

Figure 8: Model for epigenetic regulation of 14q32 miRNA cluster

There are three differentially methylated regions present in the promoter site of 14q32 miRNAs. DNA methylation and Histone acetylation at these sites can lead to epigenetic alteration in the miRNA expression, leading to upregulation or downregulation of these miRNAs in different disease states [18].

Role of iron in the form of heme is reported to increase DGCR8 dimerization during pri-miRNA processing [232]. Increased cytosolic iron was also shown to regulate miRNA processing by modulating the association between PCBP2 and Dicer, reducing PCBP2 multimerization and thereby altering the miRNA precursor processing [233]. However, detailed mechanism of how iron can regulate miRNA gene expression needs to be further examined.

Hypotheses and Aims

The goal of our studies was to analyze the cellular and molecular alterations associated with clear cell renal cancer pathophysiology and ovarian cancer initiation.

As stated previously, chemotherapeutic efficiency in ccRCC is sub-optimal and therefore, it is imperative to understand the factors involved in mediating resistance. It is well known that lipid and mitochondrial dysregulation are characteristics of ccRCC, however, whether these alterations are associated with chemoresistance via bioactive phospholipid LPA has not yet investigated. Therefore, *we hypothesized that LPA reverses the TEMS-mediated alteration of lipid droplets and mitochondrial networks, enhancing chemotherapeutic resistance. Further, LPA increases lipid droplets via modulation of the signaling pathways commonly altered in ccRCC.*

Additionally, mechanism of OVCA initiation and role of iron in mediating any potential changes is not yet well studied. It is known that OVCA cells are addicted to iron, and iron can lead to transformative changes in FTSECs. However, the role of iron in mediating specific miRNA alterations is a novel aspect covered in our study. *We hypothesized that long-term iron treatment can alter miRNA expression by regulating epigenetic status, which leads to the FTSEC-transformative changes potentially leading to OVCA-like characteristics*.

Based on these hypotheses, the specific aims for each study are as follows:

Specific Aim 1 (Chapter 3): We will assess whether lysophosphatidic acid can reverse temsirolimus-induced chemoresistance and the molecular alterations involved in mediating this effect.

1.1 Analyze the effect of temsirolimus on lipid droplets, cell viability, mitochondrial networks and signaling pathways altered in renal cells *in vitro*.

1.2 Determine the role of lysophosphatidic acid in counteracting these effects to mediate chemoresistance

Specific Aim 2 (Chapter 4): We will analyze whether iron can confer epigenetic changes leading to miRNA alterations in fallopian tube secretory epithelial cells.

2.1 Proteomics and microarray analyses of long-term iron treated fallopian tube secretory epithelial cells.

2.2 Inhibit methylation and deacetylation to analyze 14q32 miRNA expression

2.3 Assess the mechanism and functional effects of iron-mediated miRNA alterations

Overall Significance

These studies will help expand our understanding of the molecular mechanisms involved in chemotherapeutic responsiveness of ccRCC cells and if LPA can regulate this pathway. Further, examining the function of the miRNA cluster at 14q32 as a potential tumor suppressor in FTSECs *in vitro* and the role of iron in mediating miRNA deregulation will also contribute towards determining the cellular and molecular changes associated with ovarian cancer initiation. Both these studies will direct our focus towards exploring novel treatment strategies to target these diseases.

Chapter 2

Methods

Note to reader

Some of the materials and methods included in this chapter were derived in part or in full, from the following published articles:

- Chhabra R, Nanjundan M. PLoS One. 2020 Jun 3;15(6): e0233887. doi: 10.1371/journal.pone.0233887, included here with an open access license from PLOS ONE.
- Chhabra R, Rockfield S, Guergues J, Nadeau OW, Hill R, Stevens SM Jr, Nanjundan M. Sci Rep. 2021 Mar 18;11(1):6270. doi: 10.1038/s41598-021-85342-y), included here with an open access Creative Commons Attribution 4.0 international license from Springer nature.

See Appendix A for copyright permissions.

Contributions and Acknowledgements:

I am deeply grateful to Dr. Meera Nanjundan for her guidance with all the methods, to the undergraduate students for their kind assistance with western blot washes, to Robert Hill (Director of the CMMB Core Facilities) for his assistance with microarray and confocal microscopy, and to Dr. Stanley Stevens, Dr. Jennifer Guergues and Owen Nadeau- for their valuable contribution to the proteomics study.

Cell Culture and Propagation

Table 1: List of cell lines used in dissertation and their respective information.

Cell lines	***Cells/Tissue of Origin***	***Culture Media***	***Passage number***	***Purchased/Obtained from***
RPTEC	Primary Renal Proximal Tubule Epithelial Cells; Normal, Human	Basal Epithelial Media (supplemented with growth components)	p = n+2 – n+5	ATCC
HEK293T	Human embryonic kidney epithelial cells	RPMI-1640	p = n+2 – n+12	Dr. Gordon B Mills, MD Anderson Cancer Center
HK-2	Human papillomavirus 16 (HPV-16) transformed kidney, cortex/proximal tubule cells	K-SFM (supplemented with BPE and EGF)	p = n+4 – n+20	ATCC
769-P	Kidney Epithelial Carcinoma cells	RPMI-1640	p = 41 – 54	ATCC
786-O	Kidney Epithelial Carcinoma cells	RPMI-1640	p = 113 – 127	ATCC
A-498	Kidney Epithelial Carcinoma cells	EMEM	p = 38 – 53	ATCC
FTSECs: FT194	Human immortalized fallopian tube secretory epithelial cells	DMEM:F12 - phenol red, supplemented with 2% Ultroser G Serum Substitute	P = 30 – 52	Dr. Ronald Drapkin

The cell lines used in this dissertation are summarized in Table 1 along with information regarding their tissue of origin, culture media, passage numbers and source. All cell lines were maintained at 37°C with 5% CO_2; these were STR profiled and tested mycoplasma negative. RPTEC, 769-P, 786-O, and A-498 cells were maintained in a BSL-I incubator, while FTSEC, HK-2, and HEK293T cells were maintained in a BSL-II incubator. The RPMI-1640 (#SH30027-01 Cytiva, Marlborough, MA used for culturing 769-P, 786-O, HEK293T cells) and EMEM media with L-Glutamine ATCC: 30-2003) used for A-498 cells) was supplemented with 8% Fetal Bovine Serum (FBS) and 5% Penicillin/Streptomycin. The Keratinocyte serum free media (K-SFM, #17-005-042, Fisher Scientific, Pittsburgh, PA) used for culturing HK-2 cells) was supplemented with 5% Penicillin/Streptomycin, bovine pituitary extract (BPE) and epidermal growth factor Basal epithelial media (ATCC: PCS-400-010) used for maintaining RPTEC cells was supplemented with 5% Penicillin/Streptomycin, and Renal Epithelial Cell Growth Kit (ATCC: PCS-400-04) comprised of 0.5% FBS, 10nM Triiodothyronine, 10 ng/ml rh EGF, 100 ng/ml Hydrocortisone Hemisuccinate, 5 µg/ml rh Insulin, 1 µM Epinephrine, 5 µg/ml Transferrin, and 2.4 mM L-Alanyl-L-Glutamine. Immortalized FTSEC-FT194 cells were maintained in phenol red-free DMEM:F12 (1:1, #21041-025, ThermoFisher, Waltham, MA, USA) supplemented with 8% charcoal dextran-stripped FBS and 1% Penicillin/Streptomycin (without Phenol Red media), as previously described [19]. All cells were sub-cultured using 1 ml/T-25 flask or 2 ml/T-75 flask Trypsin-EDTA (# 25-053-Cl Corning 0.25% Trypsin, 2.21 nM EDTA 1X sodium bicarbonate)) and collected using respective complete media, apart from RPTEC and HK-2 cells which were trypsinized using 1:5 dilution of trypsin-EDTA and collected using neutralization buffer (5% FBS in PBS solution). Once collected, cells were pelleted at 1000 rpm for 5 minutes at room temperature, followed by resuspension in the respective media, counting the cells using a hemocytometer, and seeding/plating at an appropriate cell density.

Mycoplasma Testing

Supernatant from confluent cell culture flasks was collected for mycoplasma testing. Two sets of 1.5 ml eppendorf tubes per sample and two sets of 0.2ml PCR tubes were labelled, including one tube for Negative control (-) and one tube for Positive control (+). Except for the reaction mixture reagent (glycerol-based and kept directly on ice), all of the other mycoplasma test reagents (e.g., Nuclease-free water and Buffer Solution) were thawed and kept on ice until ready. When samples were ready to analyze, they were inverted to mix and 1ml aliquoted to their respective eppendorf tubes using filtered pipet tips. Next, they were centrifuged for 1 minute at 250 g, using the refrigerated centrifuge. The supernatant was then collected and then transferred to a new set of eppendorf tubes. These were then centrifuged for 10 minutes at 20,000g at 4°C. The following reagents were added to one set of PCR tubes using p10 pipet: 8 µl Nuclease-free water (add to sample and Positive control tubes); 10 µl Nuclease-free water to Negative control tube; 2.5 µl Reaction Mixture to sample, Positive, and Negative tubes; 1 µl of Buffer Solution to the Positive Control tube only. After centrifugation, media was discarded in the sink. Using p200, the pellet was suspended in 25 µl of Buffer solution and was transfer to the respective second set of 0.2ml PCR tube. These tubes were then added into thermocycler for “Instant Incubation” at 95˚C with heated lid for 3 minutes.

After 3 minutes, the Instant Incubate cycle was ended and all the samples were removed, placing directly on the rack on ice. 1.25 µl of heated sample was transferred to the respective 2nd set of PCR tubes. Samples were checked to ensure all solution was contained at the bottom of the tube. 0.2ml PCR tubes were pulse spun at 1000 rpm for 10 seconds. Negative control tube was added to the thermocycler first, then the samples. The positive control template was obtained from -20°C and prepared by adding 2 µl of stock template to 2 µl of nuclease-free water, 5 µl of positive template was added to the positive control tube which was then placed this into the thermocycler away from the samples and negative control. Standard-3 (STD-3) program was used in thermocycler for 35 cycles with the following settings:

94˚C for 30 seconds
94˚C for 30 seconds
60˚C for 2 minutes
} 35 times
72˚C for 60 seconds
72˚C for 5min
4˚C forever (hold)

Remaining samples (in Buffer solution) were stored in -20˚C freezer overnight. A 1% agarose gel was poured (with 10 µl of 10 mg/ml ethidium bromide) and this was stored overnight at 4˚C. TAE buffer (0.5X) was prepared by adding 5 ml of 50X TAE to 495 ml of nanopure Water, or 10ml of 50X TAE to 990 ml water, and was mixed thoroughly to store at 4˚C.

To analyze the samples on agarose gel, reaction PCR tubes and controls were pulse spun (using eppendorf adapters) at 1000 rpm for 10 seconds. After setting up the agarose gel and 0.5X TAE buffer in the appropriate apparatus, 2 µl of 6X loading dye was added to each sample and controls. 5 µl of DNA ladder, 10 µl of samples and controls were loaded. The agarose gel was run at 150V for approximately 1 hour and images were viewed/captured under UV light (using UV protective shield).

Cellular Treatments

Temsirolimus (TEMS, #50-811-7, Fisher Scientific, Pittsburgh, PA): TEMS, an mTOR inhibitor, was prepared by dissolving the powder in dimethyl sulfoxide (DMSO) at 10 mM concentration and filter sterilized using a 0.22-micron filter. 50 µM sub-stock was prepared by dissolving the 10 mM stock in respective media for each cell line, to be used at a final concentration of 10 µM. Control sample was prepared by adding similar volume of DMSO in respective media.

Hydroxychloroquine (HCQ, AC263011000, Fisher Scientific, Pittsburgh, PA): HCQ, an inhibitor of autophagic flux, was prepared at 50 mM stock concentration in phosphate buffer saline

(PBS) and filter sterilized using 0.22-micron filter. 25 µM final concentration was used by dilution into respective media for each cell line.

Oleic acid (#O1383, Sigma-Aldrich, St. Louis, MO): OA, an unsaturated fatty acid, was prepared in siliconized glass tubes by dissolving the stock solution in 100% ethanol to generate a 0.354 M solution stock followed by filter sterilization using a 0.22-micron filter. Sub-stocks were also prepared in siliconized tubes with 100% ethanol to use at a final concentration of 0.25 mM in respective media for each cell line.

Fatty acid-free bovine serum albumin (FAF-BSA, BP9704-100, Fisher Scientific, Pittsburgh, PA): FAF-BSA as a control for OA was prepared by dissolving in respective media for each cell line to prepare 10% BSA solution, which was then used at 1% final concentration in OA treatment. A similar concentration of FAF-BSA was used for control treatments, along with respective media and 100% ethanol. Alternatively, FAF-BSA utilized for lysophosphatidic acid (LPA) was prepared in PBS at a 0.5% stock concentration.

1-Oleoyl-2-hydroxy-sn-glycerol-3-phosphate (sodium LPA salt in chloroform, #857130C, Avanti Polar Lipids, Alabaster, AL): LPA, a bioactive phospholipid, was prepared in siliconized glass tubes. The aliquoted LPA was air-dried, followed by addition of FAF-BSA to prepare a 3.5 mM stock. Ten micromolar final concentration was prepared in respective media.

U0126 (#9903S, Cell Signaling Technology, Danvers, MA): U0126, a MAPK inhibitor, was prepared in DMSO for a 10 mM stock concentration and was then used at final concentration of 10 µM by adding it directly in respective media.

Combinatorial treatments of U0126 and LPA was done by first adding 10 µM of U0126, followed by a one-hour incubation at 37°C followed by the subsequent addition of 10 µM LPA.

5-Azacytidine (Aza, #S1782, Selleck Chemicals, Houston, TX): Aza, a nucleoside cytidine analog, was used for inhibition of DNA methyltransferases. A 50 mM stock was prepared by adding 1 mg of Aza powder into 81.9 µl of DMSO. 500µM sub-stock was prepared in respective

complete media and filtered using a 0.22-micron filter and then added directly at doses ranging from 0.5 µM to 10 µM.

Vorinostat or suberoylanilide hydroxamic acid (SAHA, #S1047, Selleck Chemicals, Houston, TX): SAHA, a histone deacetylase inhibitor, was prepared as 50 mM stock by adding 1 mg powder into 75.7 µl of DMSO. Sub-stock at 500 µM dose was prepared in respective complete media and filtered using a 0.22-micron filter and then added directly at doses ranging from 0.5 µM to 50 µM. Final concentrations selected for combinatorial treatment were 1 µM Aza and 50 µM SAHA, 24-hour post-seeding.

Knockdown via siRNA Transfection

HK-2 cells were seeded at 350,000 cells/well in six-well plates while FT194 cells were seeded at 500,000 cells/well in six-well plates or 1,000,000 cells/dish in 60 mm dishes. Following overnight adherence, cells were treated with ON-Target Plus non-targeting control siRNA (#D-001810-10-20, Dharmacon (Lafayette, CO, USA)) as control; EVI1-targeting siRNA (siB, custom designed as described previously) [19] was transfected into FT194 cells using RNAiMax (#13778-075, Invitrogen, Carlsbad, CA, USA); ribosomal protein S6 (RPS6) siRNA (#L-003024-00-0005) and ribosomal protein S6 kinase B1 (p70S6K1) siRNA (#L-003616-00-0005) was transfected in the HK-2 cells using Dharmafect I (#NC1308404, Fisher Scientific, Pittsburgh, PA).

For transfection (post cell adherence), cell culture complete media was replaced with serum-free media. Transfection mixture was prepared in eppendorf tubes with 100 µl serum free media, 5 µl of respective siRNAs and 4 µl appropriate transfection reagent. The reaction mixture was incubated at room temperature for 20 minutes and 100 µl of the reaction mixture was added into respective wells in a spiral motion dropwise, followed by placing the dishes/plates gently back to the incubator. Overlay with complete media was completed 3 hours post-transfection. Twenty-four hours post-transfection, cells were replenished with pre-warmed complete media and forty-

eight hours post transfection these were used for further protein/miRNA/RNA isolation and analysis.

miRNA mimic Transfection

Untreated and long-term FAC treated FT194 cells were seeded in 6-well plates at 250,000 cells/well and in 60 mm dishes at 500,000 cells/well. Next day after seeding (post cell adherence), cells were transfected with 200pmol (100 µl) of respective mimics: control mimic (mirVana miRNA mimic Negative control 1, #4464059, Life Technologies, Grand Island, NY) or hsa-miR-138-5p (mirVana miRNA mimic, Assay ID# MC11727, Life Technologies, Grand Island, NY), hsa-miR-432-5p (mirVana miRNA mimic, Assay ID# MC10941, Life Technologies, Grand Island, NY), or hsa-miR-127-3p (mirVana miRNA mimic, Assay ID# MH10400, Life Technologies, Grand Island, NY) using Fugene HD (Promega, Madison, MI).

Complete media in 6-well plates and 60mm dishes were replaced with serum free media. Transfection mixture was prepared in cryovials by adding 100 µl serum free media, 4 µl of respective miRNAs and 3 µl of Fugene HD. vials were flicked, tapped, and incubated at room temperature for 15 minutes. These vials were flicked and tapped again followed by addition of 100µlreaction mixture into respective wells in a spiral motion dropwise, followed by placing the dishes/plates gently back to the incubator. Overlay with complete media was completed 6 hours post-transfection. Cells were recovered with pre-warmed complete media 24 hours post-transfection, and 48 hours post-transfection these were used for protein/miRNA isolation and further analysis.

Protein Isolation and Western Blotting analysis

Total cell lysates were collected using previously described methods [234]. In brief, cells were seeded at an appropriate density, most commonly 250,000 cells/well, unless otherwise specified. Post-treatment, cells were lysed for 1 hour using the lysis buffer, containing 1 mM $MgCl_2$, 150 mM

NaCl, 1% Triton X-100, 10% glycerol, 1 mM EGTA, 50 mM HEPES and protease inhibitor tablet (Roche, Madison, WI), with nanopure water. Following lysis, the cells were gently scraped with cell scrapers and the cell extract was collected in eppendorf tubes. This was centrifuged at 14,000

Table 2: Antibodies list for Western Blotting analysis.

Antibody	***Company***	***Catalog numbers***	***Dilutions***	***Secondary antibody***
ALDH1A2	Cell Signaling Technology	83805	1:1000	Rabbit Polyclonal
Acetyl Histone H3 (Lys9/Lys14)	Cell Signaling Technology	9677	1:1000	Rabbit polyclonal
ATG7	Molecular biolabs (MBL) International	PM039	1:1000	Rabbit Polyclonal
Beclin-1	Cell Signaling Technology	3738S	1:1000	Rabbit Polyclonal
B-catenin	Cell Signaling Technology	9587	1:1000	Rabbit polyclonal
BMI1	Cell Signaling Technology	6964	1:1000	Rabbit monoclonal
Cas9	Cell Signaling Technology	14697	1:1000	Mouse monoclonal
Cyclin D1	Santa Cruz biotechnology	sc-718	1:1000	Rabbit polyclonal
Cyclin E	Santa Cruz biotechnology	sc-247	1:500	Mouse monoclonal
CRYAB	Cell Signaling Technology	45844	1:500	Rabbit Monoclonal
DRP1	Cell Signaling Technology	8570	1:1000	Rabbit Monoclonal
DNMT1	Cell Signaling Technology	5032	1:1000	Rabbit Monoclonal
EVI1	Cell Signaling Technology	2593	1:500	Rabbit Monoclonal
hVPS34	Cell Signaling Technology	3358	1:1000	Rabbit Monoclonal
ITGA2	Invitrogen (ARCO457)	MA5-35243	1:1000	Rabbit monoclonal
LC3B	Cell Signaling Technology	2775	1:1000	Rabbit Polyclonal
MAPK	Cell Signaling Technology	4695S	1:1000	Rabbit Monoclonal
p-AKT (Ser 473)	Cell Signaling Technology	4060	1:1000	Rabbit Monoclonal
p-AKT (Thr 450)	Cell Signaling Technology	9267	1:500	Rabbit Polyclonal

Table 2 (Continued)

p-AKT (Thr 308)	Cell Signaling Technology	9275	1:500	Rabbit Polyclonal
Pan-AKT	Cell Signaling Technology	4685	1:1000	Rabbit Monoclonal
Pan-Actin	Cell Signaling Technology	4968	1:1000/1:50	Rabbit Polyclonal
PARP	Cell Signaling Technology	9542	1:1000	Rabbit Polyclonal
p-DRP1 (Ser-616)	Cell Signaling Technology	4494	1:1000	Rabbit Monoclonal
Perilipin	Santa Cruz Biotechnology	SC-390169	1:500	Mouse Monoclonal
p-GSK3	Cell Signaling Technology	9331S	1:1000	Rabbit Polyclonal
p-MAPK (p42/44)	Cell Signaling Technology	9101	1:750	Rabbit Polyclonal
p-S6 (Ser 235/236)	Cell Signaling Technology	4858	1:1000	Rabbit Monoclonal
P62	BD biosciences	610832	1:1000	Mouse Monoclonal
P21	Cell Signaling Technology	2946	1:500	Mouse monoclonal
Pax8	Proteintech	10336-1-AP	1:1000	Rabbit polyclonal
p70S6K	Cell Signaling Technology	2708P	1:1000	Rabbit Monoclonal
TOM20	Santa Cruz Biotechnology	SC-11415	1:7500	Rabbit Polyclonal
TOM40	Santa Cruz Biotechnology	SC-365467	1:1000	Mouse Monoclonal
TOM70	Santa Cruz Biotechnology	SC-390545	1:1000	Mouse Monoclonal
S6	Cell Signaling Technology	2217S	1:1000	Rabbit Monoclonal

rpm for 10 minutes and the supernatant was extracted. Bicinchoninic acid (BCA) assay kit (Pierce, Fischer Scientific, Pittsburgh, PA) was then used to determine the protein concentration, and all protein samples were normalized to the minimum concentration determined or 1500 ng, whichever was lowest. These lysates were analyzed by running on 8%, 10% or 12% SDS-PAGE gel followed by western blotting analysis using respective antibodies, as mentioned in table 2.

Densitometric Analysis for Western Blots via Image J

For densitometric analysis of western blot, the loading control (most commonly Pan-Actin) was first quantified, followed by analysis of the experimental bands in question and their comparison with the loading control as follows:

For quantification, scanned image of the loading control western blot was opened using ImageJ software. The desired bands were selected with rectangular box tool (default selection). Where the bands were not already horizontal, “Image->Transform->Rotate” function was used to make the bands horizontal. “1 and Yes” were typed and clicked, respectively. The rectangular box was then dragged to a clear area on the blot, followed by selection of “2” then “3” to generate a plot. Lines were then drawn at the troughs between peaks (also on both ends of the plot), ensuring they were completely vertical and extended to the bottom of the plot. Using the wand tool, the peaks on the top plot were then selected and then the generated values were copied into Excel. Then, using the wand tool, the peaks on the bottom (background) plot were selected and values generated were then copied into Excel. The background was then subtracted from the total density (total – background) and utilized to plot onto an appropriately labelled column graph. These were then saved as “Tiff” images. These steps were repeated for all sample sets for all blot exposures. The optimal exposure time(s) was identified and then utilized for normalization.

For the second part of densitometric analysis, the experimental image bands were quantified using the loading control analysis. The original Western blot page scan was opened using ImageJ software and a densitometric plot was generated as mentioned above. Appropriate loading control plot (same replicate, same side of the blot) was opened and lined up with experimental antibody plot. Vertical lines were drawn on antibody plot in the same places as on the loading control plot and total density and background values were coped into Excel file as mentioned above. Then, background value was subtracted from the total density (total – background), appropriate loading control values were copied, and density values were normalized. Normalized values were used to generate a column graph. Densitometry plot and Western blot images were saved as “Tiff” images. These steps were repeated for every replicate on every set of samples for every antibody used, for multiple exposures (if possible/applicable) and the excel file was saved.

miRNA Isolation

Forty-eight hours post-transfection or 24 hours post-treatment, miRNAs were isolated using the *mir*Vana Isolation Kit (#AM1561, ThermoFisher Scientific, Waltham, MA, USA) following the manufacturer's instructions, with modifications described below. Before starting the process, the phenol-chloroform bottle was placed in the fume hood to thaw. Once thawed, the phenol chloroform was mixed thoroughly by inversion multiple times to ensure homogeneity followed by maintenance at room temperature to enable separation of the layers.

PBS (2 ml) was added to each dish for a washing step, followed by aspiration to dryness. Lysis buffer (~450µl or depending on the cell confluency) was then added to each dish and scraped lightly using a P1000 tip, followed by collection to respective tubes. Forty-five microliters of miRNA homogenate additive (containing 2 M sodium acetate) were added to the samples and mixed by inversion followed by incubation on ice for 10 minutes. Next, 450 µl phenol-chloroform (equal volume to the lysis buffer) was added to the samples in the fume hood (by bubbling method). Each sample was then vortexed for 30 seconds and centrifuged at 10,000 rcf for 10 minutes.

After centrifugation, ~150 µl (on top of the interface) of clear liquid was carefully collected from the top aqueous layer. 1.25X volume 100% ethanol was added, followed by mixing and layering on top of a filter cartridge inside a collection tube. This was centrifuged at 10,000 rcf for 20 seconds. This was followed by an initial wash step using 700 µl of Wash Solution 1 and centrifugation at 10,000 rcf for 10 seconds. After discarding the flow-through, 500 µl of Wash Solution 2/3 was added and centrifuged at 10,000 rcf for 10 seconds. During this centrifugation, a tube with an appropriate volume of RNAase free water was placed into a heating block set at 95°C. After centrifugation, the flow-through was discarded and 500µl of Wash Solution 2/3 was again added, followed by centrifugation at 10,000 rcf for 2 minutes. The flow-through was discarded and the tubes were centrifuged at 10,000 rcf for 1 minute to remove any residual volume. The filter cartridge was then transferred to fresh eppendorf tubes and 25µl of 95°C heated RNase free water was added followed by centrifugation at maximum speed (14,000 rpm or 20,817

rcf) for 30 seconds and filter cartridge was discarded. miRNAs that were eluted were then quantified using the Nanodrop and stored at -80°C freezer for subsequent qPCR analysis.

miRNA - qPCR Analysis

Two different methods for qPCR of miRNA samples were utilized and these are described below as Method 1 and Method 2:

Method 1: 100 ng/µl of miRNA dilution was prepared for each miRNA sample and 167 ng (1.67 µl) per sample was ultimately used. cDNA was first generated using the Reverse Transcription kit (#4366596, Applied Biosystems™ TaqMan™ MicroRNA Reverse Transcription Kit). Arrangement of samples on thermocycler block was recorded and temperature changes monitored. Real-time PCR was then performed using the TaqMan RNA-to-CT 1-Step Kit (#4392938, ThermoFisher Scientific, Waltham, MA, USA) with the respective probes and primers as described in Table 9, set up in clear 96-well qPCR plates (#AB0600, Thermo Scientific™ PCR Plate). The fold-change in miRNA expression was calculated using the $2^{-\Delta\Delta CT}$ correlative method, in which Ct values were normalized to the RNU6B control (assay ID #: 001093, ThermoFisher Scientific, Waltham, MA, USA). A sample calculation with detailed steps is shown below.

Example:

I. Generation of Reverse Transcription (RT) Master Mix:

2 samples for any three miRNA analyses (2 samples X 3 miRNAs at 2.33 µl /reaction)

2.33 X 6= 13.98 µl required for each miRNA

To prepare 15 µl total RT master mix:

Nuclease free Water: 2.3961 µl

10 mM dNTPs: [(2.143/10) *15] = 3.2145 µl (final concentration = 2.413mM)

10X RT Buffer: [(1.5/7) *15] = 3.214 µl

RNase inhibitor (2U/µl): [(0.5434*15)/2] = 4.0755 µl (final concentration = 0.5434U/µl)

RT Multiscribe Enzyme: (15/7) = 2.1428 µl

Total: 15 µl

To prepare 10mM dNTP sub-stock:

(100mM) (x) = (10mM) (4 µl)

X= 0.4 µl stock + 3.6 µl water

To prepare 2U/µl RNase inhibitor sub-stock:

(20u/µl) (x) = (2U/µl) (5 µl)

X = 0.5 µl stock + 4.5 µl water

- First, 2.33 µl reaction mix/ tube was added, followed by 1.67 µl miRNA dilution and 1 µl 5X RT primer.
- This was mixed by swirling and was centrifuged briefly (1000 rpm for 5 seconds) to collect the contents at the bottom.

Total 5 µl RT reaction/ PCR tube was generated.

- PCR tubes were placed on ice and proceeded to RT reaction in thermocycler:

Cycle conditions in thermocycler:

30 minutes 16°C; 30 minutes 42°C; 5 minutes 85°C; 4°C Forever

II. qPCR Reaction

Number of reactions for three miRNA analyses (in 3 different qPCR master mix tubes) –

For each: 2 reactions*2 (Duplicates) + 1 extra -> n=5

Master mix:

PCR Mix: 10 µl X 5 = 50 µl

Water: 7 µl X 5 = 35 µl

Primer: 1 µl X 5 = 5 µl

Master mix 18 µl was added to each well +2 µl RT product (cDNA)

Total 20 µl reaction was set up to run at the following cycle conditions:

10 minutes 95°C (holding stage)

50 cycles (cycling stage):

15 seconds 95°C

60 seconds 60°C

Method 2: 250 ng of each miRNA sample was utilized. cDNA was generated first using the Reverse Transcription kit (#4366596, Applied Biosystems™ TaqMan™ MicroRNA Reverse Transcription Kit). cDNAs for all miRNA samples was generated in duplicate and a non-template water control was prepared in duplicate as well for comparison. Arrangement of samples on thermocycler block was recorded and temperature changes were monitored. Real-time PCR was then performed using the TaqMan RNA-to-CT 1-Step Kit (#4392938, ThermoFisher Scientific, Waltham, MA, USA) with the respective probes and primers as mentioned in Table 3, set up in clear 96-well qPCR plates (#AB0600, Thermo Scientific™ PCR Plate). Each cDNA duplicate sample was loaded in duplicates again, ultimately generating quadruplets for each miRNA sample. The fold-change in miRNA expression was calculated using the $2^{-\Delta\Delta CT}$ correlative method, in which Ct values were normalized to the RNU48 control (assay ID #: 001006, ThermoFisher Scientific, Waltham, MA, USA). The reason for selecting an alternative endogenous control (RNU48) in this method was based on prior experimentation showing variability in RNU6B values between different renal cancer cell lines. The literature evidence supports RNU48 as one of most common normalization probes [235, 236], which also proves to be an appropriate endogenous control for renal cell lines under our experimental conditions. A sample calculation with detailed steps is shown below.

Example:

To prepare miRNA dilution – Example sample concentration: 444.575 ng/µl

RNA stock was added 2.728 µl stock + 12.272 µl water (15 µl total volume) to generate 80.8617 ng/ µl sub-stock

This will be added to the 5 µl final cDNA sample to generate 250 ng concentration.

To Generate Master Mix for RT reaction- 10XRT buffer was added first, followed by dNTPs, RNAse inhibitor and Multiscribe RT enzyme. cDNA generation was done in duplicate, therefore, number of reactions required to prepare 5 samples (duplicates)= 10 + 2 non-template controls = 12 for each miRNA -> 2 miRNAs: 12*2 = 24

PCR tubes were taken for 24 reactions and prepared enough for 26 reactions (2 extra):

I. **RT reaction set up in a PCR tube**:

For RT reaction master mix (5 µl total cDNA reaction):

- 100 mM dNTPs stock: Final concentration 0.25 mM

(100 mM) (x) = (0.25 mM) (5 µl)

X = 0.0125 µl

0.0125 µl X 26 = 0.325 µl

- 10X RT Buffer: Final concentration 1X

(10X) (x) = (5 µl) (1X)

X = 0.5 µl 10X RT buffer in one reaction

0.5 µl X 26 = 13 µl

- RNase inhibitor (20 U/ul): Final concentration 0.25 U/µl

(20 U/µl) (x) = (0.25 U/µl) (5 µl)

X= 0.0625 µl

0.0625 µl X 26= 1.625 µl

- RT Multiscribe Enzyme (50 U/µl): Final concentration 3.33 U/ul

(50 U/µl) (x)= (3.33 U/µl) (5 µl)

X= 0.333 µl in one reaction

0.333 X 26= 8.658 µl in total master mix

Total 0.9083 µl in one reaction.

- Master mix was mixed by swirling and the appropriate volume (0.9083 µl) was added to all the PCR tubes.
- RT primer was flicked and tapped before opening. RT primer (5X at 1 µl) was added to the respective tubes, spraying the pipette thoroughly between different primers.
- miRNA sub-stock 3.0917 µl of 80.8617ng/µl was added to the respective PCR tubes to generate 250 ng final concentration in one cDNA sample.

  Overall, 0.9083 µl RT master mix + 1 µl RT Primer+ 3.0917 µl miRNA dilution were added to each tube.
- These tubes were spun down at 1000 rpm for 20 seconds in the empty (without lid) tubes.
- PCR tubes were kept in the block and made note of where the tubes were being placed.

Cycle conditions in thermocycler: 30 minutes 16°C; 30 minutes 42°C; 5 minutes 85°C; 4°C Forever

II. qPCR Reaction:

For 10 sample cDNA duplicates+2 non template control) for each miRNA= 12

Samples = 12*2 (duplicates)= 24+ 2 extra = 26 reactions for each miRNA

5 µl 2X PCR mix X 26 = 130 µl

0.5 µl Tm primer X 26 = 13 µl

3.83 µl water X 26 = 99.58 µl

Master mix (9.33 µl) was added to the respective wells in duplicates. After RT reaction was done (~1 hour 10 minutes), appropriate volume (0.67 µl) was added to the appropriate master mix added in the wells. Overall, 9.33 µl per well + 0.67 µl RT product = Total 10 µl reaction set up at the following cycle conditions:

10 minutes 95°C (holding stage) ; 50 cycles (cycling stage)

15 seconds 95°C; 60 seconds 60°C

Table 3: miRNA probes and primers information list utilized in these studies.

miRNA Probes/Primers	*Assay ID (50RT/150 PCR reactions)*
miR-432-5p	001026
miR-127-3p	000452
miR-138-5p	002284
miR-493-5p	001040
miR-431-5p	001979
miR-411-5p	001610
miR-495-3p	001663
miR-539-5p	001286
miR-323b-3p	244080_mat
miR-410-3p	001274
miR-433-5p	001028
miR-494-5p	002365

RNA Isolation and qPCR Analysis

Total RNA was isolated using the RNeasy Mini kit (QIAGEN, Valencia, CA) according to the manufacturer's instructions and previously published methods [19, 234]. Real-time PCR utilized the TaqMan RNA-to-CT One-Step Kit (#4392938, ThermoFisher Scientific, Waltham, MA) and the FAM-labelled probes and primers, as mentioned in table 4**.** β-actin (#401846, ThermoFisher Scientific, Waltham, MA) and/or Cyclophilin (PP1A, # Hs04194521_s1, ThermoFisher, Waltham, MA, USA) were used as endogenous controls, as appropriate for each experimental condition. RNA-fold changes were calculated using the $2^{-\Delta\Delta CT}$ method.

LipidTOX Staining

Lipid Droplet staining was performed as previously reported [237]. Briefly, HK-2, 769-P, 786-O and A-498 cells were seeded at 250,000 cells/well onto glass coverslips in 6-well plates. After

overnight attachment, cells were treated with 10 µM TEMS or with 0.25 mM oleic acid for 24 hours. The media was then removed from the cells and rinsed with 2 ml PBS. The cells were next fixed with 1 ml 4% formaldehyde (in PBS) for 30 minutes at room temperature. Three 2 ml PBS

Table 4: List of RNA qPCR probes/primers utilized in these studies.

RNA qPCR Probes/Primers	***Assay ID***
Phospholipid Phosphatase 1 (PLPP1)	Hs00170356_m1
Diacylglycerol O-acyltransferase 2 (DGAT2)	Hs01045913_m1
Perilipin 1 (PLIN1)	Hs00160173_m1
Cell death-inducing DFFA-like effector c (CIDEC)	Hs00535724_gH
Adipose Triglyceride Lipase (ATGL/PNPLA2)	Hs00386101_m1
Autotaxin (ATX/ENPP2)	Hs00905117_m1
hTERT	*Custom designed*: Forward Primer: 5'-CGCAGGGCTCCATCCT-3' Reverse Primer: 5'-TCCCCGCAAACAGCTTGT-3' Probe Sequence: 5'-CTCTGCAGCCTGTGCTAC-3'

washes (5 minutes each) were performed, following which 500 µl of 1:400 dilution of the lipidTOX green neutral lipid stain (#H34475, Life Technologies, Grand Island, NY) in PBS was added for 1 hour at room temperature. After incubation, lipidTOX stain solution was discarded and 2 ml PBS was added as a rinse solution. The cover slips were next mounted onto glass slides containing 20 µl DAPI. Slides were viewed and imaged at 63X (oil immersion) magnification using the PerkinElmer UltraVIEW Confocal spinning disc microscope (CMMB Core Facility, University of South Florida, Tampa, Florida).

Image J analysis of Lipid Droplets

LipidTOX stained immunofluorescence images were analyzed using Image J to quantify LD size (area covered by LD) and number (number of particles). From the “Image” option, the “color threshold” of the images was selected. This was then adjusted by using the Hue, Saturation, Brightness (HSB) color model; the hue and saturation were kept constant at 0 and the brightness using the red threshold color was adjusted but kept consistent for different treatments within an independent experiment to allow appropriate comparison to facilitate an unbiased analysis. LDs within each image were analyzed for the number of LDs as well as the area covered by each droplet by selecting “Analyze particles” and setting the size limit: “0 to infinity”. This provided a list of number and sizes of LDs associated with each particle. This was then copied into an excel file and the total number of LDs and their sizes were calculated for each image with respect to the total number of cells present (i.e., number of DAPI stained nuclei within the image) to obtain the total area covered by LDs per cell as well as the total number of LDs per cell. The values obtained from treated samples were normalized to the values obtained from the corresponding untreated samples. This was used to generate appropriate graphs representing the LDs size and numbers corresponding to each experimental treatment.

Immunofluorescence

Immunofluorescence staining methods have been previously described [237, 238]. Briefly, HK-2, 769-P, 786-O and A-498 cells were seeded onto glass coverslips at 250,000 cells/well (in 6-well plates). After overnight attachment, cells were treated with 10 µM TEMS or with 0.25 mM oleic acid for 24 hours. Next day, the media was discarded, and cells washed with 2 ml PBS. The cells were then fixed with 1 ml/well 4% formaldehyde (prepared in PBS) for 30 minutes. This was followed by rinsing with 2 ml PBS and incubation with 1 ml/well blocking solution (1 ml blocking solution was prepared by adding 50 µl of 100% goat serum to generate 5% final concentration; 5 µl of 20% Triton X-100 to generate 0.1% final concentration and 945 µl PBS) at room temperature

for 1 hour. The cells were then rinsed again with 2 ml PBS. The coverslips were then placed into respective primary antibody (50µl each) onto petri dishes overnight inside a humidifying chamber at 4°C. Primary antibody was next prepared (1% goat serum, 0.1 % Triton X-100 and appropriate volume of primary antibody, at an appropriate concentration, in PBS). Mitochondrial networks were assessed using antibodies targeting TOM20 (1:100) or TOM70 (1:100) followed by incubation using the appropriate fluorophore-conjugated secondary antibodies. The secondary antibody was prepared (1% goat serum, 0.1% Triton X-100 in PBS) at 500µl for each coverslip. The coverslips were removed from the petri dishes inside the humidifying chamber and placed into respective wells containing 2ml PBS. The cells were then washed with 2 ml PBS three times, each for 5 minutes. The secondary antibody was then applied dropwise to the center of coverslip and incubated for 1 hour at room temperature. PBS (2 ml) was added 3 times, each for 5 minutes. Coverslips were next mounted onto glass slides containing 20 µl anti-fade DAPI solution, which were viewed and imaged using the 63X objective (oil immersion) on the PerkinElmer UltraVIEW Confocal spinning disc microscope (CMMB Core Facility, University of South Florida, Tampa, Florida). For quantification, the mitochondrial patterns were categorized according to the following five categories: (1) Tubular elongated; (2) Tubular shortened; [27] Tubular shortened fragmented; (4) Fragmented mitochondria; and (5) Fused not elongated [18]. One hundred cells per sample were assessed and cells were assigned to these five categories.

Crystal Violet Cell Viability Assay

First, 160 ml of nanopure water was added to the stock CV stain bottle. Methanol (40 ml) was measured in a 50 ml tube and added to the water inside the CV stain bottle. One gram of 0.5% crystal violet powder was next added to the bottle followed by mixing by gently swirling.

HK-2, 769-P, 786-O and A-498 cells were seeded in a 96-well plate at 7,500 cells for TEMS and OA treatment; 769-P and 786-O cells were seeded at 4,000 cells per well and 786-O and A-498 cells at 2000 cells/well in 96-well plate for HCQ and TEMS combinatorial treatment;

and HK-2 cells were seeded at 125,000 cells per well in a 6-well plate. After cellular treatment for appropriate time periods, cells were stained with 100 µl with crystal violet for 15 minutes, followed by extensive washing with nanopure water and overnight drying. Next day, 200 µl of Sorenson's buffer was added to each sample for solubilization and incubated for 2 hours at room temperature on a rotating platform, followed by reading at 570 nm with a Biotek plate reader according to previously published methods [237, 239].

Total Cholesterol Measurement

769-P and HK-2 cells were seeded at 125,000 cells whereas 786-O and A-498 cells were seeded at 62,500 cells in 6-well plates; all cells were kept in culture for 72 hours. Total protein lysates were collected and normalized using the BCA assay as previously described [234]. In these samples, the Amplex Red Cholesterol Assay Kit (#A12216) obtained from Life Technologies (Grand Island, NY) was utilized to assess total cholesterol levels as previously described [237]. Briefly, the cholesterol standards were prepared as detailed in table 5.

Table 5: Cholesterol assay standard concentrations and composition.

Concentrations (µg/ml)	***Component H (Cholesterol reference standard) (µl)***	***IX Reaction buffer (µl)***
0	0	1000
2.5	1.25	998.75
5.0	2.5	997.50
7.5	3.75	996.25
10	5	995

Next, 1X reaction buffer was prepared by adding 2 ml of 5X reaction buffer to 10 ml of nanopure water (5X reaction buffer contains: 0.5 M potassium phosphate (used to maintain pH

7.4), 0.25 M NaCl, 25 mM cholic acid and 0.5% Triton X-100). The Amplex Red working solution was then prepared as follows:

1X Reaction buffer (thaw at room temperature and keep on ice): 1205 µl

Amplex red (at room temperature): 18.75 µl

HRP (on ice): 12.5 µl

Cholesterol oxidase (on ice): 12.5 µl

Cholesterol esterase (on ice): 1.25 µl

The positive controls were prepared by diluting the 20 mM H_2O_2 working solution to 10 µM in 1X Reaction Buffer by adding 0.25 µl in 500ul 1X reaction buffer. Standards (50 µl) were next added to a black 96-well plate in duplicate. The positive control was added (50 µl) to a black 96-well plate. No cholesterol control (negative control) was prepared directly in well by adding 10µl of RPPA lysis buffer followed by 40 µl of 1X reaction buffer. Next, 10 µl sample was added to the plate followed by 40 µl of 1X reaction buffer. The pre-prepared Amplex Red solution was next added to all the standards, controls, and samples (50 µl). The plate was then incubated for 30 minutes at 37°C. The fluorescence was then measured in a fluorescence microplate reader using an excitation in the range of 528/20 nm with an emission at 590/35 nm.

Mammalian Antibiotic Selection for Stable Cell Line Generation

For identification of an appropriate antibiotic dose for stable cell line generation, cells were seeded in 96-well plate. Cells were generally seeded at 2500 cells/well for half plate and 5000 cells/well (96-well plate subdivided in half), except for the primary normal RPTEC cells which were seeded at 2500 cells/well density (due to limiting cell numbers).

Following overnight adherence, cells were next treated with the appropriate doses of antibiotics (puromycin or blasticidin in combination with puromycin) along with a control column of cells (untreated). 48-hours post-treatment, the plates were removed from the incubator for CV staining (please see CV staining section for details).

Proteomics and microarray analysis

Please refer to Chapter 4 for detailed methodology.

Bioinformatics analysis of EVI1 at miR-138 promoter site

Please refer to Chapter 4 for detailed methodology.

Table 6: Antibiotic doses for selection of stable cell lines used via CRISPR-Cas9.

Cell Line	***Antibiotic***	***Dose selected***
RPTEC	Puromycin	0.75 µg/ml
HEK293T	Puromycin	2 µg/ml
HEK293T	Blasticidin	3.5 µg/ml
HK-2	Puromycin	0.1 µg/ml
769-P	Puromycin	1 µg/ml
786-O	Puromycin	1 µg/ml
A-498	Puromycin	1 µg/ml
FT194-FAC	Puromycin	0.75 µg/ml
FT194-FAC	Blasticidin	5 µg/ml

Chronic Iron exposure of FTSECs

Please refer to Chapter 4 for details and Dr. Stephanie Rockfield's thesis (pages 108-109). The detailed timeline for maintenance of long-term iron (Ferric ammonium citrate (FAC)) treated and untreated FT194 cells is located on the Cloud Box storage drive at the University of South Florida in Stephanie Rockfield's "Experimental_Results_2018" within the subfolder "Mar 5 through Mar 11":" FT194 Rep 1 Timeline" and "Updated Timeline for FT194 cells".

Statistical analysis

All data obtained was analyzed using the Graphpad Prism software, version 6.04 (La Jolla, CA, USA). Error bars represent the mean ± SD and p-values were determined through the non-parametric Student's t-test for which "ns" represents non-significant values, * indicates $p \leq 0.05$, ** indicates $p \leq 0.01$, *** indicates $p \leq 0.001$, and **** indicates $p \leq 0.0001$. Fold changes and percent reductions were calculated from the average of at least three independent experiments.

Chapter 3

Lysophosphatidic Acid reverses Temsirolimus-induced changes in lipid droplets and mitochondrial networks in renal cancer cells

Note to Reader

This chapter is a reorganized and reformatted version of the published article (Chhabra R, Nanjundan M. PLoS One. 2020 Jun 3;15(6): e0233887. doi: 10.1371/journal.pone.0233887). This has been reproduced here with an open access license from PLOS ONE (see **Appendix A** for copyright permissions).

Contributions and Acknowledgements

I am deeply grateful to my mentor Dr. Meera Nanjundan for her valuable guidance and conceptualization of the study. We worked collaboratively on the experiments, methodology and data analysis. I am also highly thankful to Dr. Stephanie Rockfield, Brandon Ramos, and Nabila Rehman for their kind assistance in quantifying immunofluorescence, and to Robert Hill (Director of the CMMB Core Facilities) for his assistance with flow cytometry and confocal microscopy.

Introduction

Renal cell cancer is one of the most common urological malignancies. Contributing factors to disease pathogenesis include smoking, obesity, as well as mutations in Von Hippel-Lindau (VHL) [240]. Of the five major subtypes of RCC, clear cell RCC (ccRCC) is the most common and lethal subtype; it is a metabolic disease characterized by dysregulated lipid metabolism, altered gene

regulation due to multiple genomic aberrations, and increased abundance of lipid droplets [77, 114, 240, 241]. Regrettably, the overall patient survival rate is <15% for advanced RCC disease [240] and thus an improved understanding of the underlying mechanisms of RCC pathogenesis is direly needed to develop improved treatment regimens. There currently exists several first-line targeted therapies which are FDA approved for ccRCC, including mTOR targeting agents [6]. The PI3K/AKT/mTOR pathway is highly deregulated in ccRCC [242]; targeting mTOR (which modulates cellular survival, blood vessel development, and nutrients) with rapamycin can modulate LD formation [243]. Specifically, mTORC1 can regulate the lipogenesis and lipolysis pathways via peroxisome proliferator-activated receptor gamma (PPAR-γ) and sterol regulatory element-binding protein 1 (SREBP1) [242, 243]. Notably, LDs can physically associate with mitochondria at defined contact sites; these organellar interactions promote cellular protection from stress via the process of β-oxidation (the breakdown of fatty acids to acetyl-CoA, which can then be utilized in the citric acid cycle to generate cellular energy) [244]. However, the role of mTOR clinical targeting agents (including Rapalogs such as TEMS) [245] in the regulation of mitochondrial networks and LD biogenesis has not yet been investigated in ccRCC.

mTOR inhibitors are associated with low clinical efficacy and this may be due to the activation of the cytoprotective autophagic pathway (a “self-eating” mechanism) [246] which may then antagonize the cell death promoting effects of such inhibitors. Indeed, improvements to cellular sensitivity to mTOR inhibitors has been demonstrated by co-targeting of the autophagic pathway [94]. In a phase I clinical trial combining TEMS with hydroxychloroquine (HCQ), there was improved clinical response in melanoma patients [94, 247]. Another potential contributor to diminished cellular sensitivity to mTOR inhibitors may include the presence of the potent lipid mitogen, lysophosphatidic acid (LPA), which activates G-protein coupled receptors to increase cellular proliferation, migration, and invasive potential via activation of the AKT pathway [248, 249]. This mitogen is produced via the action of autotaxin (ATX), a member of the endonucleotide pyrophosphatase and phosphodiesterase family of enzymes (ENPP2), which elicits

lysophospholipase D (lysoPLD) activity (which hydrolyses lysophosphatidylcholine (LPC) to generate LPA [248, 249]. Interestingly, ATX mRNA and protein in addition to its lysoPLD activity are elevated in RCC (relative to normal epithelium) [135, 250, 251]. Furthermore, the LPA-ATX axis can contribute to resistance against sunitinib in RCC pathogenesis [135]. Although a derivative of LPA (phosphatidic acid, PA) has been shown to contribute to LD enlargement by promoting their fusion [137], to the best of our knowledge, it remains unclear whether LPA can modulate lipid droplet abundance, a key characteristic of ccRCC, in renal cancer cells.

Herein, we have analyzed the effect of TEMS in a series of ccRCC cell lines (769-P, 786-O, and A-498) together with an immortalized normal human kidney cell line (HK-2) to identify alterations in signaling, lipid droplet formation, and mitochondrial networks following treatment with TEMS alone. We also assessed whether combinatorial treatment of TEMS with the autophagic inhibitor, hydroxychloroquine (HCQ) could modulate cellular viability and lipid droplet abundance. Finally, we investigated whether the presence of LPA could hinder the effect of TEMS treatment in the ccRCC cell lines in terms of lipid droplet abundance and AKT/mTOR signaling. Collectively, our results identify that the LPA-ATX signaling axis may be an important target for combating the resistance acquired by RCC cells towards molecular-based therapies.

Materials and methods

Cell culture

Human epithelial renal cancer cell lines (769-P, 786-O, and A-498) and an immortalized kidney proximal tubule cell line (HK-2) [252] were purchased from ATCC (Manassas, VA). HK-2 cells were cultured in Keratinocyte-serum free media (K-SFM, #17-005-042, Fisher Scientific, Pittsburgh, PA) supplemented with 50 µg/ml bovine pituitary extract (BPE, #10450-013) and 5 ng/ml human recombinant epidermal growth factor (EGF, #13028-014). 769-P and 786-O cells were grown in RPMI 1640 media containing 8% fetal bovine serum (FBS) and 1% penicillin/streptomycin whereas A-498 cells were cultured in EMEM media supplemented with 8%

FBS and 1% penicillin/streptomycin. All cell lines used in this manuscript were authenticated by Short Tandem Repeat (STR) profiling (Genetica DNA Laboratories, Cincinnati, OH) and were tested to be mycoplasma negative. For the experiments presented in this manuscript, the above cell lines were utilized at the following passage numbers: (1) 769-P cells, p = 41-54; (2) 786-O cells, p = 113-127; [27] A-498 cells, p = 38-53; and (4) HK-2 cells, p = n+4 – n+20.

Cell treatments

A 10 mM stock of the mTOR inhibitor, Temsirolimus (TEMS, #50-811-7, Fisher Scientific, Pittsburgh, PA) was prepared by reconstitution in dimethyl sulfoxide (DMSO) and used at a final concentration of 10 µM. Oleic acid (#O1383, Sigma-Aldrich, St. Louis, MO) was reconstituted in 100% ethanol to prepare a 0.35 M solution, which was utilized at a final concentration of 0.25 mM. The autophagic flux inhibitor, hydroxychloroquine (HCQ, AC263011000, Fisher Scientific, Pittsburgh, PA), was prepared in phosphate buffered saline (PBS) at 50 mM and used at a final concentration of 25 µM. The MAPK inhibitor, U0126 (#9903S, Cell Signaling Technology, Danvers, MA), was reconstituted in DMSO at a concentration of 10 mM and utilized at a final concentration of 10 µM.

Fatty acid-free bovine serum albumin (FAF-BSA, BP9704-100, Fisher Scientific, Pittsburgh, PA) was dissolved in PBS to generate a 0.5% stock solution. 1-Oleoyl-2-hydroxy-sn-glycero-3-phosphate (sodium LPA salt in chloroform, #857130C, Avanti Polar Lipids, Alabaster, AL) was air-dried and reconstituted in 0.5% FAF-BSA to generate a stock solution of 3.5 mM and used at a final concentration of 10 µM.

siRNA transfections

HK-2 cells were seeded at 350,000 cells/well in 6-well plates. After overnight adherence, cells were transfected with the following siRNA using Dharmafect I (#NC1308404, Fisher Scientific, Pittsburgh, PA) according to previously published methods [19, 237]: ribosomal protein S6

(RPS6) siRNA (#L-003024-00-0005), ribosomal protein S6 kinase B1 (p70S6K1) siRNA (#L-003616-00-0005), or non-targeting ON-TARGETplus (D-001810-10-20) siRNA (Dharmacon, Lafayette, CO). The day after transfection and following cell recovery, cells were treated with 10 µM LPA (or with an equivalent volume of 0.5% BSA) for 24 hours followed by protein analyses or immunofluorescence LD staining (as described below).

Protein isolation and western analyses

Using previously published methodology [19, 234, 237], protein lysates were collected and normalized to at least 1,000 µg/ml using the Bicinchoninic Assay (BCA, Fisher Scientific, Pittsburgh, PA). The samples were then run on 10% SDS-PAGE gels and analyzed by western blotting using primary antibodies at the following dilutions: (1) Beclin-1 rabbit polyclonal (#3738, 1:1000), DRP1 rabbit monoclonal (#8570, 1:1000), hVPS34 rabbit monoclonal (#3358, 1:1000), LC3B rabbit polyclonal (#2775, 1:1000), p-AKT (Ser-473) rabbit monoclonal (#4060, 1:1000), p-GSK3 (Ser-21/Ser-9) rabbit polyclonal (#9331, 1:1000), p-S6 ribosomal protein (Ser-235/236) rabbit monoclonal (#4858, 1:1000), Pan-Actin rabbit polyclonal (#4968, 1:500), PARP rabbit polyclonal (#9542, 1:1000), p-DRP1 (Ser-616) rabbit monoclonal (#4494, 1:1000), p-p42/44 MAPK (Thr-202/Tyr-204) rabbit polyclonal (#9101, 1:750), Pan-AKT rabbit monoclonal (#4685, 1:1000), p42/44 MAPK rabbit monoclonal (#4695, 1:1000), p70S6K rabbit monoclonal (#2708, 1:1000), and S6 rabbit monoclonal (#2217, 1:1000) which were obtained from Cell Signaling Technology (Danvers, MA); (2) p62 mouse monoclonal (#610832, 1:1000) was obtained from BD Biosciences (San Jose, CA, USA); [27] Perilipin mouse monoclonal (#SC-390169, 1:500), TOM20 rabbit polyclonal (#SC-11415, 1:7500), TOM40 mouse monoclonal (#SC-365467, 1:1000), and TOM70 mouse monoclonal (#SC-390545, 1:1000) were obtained from Santa Cruz Biotechnology (Dallas, TX, USA); and (4) ATG7 rabbit polyclonal (#PM039, 1:1000) from MBL International Corporation (Woburn, MA, USA).

RNA isolation and real-time PCR

Total RNA was isolated using the RNeasy Mini kit (QIAGEN, Valencia, CA) according to previously published methods [19, 234]. Real-time PCR utilized the TaqMan RNA-to-CT One-Step Kit (#4392938, ThermoFisher Scientific, Waltham, MA) and the following FAM-labelled probes and primers: (1) Phospholipid Phosphatase 1 (PLPP1), Hs00170356_m1; (2) Diacylglycerol O-acyltransferase 2 (DGAT2), Hs01045913_m1; [27] Perilipin 1 (PLIN1), Hs00160173_m1; (4) Cell death-inducing DFFA-like effector c (CIDEC), Hs00535724_gH; (5) Adipose Triglyceride Lipase (ATGL/PNPLA2) Hs00386101_m1; and (6) Autotaxin (ATX/ENPP2), Hs00905117_m1. Normalization of CT values was performed using β-actin (#401846, ThermoFisher Scientific, Waltham, MA) and RNA-fold changes were calculated using the formula $2^{-\Delta\Delta CT}$.

Cell viability assay

Cells were seeded at 7,500 cells (Fig 2B) or at 4,000 cells (Fig 4C) per well in a 96-well plate or at 125,000 cells per well (Fig 5B) in a 6-well plate. After cellular treatment for appropriate time periods, cells were then stained with crystal violet for 15 minutes, extensive washing with nanopure water, and overnight drying. Next, samples were solubilized with 200 µl of Sorenson's buffer, incubated for 2 hours at room temperature on a rotating platform, and then read at 570 nm with a Biotek plate reader according to previously published methods [237, 239].

Mitochondrial network staining via immunofluorescence

Immunofluorescence staining methods have been previously described [237, 238]. Briefly, cells were seeded onto glass coverslips at 250,000 cells/well (in 6-well plates). After overnight attachment, cells were treated with 10 µM TEMS or with 0.25 mM oleic acid for 24 hours. Mitochondrial networks were assessed using antibodies targeting TOM20 (1:100) or TOM70 (1:100) followed by incubation using the appropriate fluorophore-conjugated secondary

antibodies. Coverslips were mounted using anti-fade solution (containing DAPI) onto glass slides which were viewed and imaged using the 63X objective (oil immersion) on the PerkinElmer UltraVIEW Confocal spinning disc microscope (CMMB Core Facility, University of South Florida, Tampa, Florida). For quantification, the mitochondrial patterns were categorized according to the following five categories: (1) Tubular elongated; (2) Tubular shortened; Tubular shortened fragmented; (4) Fragmented mitochondria; and (5) Fused not elongated [237]. One hundred cells per sample were assessed and cells were assigned to these five categories.

Lipid droplet (LD) staining using LipidTOX

LD staining was performed as previously reported [237]. Briefly, cells were seeded at 250,000 cells/well onto glass coverslips in 6-well plates. After overnight attachment, cells were treated with 10 µM TEMS or with 0.25 mM oleic acid for 24 hours. LDs were stained using LipidTOX neutral lipid dye. Slides were viewed and imaged at 63X (oil immersion) magnification using the PerkinElmer UltraVIEW Confocal spinning disc microscope (CMMB Core Facility, University of South Florida, Tampa, Florida).

LipidTOX stained immunofluorescence images were analyzed using Image J to quantify LD size (area covered by LD) and number (number of particles). The color threshold of the images analyzed were adjusted by using the Hue, Saturation, Brightness (HSB) color model; the hue and saturation were kept constant at 0 and the brightness using the red threshold color was varied but kept consistent for different treatments with an independent experiment to allow appropriate comparison between them to facilitate an unbiased analysis. LDs within each image were analyzed for the number of LDs as well as the area covered by each droplet (size: 0 to infinity). The total number of LDs and their sizes were then calculated for each image with respect to the total number of cells present (i.e., number of DAPI stained nuclei within the image) to obtain the total area covered by LDs per cell as well as the total number of LDs per cell. The values obtained

from treated samples were normalized to the values obtained from the corresponding untreated samples.

Measurement of cholesterol

Total protein lysates were normalized using the BCA assay as previously described [237]. In these samples, the Amplex Red Cholesterol Assay Kit (#A12216) obtained from Life Technologies (Grand Island, NY) was utilized to assess total cholesterol levels as previously described [237].

Statistical analyses

All experiments were performed independently at least three times. The error bars shown in all displayed figures represent standard deviations; p-values were obtained using the standard student's t-test using the GraphPad Prism software (**** = $p \leq 0.0001$, *** = $p \leq 0.001$, ** = $p \leq 0.01$, * = ≤ 0.05, and ns = not significant ($p>0.05$)).

Results

Comparative analyses of normal and a subset of malignant renal cell lines

It is well established that genomic aberrations are characteristic of numerous cancer types and such alterations provide insight into patient survival as well as response to chemotherapeutic regimens [253, 254]. In ccRCC, loss of 3p (which harbors the VHL gene) appears to be an obligate event in RCC pathogenesis [254, 255]. The additional loss of chromosome 14q leads to increased aggressiveness of ccRCC and is associated with a poor patient outcome [254, 256]. Apart from these 3p and 14q alterations, gain at 5q (harboring SQSTM1) is another common alteration in ccRCC [54, 254]. To correlate responsiveness of ccRCC cell lines to established forms of treatments with extent of genomic aberrations, we analyzed a subset of malignant clear cell renal cell lines, via The Cancer Genome Atlas (TCGA) [257, 258]. Indeed, TCGA analysis showed that 769-P cells contained the least percentage of genomic alterations at 17.9%, followed

by 786-O at 43.9%, and A-498 at 61.5% (Fig 1A). Specifically, the 769-P and A-498 cells were characterized by extensive deletions at both the 3p and 14q loci; however, although the 786-O cell line contained 14q deletions, it was lacking chromosomal losses at the 3p locus.

Since the AKT/mTOR and autophagy pathway has been reported to be dysregulated in a variety of tumors including ccRCC [242, 259, 260] with potential to alter chemotherapeutic cellular response, we assessed the baseline expression and activation status of key signaling mediators in the AKT/mTOR pathway across a subset of malignant renal cancer cell lines. As presented in Fig 9B, the activation status of phospho-S6 was elevated in 769-P and 786-O cells relative to A-498 cells whereas phospho-AKT was markedly elevated in 786-O and A-498 cells relative to 769-P cells. These patterns, however, did not correlate with the 3p and 14q TCGA-defined extent of genomic aberrations. Similarly, no association was uncovered with lipidated LC3B and other key autophagic markers (Fig 9B) as identified by immunofluorescence LipidTOX staining and their quality/abundance did not appear to be correlated with the extent of genomic alteration at 3p and 14q (Fig 9C). Since ccRCC is characterized by the presence of LDs [240, 241] and lipidomic analyses have uncovered alterations within the lipidome [261], we next assessed the quality and abundance of LDs across these cell lines.

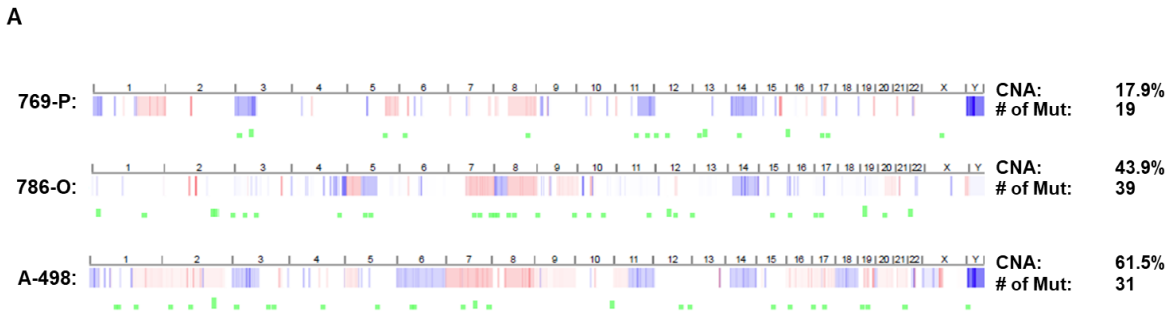

Figure 9: Status of genetic alterations, AKT/mTOR pathway, and LDs across normal and malignant renal cell lines (*Continued on next page)

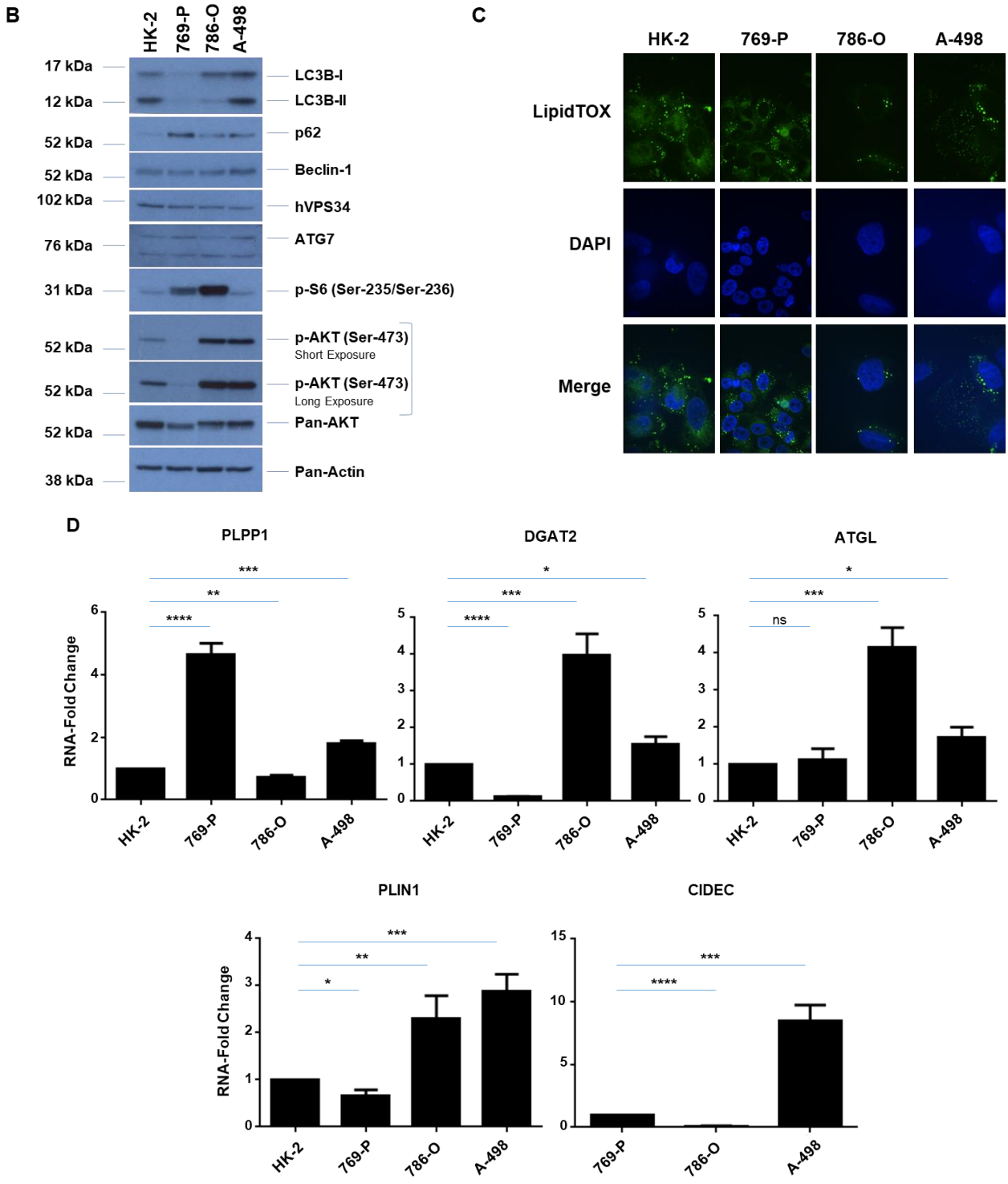

Figure 9: Status of genetic alterations, AKT/mTOR pathway, and LDs across normal and malignant renal cell lines (*Continued on next page)

Figure 9: Status of genetic alterations, AKT/mTOR pathway, and LDs across normal and malignant renal cell lines

(A) Copy number alterations (CNA) across three malignant ccRCC cell lines (769-P, 786-O, A-498) and mutational status [165] derived from TCGA. (B) Western blot analyses of ccRCC cell lines and HK-2 cells with the indicated antibodies. Three independent experiments were performed, and representative blots are displayed. (C) LD assessment of ccRCC cell lines and HK-2 cells via immunofluorescence staining using LipidTOX. Three independent experiments were performed, and representative images are displayed. (D) Real-time PCR analyses of genes involved in LD biogenesis and regulation in ccRCC cell lines and HK-2 cells. Data shown is the composite of three independent experiments.

All cell lines assessed contained LDs Furthermore, the RNA levels (via real-time PCR) of key mediators involved in LD formation/turnover such as phospholipid phosphatase 1 (PLPP1, which converts PA to DAG), diacylglycerol acyltransferase 2 (DGAT2, which converts DAG to TAG), adipose triglyceride lipase (ATGL, which regulates lipolysis), and cell death inducing activator like effector C (CIDEC, involved in LD enlargement) were more elevated in the A-498 cell line (relative to the normal immortalized HK-2), a cell line associated with increased genomic aberrations. All malignant renal cell lines had detectable expression of these LD markers with the exception of CIDEC in HK-2 cells (Fig 9D).

TEMS reduces cellular viability in normal and malignant renal cell lines

Since targeting the mTOR pathway is a part of the chemotherapy regimen for advanced kidney cancer patients [242], we next assessed whether the responsiveness to this agent was correlated with the extent of genomic aberrations at 3p and at 14q. Thus, we first tested a variety of doses of the mTOR inhibitor (100 nM to 10 µM of TEMS) in 769-P, 786-O, A-498 malignant renal cancer cells as well as the normal immortalized HK-2 cell line. Cell lysates were collected following a 24-hour treatment period and analyzed via western blotting for mTOR pathway mediators as well as

autophagy markers. As shown in Fig 10A, phospho-S6 was markedly reduced with TEMS treatment across all four cell lines, which validated mTORC1 inhibition. Phospho-AKT (at Ser-473) increased in the 769-P and 786-O cells as well as the HK-2 cells with increasing doses of TEMS whereas in the A-498 cells, the activation status of AKT decreased. With respect to the autophagy pathway, both lipidated LC3B and p62 were subtly reduced with increasing doses of TEMS in HK-2 as well as 786-O and A-498 cells. Since we noted that the TEMS-induced cellular changes were most striking at 10 µM, this dose was selected to assess changes in cellular viability across these four renal cell lines. We noted that all cell lines were susceptible to growth inhibition in response to TEMS up to 3 days of treatment (Fig 10B). Specifically, the cell numbers of HK-2, 786-O, 769-P, and A-498 were reduced by 42.6%/70.5%, 26.9%/67.7%, 16.8%/55.5%, and 19.3%/53.4%, respectively on day 1/day 3 of treatment, respectively, although this was not accompanied by alterations in PARP cleavage (a marker of caspase-dependent apoptosis) (Figure 10A).

TEMS alters LD abundance and mitochondrial networks in malignant renal cell lines

Since increased LDs are a characteristic feature of ccRCC [240, 241], we next assessed whether LD size and/or abundance was altered by targeting the mTOR pathway with TEMS. Thus, we treated the three malignant cell lines (769-P, 786-O, and A-498) and the normal immortalized HK-2 cells with TEMS for 24 hours followed by staining with LipidTOX. As shown in Fig 11A, we observed increased LD abundance in 769-P and 786-O cells, smaller more numerous numbers of LDs in A-498 cells, and a slight LD increase in HK-2 cells. Furthermore, the mRNA levels of lipid droplet regulators (PLPP1, CIDEC, DGAT1, ATGL and PLIN1) following 24-hours of TEMS treatment showed significantly marked alterations in their expression (Fig 11B), notably in the malignant renal cell lines. Interestingly, ATGL contributes to the process of lipolysis, which may lead to the increased numbers of LDs following TEMS treatment in A-498 cells.

Since LDs are composed of cholesteryl esters as well as triacylglycerides and since cellular cholesterol is linked with cancer progression [262], we next assessed total cellular cholesterol levels upon 72 hours of TEMS treatment in the three malignant RCC cell lines as well as HK-2 cells. Using the Amplex Red Assay, we noted that cholesterol was significantly higher in the malignant ccRCC cells (769-P, 786-O, and A-498) relative to the normal immortalized kidney HK-2 cell line (Fig 11C). However, TEMS treatment did not have any effect on cholesterol in any of these cell types. These data suggest that the changes in lipid droplets observed upon TEMS treatment do not alter total cellular cholesterol levels.

Although LDs interact with mitochondria to promote energy production via the β-oxidation pathway [244], the role of TEMS in regulating mitochondrial networks has not yet been investigated in ccRCC. Thus, we analyzed whether mitochondrial networks are affected by 10 μM TEMS following 72-hours treatment in renal cells. We detected mitochondrial alterations via immunofluorescence staining of both TOM20 as well as TOM70 (outer mitochondrial membrane proteins which facilitate the movement of pre-proteins through the TOM40 translocation pore) [263]. As shown in Fig 3D, we observed that the fragmented mitochondrial appearance (in control cells) changed to a fused tubular elongated structure following TEMS treatment. To assess whether expression of these mitochondrial proteins was altered, we performed western blot analyses of renal cells treated for 72 hours with 10 μM TEMS. As shown in Fig 11E, we identified that TOM20, TOM40, and TOM70 proteins were decreased following TEMS treatment in the malignant renal cancer cell lines (most notably in 786-O cells) in addition to HK-2 cells. Interestingly, these changes coincided with decreased protein expression of perilipin, p62, and the DRP1 (Dynamin-related protein1) mitochondrial fission protein. Further, marked alterations in the lipidated form of LC3B was noted in the malignant renal cell lines and the total protein levels of the DNA repair mediator PARP were reduced upon TEMS treatment suggesting that mTORC1 inhibition may deregulate autophagy as well as downregulate the DNA repair mechanism.

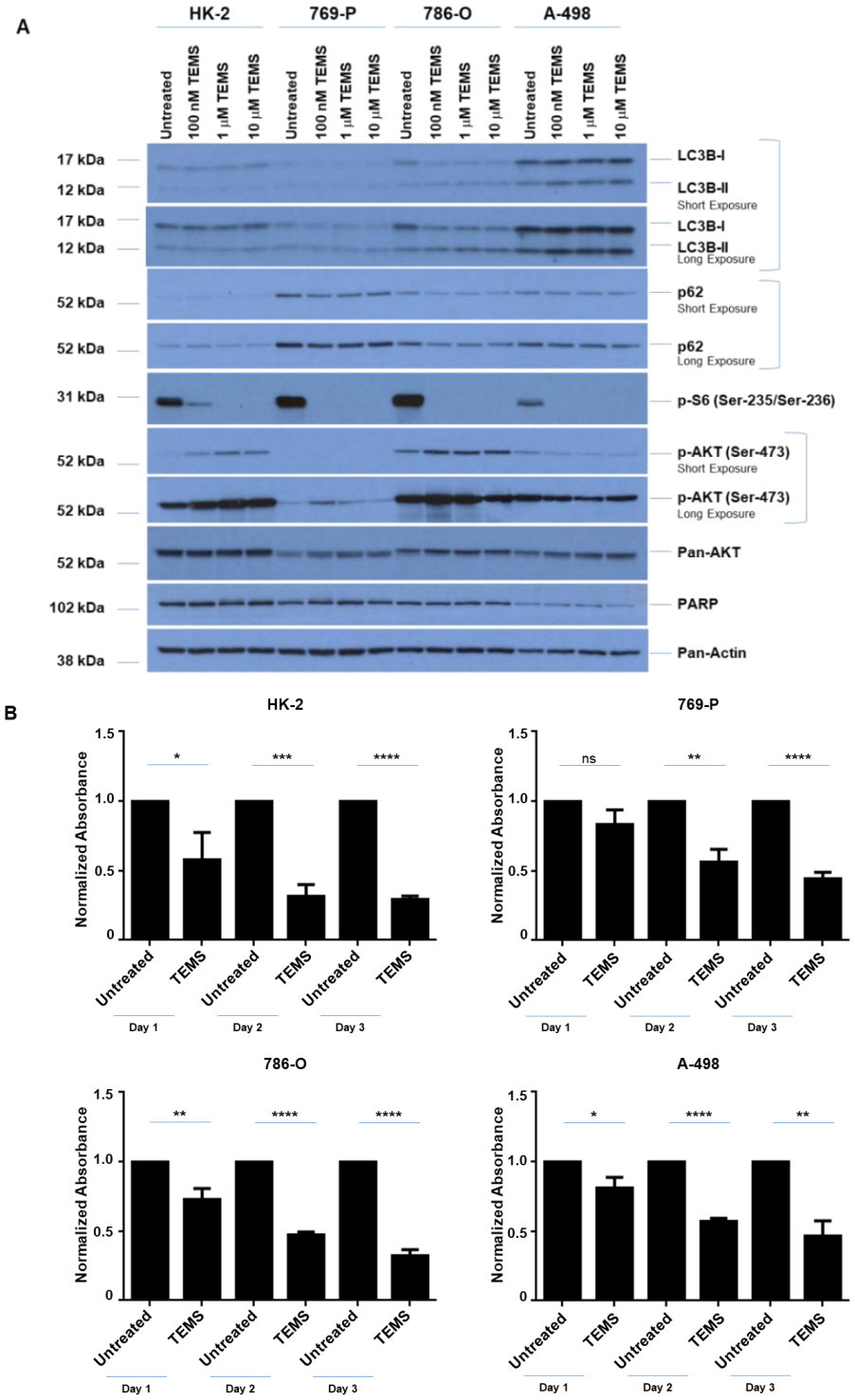

Figure 10: TEMS alters activation status of AKT/mTOR, expression of autophagic mediators and reduces cellular viability in normal and malignant renal cell lines (*Continued on next page)

Figure 10: TEMS alters activation status of AKT/mTOR, expression of autophagic mediators, and reduces cellular viability in normal and malignant renal cell lines

(A) Western blot analyses of ccRCC cell lines and HK-2 cells treated with increasing doses of TEMS (100 nM – 10 µM) with the indicated antibodies. Three independent experiments were performed, and representative blots are displayed. (B) Assessment of cellular viability in ccRCC cell lines and HK-2 cells at Day 1 – 3 in response to 10 µM TEMS. The composite of three independent experiments is displayed.

Oleic acid alters LD abundance and cellular viability of normal immortalized HK-2 cells

Lipid metabolic pathways are commonly exploited by cancer cells, which contribute to increased cellular proliferation and survival [264]. Since exogenous lipid supply (i.e., fatty acids) can increase LDs [265] and we noted that TEMS increases LD abundance, we next assessed whether oleic acid could modulate pathways similar to TEMS. Thus, we treated renal cells (three malignant and a normal immortalized HK-2 cell line) with 0.25 mM oleic acid (selected after testing a range of doses from 250 nM to 2.5 mM) [266-268].

First, we investigated whether exogenous presentation of oleic acid (for 24-hours) to these cell lines could modulate lipid droplet formation. As shown in Fig 12A, oleic acid treatment increased lipid droplet size in all four cell lines with statistically significant alterations in HK-2, 769-P, and A-498 cells; in 769-P cells, the number of lipid droplets also significantly increased. However, western blot analyses showed variable alterations in phospho-S6 levels and LC3B-II with no change in p62, phospho-AKT, or TOM20 (Fig 12B) across the four cell types treated with oleic acid for 72 hours. These results suggest that the mechanism of LD increase via oleic acid may differ to that mediated by TEMS and across different cell types. Furthermore, we identified that oleic acid could alter HK-2 cell viability (but not the malignant cancer cells) when treated up to three days (Fig 12C).

These results suggest that excess fatty acids and possibly LD formation may have a

negative effect on the viability of normal cells whereas the renal cancer cells may utilize this monounsaturated fatty acid for essential cellular metabolic processes to support their current proliferative and survival capacity.

Hydroxychloroquine (HCQ) alters LDs and synergizes with TEMS to reduce cellular viability in renal cell lines

Since the PI3K/AKT/mTOR pathway negatively regulates autophagy, effective renal cancer cell treatment with mTOR inhibitors (such as TEMS) may thus be antagonized by the resulting increased cellular protective autophagy [245, 246]. Indeed, induction of autophagy with mTORC1 inhibition has previously been reported, and thus may provide a mechanism underlying low patient

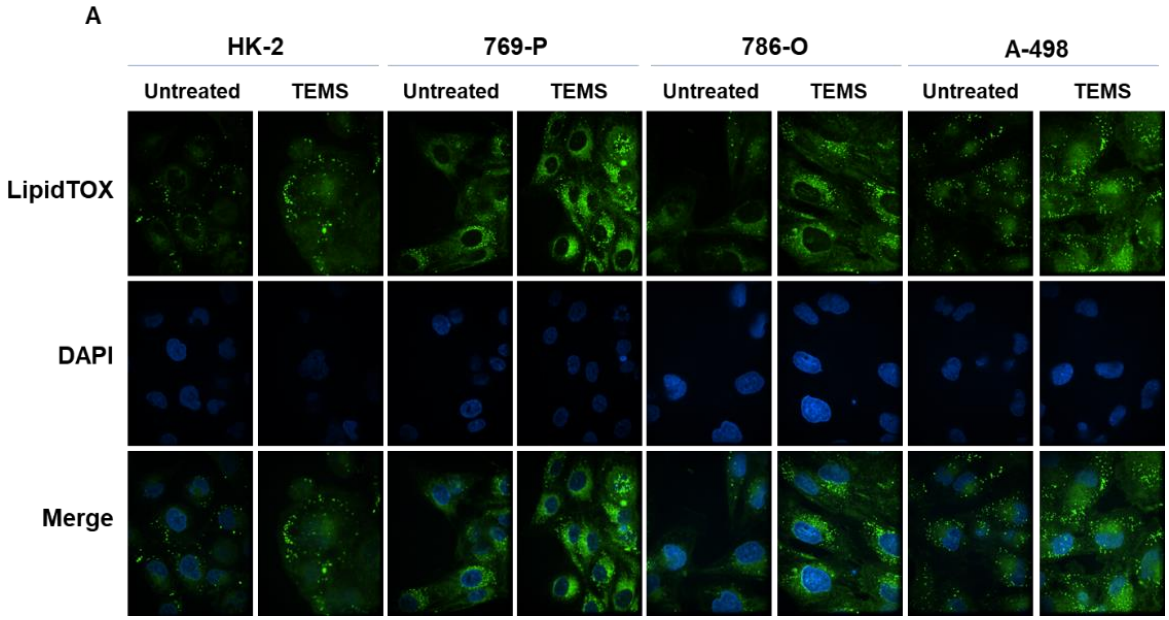

Figure 11: TEMS alters LD abundance and mitochondrial networks in malignant renal cell lines (*Continued on next page)

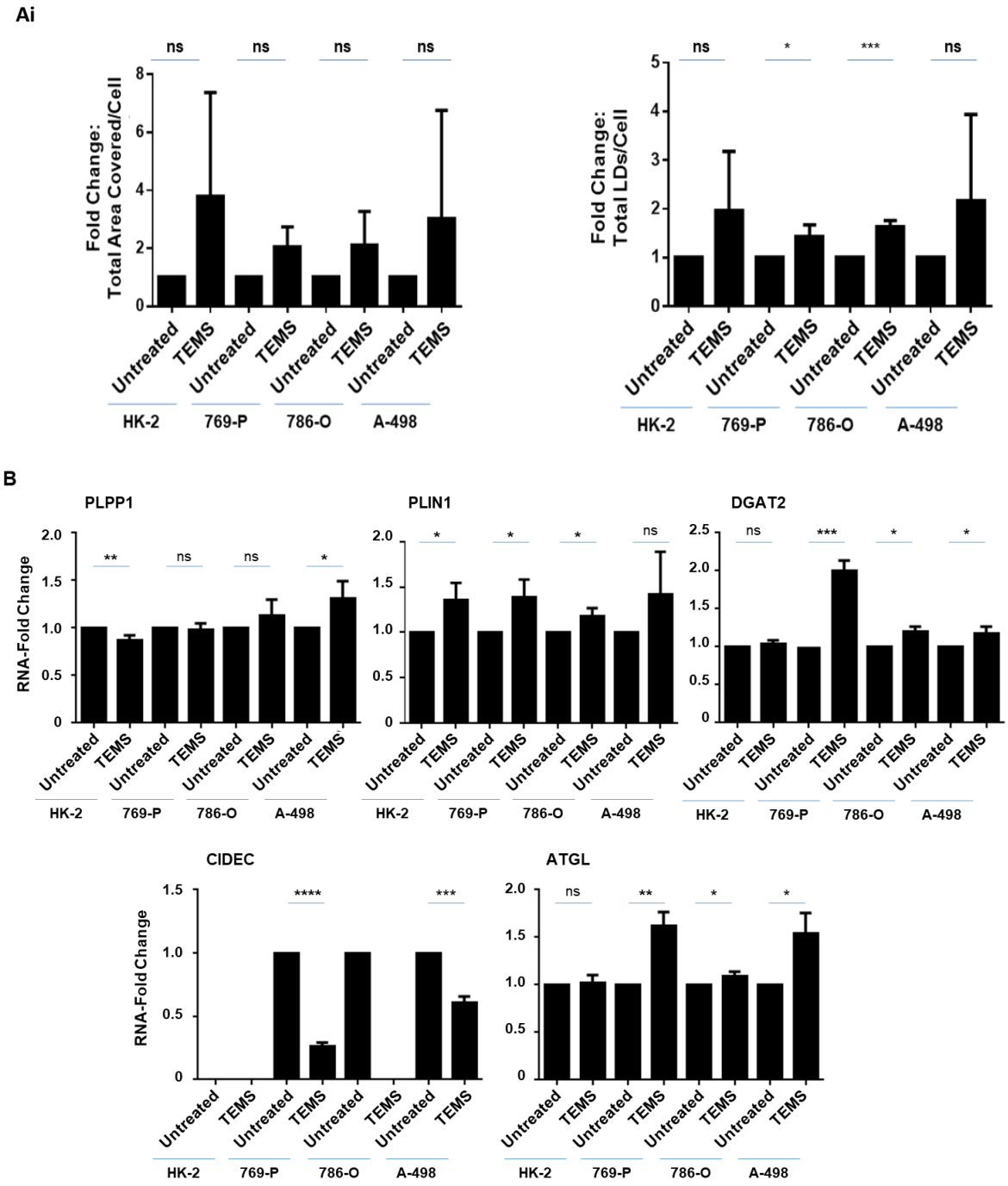

Figure 11: TEMS alters LD abundance and mitochondrial networks in malignant renal cell lines (*Continued on next page)

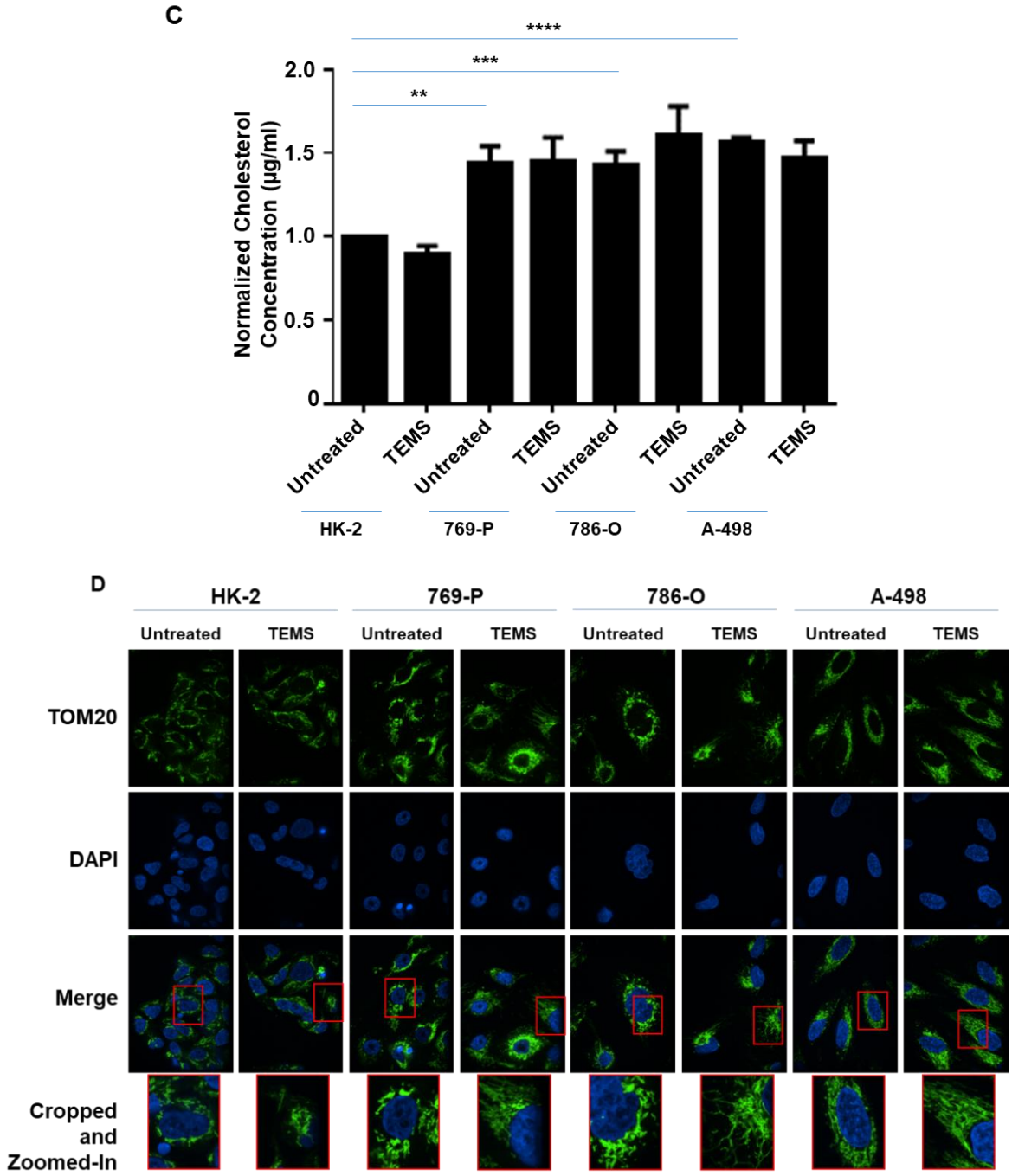

Figure 11: TEMS alters LD abundance and mitochondrial networks in malignant renal cell lines (*Continued on next page)

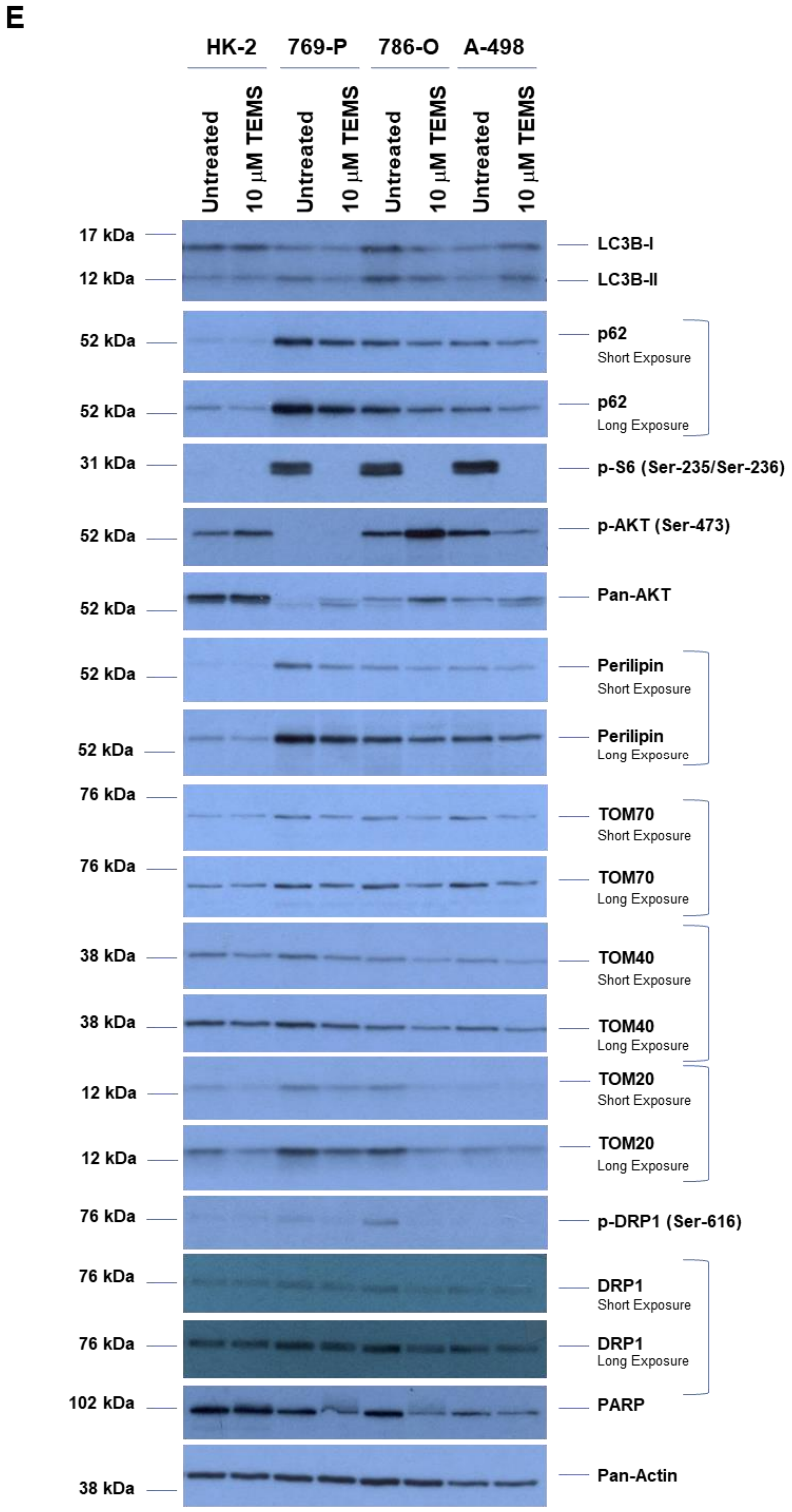

Figure 11: TEMS alters LD abundance and mitochondrial networks in malignant renal cell lines (*Continued on next page)

Figure 11: TEMS alters LD abundance and mitochondrial networks in malignant renal cell lines

(A) LD assessment of ccRCC cell lines and HK-2 cells in response to 24-hour treatment with 10 µM TEMS via immunofluorescence staining using LipidTOX. Three independent experiments were performed, and representative images are displayed as well as quantification of Total Area Covered/Cell and Total LDs/Cell (presented as normalized fold-change). (B) Real-time PCR analyses of genes involved in LD biogenesis and regulation in ccRCC cell lines and HK-2 cells in response to 24-hour treatment with 10 µM TEMS. Data shown is the composite of three independent experiments. (C) Assessment of total cholesterol levels in ccRCC cell lines and HK-2 cells in response to 72-hour treatment with 10 µM TEMS. The composite of three independent experiments is displayed. (D) Mitochondrial network assessment of ccRCC cell lines and HK-2 cells in response to 24-hour treatment with 10 µM TEMS via immunofluorescence staining of TOM20. Three independent experiments were performed, and representative images are displayed. (E) Western blot analyses of ccRCC cell lines and HK-2 cells treated for 72-hours with 10 µM TEMS with the indicated antibodies. Three independent experiments were performed, and representative blots are displayed.

response rates in clinical trials to mTOR inhibitors [94, 247]. In this regard, we assessed whether the combinatorial treatment of hydroxychloroquine (HCQ) with TEMS alters LD abundance in the normal and malignant renal cell lines. We first validated HCQ activity by treating cells (769-P, 786-O, A-498 and HK-2) with 25 µM HCQ alone or in combination with 10 µM TEMS and then detecting lipidated LC3B levels via western blot analyses. As shown in Fig 13A, we observed that LC3B-II and p62 protein levels were increased indicating that autophagic flux was effectively inhibited. Further, we noted a significant reduction in cellular viability in response to the combinatorial HCQ and TEMS treatment in the malignant cell lines but not in the normal HK-2 cells (Fig 13B). These findings suggest that the combinatorial treatment of autophagic and mTOR inhibition is more effective than the individual treatment regimens.

Interestingly, upon LipidTOX staining, we noted that the LDs appeared to be sequestered within an autophagosomal compartment (Fig 13C); indeed, HCQ mediates inhibition of the autophagosome-lysosome fusion event [246]. Altogether, these findings suggest that HCQ dominates TEMS-induced alterations in LD abundance potentially leading to diminished LD turnover.

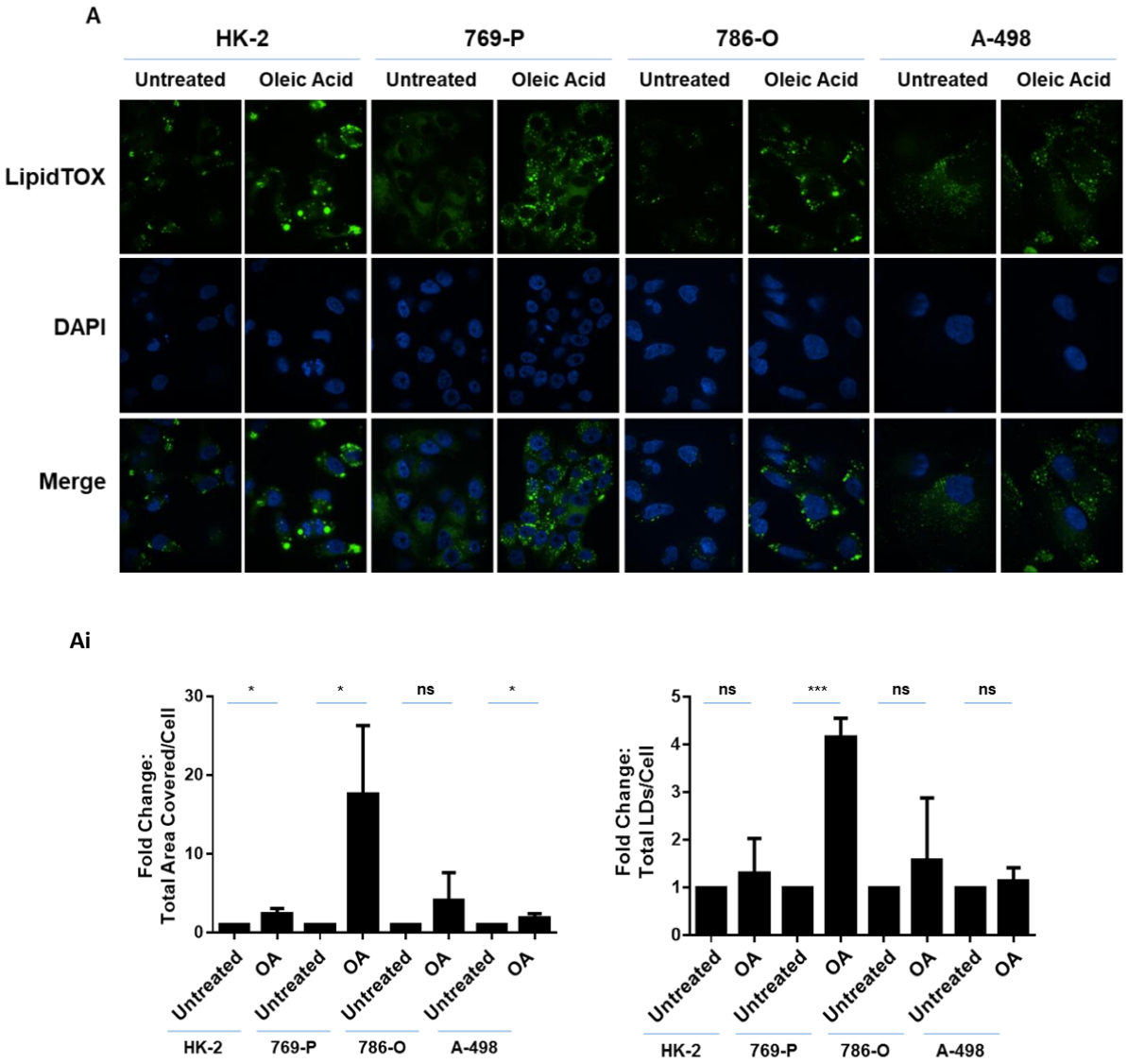

Figure 12: Oleic acid alters LD abundance and cellular viability of normal immortalized HK-2 cells (*Continued on next page)

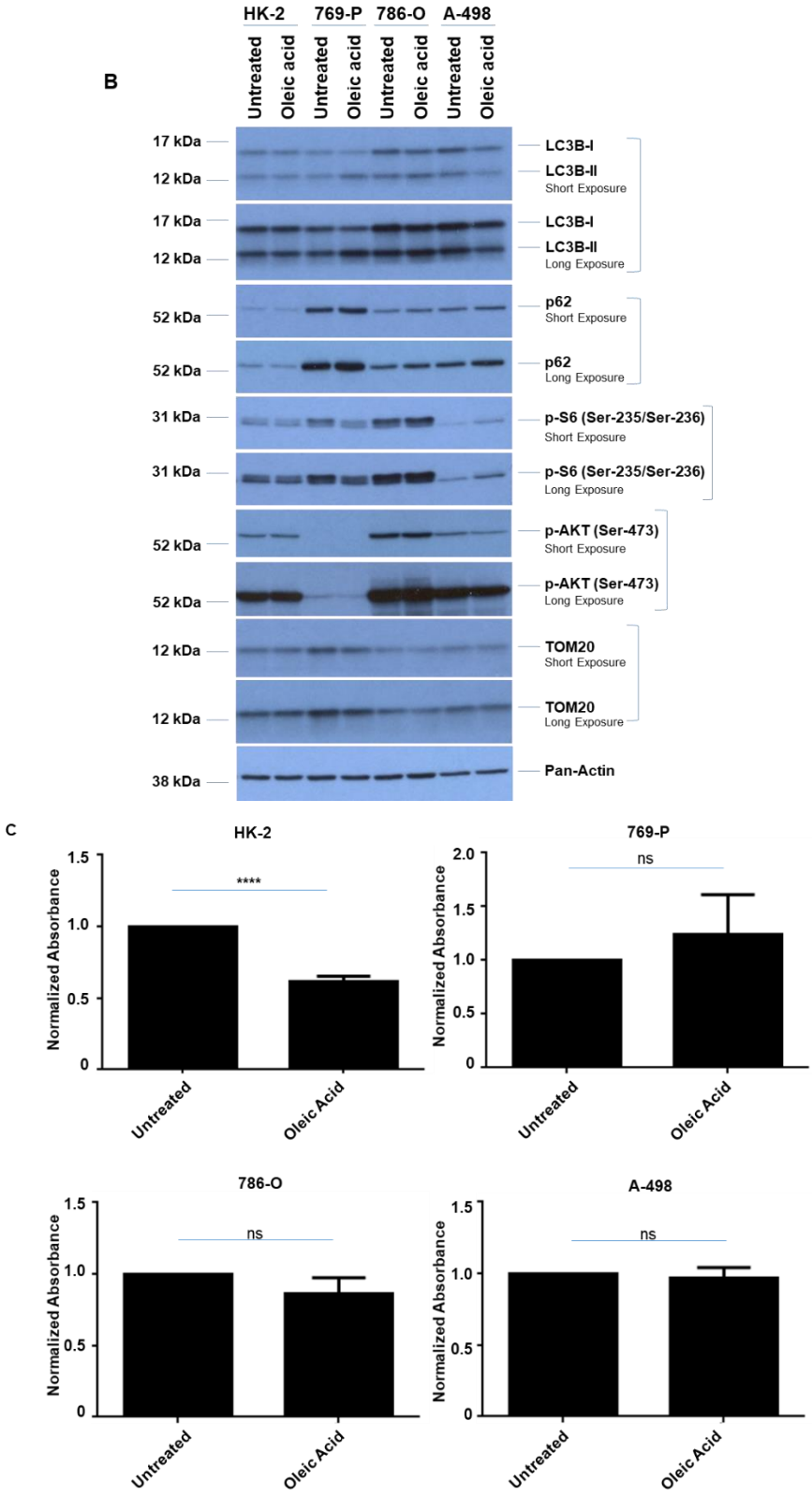

Figure 12: Oleic acid alters LD abundance and cellular viability of normal immortalized HK-2 cells (*Continued on next page)

Figure 12: Oleic acid alters LD abundance and cellular viability of normal immortalized HK-2 cells

(A) LD assessment of ccRCC cell lines and HK-2 cells in response to 24-hour treatment with 0.25 mM oleic acid via immunofluorescence staining using LipidTOX. Three independent experiments were performed, and representative images are displayed as well as quantification of Total Area Covered/Cell and Total LDs/Cell (presented as normalized Fold-Change). (B) Western blot analyses of ccRCC cell lines and HK-2 cells treated for 72 hours with 0.25 mM oleic acid with the indicated antibodies. Three independent experiments were performed, and representative blots are displayed. (C) Assessment of cellular viability in ccRCC cell lines and HK-2 cells at Day 3 in response to 0.25 mM oleic acid. The composite of three independent experiments is displayed.

LPA antagonizes TEMS-induced cellular alterations in a malignant renal cell line

LPA is a potent mitogenic lipid that mediates its extracellular effects via binding and activation of G-protein coupled receptors [248, 249]. Although LPA is elevated (along with autotaxin (ATX)) in kidney cancers [135, 250, 251] and can promote malignancy of patient-derived tumor cells [136], the role of this mitogenic lipid in chemotherapeutic resistance with the mTOR inhibitor, TEMS, has not yet been explored. First, we assessed whether ATX levels were altered by TEMS treatment in the malignant and normal renal cell line via real-time PCR. As shown in Fig 14A (top and bottom panels), we noted that ATX mRNA was significantly reduced following 24-hours of TEMS treatment and unexpectedly, these levels were significantly lower in ccRCC cells in comparison to HK-2 cells.

Since LPA mediates its effects via GPCRs to activate multiple intracellular signaling pathways including AKT/mTOR [248, 249], we next assessed whether addition of LPA alters the AKT/mTOR pathway in a malignant renal tumor cell line. The dose of LPA utilized (10 µM) was based on reported pathophysiological concentrations identified within tumors and in serum [269]. Specifically, we selected A-498 cells to investigate whether LPA modulates TEMS

responsiveness since these cells displayed marked changes in LDs and mitochondrial networks in addition to harboring the most genomic aberrations (out of the three malignant RCC lines studied herein). We cultured A-498 cells in both serum free media (SFM) and complete media to determine the effect of exogenously presented LPA in these cells. As shown in Fig 14B, we observed that the reduction in protein expression in phospho-S6, TOM20, TOM70, LC3B-II, and p62 under both culture conditions (consistently noted in SFM) were increased nearly to baseline control levels in the presence of LPA with TEMS. We next assessed whether LPA could antagonize TEMS-induced alterations in mitochondrial networks via immunofluorescence analyses (staining for TOM20 and TOM70) in A-498 cells (Fig 14C and 14D).

Since the SFM culture conditions led to shrunken cells, which resulted in challenges in assessing the mitochondrial networks, we focused this assessment using A-498 cells maintained in complete media. In control cells, we observed mitochondrial networking (staining for TOM20 and TOM70 were similar) close to the nuclear compartment of which most had a fragmented appearance (with a few extensions). LPA treatment alone did not modulate this mitochondrial network and TEMS treatment, itself, caused the mitochondrial network to become more extended (Fig 11D). Interestingly, the addition of LPA with TEMS cause a marked rearrangement of the mitochondrial networks to a tubular shortened form, which we quantified (bottom panels, Fig 14C and 14D). These findings suggest that LPA has the ability to partially antagonize the cellular response to TEMS. Since the contribution of LPA in modulating LD biogenesis remains unknown which may thus contribute to its pro-tumorigenic effect, we next investigated LD formation upon cellular treatment with LPA in A-498 cells using CM (Fig 15A) culture conditions. In control cells, we observed that 60-70% cells contained large LDs homogeneously dispersed in the cytoplasm with the remaining 30-40% of the cell population containing finer LDs. In the presence of LPA, nearly the entire cell population contained large LDs that were homogeneously dispersed in the cytoplasm. In contrast to TEMS-treated cells which contained finer LDs in 80% of the cell population, the combinatorial treatment of TEMS with LPA resulted in nearly the entire population

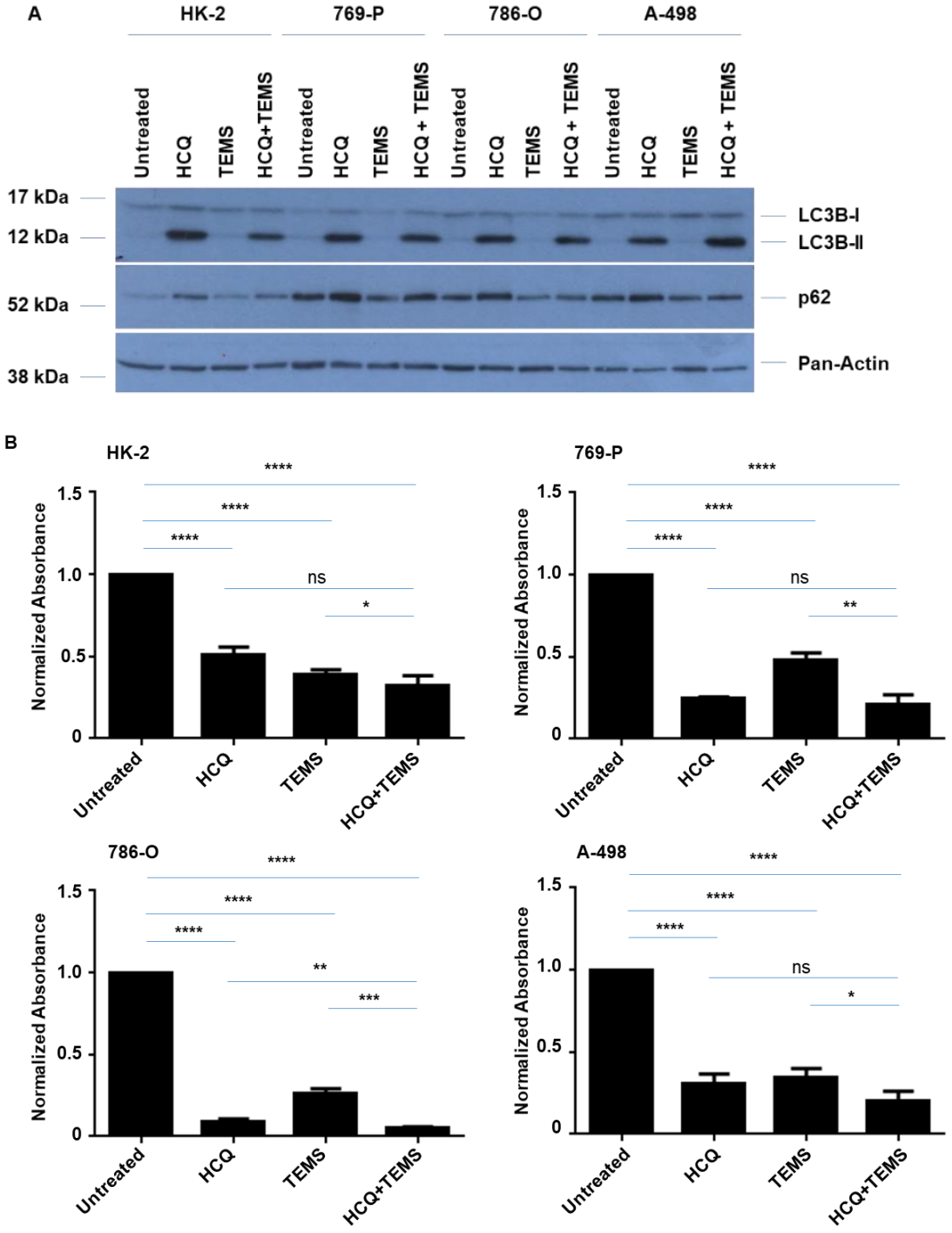

Figure 13: Hydroxychloroquine alters LDs and synergizes with TEMS to reduce cellular viability in renal cell lines (*Continued on next page)

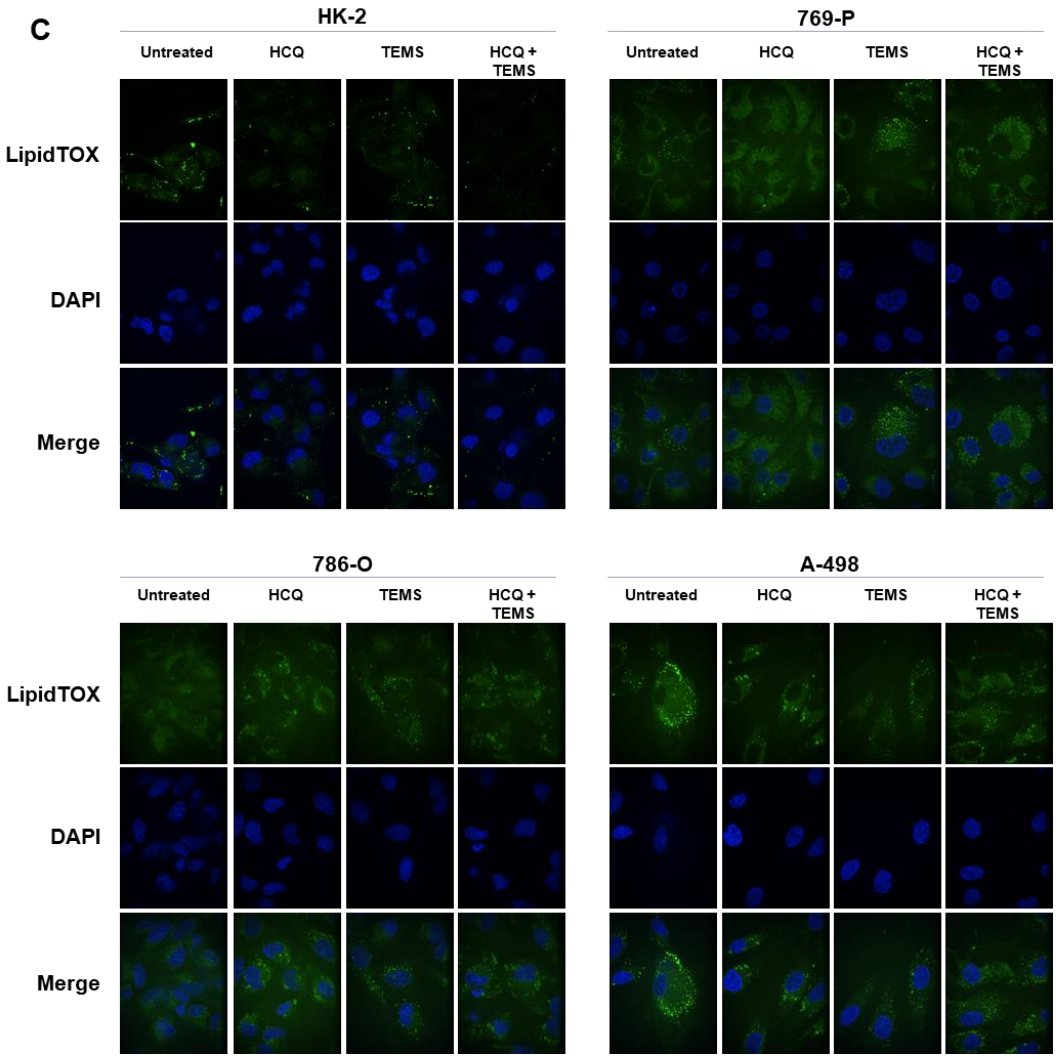

Figure 13: Hydroxychloroquine alters LDs and synergizes with TEMS to reduce cellular viability in renal cell lines

(A) Western blot analyses of ccRCC cell lines and HK-2 cells treated for 72 hours with 25µM HCQ and/or 10µM TEMS with the indicated antibodies. Three independent experiments were performed, and representative blots are displayed. (B) Assessment of cellular viability in ccRCC cell lines and HK-2 cells at Day 3 in response to 25 µM HCQ and/or 10 µM TEMS. The composite of three independent experiments is displayed. (C) LD assessment of ccRCC cell lines and HK-2 cells in response to 24-hour treatment with 25 µM HCQ and/or 10 µM TEMS via immunofluorescence staining using LipidTOX. Three independent experiments were performed, and representative images are displayed.

containing large LDs homogeneously distributed throughout the cell cytoplasm. These findings suggest that LPA may antagonize the LD-induced changes mediated by TEMS.

LPA increases LDs in renal cell lines and alters cellular viability of the normal immortalized HK-2 cells

The alterations in LDs mediated by LPA in A-498 cells were generalizable to other renal cell lines including two other malignant cell lines (769-P and 786-O cells) as well as the normal immortalized HK-2 cells (Fig 15B). Indeed, we uncovered that LPA caused the formation of larger LDs in all of these renal cell lines. To assess the mechanism underlying alterations in LD formation upon LPA treatment, we performed western blot analysis using lysates from HK-2 cells maintained in complete media culture conditions treated with LPA across a time course (30 minutes up to 24 hours). As shown in Fig 15C, we observed MAPK and S6 activation in the absence of phospho-AKT or phospho-GSK3 alterations as early as 30 minutes following LPA addition. These levels

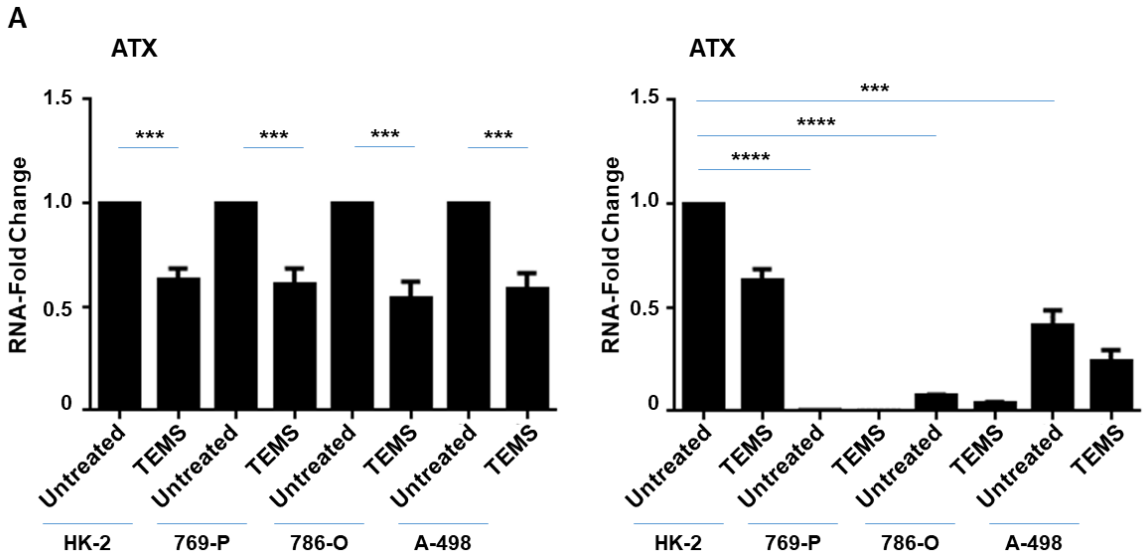

Figure 14: Lysophosphatidic acid antagonizes TEMS-induced mitochondrial alterations in a malignant renal cell line (*Continued on next page)

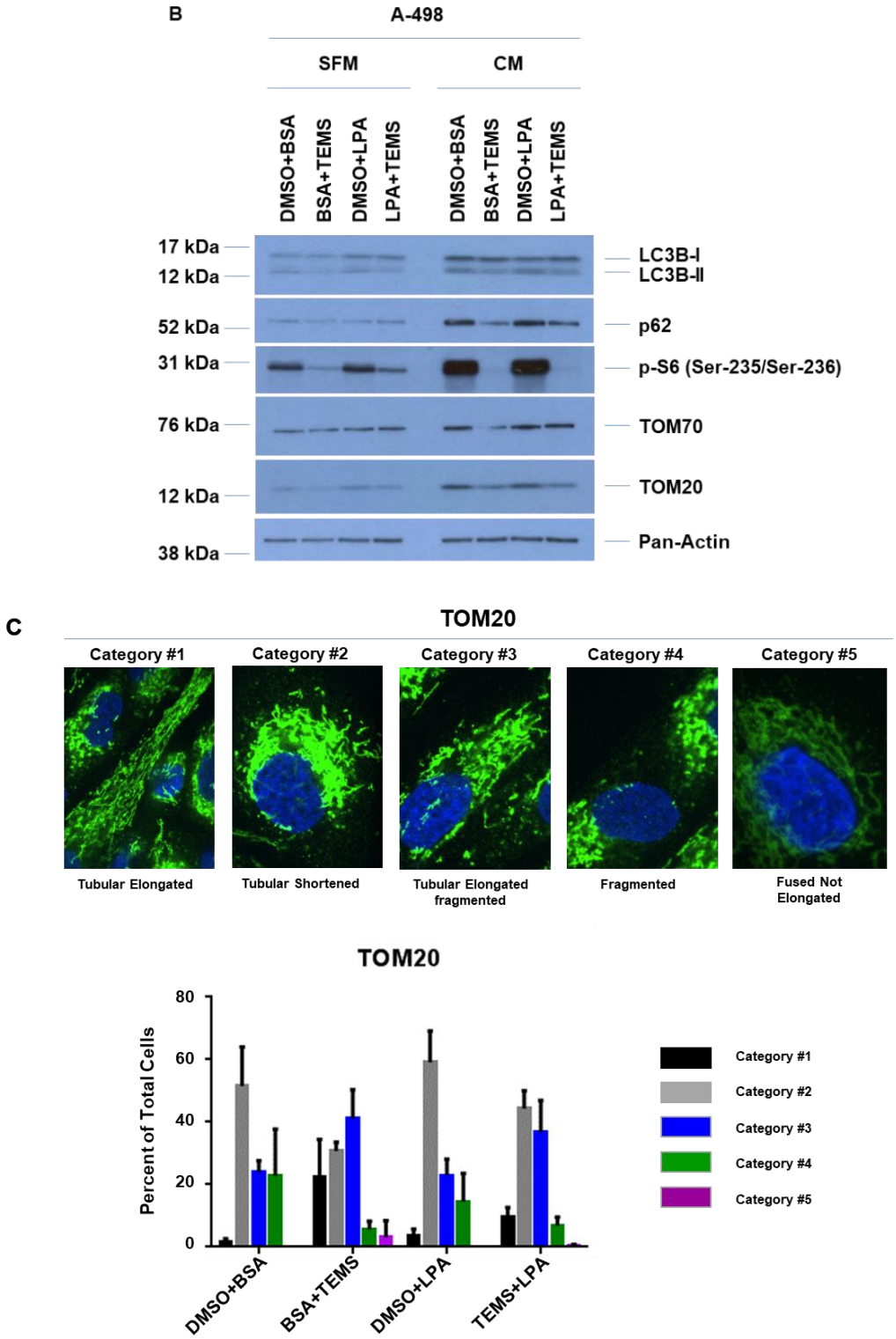

Figure 14: Lysophosphatidic acid antagonizes TEMS-induced mitochondrial alterations in a malignant renal cell line (*Continued on next page)

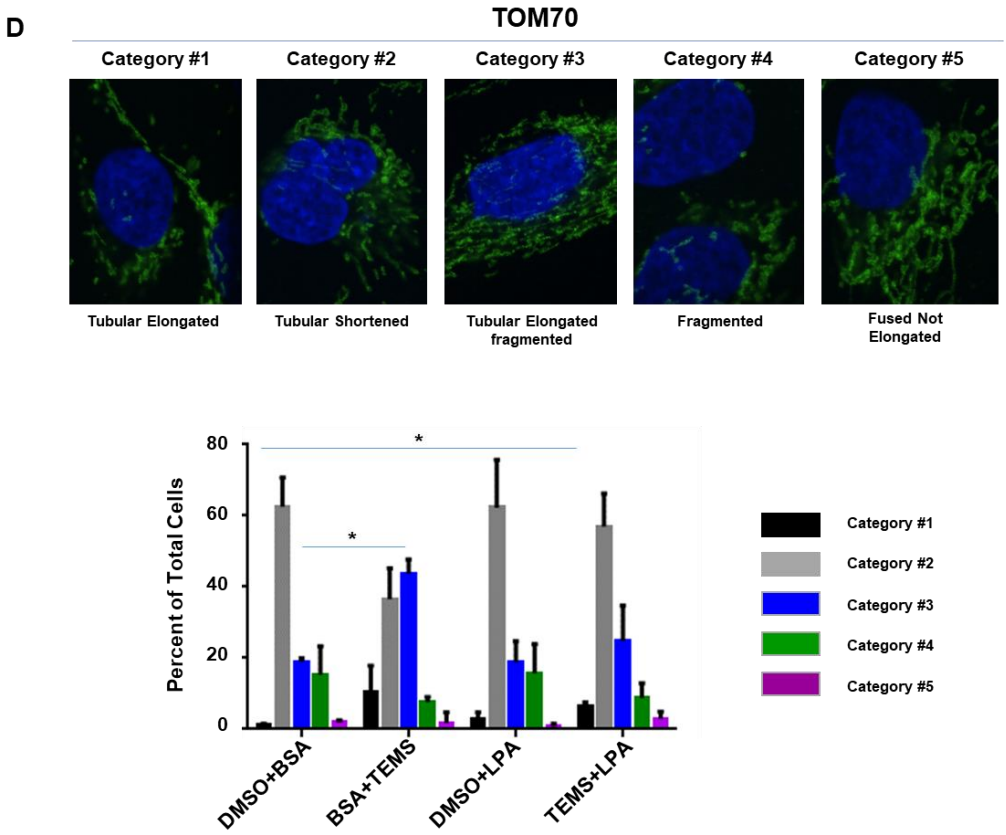

Figure 14: Lysophosphatidic acid antagonizes TEMS-induced mitochondrial alterations in a malignant renal cell line

(A) Real-time PCR analyses of ATX in ccRCC cell lines and HK-2 cells in response to 24-hour treatment with 10 µM TEMS. Data shown is the composite of three independent experiments. Left panel, normalized to each cell line (untreated). Right panel, normalized to HK-2 cells (untreated). (B) Western blot analyses of A-498 cells (grown in CM or SFM media conditions) treated with 10 µM TEMS in the absence or presence of 10 µM LPA with the indicated antibodies. Three independent experiments were performed, and representative blots are displayed. (C) Mitochondrial network assessment of A-498 cells in response to 24-hour treatment with 10 µM TEMS with/without 10 µM LPA via immunofluorescence staining of TOM20. Three independent experiments were performed, and representative images are displayed. (D) Mitochondrial network assessment of A-498 cells in response to 24-hour treatment with 10 µM TEMS with/without 10 µM LPA via immunofluorescence staining of TOM70. Three independent experiments were performed, and representative images are displayed.

appeared to be sustained up to 24 hours of LPA treatment. These changes were accompanied by elevated mRNA levels of DGAT2 in HK-2 cells (Fig 15D) suggesting that the increased LDs may be due to increased production and activity of enzymes in LD biogenesis.

As shown in Fig 15E, we observed a statistically significant increase in cell viability in HK-2 cells following LPA treatment for 3 days. These findings suggest that LPA can enhance the tumor-promoting effect of kidney cells in vitro. To determine whether LPA-induced activation of the MAPK and/or S6 signaling cascade contributed to the LPA-induced LD formation in HK-2 cells, we inhibited MAPK using 10 µM of U0126 and inhibited S6 as well as p70S6K using siRNA. We confirmed the effectiveness of these inhibitors via western blot analyses (Fig 16A at (30 minutes of LPA treatment) and Fig 16B).

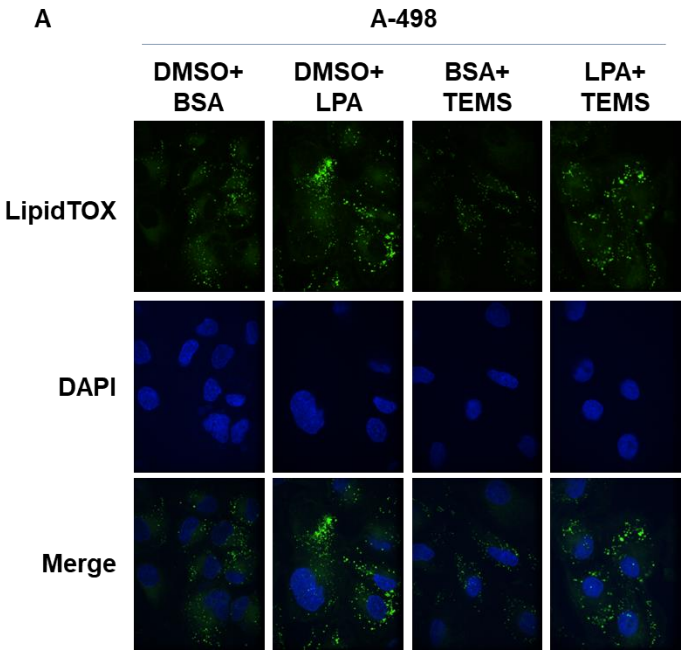

Figure 15: Lysophosphatidic acid increases LDs in a malignant renal cell line (*Continued on next page)

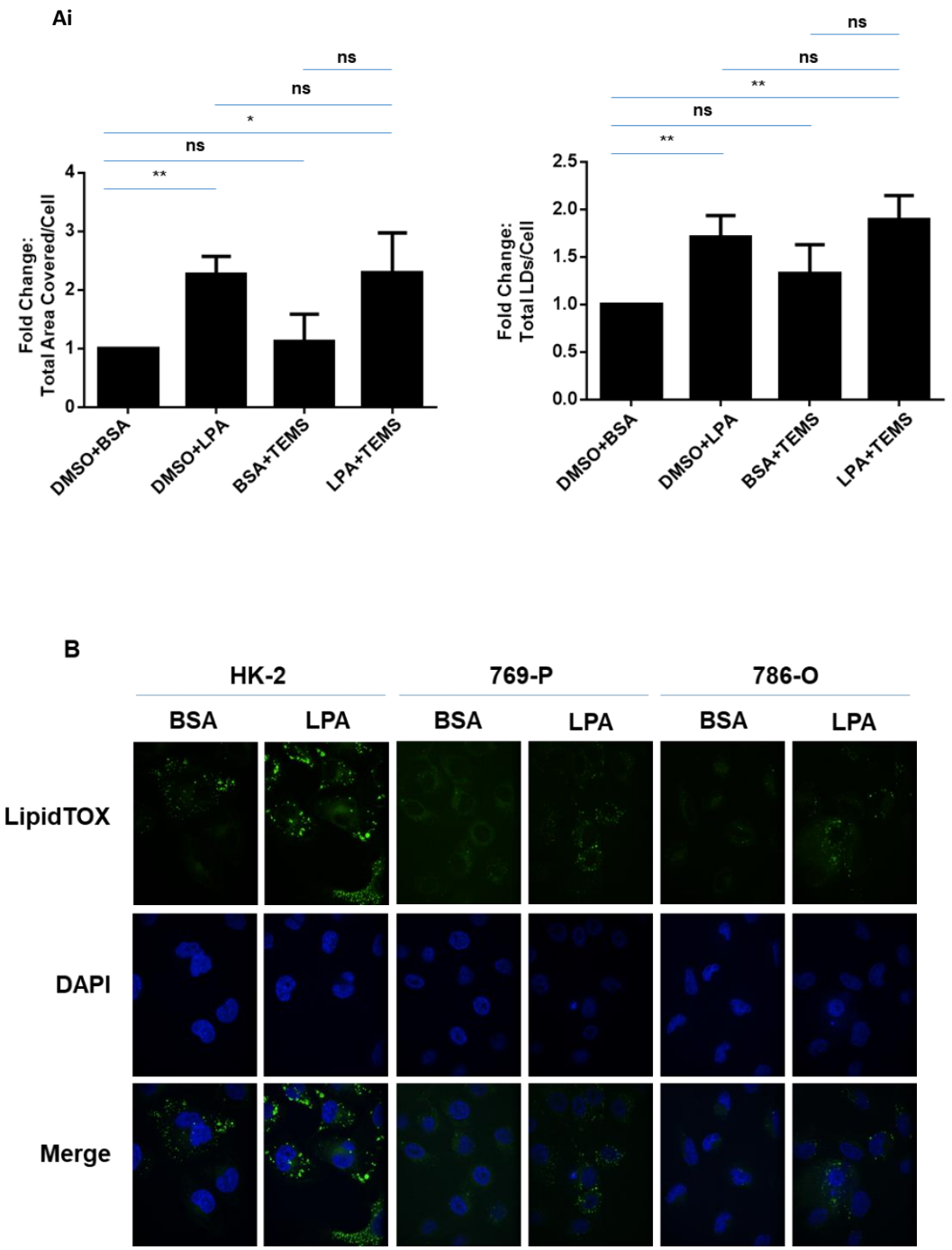

Figure 15: Lysophosphatidic acid increases LDs in a malignant renal cell line (*Continued on next page)

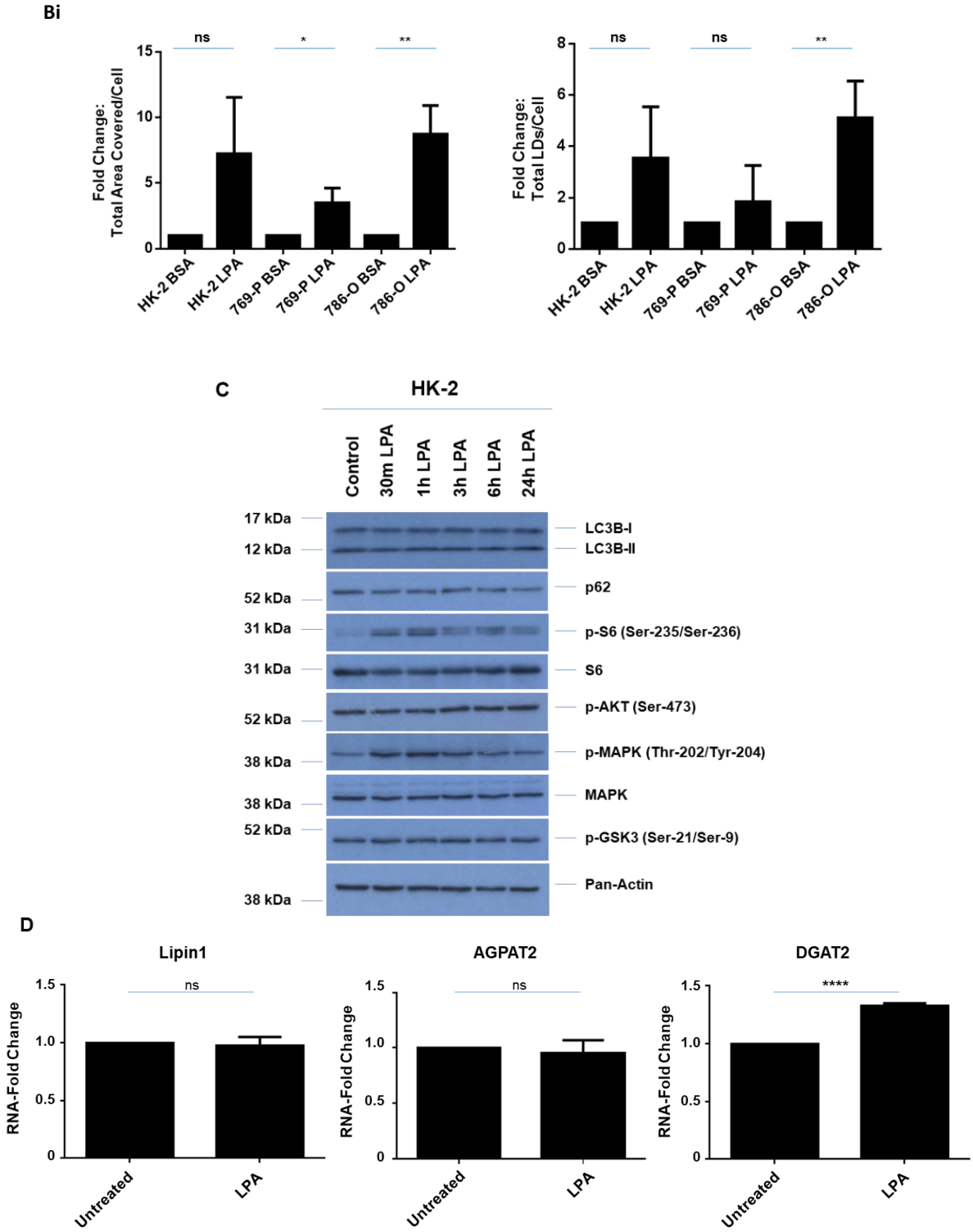

Figure 15: Lysophosphatidic acid increases LDs in a malignant renal cell line (*Continued on next page)

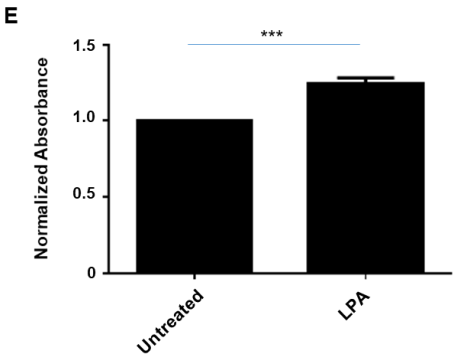

Figure 15: Lysophosphatidic acid increases LDs in a malignant renal cell line

(A) LD assessment of A-498 cells in response to 24-hour treatment with 10 µM LPA in the absence/presence of 10 µM TEMS via immunofluorescence staining using LipidTOX. Three independent experiments were performed, and representative images are displayed as well as quantification of Total Area Covered/Cell and Total LDs/Cell (presented as normalized Fold-Change). (B) LD assessment of ccRCC cell lines and HK-2 cells in response to 24-hour treatment with 10 µM LPA in the absence/presence of 10 µM TEMS via immunofluorescence staining using LipidTOX. Three independent experiments were performed, and representative images are displayed as well as quantification of Total Area Covered/Cell and Total LDs/Cell (presented as normalized Fold-Change). (C) Western blot analyses of HK-2 cells treated with 10 µM LPA across a time course (30 minutes to 24 hours) with the indicated antibodies. Three independent experiments were performed, and representative blots are displayed. (D) Real-time PCR analyses of genes involved in LD biogenesis and regulation in HK-2 cells in response to 24 -hour treatment with 10 µM LPA. Data shown is the composite of three independent experiments. (E) Cell viability in HK-2 cells was assessed following LPA treatment for 3 days. Data shown is the composite of three independent experiments.

We also analyzed LD abundance using LipidTOX (Fig 16C and 16D) and noted increased numbers of finer LDs associated following MAPK inhibition; however, the larger LDs induced by LPA alone were reduced following co-treatment with TEMS. Interestingly, we noticed that S6 protein reduction led to an increased number and size of LDs even in the absence of LPA, which

was further enhanced with addition of LPA. These findings suggest that LPA mediates alterations in LDs partially via MAPK activation and was independent of S6/p70S6K.

Discussion

Kidney tumors harbor a myriad of genetic alterations, including mutation or loss of the VHL gene, a tumor suppressor which is a common occurrence in >90% of clear cell kidney cancer cases

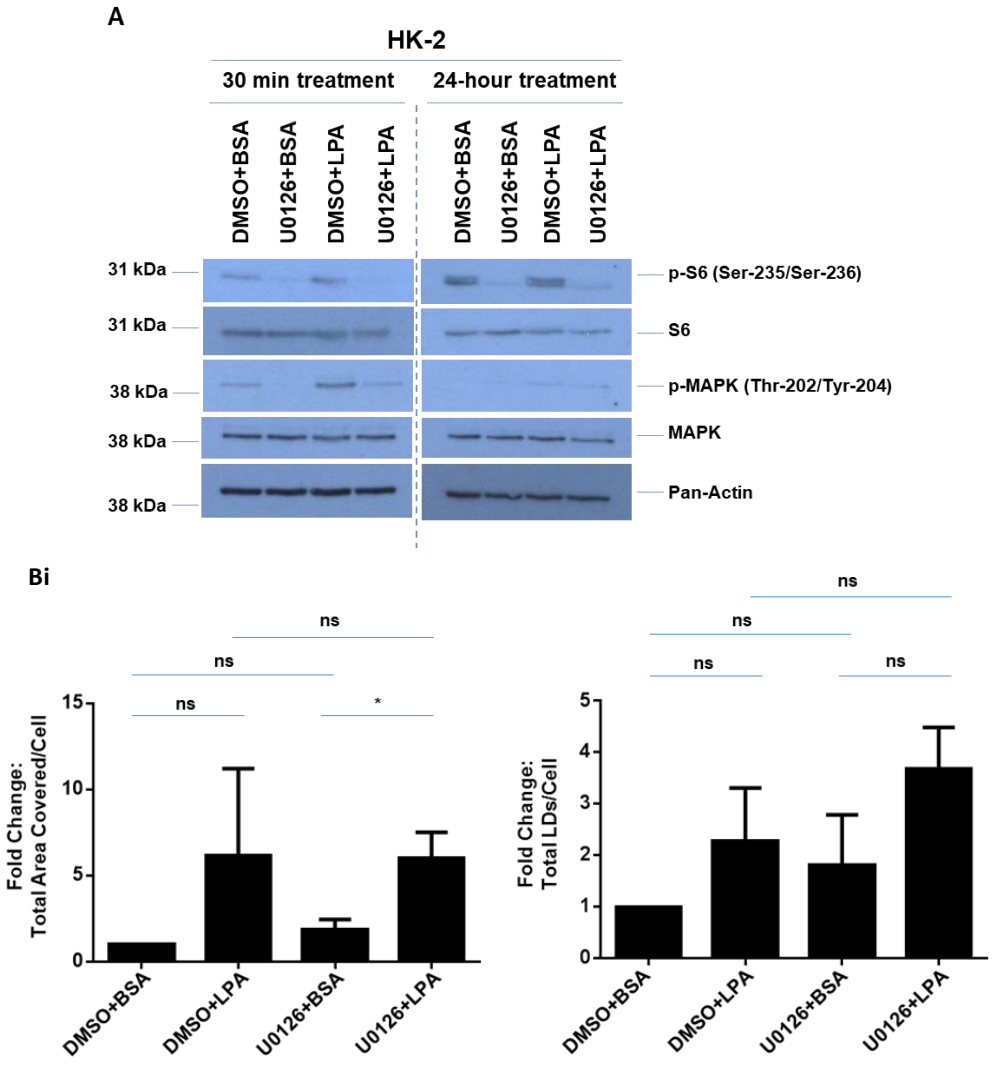

Figure 16: Lysophosphatidic acid alters LD abundance via the MAPK pathway and cellular viability in HK-2 cells (*Continued on next page)

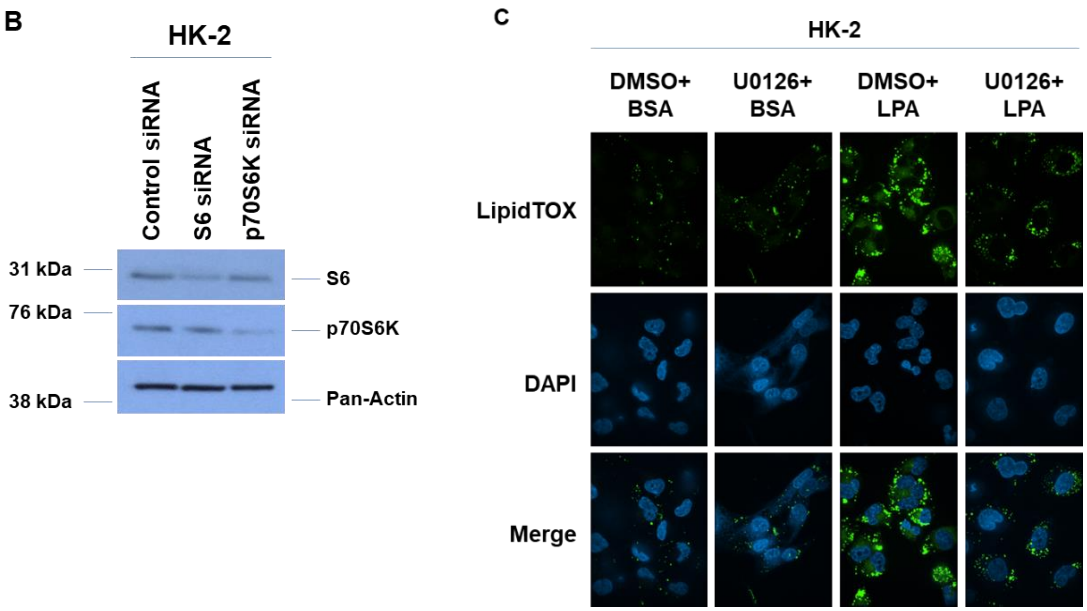

Figure 16: Lysophosphatidic acid alters LD abundance via the MAPK pathway and cellular viability in HK-2 cells

(A) Western blot analyses of HK-2 cells treated with 10 µM LPA in the absence of presence of U0126 for 30 minutes (left panels) or 24 hours (right panels) with the indicated antibodies. Three independent experiments were performed, and representative blots are displayed. (B) Western blot analyses of HK-2 cells treated with S6 or p70S6K siRNA with the indicated antibodies. Three independent experiments were performed, and representative blots are displayed. (C) LD assessment of HK-2 cells in response to 24-hour treatment with 10 µM LPA in the absence/presence of U0126 via immunofluorescence staining using LipidTOX. Three independent experiments were performed, and representative images are displayed as well as quantification of Total Area Covered/Cell and Total LDs/Cell (presented as normalized Fold-Change). (D) LD assessment of HK-2 cells in response to 24-hour treatment with 10 µM LPA in the absence/presence of siRNA targeting S6 or p70S6K via immunofluorescence staining using LipidTOX. Three independent experiments were performed, and representative images are displayed as well as quantification of Total Area Covered/Cell and Total LDs/Cell (presented as normalized Fold-Change).

[240, 254]. The ccRCC cell lines used for this study (769-P, 786-O and A-498) are associated with aberrations in VHL (TCGA data: Fig 9A). mTOR is a downstream effector of PI3K/AKT, a pathway that is well-established to be hyperactivated in ccRCC. Furthermore, several agents targeting mTOR have been developed including FDA-approved drugs such as everolimus and temsirolimus (TEMS). However, resistance to these agents has been a major contributor to suboptimal overall survival rates.

We now have identified that the mTOR inhibitor TEMS alters LD quality in both RCC and normal immortalized HK-2 cells, possibly to enhance lipid mobilization, which antagonizes cellular sensitivity to the treatment (Fig 10B and 11A). We also demonstrate that TEMS reduces expression of autophagy markers, which is accompanied by a decrease in expression of mitochondrial membrane proteins (TOM20, TOM40, and TOM70) and mitochondrial fused networks (Fig 11D and 11E). These cellular alterations may serve to relieve cellular stress induced by TEMS, thus promoting β-oxidation and fatty acid flux [244]. Since mitochondrial networks are highly dynamic in cancer and contribute to cancer cell proliferation, migration and altered cellular metabolism [270], it is notable that LDs have been found in close proximity to the ER and mitochondrial compartments to facilitate lipid exchange across these organelles [271]. Thus, the mitochondrial remodeling noted following TEMS treatment in the malignant renal cancer cell lines may thus promote increased energy usage to antagonize responsiveness to the mTOR inhibitor. Remodeling of mitochondria is likely to occur via regulated fission and fusion dynamics involving proteins present in the outer and inner mitochondrial membrane including MFN1/2, Opa1, and DRP1 [270, 271]. Furthermore, there is another report that describes that inhibitor of mTOR can lead to hyperfused and branched mitochondria, for which the underlying mechanism is thought to involve reduced expression of the mitochondrial fission process 1 (MTFP1) and DRP1 mitochondrial recruitment which may then regulate cellular survival [272].

With respect to increased LDs in response to exogenous supplementation with oleic acid, this cellular response appears to be similar to that with fatty acid synthase (FAS) inhibitors along

with mTOR inhibitors which results in synergistic toxicity in breast cancer cells. Moreover, the mTOR inhibitor can modulate expression of FASN, which implicates the PI3K/AKT/mTOR pathway in its regulation [273]. Thus, these pathways may be similarly involved with oleic acid exogenous supplementation in our renal cell lines.

Suboptimal or ineffective cellular responses to mTOR inhibitors may be due to activation of cytoprotective pathways including autophagic flux [94, 259, 260, 274]. We now demonstrate that the autophagic flux inhibitor (HCQ) alters LD abundance in both malignant and normal renal cell lines (Fig 13C). The accumulation of LDs with HCQ appeared to occur within autophagosomes, implicating inhibition of the lipophagy pathway and hence promoting synergistic cytotoxicity of HCQ and TEMS. Recently, combinatorial treatment of HCQ with the mTOR inhibitor Everolimus was assessed in a phase 1 clinical trial, which showed promise as an effective therapeutic regimen [259]. Additional pathways that may antagonize mTOR inhibitors include feedback activation of the AKT signaling pathway [275, 276]. Indeed, targeting components in these upstream PI3K-AKT cascade (as a multipronged approach) has been tested [275, 276].

Since ATX (which generates the potent LPA mitogen via its potent lyso-PLD activity) is elevated in ccRCC [250, 269] and has been shown to mediate chemotherapeutic resistance to sunitinib [135], this may be another mechanism underlying resistance to mTOR inhibitors. Indeed, we noted that LPA could antagonize the cellular responsiveness of malignant renal cell lines to TEMS, in terms of LDs and mitochondrial remodeling. LPA is linked to promotion of cell survival and proliferation. For example, treatment of a rat myocardial infarction model with LPA promoted cardiac hypertrophy which coincided with autophagic inhibition [277]; furthermore, this was noted to occur via activation of the AKT/mTOR pathway [277]. Activation of this pathway following LPA treatment is well established, as defined from other studies as well [278-280]. Therefore, in future work, we will investigate the combinatorial treatment of LPA with TEMS compared to LPA alone in RCC cell lines.

Furthermore, since we demonstrated that LPA with TEMS treatment resulted in a rearrangement of mitochondrial networks to a tubular shortened form, this could involve altered LDs and autophagic response, leading to altered mitochondrial structures. Indeed, it is reported that starvation can promote movement of autophagy-mediated LDs to mitochondria (needed for fatty acid β-oxidation, where fatty acids are made available via the action of neutral lipases), thus affecting fusion dynamics [244]. Such LDs are noted to be in close proximity to mitochondria to allow the uptake of fatty acids. Based on this report, we propose that LPA-induced LD formation and TEMS-induced autophagy may work coordinately to alter mitochondrial networks [244]. In our results, we show that LPA and TEMS combinatorial treatment results in a tubular shortened form of mitochondrial networking, suggesting that there may be resultant alterations in fatty acid movement and hence, altered β-oxidative activity. Thus, altered mitochondrial networking may result in restricted movement of fatty acids from lipid droplets to mitochondria (possibly, its expulsion from the cells thus a reduction in fatty acid metabolism would ensue) and hence, lipid accumulation in LDs.

Interestingly, we also noted that ATX mRNA levels were reduced with TEMS treatment (Fig 14A). Although we did not measure LPA content in the culture media following TEMS treatment, we propose that LPA may be elevated with mTOR inhibition and thus may downregulate ATX expression in a feedback loop [281]. In future work, the contribution of LDs to LPA-mediated drug resistance in renal cancers could be investigated. We propose that targeting the LPA/ATX axis may be a strategy to improve the sensitivity of ccRCC tumors to chemotherapeutic agents.

The molecular mechanisms involved in chemotherapeutic resistance in ccRCC are not well established. Herein, we identify that LPA can antagonize the cellular response of renal cancer cells to TEMS, specifically altering lipid droplets and mitochondrial networks. Moreover, in normal immortalized renal cells, we discovered that LPA induced LD formation in a MAPK-dependent manner, which was accompanied by changes in DGAT2 and cellular viability. Overall, this study

implicates the LPA signaling pathway as an important target for combating the resistance acquired by RCC cells towards molecular-based therapies.

Chapter 4

Global miRNA/Proteomic Analyses Identify miRNAs at 14q32 and 3p21, Which Contribute to Features of Chronic Iron-Exposed Fallopian Tube Epithelial Cells

Note to Reader

This chapter is a reorganized and reformatted version of the published article (Chhabra R, Rockfield S, Guergues J, Nadeau OW, Hill R, Stevens SM Jr, Nanjundan M. Sci Rep. 2021 Mar 18;11(1):6270. doi: 10.1038/s41598-021-85342-y). This has been reproduced here with an open access Creative Commons Attribution 4.0 international license from Springer nature (see **Appendix** for copyright permissions).

Contributions and Acknowledgements

I am deeply grateful to my mentor Dr. Meera Nanjundan for her valuable guidance and conceptualization of the study. We worked collaboratively on the experiments, methodology and data analysis. I am highly thankful to Dr. Stephanie Rockfield for her assistance with miRNA/Proteomics IPA analyses, figure preparation and generation of long-term FAC treated fallopian tube secretory epithelial cells with Dr. Meera Nanjundan. I gratefully acknowledge Dr. Jenny Guergues for bioinformatics [282] and statistical analysis; Robert Hill for performing miRNA array and analysis; Dr. Owen W. Nadeau for sample processing and Mass Spectrometric analysis, and Dr. Stanley M. Stevens Jr. for proteomics and IPA analysis.

Introduction

Iron is essential for maintenance of cellular homeostasis and organismal survival [283]. Iron participates in Fenton reactions, yielding reactive oxygen species (ROS) that are highly damaging to macromolecules including proteins, lipids, and nucleic acids [284]. Increased intracellular iron accumulation is a key feature of ferroptosis, a programmed cell death mechanism that is characterized by increased lipid peroxidation [285, 286]. In contrast, deregulated expression of mediators involved in iron metabolism (i.e., Transferrin Receptor) leads to increased intracellular labile iron that promotes increased cellular proliferative capacity and cancer pathogenesis [171, 287]. In our prior report, in response to supraphysiological levels of NTBI (non-transferrin bound iron, presented as ferric ammonium citrate (FAC)), we performed a proteomics screen utilizing reverse phase protein array (RPPA) to identify global proteomic alterations, which confirmed RAS- and MAPK-dependency in short-term iron-exposed ovarian cancer cell lines[239, 288].

High-grade serous ovarian cancer is the deadliest gynecological malignancy in women for which the fallopian tube secretory epithelial cell (FTSEC) type is now considered an established precursor cell [289]. Our recent findings have identified that chronic iron exposure contributes to upregulated EVI1 (a transcriptional regulator, amplified at 3q26.2) and TERT expression, accompanied by increased cell numbers and migration in FTSECs [19]. However, to our knowledge, an assessment of global alterations induced by this mode of iron exposure in FTSECs has yet to be performed and is thus necessary to identify comprehensive cellular changes for which improved treatment regimens may be designed. Furthermore, since miRNAs elicit both oncogenic and tumor suppressive functions by altering the expression of multiple protein targets, a global miRNA screening approach in chronic iron exposed FTSECs is deemed to be an additional highly valuable experimental approach.

Herein, we utilized a multiomics approach using the GeneChip miRNA 4.1 microarray and mass spectrometry-based proteomics to identify deregulated miRNAs and protein targets, respectively, in chronic iron exposed and transformed FTSECs. We applied stringent statistical

approaches to identify the most significantly deregulated hits and integrated both of these analyses using Ingenuity Pathway Analysis [282]. A majority of the identified downregulated miRNAs are located at the 14q32 locus, a highly aberrant chromosomal region in multiple tumor types [224, 290, 291]. Since 14q32 miRNAs can be regulated by differentially methylated promoter regions (i.e., DLK1-DMR, IG-DMR and MEG3-DMR [292-295]), we investigated whether FAC could epigenetically alter the methylation and acetylation status in genomic regions potentially involved in miRNA regulation. Inhibition of methyltransferases and histone deacetylases using 5-Azacytidine (AZA) and Suberoylanilide Hydroxamic Acid (SAHA), respectively, resulted in rescuing the expression of miR-432-5p, miR-127-3p, with minimal effects on miR-138-5p expression. IPA analyses identified notable proteomic targets of key miRNAs including ALDH1A2 (for miR-138-5p target) and PAX8 (for miR-432-5p, miR-127-3p, and miR-138-5p). Although these targets could not be validated experimentally, TERT RNA was identified to be partially regulated by miR-138-5p. From a functional perspective, overexpression of these miRNAs reversed cell survival induced by chronic iron exposure in FT194 cells.

Materials and methods

Experimental design and statistical rationale

Understanding the mechanism underlying transformation of FTSECs requires the use of an *in vitro* model system, such as immortalized FT194 cells, generated via SV40 LTAg and hTERT stable expression, characterized by p53 inactivation, as described previously [296]. We previously reported the generation of oncogenically transformed FT194 cells; briefly, these were produced by stable overexpression of c-Myc^{T58A}, H-Ras^{V12A}, and SV40 LTAg [19]. In addition, we described the generation of a transformed-like FTSEC cell line following chronic iron overload (with 250 nM Ferric Ammonium Citrate (FAC) for > 60 days in culture) which was characterized by alterations in oncogene expression (based on a focused approach) and survivability[19]. Briefly, the FTSECs

were seeded at 500 cells/well in 6 well plates and subsequently treated with a range of FAC doses (0, 25 nM, 250 nM, 2.5 µM, 25 µM, or 250 µM), as previously described[19]. Cell growth was continually monitored, and cultures propagated in FAC-containing media (with media replenishments every 4 days). Cells treated with 250 nM FAC elicited greater cell numbers (compared with Untreated cells or other iron doses) and was therefore selected for expansion and experimentation along with Untreated control cells which were maintained concurrently. Our prior attempts with mM FAC doses similar to those previously reported [189, 297] was highly toxic and therefore not further pursued.

To further characterize global changes in an unbiased manner, we prepared experimental samples from Untreated [36], FAC-treated (FAC), control virus (CV), and oncogenic cocktail virus (OCV) infected FT194 cells; these were utilized for both noncoding RNA microarray and proteomic analyses. Specifically, the proteomic study utilized flash frozen cell pellets (UNT/FAC or CV/OCV) of ~500,000 cells per replicate, based on the protein extraction yield obtained by the S-trap sample processing approach previously reported by us [298, 299]. For LFQ-based quantitation of protein expression, 5 replicates (from the same “batch” of UNT/FAC or CV/OCV cells) per group were utilized based on the expected quantitation precision of our approach obtained for cell lines [299]. For a statistical power of 90% with alpha=0.05 and n=5 replicates per group, an effect size of 2.348 would be needed based on using a two-tailed, unpaired t-test. The average coefficient of variation for each group was calculated for LFQ intensities obtained experimentally and then used to determine the fold change to achieve this effect size, which was then compared to the z-score cutoff used in this study (|z-score|>1). A conventional FDR correction approach (e.g., Benjamini-Hochberg) was not employed given the tendency for decreased sensitivity; however, a combined filtering approach that considers variance and fold change was used (Welch’s t-test $p < 0.05$ and |z-score|>1), which has been shown to adequately control FDR while maintaining sensitivity [300].

For the miRNA analyses, total RNA was isolated from 3 replicates (from the same “batch” of UNT/FAC or CV/OCV cells), quantified by Nanodrop, and then analyzed using the GeneChip 4.1 Array (#902409, ThermoFisher Scientific, Waltham, MA, USA). The miRNA array contained 30,424 mature miRNAs, of which 2,578 were of human origin. To obtain a statistically relevant dataset of differentially expressed miRNA targets, an approach was applied of a >2-fold change cutoff along with an FDR-adjusted p-value <0.05 top miRNA targets were selected to generate volcano plots and Venn diagrams.

Cell culture and treatments

Human immortalized FTSECs (FT194) were provided by Dr. Ronald Drapkin (Department of Obstetrics and Gynecology, University of Pennsylvania, Philadelphia, PA, USA)[296]. These cells were immortalized by SV40 LTAg and hTERT, and were maintained in DMEM:F12 (1:1, #15–090-CV, Corning Incorporated, Corning, NY, USA) with phenol red, supplemented with 2% Ultroser G Serum Substitute (#67042, Crescent Chemical Company, Islandia, NY, USA) and 1% penicillin-streptomycin, as previously described [19]. Long-term FAC treated (annotated FAC or F) and the corresponding Untreated FT194 (annotated UNT or U) cells were maintained in phenol red-free DMEM:F12 (1:1, #21041-025, ThermoFisher, Waltham, MA, USA) with 8% charcoal dextran-stripped FBS and 1% penicillin/streptomycin (denoted as -PR media), as previously described[19]. Cells were incubated at 37°C in a 5% CO_2 environment. Cell lines were tested for mycoplasma and confirmed to be negative. Chronic iron-treated (250 nM for greater than 60 days) immortalized FT194 cells were maintained in 250 nM ferric ammonium citrate (FAC) (day 111 to 170 and p=30-52) [19]. Oncogenic cocktail virus infected (OCV) and control virus infected FT194 cells (CV) cells generated by retroviral transduction of c-Myc^{T58A}, H-Ras^{V12A}, and SV40 LTAg cDNAs were generated previously[19] and were used herein at passages of RV+11.

FAC (#I72-500, Fisher Scientific, Pittsburgh, PA, USA) stock was prepared in PBS and used at a final concentration of 250 nM [19]. Stocks for the DNMT1 inhibitor, 5- Azacytidine (AZA,

#S1782, Selleck Chemicals, Houston, TX) and the HDAC inhibitor, SAHA (#S1047, Selleck Chemicals, Houston, TX) were prepared in dimethylsulfoxide (DMSO). Both drugs were utilized at 0.5 µM, 1 µM, 5 µM, 10 µM, 25 µM and 50 µM final concentrations, which were based on a literature review of the most appropriate doses[5, 301-303]. A dose range of 0.5 µM to 10 µM of AZA and 0.5 µM to 50 µM of SAHA (as mentioned previously [5, 301-303]) were initially tested individually for 24 hours in both Untreated and FAC-exposed FT194 cells (results not shown); the optimal dose was then selected for further experiments. Following optimization studies, 1 µM AZA and 50 µM SAHA doses were selected for use.

Mass spectrometry-based proteomic analyses

Suspension trap (S-trap) sample processing of each experimental group (U, F, CV, OCV) was performed as previously described [299] using an approximate 500,000 cell count for each group (n=5 per group). Tryptic peptide concentrations were normalized based on the original protein concentration measurements determined by a Pierce 600 nm protein assay (Thermo Fisher Scientific). LC-MS/MS analysis of the cell lysate digests was performed using a hybrid quadrupole-Orbitrap instrument (Q Exactive Plus, Thermo Fisher Scientific) coupled to an Ultimate 3000 UPLC system (Thermo Fisher Scientific). Digested samples were first concentrated on a 2 cm x 75 µm ID PepMap C18 trap column (Thermo Fisher Scientific) followed by separation on a 55°C-heated, 75 cm x 75 µm ID C18 PepMap column (Thermo Fisher Scientific). A 120 min gradient from 2-28% B, where B was 0.1% formic acid in 80% acetonitrile:20% water was used to separate peptides, as described in our prior publication[298]. An additional ramp to 40% B over 15 min followed by a wash at 95% B was implemented. For mass spectrometric analysis, data-dependent acquisition [9] with a top-10 method was utilized. The full MS spectra were acquired in the m/z range of 375-1200 at 70,000 resolutions followed by MS/MS scans at 17,500 resolutions. AGC target counts of 1E6 and 5E4 with maximum IT values of 20 and 50 ms for MS1 and MS2 were utilized, respectively. A normalized collision energy of 28 and isolation window of

1.6 m/z was employed with charge state exclusion set for unassigned, 1, 6-8, and >8. Dynamic exclusion was set for 20 sec with isotope exclusion enabled and the peptide match setting to preferred. All details of the mass spectrometry data acquisition and LC parameters are embedded in the raw data files, which have been deposited to the Proteome Xchange Consortium via the PRIDE [304] partner repository with the dataset identifier PXD018416.

MaxQuant (version 1.6.6.0) was used to search raw files against the Uniprot protein database for *Homo sapiens* (version UP000005640, 71607 entries). Search parameters included the variable modifications of N-terminal protein acetylation and methionine oxidation as well as the constant modification of cysteine by carbamidomethylation. An additional database of known contaminants provided with MaxQuant was utilized where the first search tolerance was set to 20 ppm followed by a main search tolerance of 4.5 ppm, as described in our earlier work[298, 299]. Furthermore, a search strategy using reversed sequences in a decoy database was employed to achieve protein and peptide FDR values of less than 1%[298, 299]. Label free quantification (LFQ)-based quantitation was enabled, with a minimum ratio count of 1, and the “match-between-runs” feature using default settings was employed to increase proteomic identification, as described in our earlier work [298, 299].

The resulting Protein-Groups text file generated by MaxQuant was edited by removing the reverse and contaminant sequences as well as proteins only identified by modification (similarly described in our earlier work) [298]. The file was then uploaded into Perseus (version 1.6.1.1) [298] twice for separate analysis of FAC-treated FT194 cells (F) relative to Untreated FT194 cells (U), and oncogenic cocktail virus infected FT194 cells (OCV) relative to control virus infected cells (CV). Each file was then analyzed whereby LFQ values were $\log_2$-transformed and proteins were removed that had missing values in more than just 2 out of the 5 replicates, similarly described in our earlier work[298]. The imputation function was utilized where missing values were replaced using width parameters of 0.3 for both and downshift parameters set to 1.8 and 1.75 for F vs. U and OCV vs. CV, respectively [298]. The average ratio of treatment over control was then

calculated in Excel along with a Welch's t-test (p-value < 0.05) and z-score (z-value > 1), similarly described in our earlier work [298]. These filtered lists containing protein identification and average ratio of each comparison were then uploaded to Ingenuity Pathway Analysis [282] in order to determine upstream regulator overlap and activity, over-represented canonical pathways, as well as other biological and disease functions (p < 0.05, Fisher's exact test), similarly described in our earlier work [298]. Additionally, differentially expressed miRNAs (described below) were uploaded into IPA and paired against the proteins identified from proteomic analysis, which are known (experimentally determined) or predicted (moderate or high confidence) downstream targets of the miRNAs, through the miRNA Target Filter function. Paired miRNA-protein targets were filtered to include those in which the observed miRNA up- or down-regulation resulted in down- or up-regulation of the protein target, respectively. The corresponding network was reconstructed in IPA to demonstrate the potential regulatory role of each selected miRNA on the protein expression profile obtained.

MicroRNA microarray

Total RNA was isolated from FT194 cells maintained in 250 nM FAC for 104 days (p=31) along with parental untreated FT194 cell line cultured simultaneously. In addition, total RNA was isolated from CV and OCV-infected FT194 cell lines (p=RV+12). RNA isolation was performed using the RNeasy Kit (#74106, QIAGEN, Valencia, CA, USA) according to manufacturer's instructions. Total RNA was quantified by Nanodrop and then analyzed using the GeneChip 4.1 Array (#902409, ThermoFisher Scientific, Waltham, MA, USA). The miRNA array contained 30,424 mature miRNAs, of which 2,578 were of human origin. To obtain a statistically relevant dataset of differentially expressed miRNA targets, an approach was applied of a >2-fold change cutoff along with a non-adjusted p-value <0.05 top miRNA targets were selected to generate volcano plots and Venn diagrams. miRNA array and proteomics data were combined in Ingenuity

Pathway Analysis [282] to associate miRNAs with top proteomic hits. Thirty-five miRNAs had 28 protein targets identified in the proteomic screen in FAC-treated (compared to Untreated) FT194 cell samples whereas 45 miRNAs had 74 protein targets identified in the proteomic screen in transformed OCV (compared to control virus transfected), both with a cutoff of >4-fold change to focus on the "top hits" of biological relevance. The experimental strategy is depicted in Fig. 1.

MicroRNA transfection

Untreated and FAC-treated FT194 cells were seeded at 250,000 cells (for protein isolation) in 6-well plates and 500,000 cells (for miRNA isolation) in 60 mm dishes. After overnight cell adherence, cells were transfected with 200 pmol control mimic (mirVana miRNA mimic Negative control 1, #4464059, Life Technologies, Grand Island, NY) or hsa-miR-138-5p (mirVana miRNA mimic, Assay ID# MC11727, Life Technologies, Grand Island, NY), hsa-miR-432-5p (mirVana miRNA mimic, Assay ID# MC10941, Life Technologies, Grand Island, NY), or hsa-miR-127-3p (mirVana miRNA mimic,Assay ID# MH10400, Life Technologies, Grand Island, NY) using Fugene HD (Promega, Madison, MI). Twenty-four hours post-transfection, cells were recovered and at 48 hours post-transfection, protein lysates, total RNA, or miRNA were then collected.

MicroRNA isolation for real-time PCR

miRNA was isolated using the *mir*Vana Isolation Kit (#AM1561, ThermoFisher Scientific, Waltham, MA, USA) following the manufacturer's protocol. miRNA was quantified by Nanodrop, and real-time PCR was performed using the TaqMan RNA-to-CT 1-Step Kit (#4392938, ThermoFisher Scientific, Waltham, MA, USA) with the following primer/probe sets: miR-432-5p (assay ID #: 001026), miR-127-3p (assay ID #: 000452), and miR-138-5p (assay ID #: 002284). The fold-change in miRNA expression was calculated using the $2^{-\Delta\Delta CT}$ correlative method, in which

C_T values were normalized to the RNU6B control (assay ID #: 001093, ThermoFisher Scientific, Waltham, MA, USA).

Protein isolation, SDS-PAGE, and western blotting

Cell lysates were collected for separation on appropriate percentage SDS-PAGE gels and protein expression analyzed via western blotting using previously published methods[234, 237]. Western blotting was performed using the following Cell Signaling Technology (Danvers, MA, USA) primary antibodies: DNMT1 rabbit monoclonal (1:1000, #5032), EVI1 rabbit monoclonal (1:500, #2593), Pan-Actin rabbit polyclonal (1:1000, #4968), Acetyl Histone H3 (Lys9/Lys14) rabbit polyclonal (1:1000, #9677), ALDH1A2 rabbit polyclonal (1:1000, #83805), and CRYAB rabbit monoclonal (1:1000, #45844). ITGA2 rabbit monoclonal (1:1000, MA535243) was obtained from ThermoFisher Scientific (Waltham, MA, USA). PAX8 rabbit polyclonal antibody (1:1000, #10336-1-AP) was obtained from Proteintech (Rosemont, IL, USA). The western blots were developed at multiple exposures onto film, which were all scanned using a Flatbed Scanner (HP Scanjet 5590) and inserted as images into powerpoint, without any manipulation (no contrast alterations) apart from cropping to within 6 band widths above and below the band of interest. Each developed blot (representing a specific antibody application) is presented in one powerpoint slide with space in-between, delineating different antibody applications to the same blot. The EVI1 and Pan-Actin antibodies were previously optimized in our laboratory [305]. The use of DNMT1[306], Acetyl Histone H3[307], and PAX8[308] were utilized based on prior publications and ALDH1A2 was utilized based on data available by Cell Signaling Technology.

EVI1 siRNA in FT194 cells

siRNA transfection in FT194 cells was performed as previously reported[19]. Briefly, cells were seeded in six-well plates at a density of 500,000 cells/well or at 1,000,000 cells/dish in 60 mm

dishes followed by overnight adherence. ON-Target Plus non-targeting control siRNA (#D-001810-10-20, Dharmacon (Lafayette, CO, USA)) or EVI1-targeting siRNA (siB, custom designed as described previously)[19, 305, 309] were transfected into cells using RNAiMax (#13778-075, Invitrogen, Carlsbad, CA, USA). Cells were recovered 24 hours post transfection; cell lysates and miRNAs were collected at 48 hours post-transfection for western blotting and real-time PCR, respectively.

Bioinformatics of EVI1 binding site in miR-138-5p-1 promoter region

The UCSC Genome Browser (www.genome.ucsc.edu, Human Dec. 2013 (GRCh38/hg38 Assembly) was utilized to obtain the genomic sequence (5000bp upstream) of the promoter region for miR-138-5p-1 (located at 3p21.32) and for miR-138-5p-2 (located at 16q13); miRBase was utilized to obtain the pre-miRNA sequence for these miRNAs. Previous research identified the DNA sequences that EVI1 binds to; EVI1 N-terminus binds to the sequence GACAAGATA[310, 311] while the C-terminus binds to the sequence GAAGATGAG[312, 313]. Overall, the consensus EVI1 binding sequence is TGACAAGATAA [310, 313]. Thus, these reported EVI1 binding sequences were aligned with the promoter regions for both miR-138-5p-1 and miR-138-5p-2 using the Genomatix software suite (version 3.11, http://www.genomatix.de/cgi-bin/dialign/dialign.pl).

Statistical analyses

Data from real-time PCR, densitometry, and cell counting studies were analyzed using the Graphpad Prism software, version 6.04 (La Jolla, CA, USA). Error bars represent the mean ± SD and *p*-values were determined through the non-parametric Student's *t*-test for which "ns" represents non-significant values, * indicates $p \leq 0.05$, ** indicates $p \leq 0.01$, *** indicates $p \leq$

0.001, and **** indicates $p \leq 0.0001$. Fold changes and percent reductions were calculated from the average of at least three independent experiments.

Results

miRNA and proteomic profiling of chronic FAC-treated and oncogenically transformed FTSECs

Elucidating molecular mechanisms involved in initiation and progression of ovarian cancer is essential towards developing novel therapeutic strategies. We have previously identified a subset of genes (including EVI1, located at 3q26.2 in HGSOC) that were altered following long-term iron exposure in FTSECs [19]. However, to acquire a comprehensive understanding of the iron-induced alterations, a global mass spectrometry-based proteomics analysis was performed in FAC-exposed and Untreated FT194 cells. We then compared the resultant proteomic alterations to OCV- and CV-infected FT194 cells, as generated previously [19]. For FAC-exposed FT194 cells compared to Untreated cells, 4,402 total proteins were identified with 3,968 quantifiable proteins after filtering. In OCV-infected compared to CV-infected FT194 cells, 4,691 total proteins were identified with 4,148 quantifiable proteins after filtering. The average coefficient of variation for the LFQ values of CV-infected, OCV-infected, FAC-treated, and Untreated FT194 cells was 25.4, 21.4, 21.9, and 19.6%, respectively. The median coefficient of variation for the LFQ values of CV-infected, OCV-infected, FAC-treated, and Untreated FT194 cells was 16.8, 13.7, 15.0, and 11.7%, respectively. Statistically significant “top hits” were obtained using Welch’s t-test ($p < 0.05$) and z-score (z-score >1) which identified 700 protein targets in the OCV (relative to CV) cells and 459 protein targets in iron-exposed FTSECs (relative to untreated).

To achieve the effect size corresponding to a statistical power of 0.9 based on our experimental conditions, a fold-change of ~1.7-1.8 would be needed (assuming the global average of the coefficient of variation determined for each group), which is consistent with the

implemented z-score cutoff. Additional restrictions were applied to this data set to identify the protein targets that had LFQ intensity ratio of ≥ 2 or ≤ 0.5. Using this strategy, we thus identified 622 targets for OCV (relative to CV) and 243 targets for FAC-exposed FTSECs (relative to Untreated) (Fig. 17). The list of total quantifiable as well as differentially expressed proteins are provided as supplemental Tables 7 and 8.

Since alterations in miRNAs can contribute to cancer pathogenesis by targeting multiple protein targets [282, 314], we performed microRNA array profiling using the GeneChip miRNA 4.1 Array. We compared chronic FAC-exposed FTSECs relative to Untreated cells as well as OCV- relative to CV-infected FTSECs, which identified a total of 65 and 78 unique non-coding RNAs, respectively, including mature miRNAs and snoRNAs (7 snoRNAs were repeated as duplicates in the dataset resulting in a total of 71 and 79 ncRNAs identified in FAC/UNT and OCV/CV analyses, respectively), with at least a 2-fold change (p-value >0.05, displayed as a heat map, volcano plot, and Venn diagram (Fig. 18A – 18E).

There were 42 upregulated, 29 downregulated miRNAs in FAC-treated (relative to Untreated) and 45 upregulated, 34 downregulated miRNAs in OCV (relative to CV). miRNAs downregulated in FAC-treated (relative to Untreated) cells showed higher fold change (X-axis) and statistical significance (p-value at Y-axis) compared to OCV cells (relative to CV) (Fig. 18C and 18D*)*. Since the quantity of changes are more numerous in the OCV versus CV FTSEC comparison (relative to FAC versus Untreated FTSEC), this suggests that the combination of p53 inactivation, c-Myc^{T58A} expression, and H-Ras^{V12A} expression (within the OCV cocktail) may mediate increased neoplastic cellular alterations.

Since alterations in protein expression can be regulated post-transcriptionally by miRNAs, we integrated the top miRNA hits with the protein targets using IPA to identify associations between the two analyses. Integrated proteomics and microarray analyses identified 35 miRNAs in FAC-treated FT194 cells (relative to Untreated) and 45 miRNAs in OCV cells (relative to CV

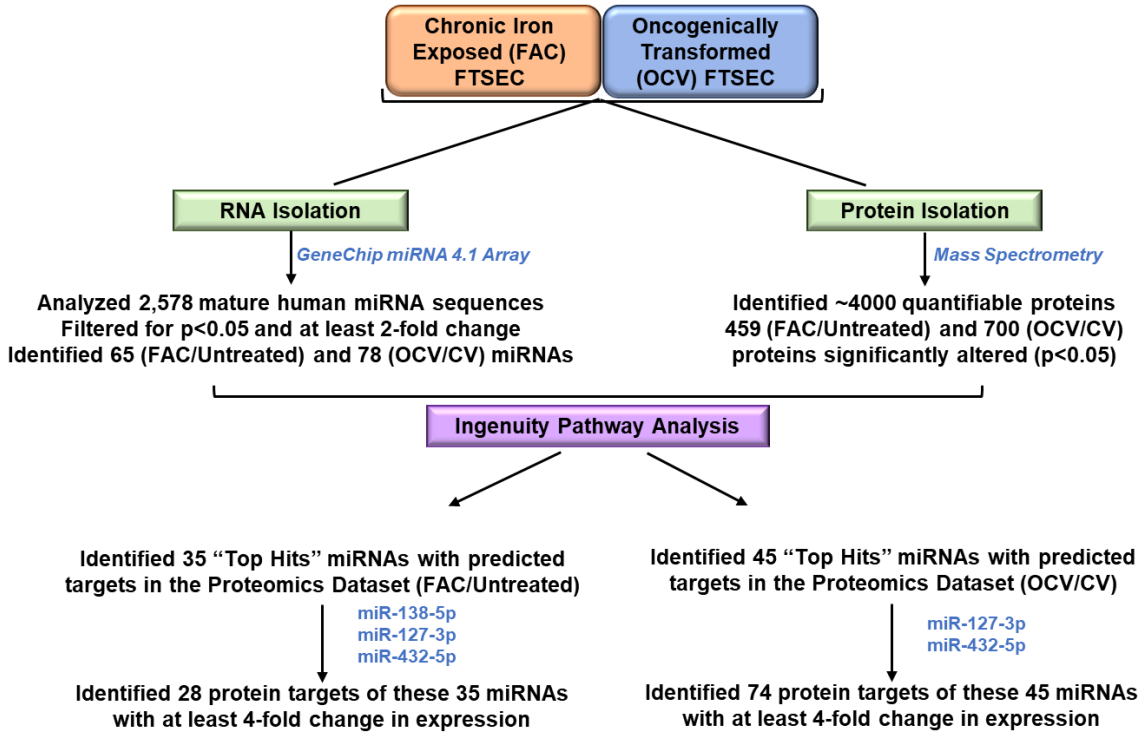

Figure 17: Schematic representation of the proteomics and microarray experimental strategy and analyses in FTSECs

Global proteomics analyses via mass spectrometry and miRNA analysis via Gene Chip miRNA 4.1 array were performed using chronic iron treated FT194 cells (p=30 at day 104 of FAC treatment) and transformed FT194 cells (p=RV+11) (with their corresponding control cells). This was followed by implementation of IPA to identify "top hits" of altered miRNA associated with protein changes.

cells) with the following characteristics: (1) >2-fold change and (2) with direct protein targets that were altered with respect to miRNA levels (Fig. 19A and 19B).

Twenty of the 35 miRNAs (57.14%) altered in FAC-treated cells (relative to Untreated) were located at chromosome 14q32 (Fig. 19A), while only 9 out of the 45 miRNAs (20%) altered

in OCV cells (relative to CV) were located at this region (Fig. 19B). This region, amongst others, also harbors common fragile sites (Table 7 and Table 8), possibly rendering the chromosomal loci susceptible to replication stress, which is known to impact genomic stability in many cancers [315]. Interestingly, the 14q32 locus contains a cluster of 54 miRNAs, one of the largest miRNA clusters in the human genome[204]. Many of these miRNAs appear to be downregulated in multiple cancer types associated with tumor suppressive properties [5, 215, 290, 316-319] and oncogenic properties [320]. From the miRNA profiling, we identified that two miRNAs from this cluster, miR-432-5p and miR-127-3p, were 97.9- and 111.7-fold downregulated, respectively, in FAC-treated cells in contrast to only 11.7-fold downregulated in OCV cells. These results were validated by real-time PCR in FAC-treated FT194 cells (Fig. 19C and 19D), which showed a 99.9% reduction for miR-432-5p and miR-127-3p (p-value < 0.0001) in FAC-treated relative to Untreated FT194 cells.

Additionally, among other highly dysregulated miRNAs from other genomic regions such as 3p21.31, we identified that miRNA-138-5p (located at 3p21) was 16.3-fold downregulated with chronic FAC-exposure in FT194 cells (Fig. 19A) and validated via qPCR to be 90.1% reduced (p-value < 0.0001, Fig. 19E). miR-138-5p also appears to be commonly downregulated in multiple cancers [321-324]. We identified 28 protein targets in FAC-treated relative to Untreated cells and 74 protein targets in OCV relative to CV cells out of the total statistically significant “top hits” ($p < 0.05$ and z-value > 1), which were associated with characteristics of gynecological cancers (Fig. 20A and 20B).

In Fig. 20C, we validated two of these “top hits”, namely CRYAB and ITGA2 via western blotting, which have roles as molecular chaperones [325] and in adhesion to the extracellular matrix [326], respectively. The number of identified proteins and miRNAs from the OCV FT194 cells (relative to CV) were higher as compared to FAC-exposed cells (relative to Untreated), which suggests that the extent of neoplastic alterations induced by the oncogenic cocktail (hTERT, LTAg, c-

Myc^{T58A}, and H-Ras^{V12A}) is more extensive than that induced by iron exposure (see Experimental Procedures).

Table 7: List of common fragile sites in FAC-exposed relative to Untreated FT194 cells

FAC vs. Untreated					
miRNA ID	**Genomic Location**	**Fold Change**	**FDR p-value**		**Nearest Common Fragile Site**
miR-34a-5p	1p36.22	6.85	0.02890000	*	FRA1A (1p36)
miR-138-5p	3p21.31	-16.25	0.00000189	****	FRA3A (3p24.2); FRA3B (3p14.2)
hsa-miR-7110-5p	3q21.1	2.29	0.49900000	NS	FRA3D (3q25)
miR-145-5p	5q32	-2.38	0.45400000	NS	FRA5C (5q31.1)
miR-146a-5p	5q33.3	10.26	0.31070000	NS	FRA5C (5q31.1)
mir-182-5p	7q32.2	-9.19	0.03020000	*	FRA7G (7q31.2); FRA7H (7q32.3
miR-31-5p	9p21.3	2.32	0.06330000	NS	N/A
miR-1296-5p	10q21.3	-5.42	0.08800000	NS	FRA10D (10q22.1)
miR-210-3p	11p15.5	-2.09	0.01260000	*	FRA11C (11p15.1)
miR-708-5p	11q14.1	3.44	0.00660000	**	FRA11F (11q14.2)
miR-34c-3p	11q23.1	3.83	0.19130000	NS	FRA11G (11q23.3)
miR-125b-5p	11q24.1	2.45	0.48070000	NS	FRA11G (11q23.3)
miR-125b-1-3p	11q24.1	2.45	0.48070000	NS	FRA11G (11q23.3)
miR-615-3p	12q13.13	-15.09	0.00009200	****	N/A
miR-17-3p	13q31.3	2.24	0.16410000	NS	FRA13D (13q32)
miR-127-3p	14q32.2	-111.69	0.00000003	****	FRA14C (14q24.1)
miR-432-5p	14q32.2	-97.87	0.00000009	****	FRA14C (14q24.1)
miR-433-3p	14q32.2	-22.41	0.00000703	****	FRA14C (14q24.1)
miR-493-3p	14q32.2	-11.59	0.00730000	**	FRA14C (14q24.1)
miR-431-5p	14q32.2	-6.02	0.06480000	NS	FRA14C (14q24.1)
hsa-miR-770-5p	14q32.2	-2.45	0.25680000	NS	FRA14C (14q24.1)
miR-342-5p	14q32.2	-2.34	0.41920000	NS	FRA14C (14q24.1)
miR-409-3p	14q32.31	-49.16	0.00000034	****	FRA14C (14q24.1)
miR-382-5p	14q32.31	-37.07	0.00020000	***	FRA14C (14q24.1)
miR-379-5p	14q32.31	-23.84	0.00002020	****	FRA14C (14q24.1)
miR-487b-3p	14q32.31	-22.55	0.00040000	***	FRA14C (14q24.1)
miR-485-3p	14q32.31	-18.02	0.00030000	***	FRA14C (14q24.1)
hsa-miR-654-5p	14q32.31	-9.37	0.00010000	****	FRA14C (14q24.1)
hsa-miR-1185-1-3p	14q32.31	-8.64	0.00009730	****	FRA14C (14q24.1)
miR-485-5p	14q32.31	-5.98	0.00660000	**	FRA14C (14q24.1)
miR-323a-5p	14q32.31	-5.85	0.00005460	****	FRA14C (14q24.1)
miR-134-5p	14q32.31	-3.58	0.24840000	NS	FRA14C (14q24.1)
miR-487a-5p	14q32.31	-3.04	0.41920000	NS	FRA14C (14q24.1)
miR-409-5p	14q32.31	-2.54	0.61360000	NS	FRA14C (14q24.1)
miR-329-3p	14q32.31	-2.52	0.25680000	NS	FRA14C (14q24.1)

Note: >2-fold change cutoff along with an FDR-adjusted p-value <0.05 (**** p<0.0001; *** p<0.001; ** p<0.01; * p<0.05; NS >0.05).

Table 8: List of common fragile sites in OCV relative to CV FT194 cells

OCV vs. CV					
miRNA ID	**Genomic Location**	**Fold Change**	**FDR p-value**		**Nearest Common Fragile Site**
hsa-miR-4632-5p	1p36.22	2.6	0.61160000	NS	FRA1A (1p36)
miR-34a-5p	1p36.22	2.08	0.64000000	NS	FRA1A (1p36)
miR-128-3p	2q21.3	-2.11	0.43710000	NS	FRA2F (2q21.3)
miR-378a-3p	5q32	7.66	0.00460000	**	FRA5C (5q31.1)
miR-584-5p	5q32	2.67	0.73370000	NS	FRA5C (5q31.1)
miR-378a-5p	5q32	2.17	0.49590000	NS	FRA5C (5q31.1)
miR-146a-5p	5q33.3	11.43	0.08990000	NS	FRA5C (5q31.1)
miR-4640-5p	6p21.33	3.72	0.49590000	NS	FRA6C (6p22.2)
miR-589-3p	7p22.1	-2.2	0.88380000	NS	FRA7B (7p22)
miR-182-5p	7q32.2	-3.58	0.49590000	NS	FRA7G (7q31.2); FRA7H (7q32.3
miR-6850-5p	8q24.3	2	0.87770000	NS	FRA8D (8q24.3)
let7e-5p	9q22.32	-3.92	0.00001450	****	FRA9D (9q22.1)
miR-455-3p	9q32	4.77	0.00040000	***	FRA9E (9q32)
miR-1343-5p	11p13	2.31	0.61160000	NS	FRA11E (11p13)
miR-210-3p	11p15.5	-2.19	0.10890000	NS	FRA11C (11p15.1)
miR-139-5p	11q13.4	8.53	0.00040000	***	FRA11H (11q13)
miR-125a-5p	11q24.1	-4.65	0.00008670	****	FRA11G (11q23.3)
miR-615-3p	12q13.13	3.55	0.02630000	*	N/A
miR-17-5p	13q31.3	4.75	0.33370000	NS	FRA13D (13q32)
miR-18a-5p	13q31.3	3.9	0.25760000	NS	FRA13D (13q32)
miR-18a-3p	13q31.3	3.79	0.12120000	NS	FRA13D (13q32)
miR-92a-3p	13q31.3	2.48	0.00460000	**	FRA13D (13q32)
miR-127-3p	14q32.2	-11.76	0.00001450	****	FRA14C (14q24.1)
miR-432-5p	14q32.2	-11.75	0.00010000	****	FRA14C (14q24.1)
miR-433-3p	14q32.2	-2.62	0.53880000	NS	FRA14C (14q24.1)
miR-134-5p	14q32.31	-6.06	0.61160000	NS	FRA14C (14q24.1)
miR-409-3p	14q32.31	-6.04	0.00040000	***	FRA14C (14q24.1)
miR-382-5p	14q32.31	-3.22	0.18450000	NS	FRA14C (14q24.1)
miR-370-3p	14q32.31	-3.13	0.17770000	NS	FRA14C (14q24.1)
miR-485-3p	14q32.31	-2.22	0.58160000	NS	FRA14C (14q24.1)
miR-487b-3p	14q32.31	-2.04	0.87160000	NS	FRA14C (14q24.1)
miR-3180	16p13.11	2.82	0.87770000	NS	N/A
miR-744-5p	17p12	-2.21	0.03970000	*	N/A
miR-6776-5p	17p13.3	2.72	0.87770000	NS	N/A
hsa-miR-6779-5p	17q12	3.24	0.04560000	*	N/A
miR-27b-3p	19p13.12	-2.31	0.65520000	NS	N/A
miR-23b-3p	19p13.12	-2.14	0.24790000	NS	N/A
miR-769-5p	19q13.32	-2.62	0.61160000	NS	N/A
hsa-miR-99b-5p	19q13.41	-4.88	0.00460000	**	N/A
miR-125a-3p	19q13.41	-3.51	0.24790000	NS	N/A
miR-296-3p	20q13.32	3.11	0.00460000	**	N/A
miR-941	20q13.33	2.87	0.87720000	NS	N/A
miR-99b-3p	21q21.1	-4.18	0.00040000	***	N/A
miR-500a-5p	Xp11.23	2.03	0.84280000	NS	N/A
miR-424-3p	Xq26.3	5.6	0.13100000	NS	FRAXD (Xq27.2)

Note: >2-fold change cutoff along with an FDR-adjusted p-value <0.05 (**** p<0.0001; *** p<0.001; ** p<0.01; * p<0.05; NS >0.05)

A

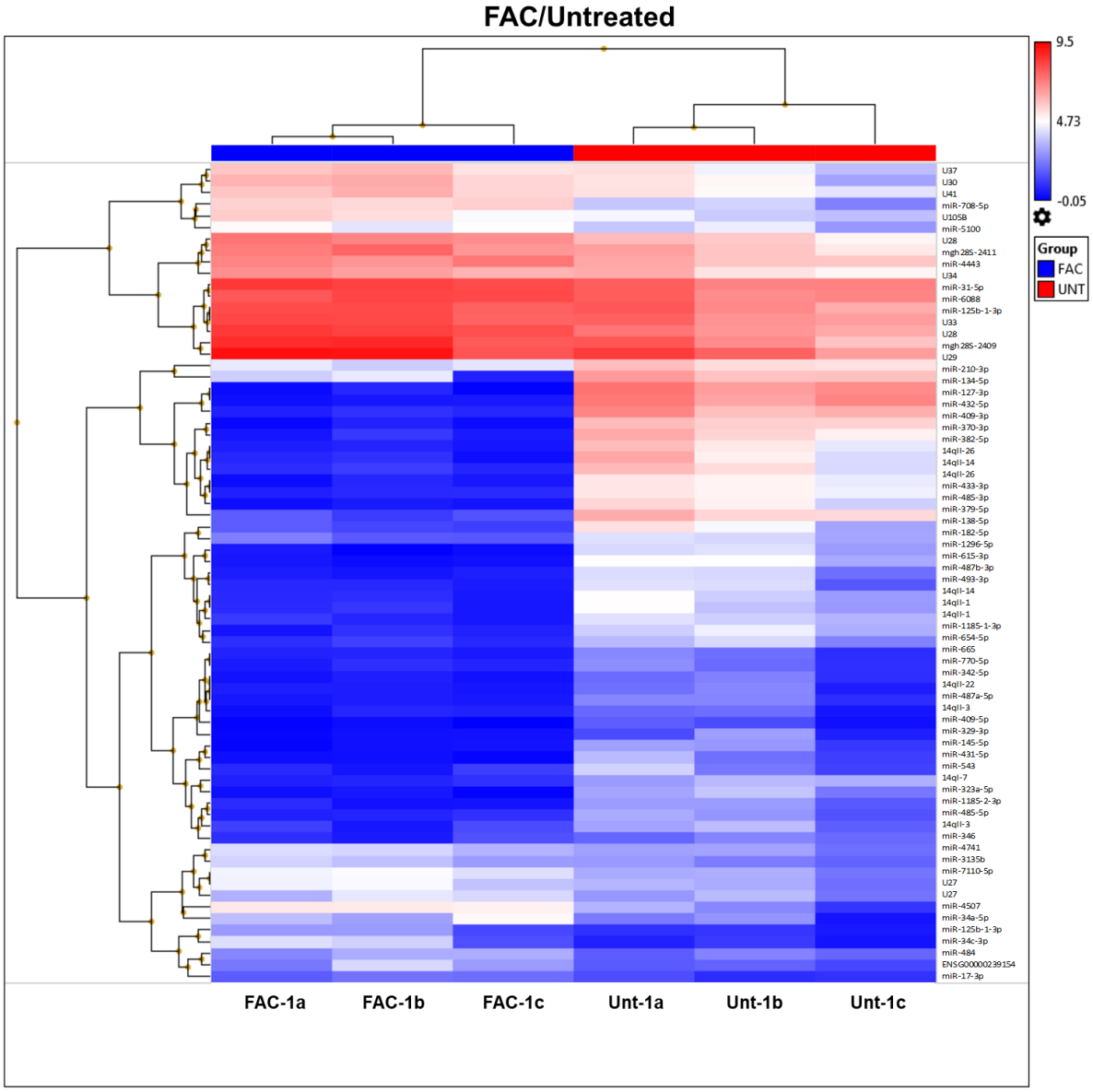

Figure 18: Altered miRNAs identified from microarray analysis in FTSECs (*Continued next page)

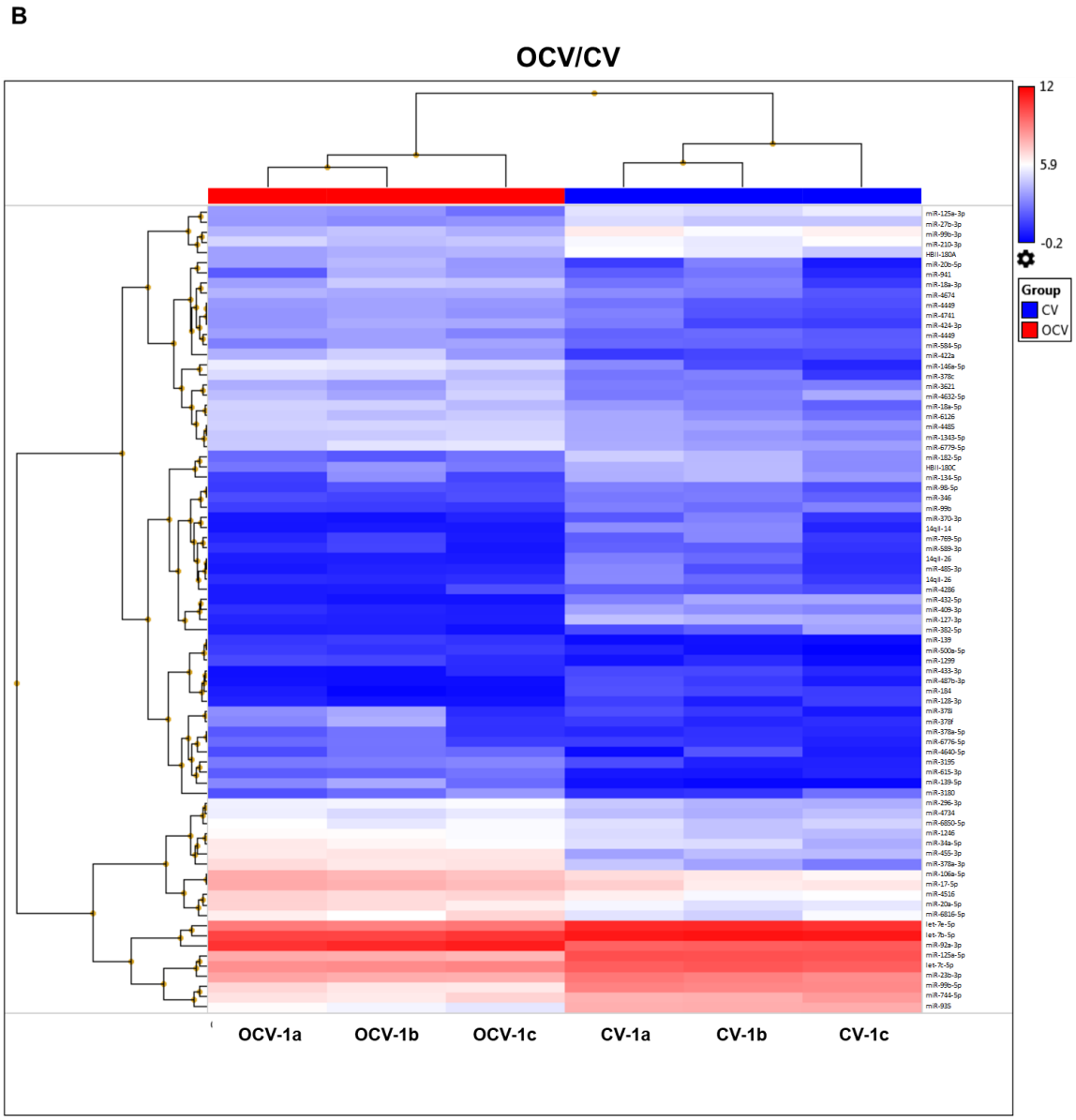

Figure 18: Altered miRNAs identified from microarray analysis in FTSECs (*Continued next page)

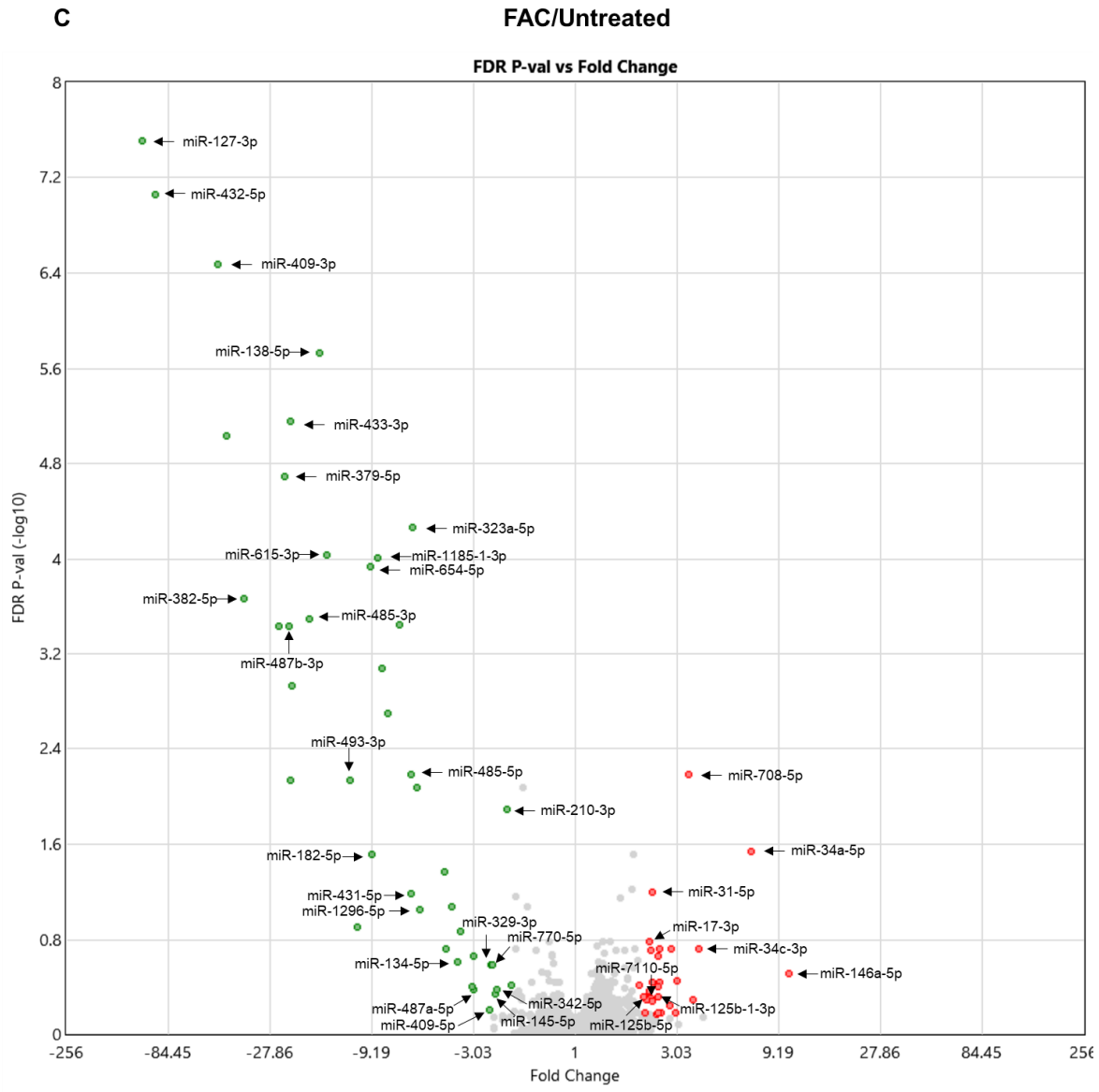

Figure 18: Altered miRNAs identified from microarray analysis in FTSECs (*Continued next page)

Figure 18: Altered miRNAs identified from microarray analysis in FTSECs (*Continued next page)

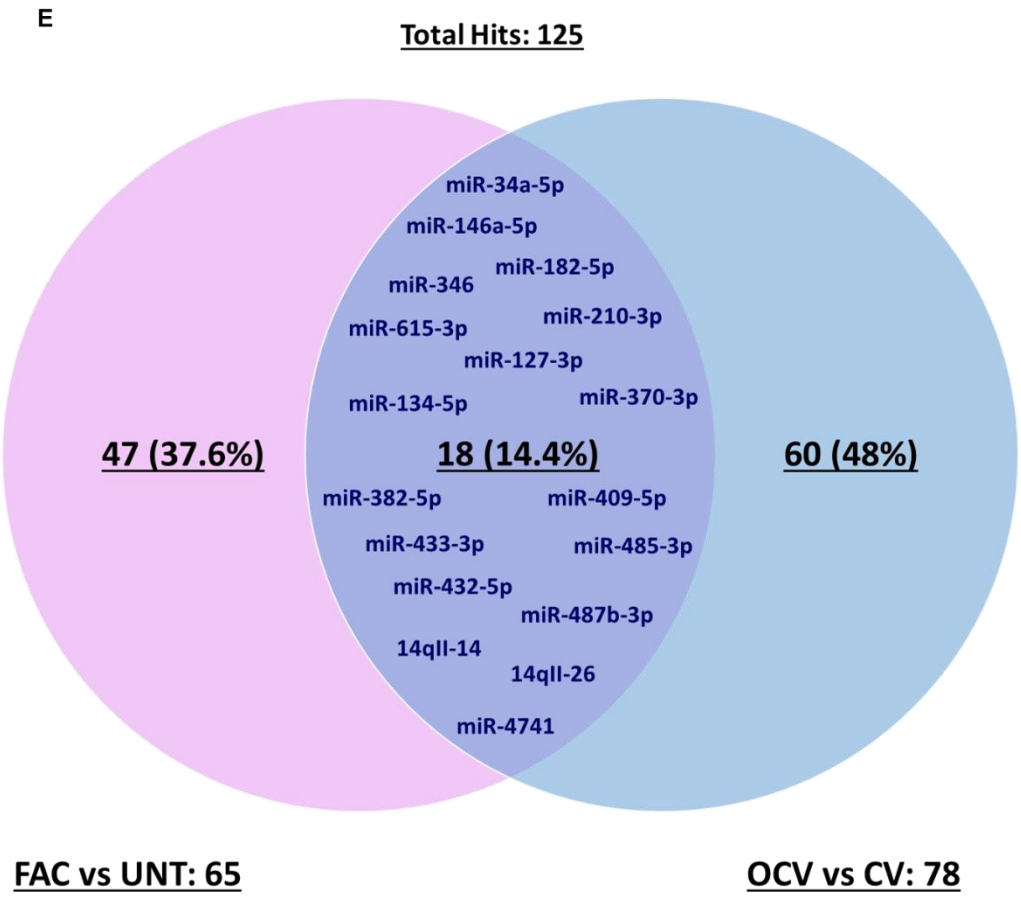

Figure 18: Altered miRNAs identified from microarray analysis in FTSECs

Heat Map representing miRNAs derived from the microarray analysis showing a decrease [1] and increase (Red) in miRNAs with (**A**) FAC treatment (FAC-1a, 1b, 1c) compared to Untreated and (**B**) transformed OCV- relative to CV-infected FT194 cells. Dysregulated miRNAs are displayed as Volcano Plots in (**C**) FAC-treated vs Untreated FT194 cells, (**D**) Transformed (OCV/CV) and (**E**) dysregulated miRNAs are displayed in a Venn diagram showing 18 common (overlapping) miRNAs between FAC-treated relative to Untreated as well as transformed OCV relative to CV analyses.

These ”hits” were not validated due to the expectation that oncogenic transformation of FTSECs would lead to a comparatively larger array of alterations recapitulating more closely tumorigenic profiles of ovarian tumors relative to chronic iron exposed FTSECs, which is the main focus of this study. As the protein targets from the FAC versus Untreated analyses were found to be involved in multiple signaling and molecular pathways (Fig. 20D and Table 9), we further investigated the mechanism of FAC-induced dysregulation in FT194 cells, specifically focusing on analyzing the mechanism by which FAC alters miR-138-5p, miR-432-5p and miR-127-3p levels to potentially contribute towards increased tumorigenesis.

FAC-induced epigenetic regulation of PAX8

Integrated microarray and proteomics analyses were used to identify the most common protein targets of miR-432-5p, miR-127-3p, and miR-138-5p in FAC-treated cells relative to Untreated (Fig. 21A – 21C) as well as in OCV (relative to CV) FT194 cells (Fig. 22 – 24). Via IPA, the analyses identified PAX8 (Paired Box 8) as a potential common target of miR-432-5p, miR-127-3p, and miR-138-5p involved in ovarian cancer pathophysiology (Fig. 21D). Global proteomic analyses demonstrated that PAX8 was increased 1.7-fold in FAC-exposed FT194 cells, which was validated by western blotting and densitometric analyses (Fig. 25A, left and right panels).

Since iron-overload conditions are associated with epigenetic changes in various human tissues [327, 328] and epigenetic modification of PAX8 is reported in ovarian cancer [329, 330], we next investigated whether FAC-induced increase of PAX8 could be altered with AZA and/or SAHA treatment. As shown in Fig. 25A, we observed a 95.6%-fold reduction in PAX8 protein following combinatorial treatment of SAHA and AZA. These results suggest that the increased PAX8 protein is epigenetically regulated as a result of chronic iron treatment in FT194 cells.

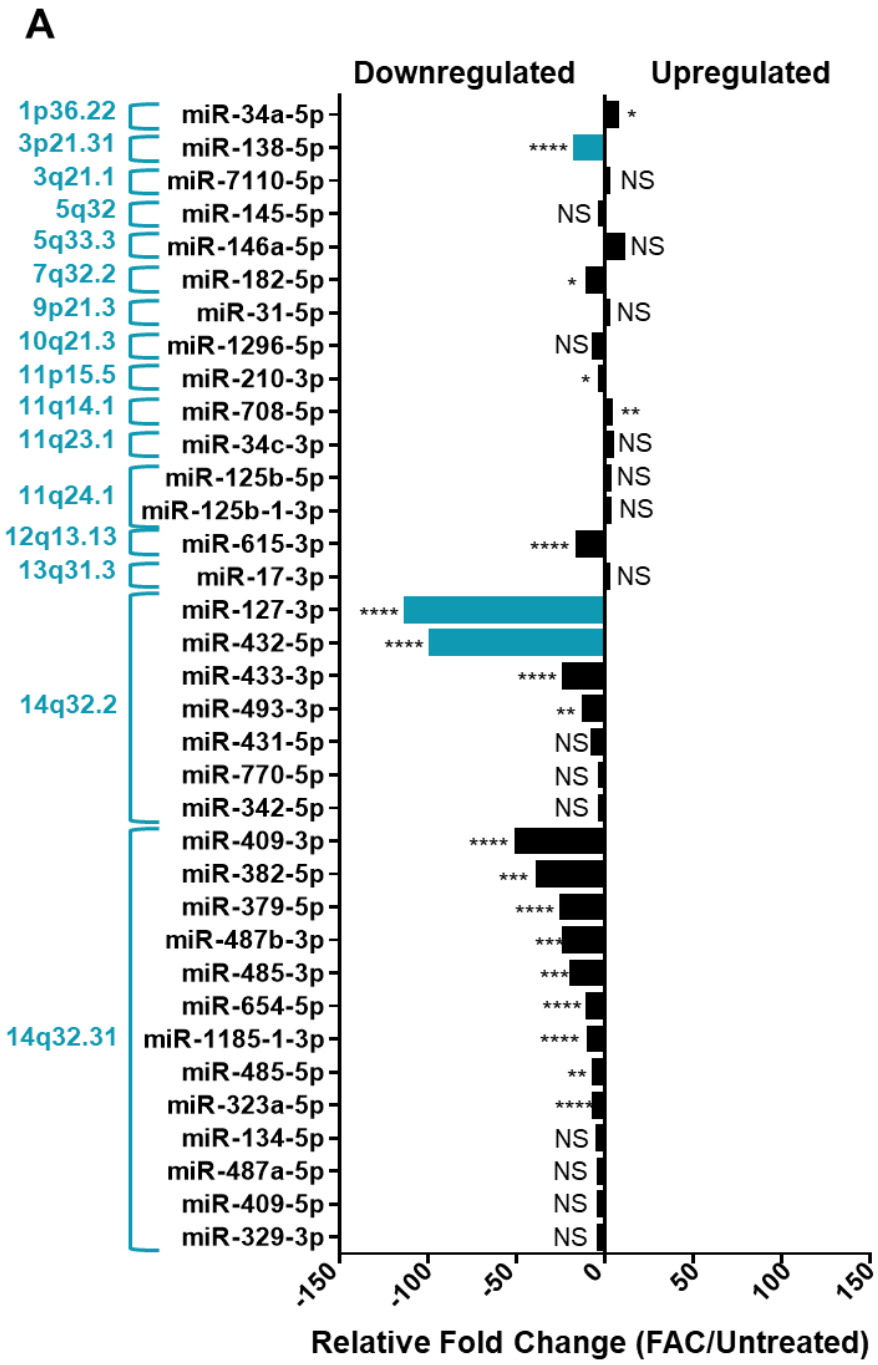

Figure 19: Top miRNAs altered in FT194 cells, and their genomic locations (*Continued next page)

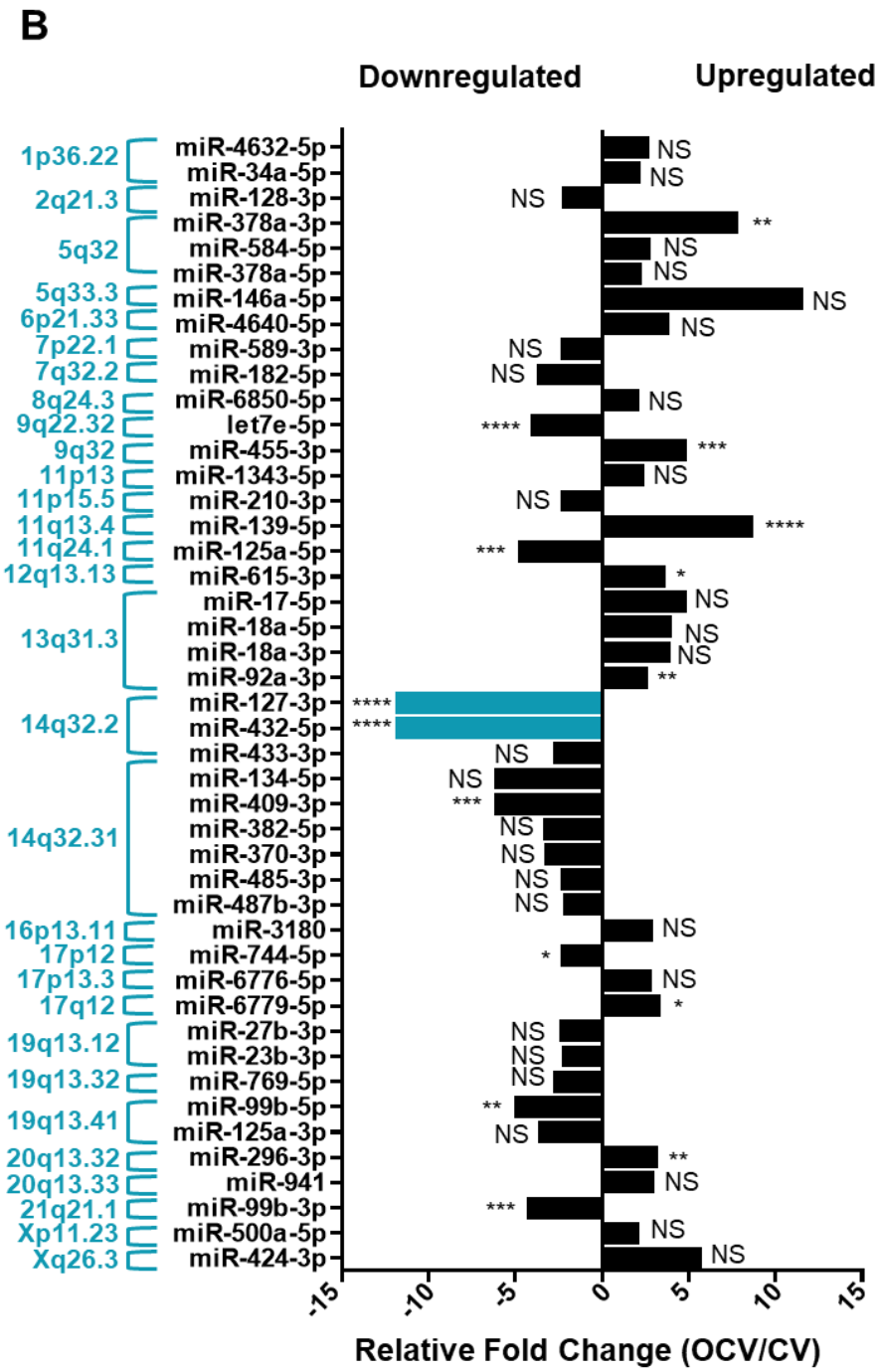

Figure 19: Top miRNAs altered in FT194 cells, and their genomic locations (*Continued next page)

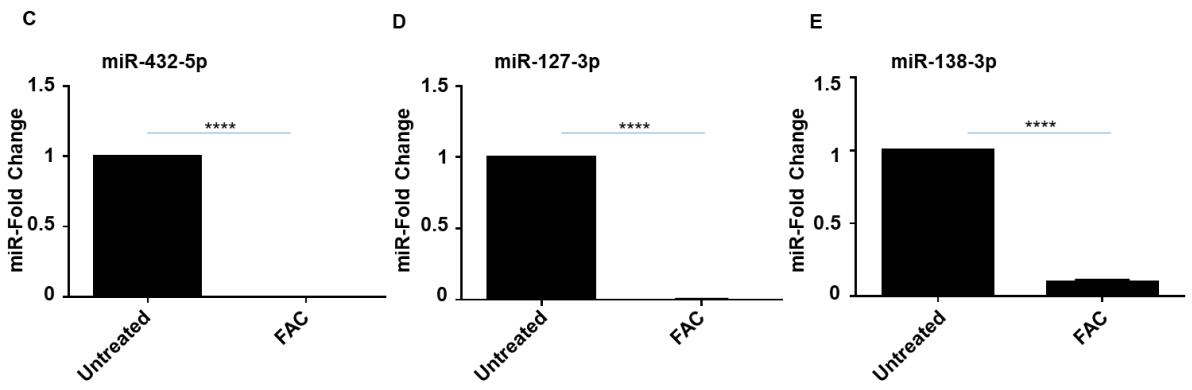

Figure 19: Top miRNAs altered in FT194 cells, and their genomic locations

These graphs show the miRNA targets (analyzed via microarray profiling) which correlate with the protein changes (analyzed via mass spec proteomics analysis) as predicted by IPA. The relative fold change of miRNAs is represented and organized according to their genomic locations in (A) 250 nM FAC-treated FT194 cells compared to untreated, and (B) FT194 transformed cells via Oncogenic cocktail virus (OCV), compared to control virus (CV) cells. Real-time PCR analysis of (C) miR-432-5p, (D) miR-127-3p, and (E) miR-138-5p was performed after isolating total miRNAs from 250 nM FAC-treated cells as compared to the untreated, at days 111 and 124 of FAC treatment (p=33 and 37), to validate the downregulation of these miRNAs as predicted by IPA analysis. RNU6B was used as a reference control and the data represents composite of three independent experiments.

FAC-induced epigenetic regulation of miRNAs at 14q32 and 3p21

miRNAs are also regulated by epigenetic mechanisms [331-333] and miRNAs at chromosome 14q32 appear to be transcribed as a polycistronic miRNA cluster under control of epigenetic mechanisms [334, 335]. In specific cancers, there is evidence to support hypermethylation at the 14q32 differentially methylated CpG regions (DMRs) which leads to cancer development [5, 223]; furthermore, promoter hypoacetylation, which can recruit HDACs through methyl CpG binding proteins can also regulate gene expression at this locus [336].

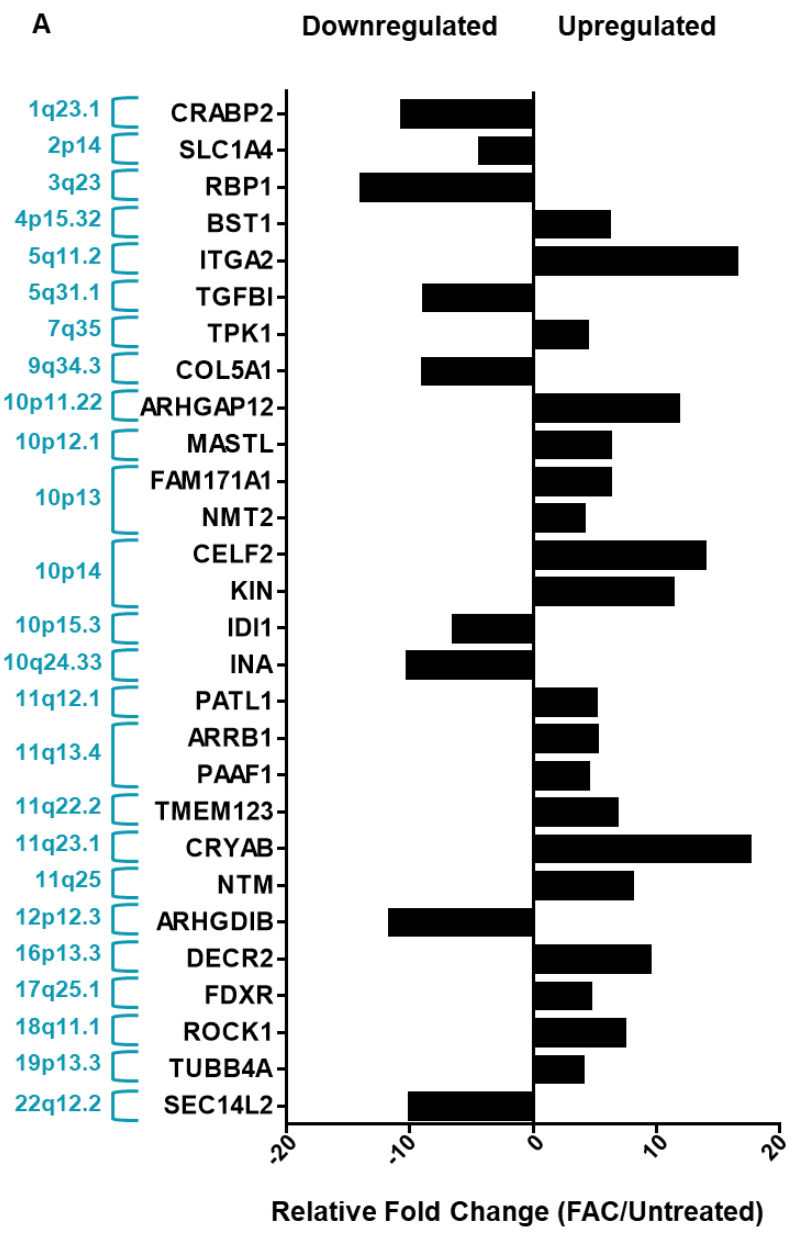

Figure 20: Protein targets and their genomic locations associated with top miRNAs altered in FT194 cells (*Continued next page)

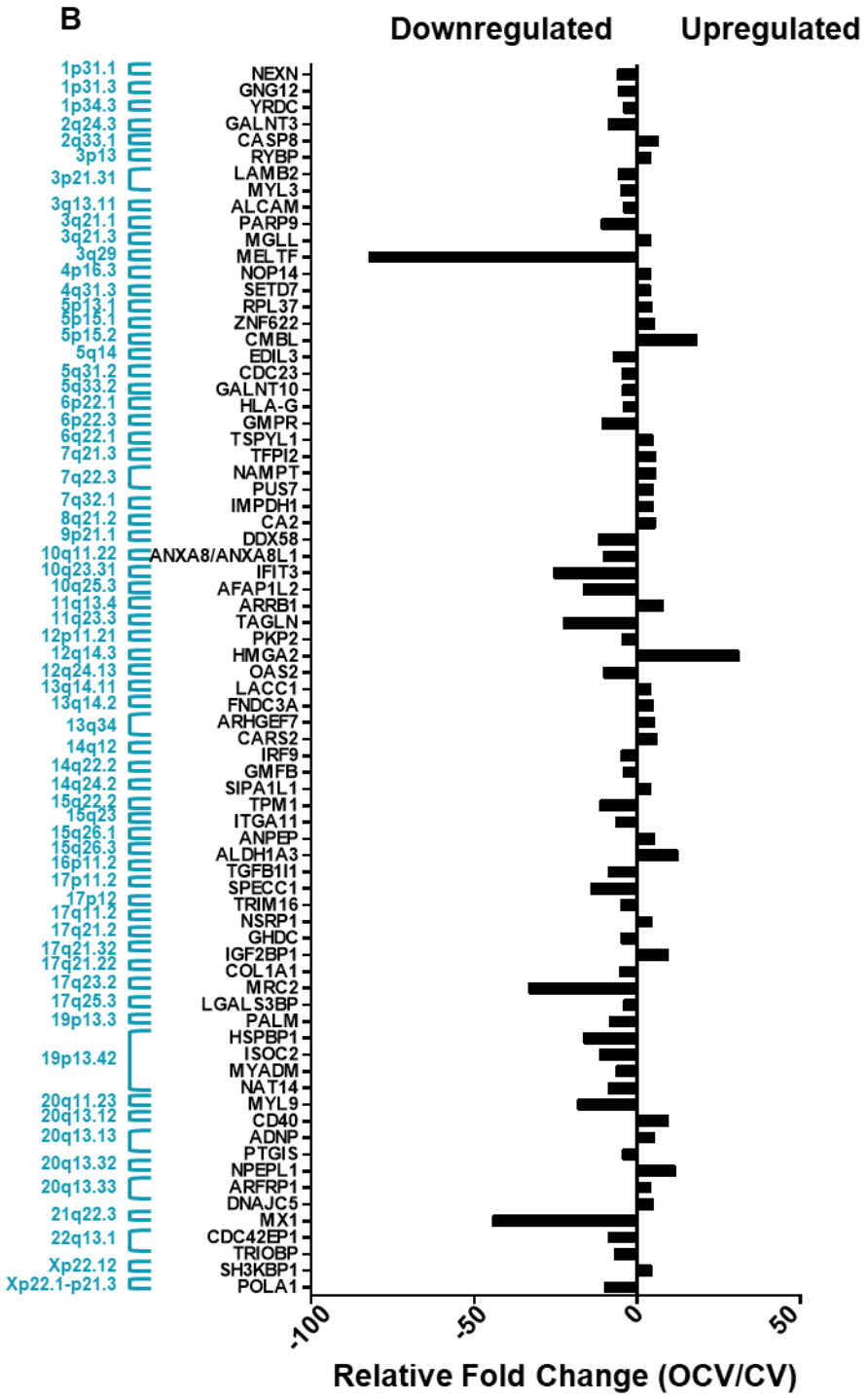

Figure 20: Protein targets and their genomic locations associated with top miRNAs altered in FT194 cells (*Continued next page)

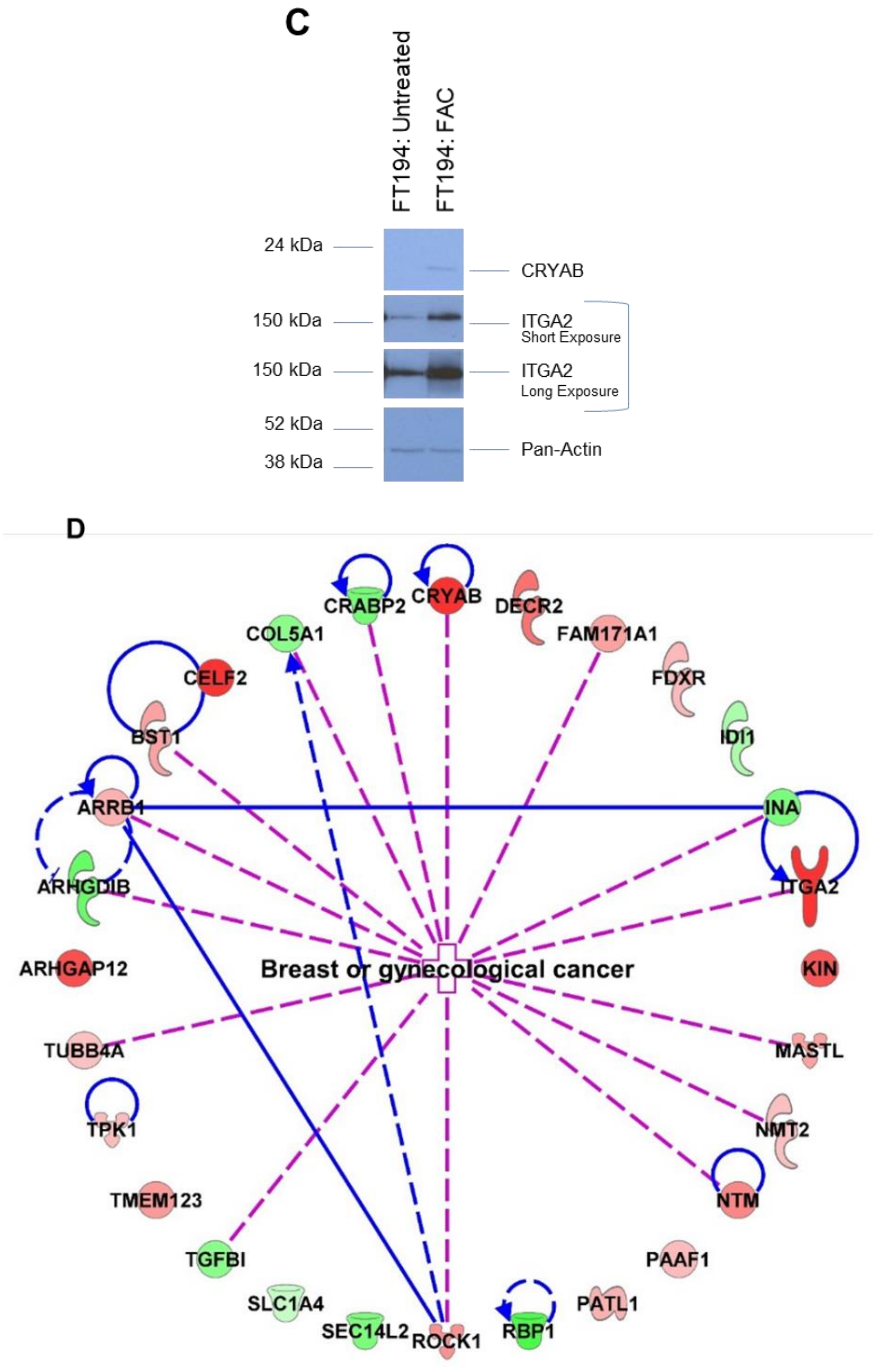

Figure 20: Protein targets and their genomic locations associated with top miRNAs altered in FT194 cells (*Continued next page)

E

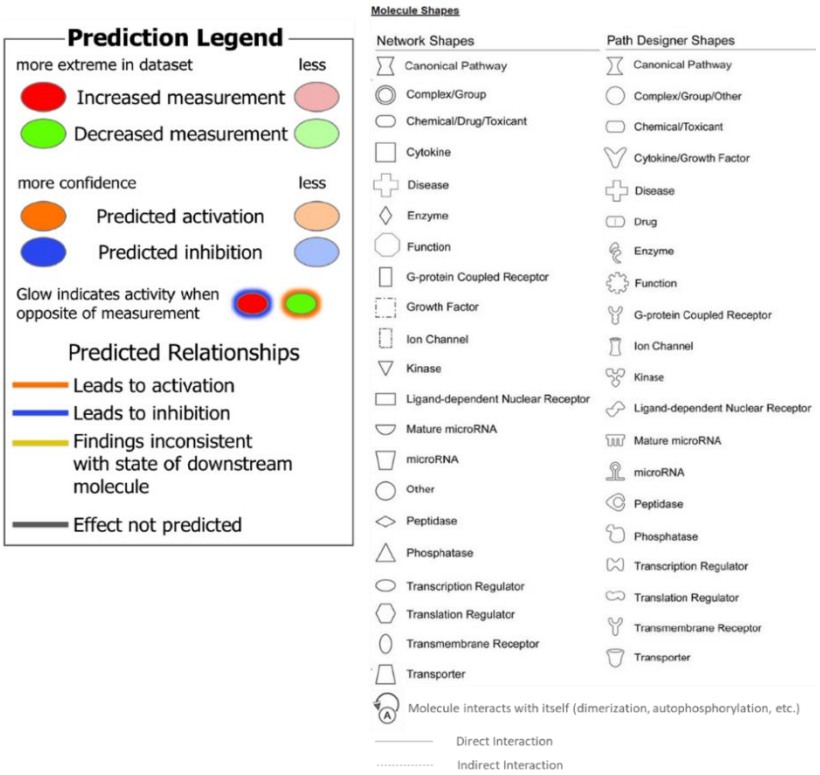

Figure 20: Protein targets and their genomic locations associated with top miRNAs altered in FT194 cells

These graphs show the protein targets associated with highly dysregulated miRNAs in FT194 cells, as determined by IPA analysis. Protein targets with >4-fold change, corresponding to the miRNAs, were compiled, and organized by their genomic locations. Relative fold change of these protein targets has been represented for (A) 250 nM FAC-treated FT194 cells compared to untreated, and (B) transformed OCV cells compared to CV cells. (C) Western Blotting analysis of 250 nM FAC-exposed and Untreated FT194 cells, using cell lysates collected at day 170 of FAC treatment (p=52). Three independent replicates were performed; representative cropped blots are displayed. White space between cropped blots delineate different antibody applications to the same blot. The full-length uncropped blots are displayed in the Supplementary Information File. (D) Top 28 protein targets altered in gynecological cancers, with >4-fold change, identified for 250 nM FAC-treated FT194 cells compared to untreated. Upregulated proteins are shown in red and downregulated proteins in green, ranging color intensity based on the fold change associated with each. The detailed legend for all molecular processes in the protein network is included in tabular form in (E).

In view of these regulatory mechanisms and the identification of twenty 14q32 miRNAs that were altered in FAC-exposed FT194 cells, we hypothesized that inhibition of DNA methylation with AZA and/or inhibition of histone deacetylases with SAHA may alter the expression of miR-432-5p and miR-127-3p (refer to Fig. 18 for “top hits” identified in the screening approach). Since miR-138-5p is associated with epigenetic changes [337, 338], we therefore investigated whether AZA and SAHA treatments could alter miR-138-5p levels. Inhibition of DNA methyltransferase with AZA was validated by western blotting for DNMT1, which showed reduced protein levels (Fig. 6A).

In addition, HDAC inhibition was validated by demonstrating increased acetyl histone H3 levels via western blotting (Fig. 25A). Although SAHA treatment was more potent alone compared to AZA alone, the combination of AZA with SAHA, resulted in a further fold-increase of 164.8, 48.8 and 2.3 in miR-432-5p, miR-138-5p, and miR-127-3p levels, respectively, as measurement via real-time PCR (Fig. 25B – 25D). These results can be explained by the ability of the HDAC inhibitor, SAHA, to inhibit not only HDAC but also DNMT1 protein expression via inhibition of MAPK and thus the DNA methylation status [339]. HDAC inhibitors can also target DNMTs for degradation via the ubiquitin-proteasome-pathway by an Hsp90 chaperone mediated mechanism [340]. On the other hand, AZA specifically inhibits only DNMTs [341].

FAC-induced miR-138-5p downregulation is mediated independently of EVI1

We have previously reported that telomerase reverse transcriptase (TERT) can be transcriptionally regulated by EVI1 (genomically amplified at chromosome 3q26) in FAC exposed FT194 cells [19]. Prior work has shown that miR-138 levels are inversely correlated with TERT as a result of direct binding of miR-138 to the 3’-UTR of TERT [342-344]. Therefore, we hypothesized that the EVI1 may upregulate TERT transcripts in a miR-138-dependent manner.

Mature miR- 138 originates from two primary transcripts: pri-miR-138-1 (encoded on chromosome 3p21, Genecard) and pri-miR-138-2 (encoded on chromosome 16q13, Genecard).

Indeed, we identified predicted EVI1 binding sites ~2500 bp upstream of miR-138-5p-1 (Fig. 26A and Fig. 27); specifically, the C-terminal binding site, GAAGATGAG, was 100% aligned in this region, while the N-terminal and consensus sequences were imperfectly aligned (5 out of 9 nucleotides and 5 out of 11 nucleotides, respectively). To determine whether EVI1 is potentially involved in the direct regulation of miR-138-5p-1 expression in chronic iron-exposed FT194 cells, we reduced EVI1 levels using an siRNA transfection (siB) approach and validated the efficiency of knockdown via western blotting (Fig. 26B). We then determined the levels of miR-138-5p via real-time PCR analysis.

Although we confirmed that the levels of miR-138-5p were reduced following chronic FAC exposure ($p < 0.0001$), as noted previously (see Fig. 26D), its levels were not significantly altered upon siB (EVI1 knockdown) treatment in FAC-exposed FT194 cells relative to FAC-exposed parental cells ($p = 0.8509$) (Fig. 26C). These results indicate that miR-138-5p expression is regulated in an EVI1-independent manner and that other factors likely contribute to the downregulation of miR-138-5p under these conditions.

miR-138-5p partially regulates transcript expression of the stem cell marker TERT but not ALDH1A2 protein

Cancer stem cells (CSCs or tumor initiating cells) represent a subpopulation of cells that are responsible for tumor initiation and progression [345, 346]. Dysregulated iron homeostasis in CSCs may also aggravate cancer phenotypes [174, 347]. CSCs are notably characterized by the expression of stem cell markers including elevated activity by aldehyde dehydrogenase (ALDH, represented by multiple isoforms) [348], a superfamily of metabolic markers which serves as a potential poor prognostic factor of cancer [349]. One family member, ALDH1A2, is aberrantly expressed in acute lymphoblastic leukemia cells [350] and ovarian cancer [351, 352].

Interestingly, the proteomics analyses identified a 3.2-fold increase in ALDH1A2 levels upon FAC exposure in FTSEC cells and IPA analyses suggests that ALDH1A2 is a potential direct target of miR-138-5p (Fig 28C). Indeed, prior published work supports miR-138-5p involvement in ALDH1A2 regulation [353, 354]. To investigate whether ALDH1A2 is a target of miR-138-5p in human FTSECs, we transfected FAC-exposed FT194 cells with miR-138-5p mimic. Although overexpression of miR-138-5p was confirmed by real-time PCR (Fig. 28A) and western blotting demonstrated that ALDH1A2 protein was increased in iron-exposed FTSECs, its levels were not altered by miR-138-5p overexpression (Fig. 28B). These results suggest that miR-138-5p is not a regulator of ALDH1A2 expression in FTSECs. Another stem cell marker TERT [355, 356] has also been reported to be directly regulated by miR-138-5p [344, 357].

Since chronic iron exposure can induce TERT mRNA levels [19] and TERT sequence alignment with miR-138-5p mature sequence has shown direct binding (Fig. 28D) [342], we analyzed whether TERT increase is mediated via miR-138-5p. Indeed, we observed that miR-138-5p mimic transfection partially rescued the TERT mRNA levels by 25% (Fig. 28E), suggesting that FAC-induced increase in TERT transcript levels could be partially regulated via miR-138-5p. IPA analysis identified 10 upregulated proteins predicted to be downstream of either miR-432-5p (5 proteins) or miR-127-3p (5 proteins) in FT194-OCV cells relative to FT194-CV and associated with malignant solid tumors.

miR-432-5p, miR-127-3p, and miR-138-5p overexpression does not alter PAX8 protein but reduces cell numbers in FAC-treated FT194 cells

PAX8 (a member of paired box PAX gene family) is a positive marker of FTSECs [168] and is elevated in a variety of tumors [358-363]. Our prior findings demonstrated that PAX8 was upregulated following chronic iron exposure[19]; we now validate this observation and further show that it is epigenetically regulated, also supported by prior literature [330].

Furthermore, PAX8 appears to be a common target of miR-432-5p, miR-127-3p, and miR-138-5p via the IPA analyses; target analyses using bioinformatic programs (Targetscan, miRDB, miRNA.org, miRpath v.3 and miRmap) identified PAX8 to be a target of the aforementioned miRNAs in a subset of these databases (data not shown). However, western blot analyses did not identify any marked changes in PAX8 protein expression in FTSECs upon overexpression of these miRNAs (Fig. 28B and 28C).

Thus, it remains to be experimentally determined whether these miRNAs interact directly with PAX8 to regulate its expression. Since miR-432-5p, miR-127-3p, and miR-138-5p levels were reduced in chronic FAC-exposed FT194 cells (Fig. 23C - 23E) and evidence supports their tumor-suppressive role [364-366], we proposed that rescuing their expression in the chronic iron-

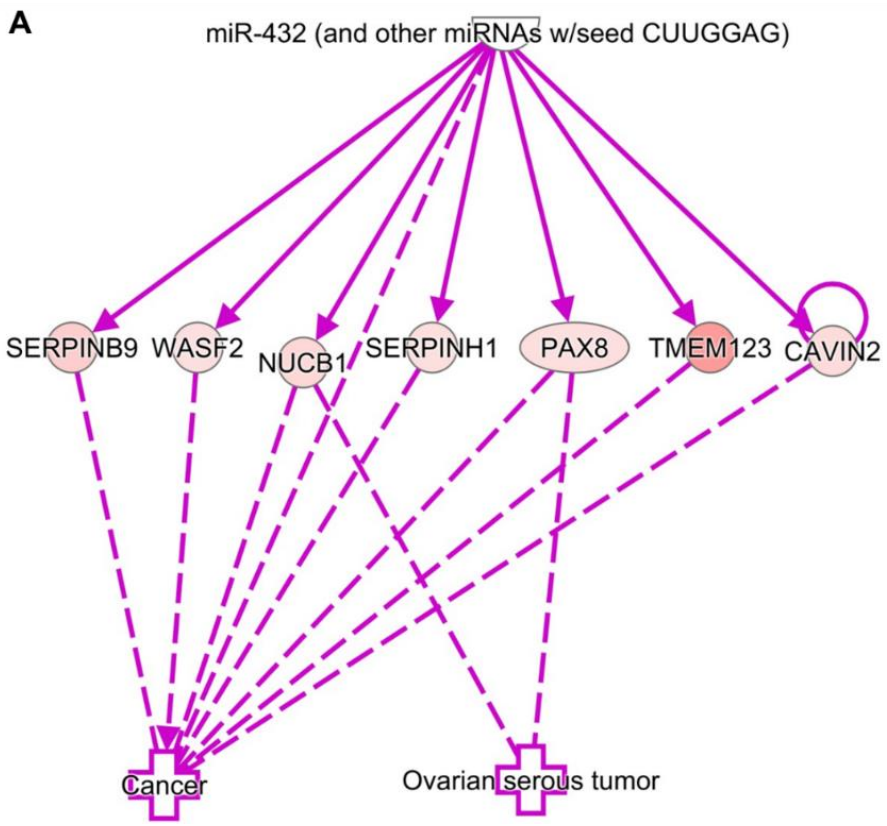

Figure 21: Protein targets of miR-138-5p, miR-432-5p, and miR-127-3p associated with gynecological cancers, predicted via IPA analysis (*Continued next page)

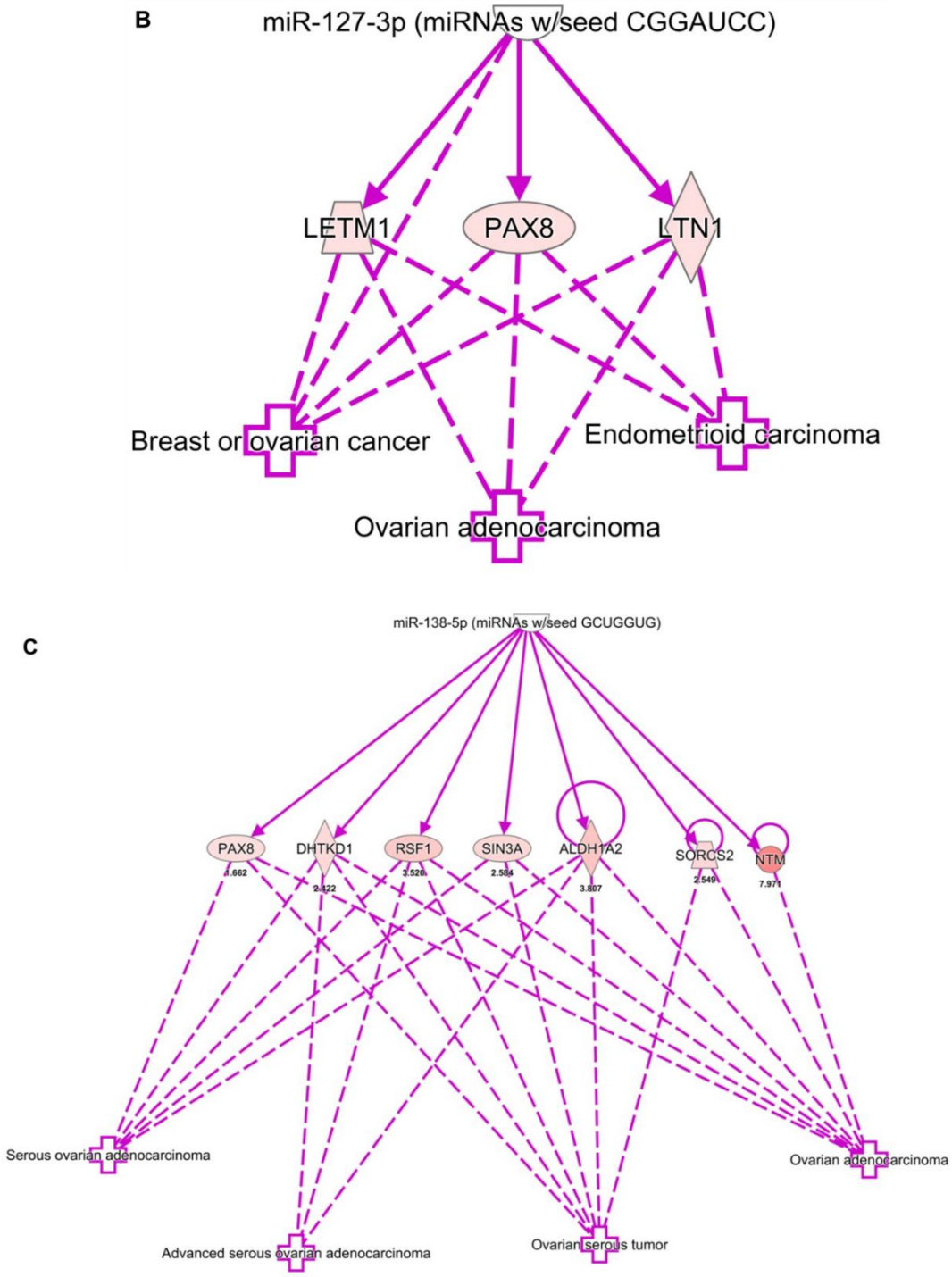

Figure 21: Protein targets of miR-138-5p, miR-432-5p, and miR-127-3p associated with gynecological cancers, predicted via IPA analysis (*Continued next page)

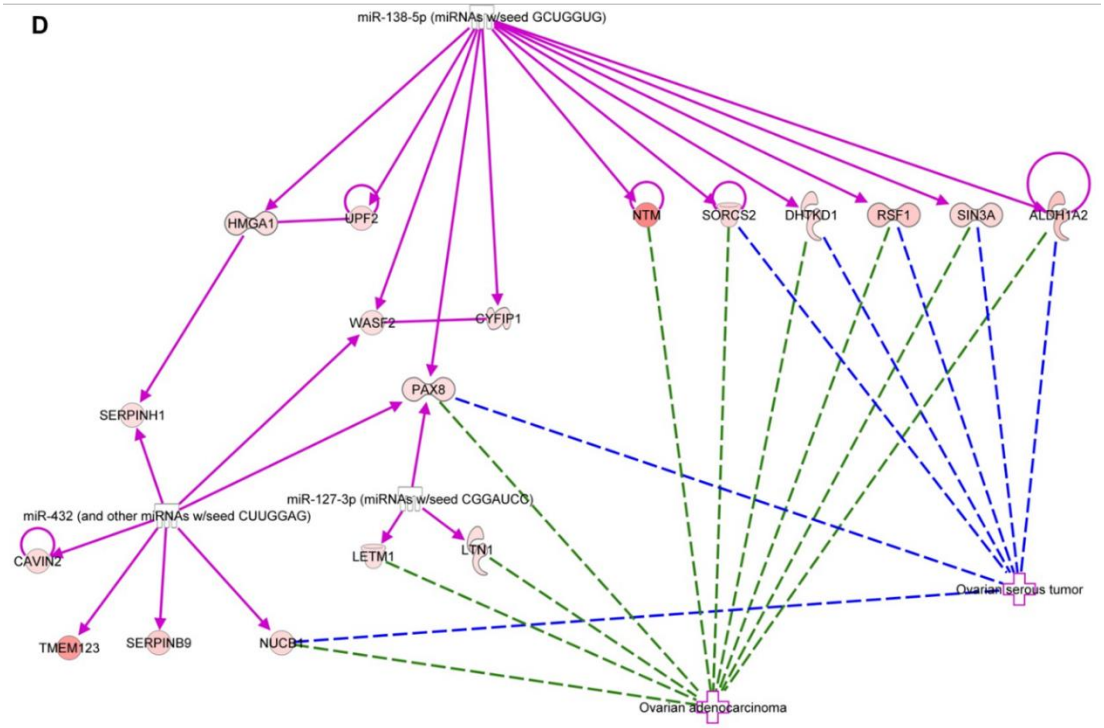

Figure 21: Protein targets of miR-138-5p, miR-432-5p, and miR-127-3p associated with gynecological cancers, predicted via IPA analysis

Protein targets of miR-138-5p, miR-432-5p, and miR-127-3p associated with gynecological cancers, predicted via IPA analysis. In co-relation with ovarian serous tumors, (a) 7 targets identified for miR-432 analysis and in correlation with gynecological malignancies, (b) 3 targets identified for miR-127-3p and (c) 7 targets for miR-138-5p analysis. (d) Combined target network analysis of miR-432, miR-127-3p and miR-138-5p in relation to their association with ovarian carcinoma revealed PAX8 as a common target of all three miRNAs

exposed FT194 cells could antagonize the FAC-induced increase in cell numbers, as previously reported [19]. Validation of miRNA overexpression for miR-432-5p, miR-127-3p, and miR-138-5p was performed by real-time PCR (Fig. 28A and 29A). Cell counting identified reduced numbers of cells in the chronic iron-exposed FT194 cells, with statistical significance following miR-432-5p expression ($p \leq 0.05$), relative to the parental FAC-exposed FT194 cell line (Fig. 29B).

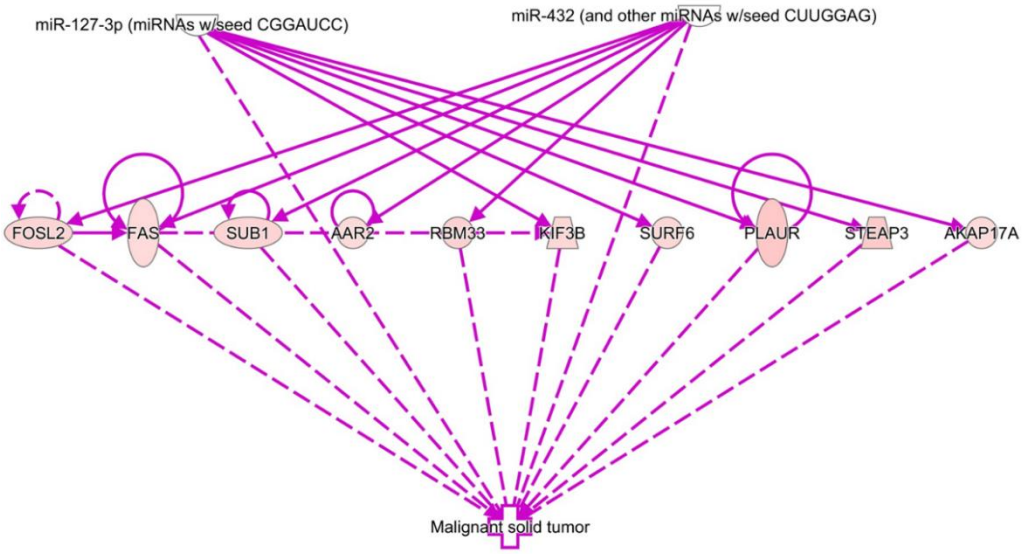

Figure 22: Protein targets of miR-127-3p and miR-432-5p, associated with malignant solid tumors, predicted via IPA analysis

IPA analysis identified 10 upregulated proteins predicted to be downstream of either miR-432-5p (5 proteins) or miR-127-3p (5 proteins) in FT194-OCV cells relative to FT194-CV and associated with malignant solid tumors.

Discussion

Iron is an important dietary component that is critical in maintenance of various cellular functions; however, it elicits activity as a mutagenic factor through its participation in Fenton reactions whereby it is involved in generating ROS that may promote DNA damage such as oxidation of DNA bases [172]. In this manner, iron may contribute to the pathophysiology of cancer. Deregulated iron levels and expression of key mediators of iron metabolism are established features of multiple tumors[178] including an established tumor “addiction” to iron [175]. Indeed, multiple studies have linked the exposure to supraphysiological levels of iron with an increased incidence of cancer including renal tumor formation in a rat model exposed to ferric nitrilotriacetate [367], iron overload patients (e.g., hemochromatosis) with an increased risk of developing liver

tumors [367, 368]. On the other hand, dietary iron (in excess) can enhance tumor formation in mice harboring abnormalities in Adenomatous polyposis coli (APC) whereas iron chelation could hinder tumor development [369]. Collectively, these reports implicate the potential tumor promoting activities of iron in various experimental systems.

Although a recent report identified that chronic iron exposure in human pancreatic ductal epithelial cell line supported epithelial-mesenchymal transition (EMT) and tumorigenesis through a p53-dependent mechanism [370], the role of chronic iron overload in ovarian cancer initiation by mediating transformation of fallopian tube secretory epithelial precursor cells (FTSECs) remains unclear [371]. Iron sources in the pelvic cavity has been suggested to originate from ovulation, retrograde menstrual reflux, and the rupture of follicles [372-374]; furthermore, a link between hemochromatosis and ovarian cancer has been reported [176]. However, there is currently limiting data regarding the contribution of iron to high grade serous ovarian tumor initiation. Recently, we reported that long-term FAC exposure (at 250 nM) to FTSECs leads to cellular changes that are reminiscent of those identified in HGSOC including alterations in EVI1,

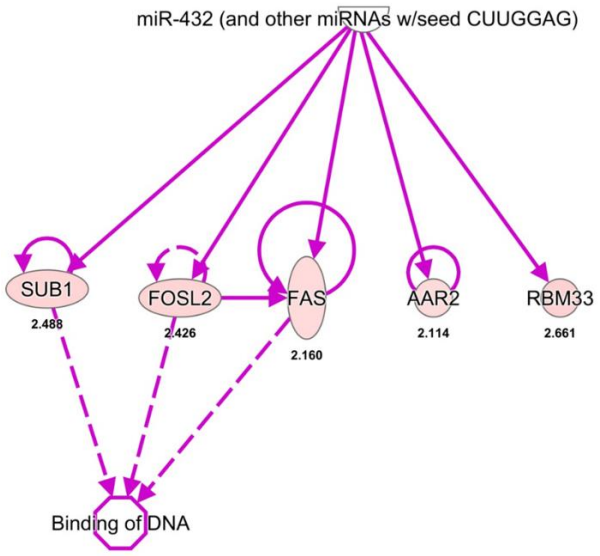

Figure 23: Protein targets of miR-432-5p, associated with binding of DNA, predicted via IPA analysis (*Continued on next page)

Figure 23: Protein targets of miR-432-5p, associated with binding of DNA, predicted via IPA analysis

IPA analysis identified 5 upregulated proteins predicted to be downstream of miR-432-5p in FT194-OCV cells relative to FT194-CV. Of these, three were associated with binding of DNA. FTSECs. iron-exposed and transformed FTSECs.

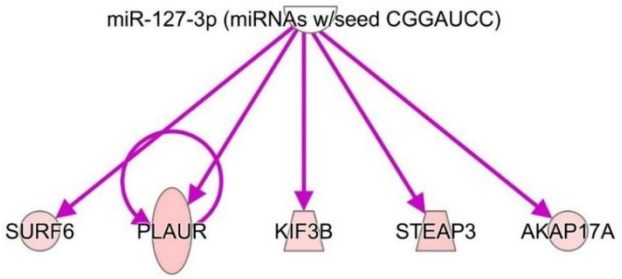

Figure 24: Protein targets of miR-127-3p, associated with binding of DNA, predicted via IPA analysis

IPA analysis identified 5 upregulated proteins predicted to be downstream of miR-127-3p in FT194-OCV cells relative to FT194-CV. Of these, three were associated with binding of DNA.

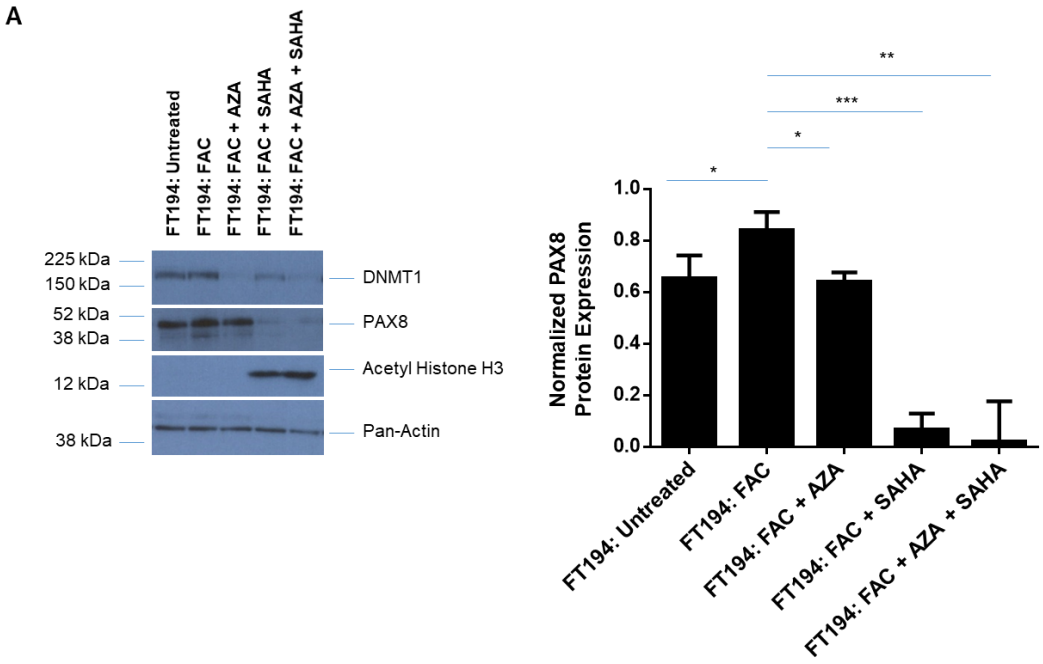

Figure 25: miR-432-5p, miR-127-3p, and miR-138-5p are epigenetically regulated by FAC (*Continued on next page)

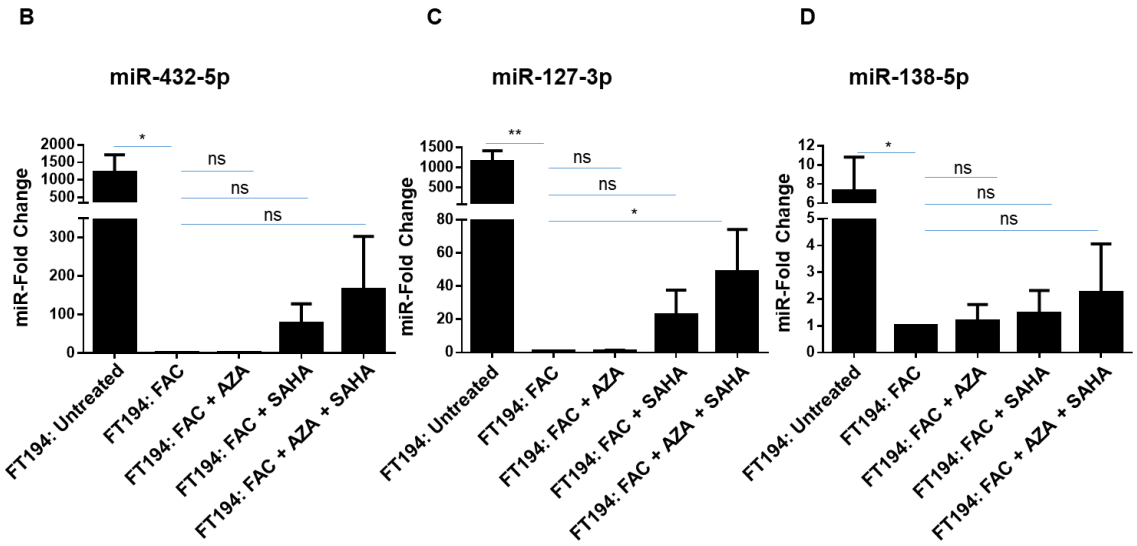

Figure 25: miR-432-5p, miR-127-3p, and miR-138-5p are epigenetically regulated by FAC
(A) Western Blotting analysis of 250 nM FAC-exposed FT194 cells treated with 1 µM AZA and/or 10 µM SAHA for 24 hours, using cell lysates collected at days 129, 134 and 137 of FAC treatment (p=38 and 39). Three independent replicates were performed; representative cropped blots and the densitometric analysis for PAX8 are displayed. Real-time PCR analyses of (B) miR-432-5p, (C) miR-127-3p, and (D) miR-138-5p in 250nM FAC-exposed FT194 cells treated with 1 µM AZA and/or 10 µM SAHA for 24 hours. The data shown represents the composite of three independent experiments. RNU6B was used as a reference control.

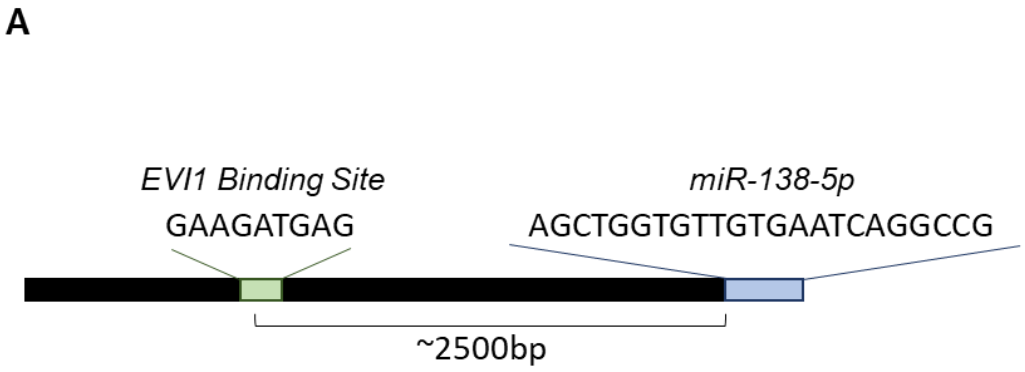

Figure 26: EVI1 knockdown does not alter miR-138-5p expression level (*Continued on next page)

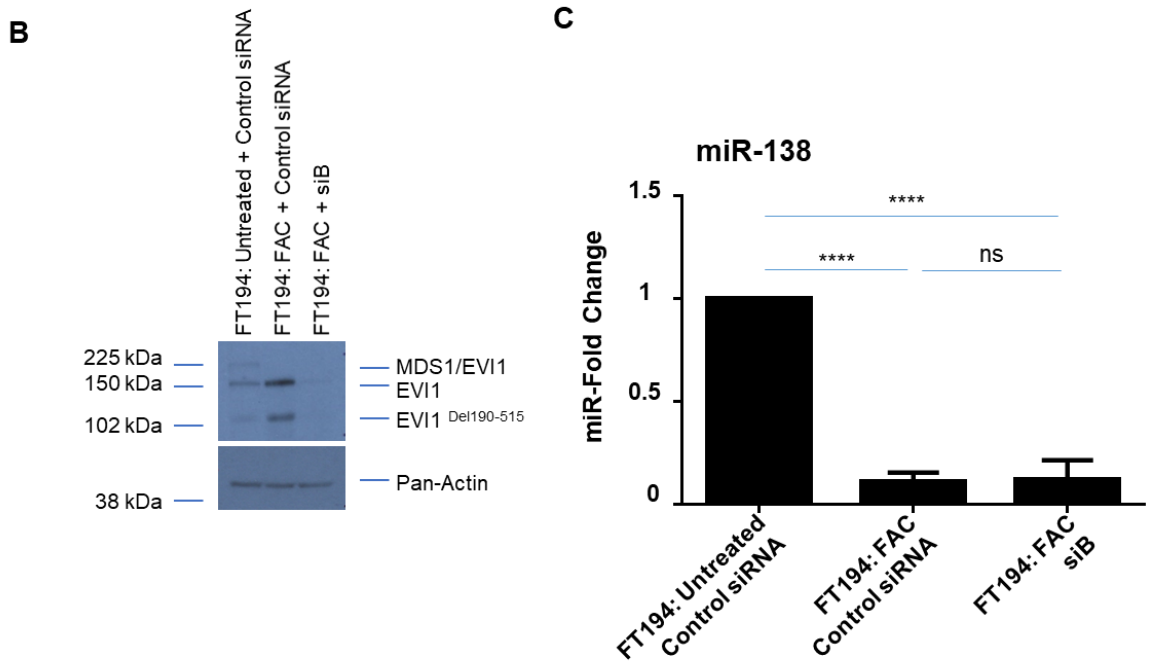

Figure 26: EVI1 knockdown does not alter miR-138-5p expression level

(A) Schematic representing the predicted EVI1 binding site upstream from miR-138-5p. EVI1 splice variants were reduced in FAC-treated FT194 cells using siRNA (siB) in FAC-treated cells. Cell lysates and miRNAs were collected at days 125 and 128 of FAC treatment (p=37 and 38). (B) Western blotting was performed to validate the knockdown. Three independent experiments were completed, and a representative blot is shown. (C) Real-time PCR of miR-138-5p was performed using RNU6B as a reference control. The data represents the composite of three independent experiments.

```
alignment position              2521...... 2531...... 2541...... 2551...... 2561...... 2571...... 2581......

Promoter_miR-138         2521   tagcctagag tcagGAAGAT GAGttaagag gtctgacagt ctattgaagt aaaattattc attacagaat
EVI1_N-term_Zn_Finger_BD    4   ---------- -----AAGAT A--------- ---------- ---------- ---------- ----------
EVI1_C-term_Zn_Finger_BD    1   ---------- ----GAAGAT GAG------- ---------- ---------- ---------- ----------
EVI1_Consensus              5   ---------- -----AAGAT Aa-------- ---------- ---------- ---------- ----------
```

Figure 27: Prediction of EVI1 binding with miR-138-5p, using Dialign Genomatrix 49 software

The genomic sequence (5000bp upstream) of the promoter region of miR-138-50 5p-1 (located at 3p21.32) was obtained from the UCSC Genome Browser (www.genome.ucsc.edu, Human Dec. 2013 (GRCh38/hg38 Assembly). The EVI1 N-terminal Zinc-finger binding, C-terminal Zinc-

finger binding and consensus sequences were previously published. Prediction of EVI1 binding with miR-138-5p-1 promoter region was completed by aligning the sequences using Genomatix software suite (version 3.11, http://www.genomatix.de/cgi-bin/dialign/dialign.pl), and the aligned region is presented.

β-catenin, and c-Myc protein expression, together with functional changes including increased cell numbers and migratory potential [19]. The work reported herein extends these findings to uncover miRNA and protein level changes under these chronic iron exposure conditions in Further, it is well recognized that aberrant expression of miRNAs is a characteristic of ovarian tumors with potential to serve as biomarkers and/or aid as potential diagnostic tools[282, 375, 376]; however, the contribution of iron in altering their expression has not yet been reported in precursors to ovarian tumors.

Thus, to comprehensively assess the iron-induced molecular changes in FTSECs, we performed an integrated miRNA and protein analysis approach in chronic iron-exposed and transformed FTSECs. To our knowledge, this is the first study to utilize a multi-omics approach to assess miRNA and protein level changes in FAC-exposed and transformed FTSECs. Herein, we have identified a subset of dysregulated miRNAs along with their corresponding protein targets via our integrated experimental approach following chronic iron exposure in FTSECs. Furthermore, we identified that several miRNAs were epigenetically dysregulated which may therefore be potentially associated with the transformative-like alterations observed in FTSECs [19]. Fig. 30 displays a proposed model of the findings presented herein.

Analyses of oncogenetically transformed FTSECs (which harbors p53 inactivation, c-Myc^{T58A} mutant, and H-Ras^{V12A} mutant) revealed a higher number of altered miRNAs and protein targets relative to long-term iron exposed cells (see Fig. 18C and 18D). This suggests that these OCV cells are likely to be more extensively transformed than FAC-treated cells. This is not surprising since iron may only be one of many contributing factors mediating tumorigenesis.

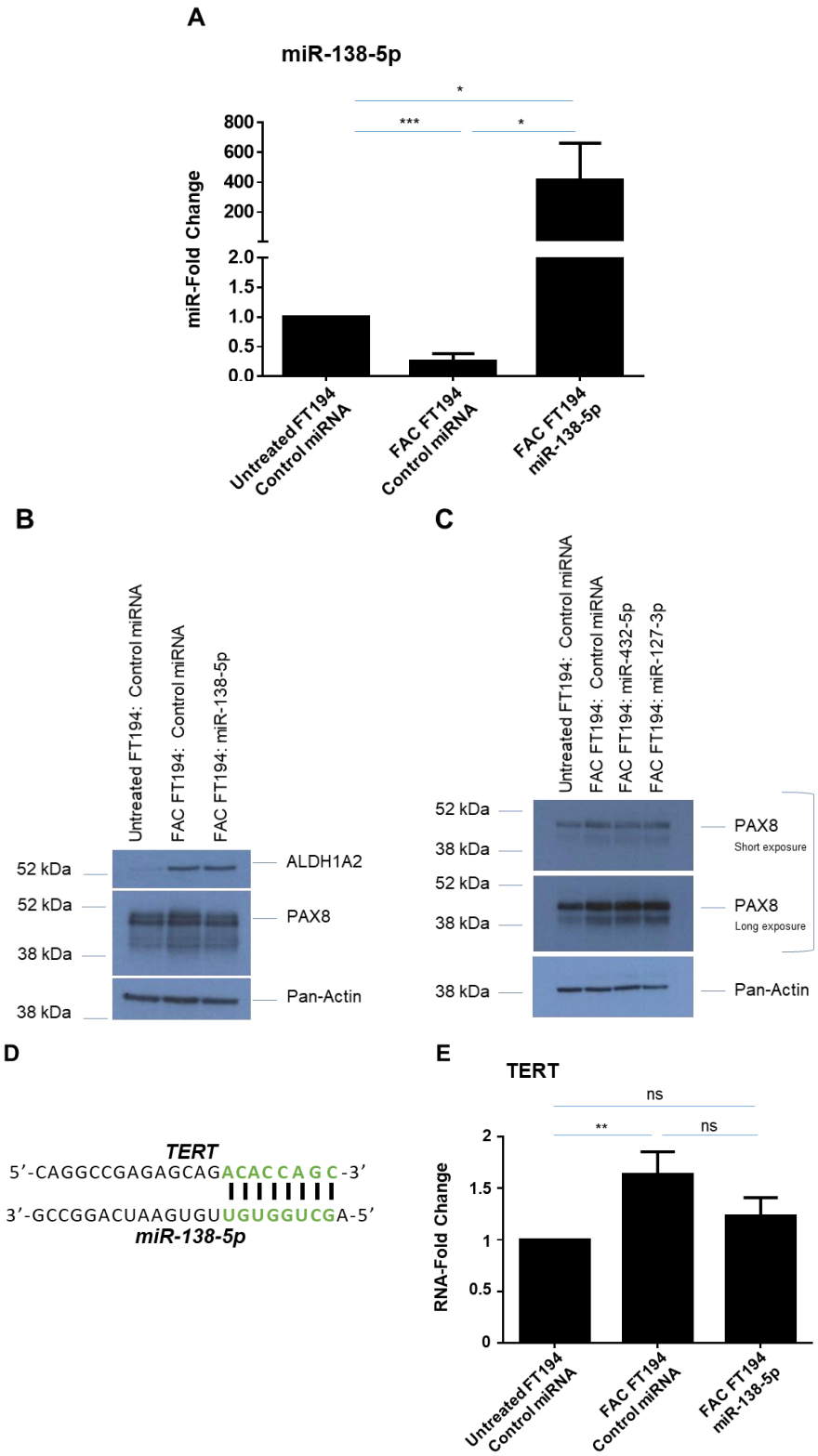

Figure 28: miR-138-5p overexpression partially regulates stem cell marker hTERT transcript levels but does not alter another stem cell marker ALDH1A2 (*Continued next page)

Figure 28: miR-138-5p overexpression partially regulates stem cell marker hTERT transcript levels but does not alter another stem cell marker ALDH1A2

(A) Real-time PCR analysis of miR-138-5p after isolating total miRNAs from miR-138-5p transfected 250 nM FAC-treated cells relative to control transfected FAC-treated and Untreated FT194 cells, at days 122, 125 and 129 of FAC treatment (p=35, 36, and 37) to validate the overexpression. (B) Western blotting was performed for cell lysates collected from miR-138-5p transfected and control transfected Untreated and FAC-treated FT194 cells to analyze ALDH1A2 levels at days 119, 122, and 126 of FAC treatment (p= 35 - 37) (C) Western blotting was performed using cell lysates collected from control or miR-432-5p or miR-127-3p, transfected Untreated and FAC-treated FT194 cells with the indicated antibodies at days 123, 131, and 137 of FAC treatment (p=35, 37, and 38). (D) The predicted miR-138-5p binding site in the TERT sequence is shown. (E) Real-time PCR analysis of TERT in miR-138-5p transfected FAC-treated FT194 cells, relative to control transfected Untreated and FAC-treated FT194 cells after isolating miRNAs at days 119, 122, and 126 of FAC treatment (p=35 - 37). The data is the composite of three independent experiments.

Indeed, profound alterations of the cellular regulatory networks may indicate the concept of “multiple events” needed to promote propagation of the tumor [377]. Our work presented herein encourages future investigations, including 3-D organoid culture and *in vivo* mouse xenografts to further explore the contribution of iron dysregulation to tumor initiation and/or the metastatic process. Two-dimensional *in vitro* culture models lack the complexity of the tumor microenvironment and thus limit physiological relevance [378]. Although murine models have been developed to investigate HGSOC pathophysiology [379, 380], these *in vivo* model systems pose challenges in terms of studying iron derived from the reproductive organs due to a lack of menstruation in mice. Therefore, alternative strategies such as intra-bursal or intraperitoneal delivery using iron dextran may be needed. Three-dimensional organoid cultures may also provide an alternative approach to investigate the response of FTSECs to exogenous iron [381].

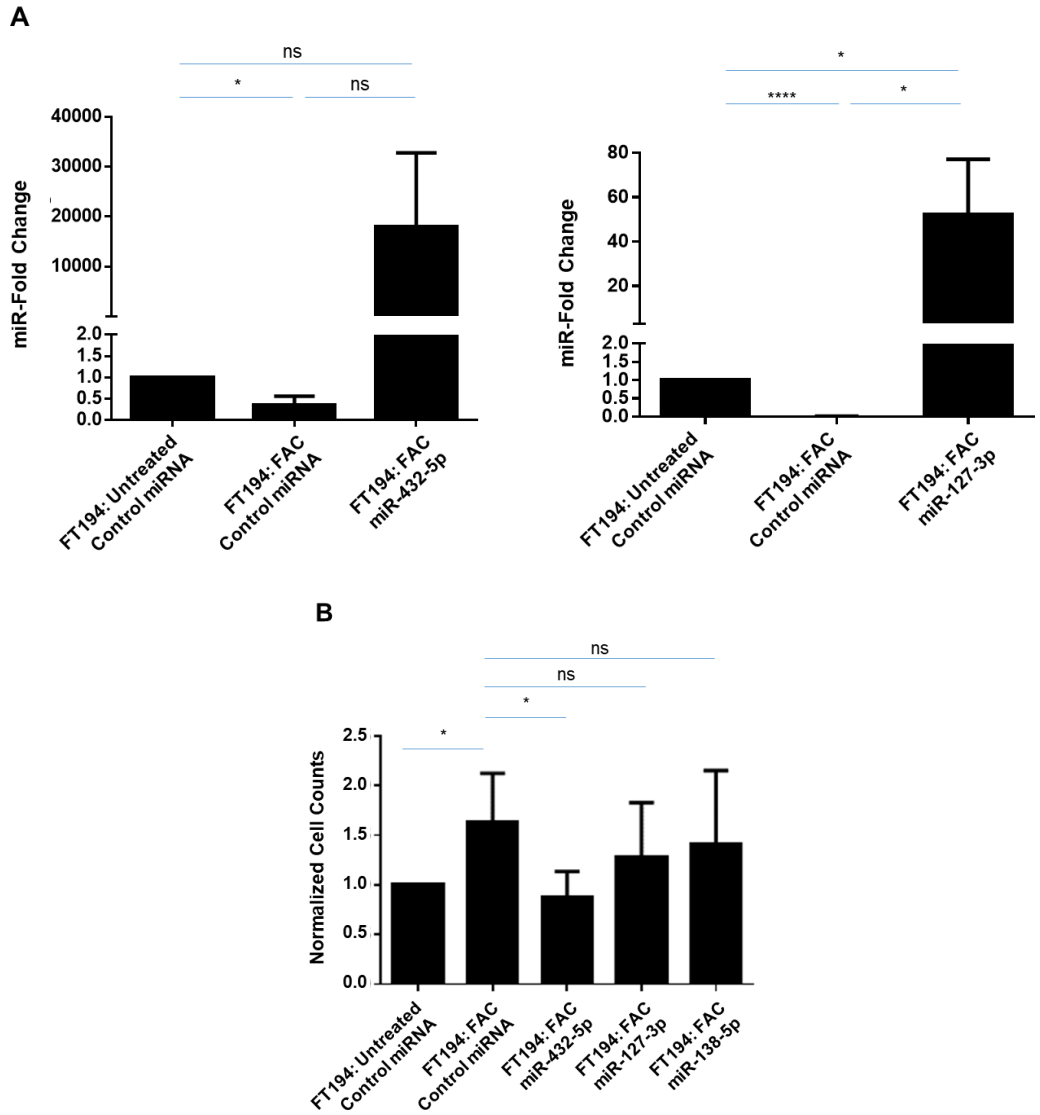

Figure 29. Overexpression of miR-432-5p, miR-127-3p and miR-138-5p in FAC-treated FT194 cells alter the cell counts and Pax8 expression level

(A) Real-time PCR of miR-432-5p and miR-127-3p was performed after isolating total miRNAs from the respective mimic-transfected 250 nM FAC-treated cells relative to the Untreated cells at days 123, 131, and 137 with FAC (p=35, 37, and 38). RNU6B was used as a reference control and the data represents a composite of three independent experiments. (B) Representation of cell counts obtained from overexpression of miR-432-5p, miR-127-3p, and miR-138-5p compared to control miRNA transfected Untreated and 250 nM FAC-treated FT194 cells. The data presented is the composite of five independent experiments.

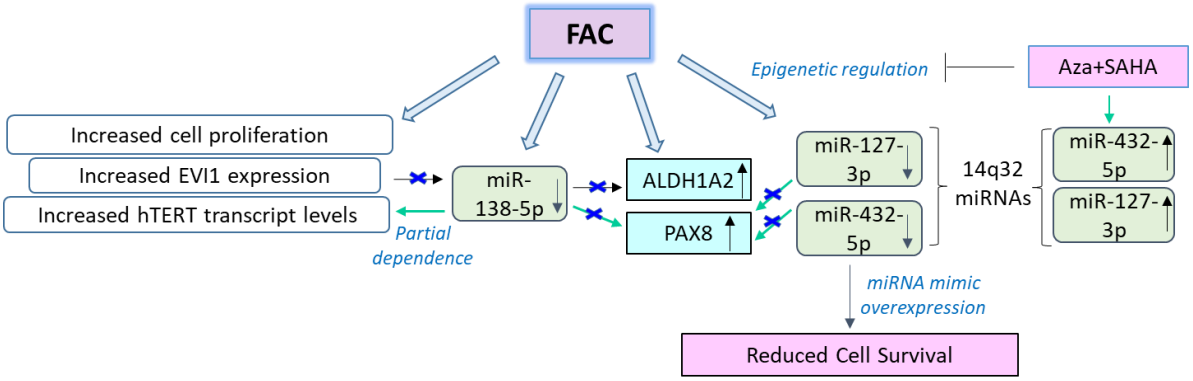

Figure 30: Proposed model for 14q32 miRNA regulation with combination of DNMT inhibition and HDAC inhibition

We previously reported that chronic iron overload contributes towards oncogenic transformative events, which potentially recapitulate early events in HGSOC transformation. Microarray analyses identified markedly reduced levels of miR-432 and miR-127 (located at 14q32) in FAC-treated FT194 cells. We propose that the FAC-induced reduction in the miRNA levels was a result of epigenetic alterations, specifically in their methylation and acetylation status. Inhibition of DNA methyltransferases (using AZA) and HDACs (using SAHA) led to a reversal of the levels of these specific miRNAs in these chronic iron exposed FTSECs. We previously reported that chronic FAC treatment of FT194 cells notably increased TERT mRNA levels[19] as well as ALDH1A2 protein (from our proteomic analyses, validated via western analysis). We now identified that overexpression of miR-138-5p (located at 3p21) could antagonize the FAC-induced TERT transcript levels; however, miR-138-5p expression did not modulate ALDH1A2 protein. The above described three miRNAs also commonly alter Pax8 protein expression, which may contribute to FAC-induced changes in FT194 cells. Green arrows denote partial regulation.

However, our initial attempts to maintain our oncogenically transformed and chronic iron exposed FTSECs in spheroid culture failed to produce spheroids (data not shown). Thus, implementation of alternative 3-D methods including hanging drop method in future studies could be implemented [382]. Interestingly, there exists literature supporting the association between iron and miRNAs. In one aspect, miRNAs can behave as iron sensors to suppress expression of proteins associated with iron regulation [228]. On the other hand, the role of iron in deregulating

miRNAs is comparatively understudied. Although cytosolic iron can regulate miRNA biogenesis by altering miRNA precursor processing [233], the role of iron-induced miRNA regulation in cancer requires further investigation. Herein, we have identified global dysregulation of miRNAs following chronic iron exposure. There is evidence implicating iron in the regulation of epigenetic control. Specifically, iron deprivation alters DNA methylation and histone deacetylation in preadipocytes [383] whereas brain iron overload reduces DNA methylation [328]. However, the specific underlying mechanism through which iron modulates these events remains to be explored. The microarray analysis presented herein, we identified 20 out of 35 miRNAs (including miR-432-5p and miR-127-3p) that were down-regulated in FAC-treated FT194 cells and also part of a large, imprinted miRNA cluster at 14q32 locus. Interestingly, there is evidence implicating epigenetic modification in the regulation of the miRNAs located within this cluster [334, 335]. miR-138-5p, although located at a different chromosomal region at chromosome 3p21, was also identified to be markedly down-regulated following iron exposure.

Current evidence supports miR-138-5p as a tumor suppressor in various cancer types [357, 384-386]. This locus harbors a tumor suppressor gene cluster comprised of 8 genes within a ~120Kb spanning region [387] whose expression can be regulated epigenetically [388]. Besides miR-138-5p, 4 miRNAs (miR-135a-1, miR-let-7g, miR-1226, miR-564) out of total 16 miRNAs at this locus have been reported to perform tumor suppressive functions in various cancers [389-393]. Furthermore, upregulation of six miRNAs has been identified in different cancer types, including miR-4271 [394], miR-191 [395-397], miR-425 [330, 398, 399], miR-4793 [71], miR-2115 [400], and miR-4443 [401], suggesting potential oncogenic functions in these cancers.

The miR-138-5p down-regulation was partially reversed via inhibition of methylation and histone deacetylases, suggesting that iron can regulate miRNA expression by mediating epigenetic changes in FTSECs. Out of the 15 miRNAs (from a total of 35 miRNAs) identified from the integrated microarray analysis (see Table 1) that are not located at 14q32, 9 are reported to be epigenetically regulated (miR-34a [302, 402], miR-145 [403], miR-182 [404], miR-31 [405],

miR-708 [406], miR-34c [407], miR-125b [408], miR-615 [409], and miR-17 [410]). Similarly, miR-17, which is a part of the 17-92 miRNA cluster located at chromosome 13q31, can also be regulated by epigenetic mechanisms [410]. We also identified 5 miRNAs at chromosome 19q13 to be altered in OCV transformed FT194 cells (relative to CV) via proteomics analysis. Notably, chromosome 19 contains a large imprinted miRNA cluster comprising 46 miRNAs, which can also be regulated via epigenetic mechanisms [411, 412]. Collectively, our miRNA analyses have verified epigenetic regulation as a common mechanism underlying miRNA expression, which is also supported by literature for miRNA cluster regulation at different loci in the human genome.

As shown in Fig. 25B, inhibition of methylation and histone deacetylation rescued the levels of miR-432-5p and miR-127-3p in chronic iron exposed FTSECs. This suggests that iron may regulate the activities of epigenetic regulators. There is also evidence that differential miRNA regulation may occur within this locus as independent miRNA regulation of 14q32 at unique miRNA promoters by nuclear receptors may be responsible [226], although there is also evidence supporting transcription of this miRNA cluster as a polycistronic transcript [204]. Since we observed differential expression of 14q32 miRNAs via our microarray analysis, this may implicate independent regulatory mechanisms for multiple miRNAs within this region.

PAX8 (a member of paired box PAX gene family) is a positive marker of FTSECs[168] and is elevated in a variety of tumors [358-363]. Our prior findings demonstrated that PAX8 was upregulated following chronic iron exposure [19]; we now validate this observation and further show that it is epigenetically regulated, also supported by prior literature[330]. Furthermore, PAX8 appears to be a common target of miR-432-5p, miR-127-3p, and miR-138-5p via the IPA analyses; target analyses using bioinformatic programs (Targetscan, miRDB, miRNA.org, miRpath v.3 and miRmap) identified PAX8 to be a target of the aforementioned miRNAs in a subset of these databases (data not shown). However, western blot analyses did not identify any marked changes in PAX8 protein expression in FTSECs upon overexpression of these miRNAs.

Table 9: Top protein targets in FAC-exposed relative to Untreated FT194 cells

Protein Target	***Alias***	***Chromosomal Location***	***Fold-Change (Welch's T-test LFQ intensity F v U)***	***UniProtKB/Swiss-Prot Summary***
ARHGAP12	Activating Protein 12	10p11.22	11.77340121	a member of a large family of proteins that activate Rho-type GTP metabolizing enzymes
ARHGDIB	Dissociation	12p12.3	0.086813615	the Rho proteins
ARRB1	Arrestin Beta 1	11q13.4	5.124634149	protein coupled receptor signaling by mediating both receptor desensitization and resensitization processes
BST1	Stromal Cell Antigen 1	4p15.32	6.122146871	ribose and nicotinate-adenine dinucleotide phosphoate
CELF2	CUGBP Elav-like Family Member 2	10p14	13.84767274	RNA-binding protein implicated in the regulation of several post-transcriptional events
COL5A1	Collagen Type V Alpha 1 Chain	9q34.3	0.112864701	Type V collagen is a member of group I collagen (fibrillar forming collagen)
CRABP2	Acid Binding	1q23.1	0.09458846	Transports retinoic acid to the nucleus
CRYAB	Crystallin Alpha B	11q23.1	17.53439428	refractive index of the lens
DECR2	2,4-Dienoyl-CoA Reductase 2	16p13.3	9.463406179	fatty enoyl-CoA esters having double bonds in both even- and odd-numbers positions in peroxisome
FAM171A1	Sequence Similarity 171	10p13	6.197873721	dynamics/plays a role in actin stress fiber formation
FDXR	Ferredoxin Reductase	17q25.1	4.595277	Serves as the first electron transfer protein in all the mitochondrial P450 systems
IDI1	Isopentenyl-Diphosphate Delta Isomerase 1	10p15.3	0.156436427	homoallylic substrate isopentenyl to its highly eletrophilic allylic isomer, dimethylallyl diphosphate
INA	Neuronal Intermediate	10q24.33	7.346539312	assemble and is involved in the morphogenesis of neurons.
ITGA2	Integrin Subunit Alpha 2	5q11.2	16.44875121	collagen, collagen C-propeptides, fibronectin, and E-cadherin
KIN	RNA Binding	10p14	11.27786487	response to DNA damage
MASTL	Associated Serine/Threonine	10p12.1	6.20270082	M phase by acting as a regulator of mitosis entry and maintenance'\
NMT2	myristoyltransferase 2	10p13	4.073197008	Adds a myristoyl group to the N-terkinal glycine residue of certain cellular and viral proteins
NTM	Neurotrimin	11q25	7.970555423	Neural cell adhesion molecule
PAAF1	ATPase Associated Factor	11q13.4	4.390010657	proteolytic activity by impairing the association of the 19S regulatiry complex with the 20S core
PATL1	Processing Body mRNA Decay	11q12.1	5.037787567	dependent decapping of mRNAs, leading to the degradation of mRNAs.
RBP1	Protein 1	3q23	0.072160245	Cytoplasmic retinol-binding protein
ROCK1	Coiled-Coil Containing Protein	18q11.1	7.346539312	Rho-kinases are serine/threonine kinases activated by RhoA GTPases
SEC14L2	SEC14 Like Lipid Binding 2	22q12.2	0.10067807	molecular and promotes their transfer between the different cellular sites
SLC1A4	Family 1 Member 4	2p14	0.235645725	threonine
TGFBI	Transforming Growth Factor Beta 1	19q13.2	0.113836913	differentation of various cell types and is invovled in various processes such as normal development, immune function, microglia function, and responses to neurodegeneration
TMEM123	Transmembrane Protein 123	11q22.2	6.71872719	Implicated in oncotic cell death, characterized by cell swelling, organelle swelling, vacuolization, and increased membrane permeability
TPK1	Pyrophosphokinas	7q35	4.34870065	thiamine pyrophosphate
TUBB4A	Class Iva	19p13.3	4.021247785	Tubulin is the major constituent of microtubules.

Note: $p < 0.05$ and z-value >1.

Future studies are needed to experimentally validate whether PAX8 is a target of these miRNAs.

Our earlier findings demonstrated that long-term iron exposure in FTSECs leads to altered expression of EVI1 variants [19]. Although we identified an EVI1 binding site within the promoter region of miR-138-5p through our bioinformatics analysis (see Fig. 27), EVI1 knockdown did not alter miR-138-5p levels implicating the involvement of other regulatory mechanisms.

The stem cell marker, ALDH1A2 [349, 413, 414] is reported to be a direct target of miR-138-5p, as identified via a proteomics screen in zebrafish embryos [353] but as of yet has not been confirmed in humans. As shown in Fig. 28B, overexpression of miR-138-5p in iron exposed FTSECs did not result in an alteration in ALDH1A2 expression; thus, this suggests that ALDH1A2 is not regulated by miR-138-5p in FTSECs. However, another stem cell marker TERT [355, 356], which has already been demonstrated to directly regulate miR-138-5p [344, 357], appears to be at least partially regulated by miR-138-5p (see Fig. 28D).

Although the quantitation accuracy of both the miRNA transcriptomic and proteomic datasets was validated through orthogonal methods such as qPCR and western blot analysis of selected targets, the miRNA target filtering through IPA is based on previously experimentally determined interactions or computational prediction (e.g., TargetScan). Potential regulatory miRNAs will need to be validated in future studies based on the expression pairing of miRNAs and proteins relevant to specific cancer-related pathways identified in our high-confidence transcriptomic and proteomic datasets. Further improvement can also be made in the proteomics-based methodology, which includes fractionation of the proteome and application of DIA approaches to enhance proteome coverage. In addition to deeper proteome coverage to reveal further differentially expressed proteins, global-scale phosphoproteomic analysis can be employed to identify altered signaling pathways, collectively providing detailed global-scale insight into changes of the molecular landscape associated with iron exposure and oncogenenic mechanisms in FTSECs.

Conclusion

Overall, the methodological approach utilized herein served to identify miRNAs and protein targets associated with long-term FAC treatment in FT194 cells. To our knowledge, this is the first study elucidating a comprehensive set of alterations at the miRNA and protein levels in chronic iron exposed FTSECs, which may identify pathways that may contribute to increased tumorigenic potential. In future studies, epigenetic mapping of chronic iron-exposed cells could be performed to further our understanding of the changes induced by long term iron treatment in fallopian tube precursors.

Data availability

The mass spectrometry proteomics data have been deposited to the Proteome Xchange Consortium via the PRIDE28 partner repository with the dataset identifier PXD018416. The RNA microarray data have been deposited to the Gene Expression Omnibus with the dataset identifier GSE150622.

Acknowledgements

This work was supported by funding from the National Cancer Institute: R21 CA178468 (to M.N.) and R03 CA212696 (to M.N.).

Author contributions

R.C. performed experiments, performed data analyses, wrote manuscript, and prepared figures. S.R. performed miRNA/Proteomics IPA analyses, wrote manuscript, and prepared figures. J.G. performed database searches, statistical analysis, bioinformatics [282], and reviewed final manuscript. R.H. performed miRNA array and analysis as well as reviewed final manuscript. O.W.N. performed sample processing, MS analysis, and reviewed final manuscript. S.M.S. Jr.

performed proteomics analysis, assisted with IPA, and wrote manuscript. M.N. conceived project, directed project, supervised project, performed experiments, directed, and performed data analyses, wrote manuscript, and prepared figures.

Chapter 5

Future Perspectives and Significance of the Study

Overview of the Major Conclusions

Tumor microenvironment is characterized by vast molecular and genomic alterations [415]. Due to the limited understanding and sub-optimal treatment regimens of different cancer types, it is imperative to identify the contributing factors. The work presented in this dissertation focuses on analyzing the changes occurring at cellular and molecular levels to study the pathophysiology of renal cancer chemoresistance towards Temsirolimus (TEMS) mediated by Lysophosphatidic acid (LPA), and miRNA alterations involved in iron-induced transformative events in the fallopian tube secretory epithelial cells.

In *Chapter 3*, we analyzed the effect of LPA in reversing the chemoresistance of ccRCC towards the mTOR inhibitor TEMS, which is an FDA approved drug. The role of LPA in promoting invasion and metastasis via Arf6 based mesenchymal pathway activation [136] and by inducing resistance towards the tyrosine kinase inhibitor, Sunitinib [135] had been previously described. However, the novel mechanistic aspect of LPA-induced lipid droplets and mitochondrial alterations possibly leading to sub-optimal efficacy of TEMS in ccRCC is described in this thesis. We compared the molecular alterations in four renal cell lines, including immortalized human kidney cell line (HK-2) and three ccRCC cell lines (769-P, 786-O, and A-498 associated with VHL mutations and varying genomic aberrations). We determined the variability in baseline and post-TEMS treatment levels in AKT/mTOR pathway markers, as hyperactivation of this pathway is one

of the common aberrations found in ccRCC patients [416]. Since ccRCC is a metabolic disease associated with accumulation of lipid droplets [114], which interact with mitochondria for production of energy [3], we also analyzed the levels of LDs, markers involved in LD biogenesis and mitochondrial network alterations in all four renal cell lines. We noticed that cells also reduced the size of LDs, increased LD abundance and hyperfuse mitochondrial networks to increase the usage and conservation of energy, conferring resistance against TEMS treatment [417]. TEMS also reduced the cellular viability in ccRCC cells, as expected [417]. When TEMS was used in combination with Hydroxychloroquine (HCQ), the autophagic flux inhibitor, LDs were found to be sequestered in autophagosomal compartments and ccRCC cellular viability was further reduced [417]. This confirmed the increased efficacy of TEMS in combination with HCQ, which has also been reported previously in a phase I clinical trial [94]. Additionally, this suggested that HCQ can dominate over the effect of TEMS-induced LD alterations.

Further, when cells were treated with a combination of TEMS and LPA, TEMS-induced molecular alterations were found to be reversed by the LPA treatment *in vitro* [417]. LPA treatment increased cellular viability in a MAPK-dependent manner in HK-2 cells and post-combinatorial treatment of TEMS and LPA, there were larger, more abundant LDs and mitochondrial networks which were found to be more fragmented in all ccRCC cells. This suggested the role of LPA in antagonizing cellular response to TEMS in renal cancer, potentially contributing to the chemoresistance [417].

Additionally, genetic aberrations also play a major role in cancer development and aggressiveness in ccRCC patients. More commonly, chromosomal arm-level aberrations have been reported [37, 418], such as loss of 3p associated with VHL inactivation (which is an obligate event in ccRCC), gain of 5q [54], and loss of 14q [37]. Interestingly, the miRNA cluster located at chromosome 14q32 is reported to be epigenetically regulated in mice (corresponds to chromosome 12F1 in mice) [204, 292] and is dysregulated in a variety of tumor types [72, 206, 215, 223, 224, 237, 290, 291, 320, 419]. Loss of heterozygosity at chromosome 14q was reported

to be associated with 49% of the 67 ovarian cancer tumors studied representing different stages, grades and sub-types [316] and eight miRNAs located at 14q32 miRNA cluster were identified to possess potential tumor suppressive functions in epithelial ovarian cancer [420], suggesting substantial contribution of this region in OVCA pathophysiology. We focused on analyzing the specific 14q32 miRNAs and their role in ovarian cancer initiation in chronic iron exposed fallopian tube secretory epithelial cells (FTSECs) in *Chapter 4*. In this chapter, we applied a multi-omics approach to examine the global protein-level alterations via Mass-spectrometry based proteomics and miRNA alterations via microarray analysis in FT194-FTSECs which were treated with 250nM ferric ammonium citrate (FAC), a non-transferrin bound iron form, for a period of >60 days. To analyze the association between these analyses, we integrated them to derive a list of miRNAs with more than two-fold change as well as direct protein targets corresponding with the miRNA alterations in FAC-FTSECs compared to Untreated [421]. Twenty out of thirty-five miRNAs were located at 14q32 locus, including the miRNAs with highest fold reduction, i.e., miR-127-3p and miR-432-5p. Additionally, another miRNA, i.e., miR-138-5p located at chromosome 3p21, was analyzed because of the potential EVI1 binding site in the promoter region of this miRNA [421]. Since EVI1 is altered in FAC-FT194 cells [19], we hypothesized that this FAC-induced alteration is miR-138 dependent. However, when EVI1 was knocked down, there was no change in miR-138 levels indicating existence of an alternate mechanism. Since 14q32 miRNA locus is epigenetically regulated [72, 223, 292, 419], we analyzed the effect of DNA methyltransferase inhibitor (AZA) and Histone deacetylase inhibitor (SAHA) on FAC-FTSECs and observed that FAC-induced reduction in miRNAs (miR-127, miR-432 and miR-138) was partially reversed with the combinatorial treatment of AZA and SAHA, suggesting that FAC possibly downregulates 14q32 miRNAs via epigenetic alterations[421]. Additionally, FAC-induced increase in hTERT mRNA levels were found to be partially reversed with miR-138 mimic transfection. FAC-induced increase in cell survival in FT194 cells was also partially reversed when miRNA mimics were overexpressed, specifically the effect was statistically significant with miR-432 overexpression

[421]. Overall, we found that 14q32 miRNAs may have a potential tumor suppressive role *in vitro* in FTSECs and these miRNAs can be epigenetically downregulated by chronic iron treatment. This can potentially contribute to the transformative features in FTSECs, ultimately leading to development of HGSOC characteristics [421].

Chapter 3 and 4: Limitations of the Studies

In *Chapter 3*, our data supported the role of LPA in mediating chemoresistance towards TEMS [417], however, we acknowledge that being an *in vitro* analysis, the findings must be carefully interpreted, and further investigation would be required via organoid cell culture in 3D [9, 422] or through *in vivo* studies, recapitulating the tumor microenvironment. Although we used 3 different ccRCC cell lines, the data cannot be generalized to all ccRCC cells and comparison with a primary renal proximal tubule cell line instead of immortalized cells (such as HK-2) could be considered. Within individual cell-based assays, the number of markers analyzed were limited, and further investigation would be required for large scale characterization of lipid and mitochondrial alterations.

In *Chapter 4*, although we identified Pax8 to be a common protein target of miR-432, miR-127 and miR-138 via proteomics and bioinformatics analyses, the protein expression of Pax8 was not changed as identified via western analysis [421]; further experimentation would be required to determine whether these miRNAs interact directly with PAX8 to regulate its expression. Additionally, ALDH1A2 was identified as a target of miR-138 via proteomics, but this data could not be validated experimentally. Potential reason for this discrepancy could be due to variability in protein expression across different study models as reported in literature, such as ALDH1A2 was identified as a direct target of miR-138 in zebrafish embryos [353], but was not identified in our study in human FTSECs [421]. We also acknowledge that the large-scale score filtering criteria of Mass-spectrometry based proteomics and Gene Chip microarray can also lead to potential false positives [423, 424]. Although these quantitative methods are sensitive and allows

large number of parallel analyses, we must consider that matching and scoring of large data sets can be specific to certain search engines/platforms optimized to particular instruments, which may differ from other algorithms and scoring systems [425]. We also focused on only 3 miRNAs for investigation, as mentioned above. miR-432 and miR-127 were the two most downregulated out of total 20 identified 14q32 miRNAs altered with chronic iron treatment in FTSECs [421]. Since miRNAs are present in the form of sub-clusters at this locus (as shown in figure 31), it is possible that many of these miRNAs work synchronously to mediate the iron-induced alterations, which requires further investigation.

14q32 miRNAs in cancer

Existing evidence and Implications

Genomically imprinted region on chromosome 14 is ~1 Mb in size and contains paternally expressed genes, such as DLK1, RTL1 and DIO3 as well as maternally expressed genes, such as MEG3, MEG8 and DIO3 [294, 426]. These imprinted genes have been reported to play significant role in various cellular pathways and diseases, including cancer [427-430]. Interestingly, this locus also contains 54 miRNAs [295] within ~300 kb region, present in form of 2 sub-clusters (as shown in Figure 31). These miRNAs have been identified to be downregulated in glioblastoma multiforme, ovarian cancers, osteosarcoma, invasive breast cancer, renal clear cell carcinoma [431, 432]. There have been reports suggesting the role of the 14q32 miRNA cluster in driving lung adenocarcinoma [206] and are differentially expressed, acting as potential biomarkers in non-alcoholic fatty acid liver disease [209]. In ovarian cancer, existing evidence suggests that eight miRNAs from this cluster can act as tumor suppressors [420] as well as allelic loss of potential tumor suppressor genes at locus 14q32 is associated with substantial increase ovarian cancer cases [316]. As summarized in Table 10, this cluster targets various

tissues/diseases in humans and their functions are co-related with upregulation or downregulation of miRNAs in cell-type specific manner.

14q32 miRNA cluster in Renal cell carcinoma

Loss of chromosome 14q32 in ccRCC is reported to be associated with increase in disease aggressiveness [433], but the role and mechanism of these miRNA aberrations in renal cancer is not well studied. We hypothesize that 14q32 miRNAs possess tumor suppressive properties in ccRCC. We performed a preliminary analysis of basal expression of eight 14q32 miRNAs (selected based on their approximate equidistant location on chromosome 14q) via RT-PCR in renal cells. The results showed highest expression in primary renal proximal tubule epithelial cells (RPTEC) and low/no expression in immortalized cell lines HEK293T and HK-2, suggesting that perhaps immortalization process can lead to 14q32 miRNA reduction (data not shown). Furthermore, we compared the 14q32 miRNA expression pattern in three ccRCC cell lines: 769-P, 786-O and A-498. Interestingly, the expression level of sub-cluster A miRNAs (miR-493, miR-431, miR-432) were low/not detectable in all three cells lines, while analysis of sub-cluster B miRNAs (miR-411, miR-495, miR-539 and miR-323b) showed miRNA expression to be highest in 769-P, followed by 786-O and A-498 (miRNA expression: 769-P>786-O>A-498) (data not shown). These expression levels were inversely related with the level of genomic aberrations in these cell lines (769-P<786-O<A-498) as expected, supporting that increased aggressiveness can lead to reduction of these miRNAs. As the expression pattern was different among sub-cluster A and B miRNAs, this also provides an indication of difference in regulation of these sub-clusters (data not shown).

To decipher the role and regulation of 14q32 miRNAs in ccRCC, we attempted to overexpress these miRNAs *in vivo* using 786-O cells. We established a renal tumor xenograft model by injecting these cells subcutaneously, followed by intratumoral administration of control adeno-associated virus or those expressing the miRNA cluster at 14q32.

Table 10: 14q32 miRNA alterations and their corresponding functions in different diseases/target tissues.

14q32 miRNA cluster	*Disease/Target*	*PMID*	*Function*
14q LOH	Renal cell carcinoma	15202004	High grade malignancy and poor survival
Loss of 14q32	Clear cell RCC	17922474	Transformation of low grade into high grade ccRCC
Downregulation of 14q32 miRNAs (focusing on miR-654-3p)	Papillary thyroid cancer	28030816	Progression of cancer: cell proliferation, adhesion, migration, and angiogenesis
Overexpression of 14q32 miRNAs (focusing on miR-323b-3p, miR-487a-3p, and miR-539-5p)	Lung adenocarcinoma	29330288	Tumor cell migratory and invasive properties
14q32 miRNA expression	Lung and liver cancer	30538122	Suppress metastatic colonization in preclinical models of lung and liver metastasis and correlates with improved clinical outcomes in patients with metastatic cancer
Downregulation of 14q32 miRNAs (focusing on miR-323-3p)	Primary human desmoplastic medulloblastoma	24093088	IPA analysis revealed various potential functions, including cell proliferation, cell cycle progression and migration
14q32 hypermethylation	Acute promyelocytic leukemia	24493669	Associated with pathogenesis of AML (hypermethylation observed in leukemic cells compared to control)
miR-379/miR-410 cluster ablation	Mouse neonates-development and metabolic pathway	25124681	Neonatal metabolic adaptation (inefficient mobilization of hepatic glycogen stores, hypoglycemia, defective gluconeogenesis)
Deletion of the miR-379/miR-410 cluster	Neonatal mice brain	26744330	Enhances anxiety-related behavior (influences behavior and energy homeostasis)
Expression of several 14q32 miRNAs	Osteosarcoma	28506242	Associated with high aggressiveness in osteosarcoma cell lines
Dlk1-Dio3 Locus-Embedded MicroRNAs	Embryonic Stem cells	29129685	Drivers of pluripotency
14q32 miRNA Cluster (focus on miR-323b-3p, miR-487a-3p, and miR-539-5p)	Lung adenocarcinoma	29330288	Metastasis and poor prognosis
Upregulation of Dlk1-Dio3 locus miRNAs	Mouse liver	31919282	Promote gluconeogenesis
14q32 miRNAs (focus on mir-376a and mir-376c)	Melanoma	22747855	14q32 miR cluster downregulated in melanoma and downregulation of miR-376a and miR-376c increases insulin growth factor 1 receptor

We were able to establish the tumor models but injecting the AAV-associated miRNAs did not alter the tumor size or volume (data not shown). Further we also isolated the tumors and analyzed miRNA expression levels of miR-410, miR-432 and miR-494 via qPCR, which were not found to be expressed (data not shown). A scientific conclusion could not be made due to technical issues with the experiment. Additionally, since multiple genomic aberrations are associated with tumor development, the subcutaneous injections of ccRCC cells may not recapitulate ccRCC microenvironment. Since AAVs were injected intratumorally, it was not feasible to estimate the efficiency of AAV-miRNA uptake by all tumor cells, which could have been different throughout the tumor. Simultaneously, *in vitro* culture of 786-O cells with AAV-associated miRNA transfection was also attempted, but miRNAs were not successfully expressed (data not shown).

To resolve these issues, we attempted to overexpress selected miRNAs from this cluster individually via miRNA mimic transfection in 786-O cells. These miRNAs were selected based on extensive literature review of the roles of all 54 miRNAs in cancer and other molecular pathways, such as lipid metabolic pathway, as ccRCC has been described as a metabolic disease characterized by dysregulated lipid metabolism and increased intracellular lipid content [99]. Top 5 miRNAs from this list and their reported roles are mentioned below in table 11, which were used for miRNA mimic transfections. We did not observe any changes in cell viability via crystal violet assay and no changes in EMT markers via western blotting (data not shown). This could possibly be due to potential technical issues with experiments; therefore, no definitive conclusions were drawn. Additionally, as miRNAs exist in the form of sub-clusters on this locus (figure 31), it is possible that these miRNAs work synergistically to exert their tumor suppressive functions. Therefore, a next possible step is overexpression of miRNA mimics together to analyze changes in cell morphology, viability, growth related functions such as cell migration and expression of EMT markers. Based on the results, lipid metabolic alterations can be examined, such as cholesterol levels and lipid droplet analysis.

An alternative approach is CRISPR-Cas9 mediated re-activation of 14q32 miRNA cluster in ccRCC cells. This approach was adapted from a lung adenocarcinoma study, which analyzed the effect of miRNA cluster hyperactivation on migration and patient prognosis in lung adenocarcinoma patients [223]. A 2-fold approach can be used to reactivate 14q32 miRNA cluster, using lentiviral infection and stable transfection of Cas9-expressing plasmid (Lenti-EFS-

Table 11: 14q32 miRNAs selected based on extensive literature review of the roles of these miRNAs in cancer and lipid metabolic pathways

miRNAs	***Cancer-related studies***	***Lipid-related studies***
miR-431-5p	Hepatocellular carcinoma, pancreatic cancer, breast cancer, medulloblastoma, Glioblastoma, colorectal cancer [434-439]	IFN-beta (involved in lipid metabolic regulation in diseases such as multiple sclerosis and hepatitis C) [440]
		Grave's disease (related with altered serum cholesterol) [441]
		Platelet function (Platelets related to lipid rafts for membrane domains) [442]
		Alzheimer's disease (AD is related to increased LDs) [443]
		Differentiation and regeneration of old skeletal muscle by targeting SMAD4 (TGF beta related to abnormal lipid metabolism) [444]
		Spinal muscular atrophy (related to abnormal fatty acid metabolism) [445]
		Myostatin regulates miR-431 expression via the Ras-MEK-ERK signaling pathway (Myostatin involved in adipogenic differentiation) [446]
miR-411-5p	Bladder cancer, Renal cell cancer, Breast cancer, head and neck squamous carcinoma, Lung adenocarcinoma [447-451]	Caloric Restriction-Mediated Induction of Lipid Metabolism Gene Expression in Liver is Enhanced by Keap1-Knockdown [452]
		Genome-wide identification of microRNA expression quantitative trait loci [453]

Table 11 (Continued)

miR-433-3p	Esophageal, cervical, pancreatic, breast, gastric and liver cancer [454, 455]	MicroRNA-433-3p promotes osteoblast differentiation through targeting DKK1 expression [456]
		miR-433-3p is one of the miRNAs regulated by rHDL [457]
		Potential therapeutic target in renal fibrosis [458]
miR-433-5p	Human glioma, Osteosarcoma, Cervical cancer, Human gastric carcinoma, Hepatocellular carcinoma, Gastric cancer, Breast cancer, Bladder cancer, nasopharyngeal carcinoma [454, 455, 459-464]	Targets HIF1a [465]
		miR-433 expression is altered in the adipose tissue of patients with non-alcoholic fatty liver disease [466]
miR-127-3p	Breast, ovarian, gastric, glioma, osteosarcoma, pancreatic cancer, Human esophageal squamous cell carcinoma [364, 461, 467-471]	miR-127-3p is one of the 4 differentially expressed miRNAs between exosomes and their original cell samples in ovarian cancer cell lines [472]
		The miR-127 gene overlaps with the miR-433 gene in a compact genomic space. CREB, which controls hepatic lipid metabolism by repression of PPARγ and induction of PGC-1 (Peroxisome proliferator-activated receptor-gamma coactivator-1), is one of the targets of miR-433 [473]
miR-432-5p	Prostate cancer, Hepatocellular carcinoma, cervical cancer, lung adenocarcinoma, colorectal cancer, breast cancer [474-479]	Expressed in bovine backfat [480]
		Inhibits myogenesis through PI3K/AKT/mTOR signaling pathway [481]

dCas9-VPR-PGK-Puro), followed by double stable cell line generation using sgRNA-expressing plasmid (pLKO-U6sgRNA_improved-EF1s-GFP-P2A-Blasticidin) (See Appendix for technical and methodological details), followed by selection with both blasticidin and puromycin for double stable cell line generation. As shown in table 6, we determined the appropriate doses of blasticidin

and puromycin for this purpose in different cell lines (dose response data not shown), which can be used in preliminary studies.

Once the double stable cell lines are generated, these will be used to assess functional properties of the miRNA cluster in relation to cell viability, migration capacity and lipid metabolic alterations. Furthermore, we can also perform metabolomics analysis in 14q32 activated renal cancer cells to analyze global metabolic pathway alterations. These cells can also be used to generate a murine orthotropic RENCA model [482] to study the effects of 14q32 miRNAs *in vivo*.

14q32 miRNA Alterations: Epigenetic Factors and Potential role of Iron

Imprinted chromosome 14q32 region is regulated by differentially methylated regions (DMRs) located upstream of miRNAs at this locus. Intergenic DMR (IG-DMR) is located between DLK1 and MEG3 genes, MEG3-DMR is located in the promoter region of MEG3 [292] and MEG8-DMR is located within intron 2 of MEG8 gene [483]. IG-DMR and MEG3-DMR are methylated on the paternal and unmethylated on the maternal allele, however, MEG8-DMR is methylated on the maternal allele [222]. Literature supports the presence of DLK1-DMR, IG-DMR and MEG3-DMR at chromosome 12p of mice [484], which correspond to the 14q32 locus in humans. DLK1-DMR has paternal allele-specific methylation during embryogenesis and the methylation pattern remains dynamic with further growth [484]. The IG-DMR is the germline primary DMR [485]. Evidence suggests that IG-DMR acts as upstream regulator of MEG3-DMR methylation pattern [294, 486] and DNA-methylation pattern of IG-DMR functionally influences MEG3- and MEG8-DMR DNA-methylation [487].

In addition to methylation, this region is also regulated by promoter acetylation, recruiting HDACs through CpG binding proteins [336]. Role of epigenetic alterations, leading to silencing of this miRNA cluster has been reported in some cancer cases [5, 223, 224, 488]. However, the role and regulation of 14q32 epigenetic alteration in renal cancer and ovarian cancer development is understudied. We showed that chronic iron exposure can alter these epigenetic changes leading

to 14q32 miRNA downregulation (as mentioned above) in FTSECs [421]. Interestingly, Iron is known to cause epigenetic alterations [225, 328] and iron accumulation in cancer cells is well known to promote tumorigenesis in different cancer types [178]. Studies suggest that iron in the form of nitrilotriacetic acid (Fe-NTA) can contribute to RCC development [489, 490] and can lead to genomic aberrations by inducing Fenton reaction in renal proximal tubules of rodents; these chromosomal aberrations were similar to human copy number alterations associated with RCC [367]. Therefore, we hypothesize that iron can also lead to silencing of 14q32 miRNAs in renal cancer by altering promoter methylation and acetylation patterns.

Additionally, since VHL mutation exists in 90% of ccRCC patients, VHL-HIFα axis is dysregulated in these tumors, leading to iron accumulation as one of the downstream effects due to increase in Transferrin Receptor 1 (TfR1) [181] and inhibition of ferritin expression at mRNA and protein level [491]. VHL-loss also leads to increased iron susceptibility in ccRCC cells [492]. This evidence supports the role of iron in ccRCC pathophysiology. As a preliminary analysis, we used a non-physiological means of altering iron levels by treating HK-2 cells with FAC (NTBI) for a period of ~3 months and we were expecting an increase in cell viability, but we did not notice any change in cellular growth or morphology (data not shown).

It is possible that either NTBI alone is not sufficient to induce any obvious cellular changes or HK-2 cells, being immortalized with EBV leading to genomic alterations [252], do not appropriately represent the renal proximal tubule cell environment and may not be susceptible to iron-induced changes. Since it has been reported that human proximal tubular epithelial cells can uptake iron in form of both transferrin bound (TBI) as well as non-transferrin bound (NTBI) forms [21], we can treat the primary renal cells (immortalized via another mechanism such as hTERT/c-Myc/LTAg/Ras overexpression) using a combination of both iron forms for long time duration then analyze if there is a direct effect on expression level of 14q32 miRNAs.

Iron can also cause epigenomic alterations via iron-dependent enzymes such as Ten-eleven translocation (TET) enzymes and Jumonji C (JmjC) domain containing demethylases [493]

and catalyze oxidative demethylation of transcription factors [494]. H_2O_2- induced oxidative stress has also been shown to induce epigenetic alterations associated with malignant transformation in human kidney epithelial cells [495]. Additionally, iron chelation by DFO can modulate histone methylation in colorectal cells [496] and enhances chemoresistance in breast cancer cells by causing promoter histone methylation in gene-specific manner [225]. Deferiprone (DFP)-mediated iron chelation can alter histone modification profile to promote anti-tumor properties in breast cancer xenograft mouse model [497]. Therefore, we can compare the ccRCC patient tumor samples and with corresponding normal kidney samples to analyze the TET and JmjC enzymatic activities as well as overall accumulated iron content before and after iron chelation. We can further examine the epigenetic modifications caused by iron on 14q32 miRNA promoter region by performing anti-histone specific Chromatin Immunoprecipitation (ChIP) and bisulphite sequencing analysis using iron-treated primary immortalized renal cells.

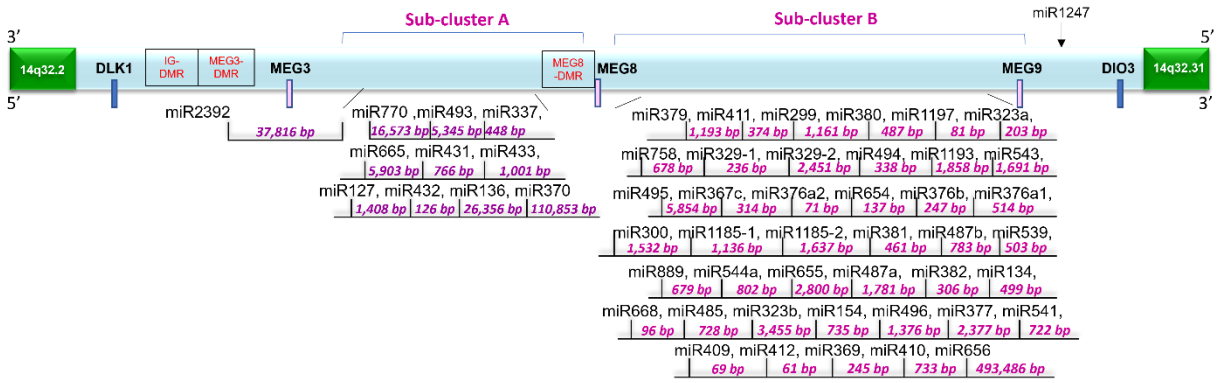

Figure 31: Schematic representation of the miRNA-clusters at 14q32 chromosomal region 54 miRNAs present in the form of 2 sub-clusters, regulated by differentially methylated regions IG-DMR, MEG3-DMR and MEG8-DMR. The distance between miRNAs as calculated through UCSC genome browser data is also included within ~300 kb region.

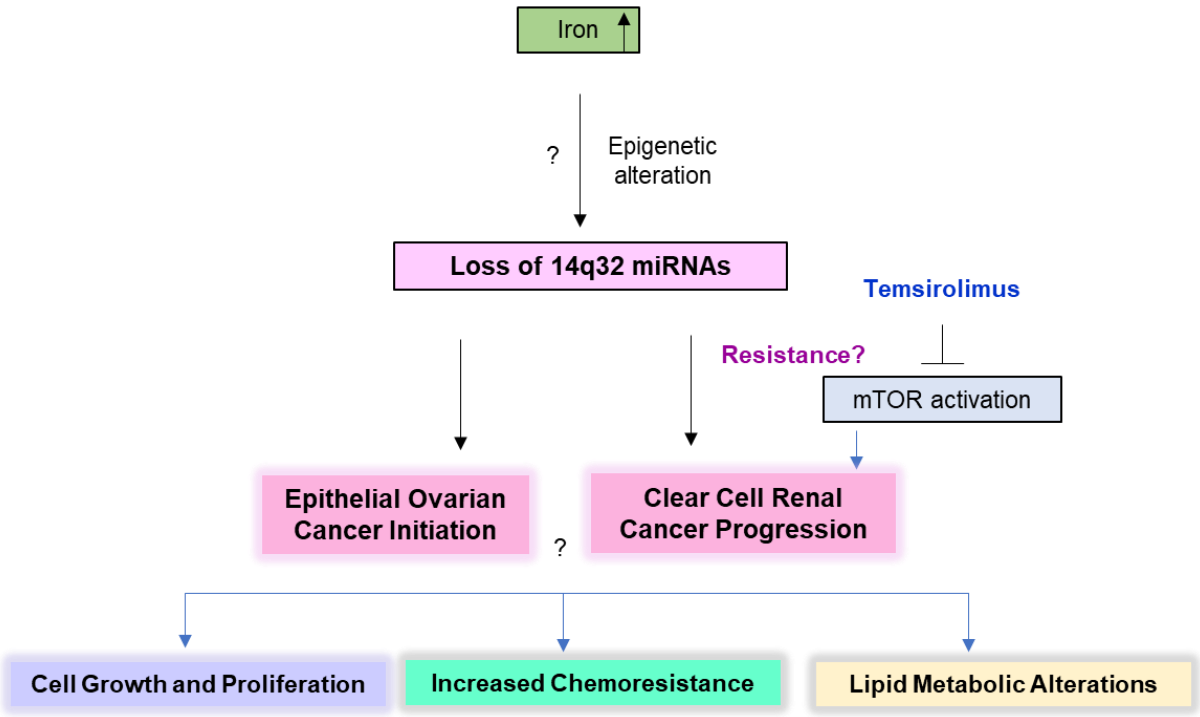

Figure 32: Overall Model of Proposed Hypothesis for Role and Regulation of 14q32 miRNAs in Epithelial Ovarian Cancer initiation clear cell Renal cancer pathophysiology
The model presented herein summarizes the potential crosstalk between increased iron content, leading to 14q32 miRNA downregulation via epigenetic silencing. This may lead to potential transformative cellular alterations leading to OVCA initiation. Additionally, 14q32 miRNA dysregulation may also be associated with increase in chemoresistance towards mTOR inhibitor drug Temsirolimus, increased RCC aggressiveness, and lipid dysregulation.

Concluding Remarks and Overall Clinical Significance

Aberrations at 14q32 region brings attention to the possible prognostic value of the miRNA cluster at this locus which may not only act as a biomarker for examining patient vulnerability towards certain diseases but can also serve as potential therapeutic target for gene-based therapies. With examination of iron-induced 14q32 miRNA downregulation, potentially caused by epigenetic alterations, leading to transformative changes in FTSECs, this data moves us one step ahead in

understanding of HGSOC initiation which has remained an open-ended question for years. It is also possible that altered iron metabolism mediates drug resistance to TEMS and the related signaling pathway markers as downstream targets of 14q32 miRNA dysregulation. Since lipid reprogramming is one of the hallmarks of ccRCC [497], assessment of the role of 14q32 miRNAs on lipid metabolism can provide direction to further understanding of altered cellular energetics in this disease. With subsequent analyses, these altered metabolic pathways can also possibly serve as diagnostic biomarkers at different stages of ccRCC [498], and a potential means of therapeutic intervention via miRNA-based gene therapy [499] to restore the tumor suppressive miRNAs and inhibit the translation of metabolic enzymes and other target proteins, hyperactivated in ccRCC patients. Additional studies would be required to establish the role of these miRNAs in cancer pathogenesis and drug resistance at both cellular and clinical level.

References

1. Fife BT, Bluestone JA: **Control of peripheral T-cell tolerance and autoimmunity via the CTLA-4 and PD-1 pathways**. *Immunological reviews* 2008, **224**:166-182.
2. Xu S, Zhang X, Liu P: **Lipid droplet proteins and metabolic diseases**. *Biochimica et biophysica acta Molecular basis of disease* 2018, **1864**(5 Pt B):1968-1983.
3. Shyu P, Jr., Wong XFA, Crasta K, Thibault G: **Dropping in on lipid droplets: insights into cellular stress and cancer**. *Bioscience reports* 2018, **38**(5).
4. Rini BI, Atkins MB: **Resistance to targeted therapy in renal-cell carcinoma**. *The Lancet Oncology* 2009, **10**(10):992-1000.
5. Oshima G, Poli EC, Bolt MJ, Chlenski A, Forde M, Jutzy JMS, Biyani N, Posner MC, Pitroda SP, Weichselbaum RR *et al*: **DNA Methylation Controls Metastasis-Suppressive 14q32-Encoded miRNAs**. *Cancer research* 2019, **79**(3):650-662.
6. Hudes G, Carducci M, Tomczak P, Dutcher J, Figlin R, Kapoor A, Staroslawska E, Sosman J, McDermott D, Bodrogi I *et al*: **Temsirolimus, interferon alfa, or both for advanced renal-cell carcinoma**. *The New England journal of medicine* 2007, **356**(22):2271-2281.
7. Hsieh JJ, Purdue MP, Signoretti S, Swanton C, Albiges L, Schmidinger M, Heng DY, Larkin J, Ficarra V: **Renal cell carcinoma**. *Nature reviews Disease primers* 2017, **3**:17009.
8. Massari F, Ciccarese C, Santoni M, Brunelli M, Piva F, Modena A, Bimbatti D, Fantinel E, Santini D, Cheng L *et al*: **Metabolic alterations in renal cell carcinoma**. *Cancer treatment reviews* 2015, **41**(9):767-776.
9. Grassi L, Alfonsi R, Francescangeli F, Signore M, De Angelis ML, Addario A, Costantini M, Flex E, Ciolfi A, Pizzi S *et al*: **Organoids as a new model for improving regenerative medicine and cancer personalized therapy in renal diseases**. *Cell death & disease* 2019, **10**(3):201.
10. Choi JW, Herr DR, Noguchi K, Yung YC, Lee CW, Mutoh T, Lin ME, Teo ST, Park KE, Mosley AN *et al*: **LPA receptors: subtypes and biological actions**. *Annual review of pharmacology and toxicology* 2010, **50**:157-186.
11. Winter JN, Fox TE, Kester M, Jefferson LS, Kimball SR: **Phosphatidic acid mediates activation of mTORC1 through the ERK signaling pathway**. *American journal of physiology Cell physiology* 2010, **299**(2):C335-344.
12. Russo P: **Contemporary understanding and management of renal cortical tumors**. *The Urologic clinics of North America* 2008, **35**(4):xiii-xvii.
13. Cairns P: **Renal cell carcinoma**. *Cancer biomarkers : section A of Disease markers* 2010, **9**(1-6):461-473.
14. Huang Q, Sun Y, Ma X, Gao Y, Li X, Niu Y, Zhang X, Chang C: **Androgen receptor increases hematogenous metastasis yet decreases lymphatic metastasis of renal cell carcinoma**. *Nature communications* 2017, **8**(1):918.
15. Davis-Dusenbery BN, Hata A: **MicroRNA in Cancer: The Involvement of Aberrant MicroRNA Biogenesis Regulatory Pathways**. *Genes & cancer* 2010, **1**(11):1100-1114.
16. Drabkin HA, Gemmill RM: **Obesity, cholesterol, and clear-cell renal cell carcinoma (RCC)**. *Advances in cancer research* 2010, **107**:39-56.

17. Kawabata H: **Transferrin and transferrin receptors update**. *Free radical biology & medicine* 2019, **133**:46-54.
18. Fournier C, Goto Y, Ballestar E, Delaval K, Hever AM, Esteller M, Feil R: **Allele-specific histone lysine methylation marks regulatory regions at imprinted mouse genes**. *The EMBO journal* 2002, **21**(23):6560-6570.
19. Rockfield S, Kee Y, Nanjundan M: **Chronic iron exposure and c-Myc/H-ras-mediated transformation in fallopian tube cells alter the expression of EVI1, amplified at 3q26.2 in ovarian cancer**. *Oncogenesis* 2019, **8**(9):46.
20. Sendamarai AK, Ohgami RS, Fleming MD, Lawrence CM: **Structure of the membrane proximal oxidoreductase domain of human Steap3, the dominant ferrireductase of the erythroid transferrin cycle**. *Proceedings of the National Academy of Sciences of the United States of America* 2008, **105**(21):7410-7415.
21. van Raaij SEG, Srai SKS, Swinkels DW, van Swelm RPL: **Iron uptake by ZIP8 and ZIP14 in human proximal tubular epithelial cells**. *Biometals : an international journal on the role of metal ions in biology, biochemistry, and medicine* 2019, **32**(2):211-226.
22. McKie AT, Barrow D, Latunde-Dada GO, Rolfs A, Sager G, Mudaly E, Mudaly M, Richardson C, Barlow D, Bomford A *et al*: **An iron-regulated ferric reductase associated with the absorption of dietary iron**. *Science* 2001, **291**(5509):1755-1759.
23. Mackenzie B, Hediger MA: **SLC11 family of H+-coupled metal-ion transporters NRAMP1 and DMT1**. *Pflugers Archiv : European journal of physiology* 2004, **447**(5):571-579.
24. Gunshin H, Mackenzie B, Berger UV, Gunshin Y, Romero MF, Boron WF, Nussberger S, Gollan JL, Hediger MA: **Cloning and characterization of a mammalian proton-coupled metal-ion transporter**. *Nature* 1997, **388**(6641):482-488.
25. Gibney ER, Nolan CM: **Epigenetics and gene expression**. *Heredity* 2010, **105**(1):4-13.
26. Russo P: **End stage and chronic kidney disease: associations with renal cancer**. *Frontiers in oncology* 2012, **2**:28.
27. Dixon SJ, Lemberg KM, Lamprecht MR, Skouta R, Zaitsev EM, Gleason CE, Patel DN, Bauer AJ, Cantley AM, Yang WS *et al*: **Ferroptosis: an iron-dependent form of nonapoptotic cell death**. *Cell* 2012, **149**(5):1060-1072.
28. Muglia VF, Prando A: **Renal cell carcinoma: histological classification and correlation with imaging findings**. *Radiologia brasileira* 2015, **48**(3):166-174.
29. Wang J, Pantopoulos K: **Regulation of cellular iron metabolism**. *The Biochemical journal* 2011, **434**(3):365-381.
30. Nemeth E, Tuttle MS, Powelson J, Vaughn MB, Donovan A, Ward DM, Ganz T, Kaplan J: **Hepcidin regulates cellular iron efflux by binding to ferroportin and inducing its internalization**. *Science* 2004, **306**(5704):2090-2093.
31. Algaba F, Akaza H, Lopez-Beltran A, Martignoni G, Moch H, Montironi R, Reuter V: **Current pathology keys of renal cell carcinoma**. *European urology* 2011, **60**(4):634-643.
32. Pandey J, Syed W: **Renal Cancer**. In: *StatPearls.* Treasure Island (FL); 2021.
33. Shi H, Bencze KZ, Stemmler TL, Philpott CC: **A cytosolic iron chaperone that delivers iron to ferritin**. *Science* 2008, **320**(5880):1207-1210.
34. Cremona M, Espina V, Caccia D, Veneroni S, Colecchia M, Pierobon M, Deng J, Mueller C, Procopio G, Lanzi C *et al*: **Stratification of clear cell renal cell carcinoma by signaling pathway analysis**. *Expert review of proteomics* 2014, **11**(2):237-249.
35. Cheville JC, Lohse CM, Zincke H, Weaver AL, Blute ML: **Comparisons of outcome and prognostic features among histologic subtypes of renal cell carcinoma**. *The American journal of surgical pathology* 2003, **27**(5):612-624.

36. Delahunt B, Bethwaite PB, Nacey JN: **Outcome prediction for renal cell carcinoma: evaluation of prognostic factors for tumours divided according to histological subtype**. *Pathology* 2007, **39**(5):459-465.
37. Cancer Genome Atlas Research N: **Comprehensive molecular characterization of clear cell renal cell carcinoma**. *Nature* 2013, **499**(7456):43-49.
38. Gnarra JR, Tory K, Weng Y, Schmidt L, Wei MH, Li H, Latif F, Liu S, Chen F, Duh FM *et al*: **Mutations of the VHL tumour suppressor gene in renal carcinoma**. *Nature genetics* 1994, **7**(1):85-90.
39. Clifford SC, Prowse AH, Affara NA, Buys CH, Maher ER: **Inactivation of the von Hippel-Lindau (VHL) tumour suppressor gene and allelic losses at chromosome arm 3p in primary renal cell carcinoma: evidence for a VHL-independent pathway in clear cell renal tumourigenesis**. *Genes, chromosomes & cancer* 1998, **22**(3):200-209.
40. Latif F, Tory K, Gnarra J, Yao M, Duh FM, Orcutt ML, Stackhouse T, Kuzmin I, Modi W, Geil L *et al*: **Identification of the von Hippel-Lindau disease tumor suppressor gene**. *Science* 1993, **260**(5112):1317-1320.
41. Xu L, Tong R, Cochran DM, Jain RK: **Blocking platelet-derived growth factor-D/platelet-derived growth factor receptor beta signaling inhibits human renal cell carcinoma progression in an orthotopic mouse model**. *Cancer research* 2005, **65**(13):5711-5719.
42. Zhang T, Niu X, Liao L, Cho EA, Yang H: **The contributions of HIF-target genes to tumor growth in RCC**. *PloS one* 2013, **8**(11):e80544.
43. Shen C, Beroukhim R, Schumacher SE, Zhou J, Chang M, Signoretti S, Kaelin WG, Jr.: **Genetic and functional studies implicate HIF1alpha as a 14q kidney cancer suppressor gene**. *Cancer discovery* 2011, **1**(3):222-235.
44. Kawakami T, Chano T, Minami K, Okabe H, Okada Y, Okamoto K: **Imprinted DLK1 is a putative tumor suppressor gene and inactivated by epimutation at the region upstream of GTL2 in human renal cell carcinoma**. *Human molecular genetics* 2006, **15**(6):821-830.
45. Duran A, Amanchy R, Linares JF, Joshi J, Abu-Baker S, Porollo A, Hansen M, Moscat J, Diaz-Meco MT: **p62 is a key regulator of nutrient sensing in the mTORC1 pathway**. *Molecular cell* 2011, **44**(1):134-146.
46. He X, Wang J, Messing EM, Wu G: **Regulation of receptor for activated C kinase 1 protein by the von Hippel-Lindau tumor suppressor in IGF-I-induced renal carcinoma cell invasiveness**. *Oncogene* 2011, **30**(5):535-547.
47. Semenza GL: **Targeting HIF-1 for cancer therapy**. *Nature reviews Cancer* 2003, **3**(10):721-732.
48. Banumathy G, Cairns P: **Signaling pathways in renal cell carcinoma**. *Cancer biology & therapy* 2010, **10**(7):658-664.
49. Hara S, Oya M, Mizuno R, Horiguchi A, Marumo K, Murai M: **Akt activation in renal cell carcinoma: contribution of a decreased PTEN expression and the induction of apoptosis by an Akt inhibitor**. *Annals of oncology : official journal of the European Society for Medical Oncology* 2005, **16**(6):928-933.
50. Kwiatkowski DJ, Choueiri TK, Fay AP, Rini BI, Thorner AR, de Velasco G, Tyburczy ME, Hamieh L, Albiges L, Agarwal N *et al*: **Mutations in TSC1, TSC2, and MTOR Are Associated with Response to Rapalogs in Patients with Metastatic Renal Cell Carcinoma**. *Clinical cancer research : an official journal of the American Association for Cancer Research* 2016, **22**(10):2445-2452.
51. Inoki K, Ouyang H, Zhu T, Lindvall C, Wang Y, Zhang X, Yang Q, Bennett C, Harada Y, Stankunas K *et al*: **TSC2 integrates Wnt and energy signals via a coordinated phosphorylation by AMPK and GSK3 to regulate cell growth**. *Cell* 2006, **126**(5):955-968.

52. Yun CW, Lee SH: **The Roles of Autophagy in Cancer**. *International journal of molecular sciences* 2018, **19**(11).
53. Bhutia SK, Mukhopadhyay S, Sinha N, Das DN, Panda PK, Patra SK, Maiti TK, Mandal M, Dent P, Wang XY *et al*: **Autophagy: cancer's friend or foe?** *Advances in cancer research* 2013, **118**:61-95.
54. Li L, Shen C, Nakamura E, Ando K, Signoretti S, Beroukhim R, Cowley GS, Lizotte P, Liberzon E, Bair S *et al*: **SQSTM1 is a pathogenic target of 5q copy number gains in kidney cancer**. *Cancer cell* 2013, **24**(6):738-750.
55. Cao Q, Bai P: **Role of Autophagy in Renal Cancer**. *Journal of Cancer* 2019, **10**(11):2501-2509.
56. Dunn WA, Jr.: **Autophagy and related mechanisms of lysosome-mediated protein degradation**. *Trends in cell biology* 1994, **4**(4):139-143.
57. Levine B, Klionsky DJ: **Development by self-digestion: molecular mechanisms and biological functions of autophagy**. *Developmental cell* 2004, **6**(4):463-477.
58. Chun Y, Kim J: **Autophagy: An Essential Degradation Program for Cellular Homeostasis and Life**. *Cells* 2018, **7**(12).
59. Mizushima N, Levine B, Cuervo AM, Klionsky DJ: **Autophagy fights disease through cellular self-digestion**. *Nature* 2008, **451**(7182):1069-1075.
60. Lipinski MM, Hoffman G, Ng A, Zhou W, Py BF, Hsu E, Liu X, Eisenberg J, Liu J, Blenis J *et al*: **A genome-wide siRNA screen reveals multiple mTORC1 independent signaling pathways regulating autophagy under normal nutritional conditions**. *Developmental cell* 2010, **18**(6):1041-1052.
61. Behrends C, Sowa ME, Gygi SP, Harper JW: **Network organization of the human autophagy system**. *Nature* 2010, **466**(7302):68-76.
62. Mathew R, Kongara S, Beaudoin B, Karp CM, Bray K, Degenhardt K, Chen G, Jin S, White E: **Autophagy suppresses tumor progression by limiting chromosomal instability**. *Genes & development* 2007, **21**(11):1367-1381.
63. White E, DiPaola RS: **The double-edged sword of autophagy modulation in cancer**. *Clinical cancer research : an official journal of the American Association for Cancer Research* 2009, **15**(17):5308-5316.
64. Li X, He S, Ma B: **Autophagy and autophagy-related proteins in cancer**. *Molecular cancer* 2020, **19**(1):12.
65. Deng Q, Wang Z, Wang L, Zhang L, Xiang X, Wang Z, Chong T: **Lower mRNA and protein expression levels of LC3 and Beclin1, markers of autophagy, were correlated with progression of renal clear cell carcinoma**. *Japanese journal of clinical oncology* 2013, **43**(12):1261-1268.
66. Lau A, Wang XJ, Zhao F, Villeneuve NF, Wu T, Jiang T, Sun Z, White E, Zhang DD: **A noncanonical mechanism of Nrf2 activation by autophagy deficiency: direct interaction between Keap1 and p62**. *Molecular and cellular biology* 2010, **30**(13):3275-3285.
67. Liu WJ, Ye L, Huang WF, Guo LJ, Xu ZG, Wu HL, Yang C, Liu HF: **p62 links the autophagy pathway and the ubiqutin-proteasome system upon ubiquitinated protein degradation**. *Cellular & molecular biology letters* 2016, **21**:29.
68. Villeneuve NF, Lau A, Zhang DD: **Regulation of the Nrf2-Keap1 antioxidant response by the ubiquitin proteasome system: an insight into cullin-ring ubiquitin ligases**. *Antioxidants & redox signaling* 2010, **13**(11):1699-1712.
69. Fabrizio FP, Costantini M, Copetti M, la Torre A, Sparaneo A, Fontana A, Poeta L, Gallucci M, Sentinelli S, Graziano P *et al*: **Keap1/Nrf2 pathway in kidney cancer: frequent methylation of KEAP1 gene promoter in clear renal cell carcinoma**. *Oncotarget* 2017, **8**(7):11187-11198.

70. Zhang J, Lefkowitz RA, Ishill NM, Wang L, Moskowitz CS, Russo P, Eisenberg H, Hricak H: **Solid renal cortical tumors: differentiation with CT**. *Radiology* 2007, **244**(2):494-504.
71. Sayagues JM, Corchete LA, Gutierrez ML, Sarasquete ME, Del Mar Abad M, Bengoechea O, Ferminan E, Anduaga MF, Del Carmen S, Iglesias M *et al*: **Genomic characterization of liver metastases from colorectal cancer patients**. *Oncotarget* 2016, **7**(45):72908-72922.
72. Manodoro F, Marzec J, Chaplin T, Miraki-Moud F, Moravcsik E, Jovanovic JV, Wang J, Iqbal S, Taussig D, Grimwade D *et al*: **Loss of imprinting at the 14q32 domain is associated with microRNA overexpression in acute promyelocytic leukemia**. *Blood* 2014, **123**(13):2066-2074.
73. Escudier B, Porta C, Schmidinger M, Rioux-Leclercq N, Bex A, Khoo V, Grunwald V, Gillessen S, Horwich A, clinicalguidelines@esmo.org EGCEa: **Renal cell carcinoma: ESMO Clinical Practice Guidelines for diagnosis, treatment and follow-updagger**. *Annals of oncology : official journal of the European Society for Medical Oncology* 2019, **30**(5):706-720.
74. McDermott DF, Regan MM, Clark JI, Flaherty LE, Weiss GR, Logan TF, Kirkwood JM, Gordon MS, Sosman JA, Ernstoff MS *et al*: **Randomized phase III trial of high-dose interleukin-2 versus subcutaneous interleukin-2 and interferon in patients with metastatic renal cell carcinoma**. *Journal of clinical oncology : official journal of the American Society of Clinical Oncology* 2005, **23**(1):133-141.
75. Sternberg CN, Davis ID, Mardiak J, Szczylik C, Lee E, Wagstaff J, Barrios CH, Salman P, Gladkov OA, Kavina A *et al*: **Pazopanib in locally advanced or metastatic renal cell carcinoma: results of a randomized phase III trial**. *Journal of clinical oncology : official journal of the American Society of Clinical Oncology* 2010, **28**(6):1061-1068.
76. Ellis LM, Hicklin DJ: **VEGF-targeted therapy: mechanisms of anti-tumour activity**. *Nature reviews Cancer* 2008, **8**(8):579-591.
77. Chan DA, Sutphin PD, Nguyen P, Turcotte S, Lai EW, Banh A, Reynolds GE, Chi JT, Wu J, Solow-Cordero DE *et al*: **Targeting GLUT1 and the Warburg effect in renal cell carcinoma by chemical synthetic lethality**. *Science translational medicine* 2011, **3**(94):94ra70.
78. Bamias A, Karavasilis V, Gavalas N, Tzannis K, Samantas E, Aravantinos G, Koutras A, Gkerzelis I, Kostouros E, Koutsoukos K *et al*: **The combination of bevacizumab/temsirolimus after first-line anti-VEGF therapy in advanced renal-cell carcinoma: a clinical and biomarker study**. *International journal of clinical oncology* 2019, **24**(4):411-419.
79. Park H, Williams K, Trikalinos NA, Larson S, Tan B, Waqar S, Suresh R, Morgensztern D, Van Tine BA, Govindan R *et al*: **A phase I trial of temsirolimus and erlotinib in patients with refractory solid tumors**. *Cancer chemotherapy and pharmacology* 2021, **87**(3):337-347.
80. Trivedi ND, Armstrong S, Wang H, Hartley M, Deeken J, Ruth He A, Subramaniam D, Melville H, Albanese C, Marshall JL *et al*: **A phase I trial of the mTOR inhibitor temsirolimus in combination with capecitabine in patients with advanced malignancies**. *Cancer medicine* 2021, **10**(6):1944-1954.
81. Hutson TE, Michaelson MD, Kuzel TM, Agarwal N, Molina AM, Hsieh JJ, Vaishampayan UN, Xie R, Bapat U, Ye W *et al*: **A Single-arm, Multicenter, Phase 2 Study of Lenvatinib Plus Everolimus in Patients with Advanced Non-Clear Cell Renal Cell Carcinoma**. *European urology* 2021, **80**(2):162-170.
82. Hwang HS, Go H, Park JM, Yoon SY, Lee JL, Jeong SU, Cho YM: **Epithelial-mesenchymal transition as a mechanism of resistance to tyrosine kinase inhibitors**

in clear cell renal cell carcinoma. *Laboratory investigation; a journal of technical methods and pathology* 2019, **99**(5):659-670.
83. Hamieh L, Choueiri TK, Ogorek B, Khabibullin D, Rosebrock D, Livitz D, Fay A, Pignon JC, McDermott DF, Agarwal N *et al*: **Mechanisms of acquired resistance to rapalogs in metastatic renal cell carcinoma**. *PLoS genetics* 2018, **14**(9):e1007679.
84. Makhov P, Joshi S, Ghatalia P, Kutikov A, Uzzo RG, Kolenko VM: **Resistance to Systemic Therapies in Clear Cell Renal Cell Carcinoma: Mechanisms and Management Strategies**. *Molecular cancer therapeutics* 2018, **17**(7):1355-1364.
85. Gotink KJ, Broxterman HJ, Labots M, de Haas RR, Dekker H, Honeywell RJ, Rudek MA, Beerepoot LV, Musters RJ, Jansen G *et al*: **Lysosomal sequestration of sunitinib: a novel mechanism of drug resistance**. *Clinical cancer research : an official journal of the American Association for Cancer Research* 2011, **17**(23):7337-7346.
86. Raimondo L, D'Amato V, Servetto A, Rosa R, Marciano R, Formisano L, Di Mauro C, Orsini RC, Cascetta P, Ciciola P *et al*: **Everolimus induces Met inactivation by disrupting the FKBP12/Met complex**. *Oncotarget* 2016, **7**(26):40073-40084.
87. Carew JS, Kelly KR, Nawrocki ST: **Mechanisms of mTOR inhibitor resistance in cancer therapy**. *Targeted oncology* 2011, **6**(1):17-27.
88. Thomas GV, Tran C, Mellinghoff IK, Welsbie DS, Chan E, Fueger B, Czernin J, Sawyers CL: **Hypoxia-inducible factor determines sensitivity to inhibitors of mTOR in kidney cancer**. *Nature medicine* 2006, **12**(1):122-127.
89. Ravaud A, Gross-Goupil M: **Overcoming resistance to tyrosine kinase inhibitors in renal cell carcinoma**. *Cancer treatment reviews* 2012, **38**(8):996-1003.
90. Buczek M, Escudier B, Bartnik E, Szczylik C, Czarnecka A: **Resistance to tyrosine kinase inhibitors in clear cell renal cell carcinoma: from the patient's bed to molecular mechanisms**. *Biochimica et biophysica acta* 2014, **1845**(1):31-41.
91. Lee CK, Marschner IC, Simes RJ, Voysey M, Egleston B, Hudes G, de Souza P: **Increase in cholesterol predicts survival advantage in renal cell carcinoma patients treated with temsirolimus**. *Clinical cancer research : an official journal of the American Association for Cancer Research* 2012, **18**(11):3188-3196.
92. Gerlinger M, Rowan AJ, Horswell S, Math M, Larkin J, Endesfelder D, Gronroos E, Martinez P, Matthews N, Stewart A *et al*: **Intratumor heterogeneity and branched evolution revealed by multiregion sequencing**. *The New England journal of medicine* 2012, **366**(10):883-892.
93. He YH, Tian G: **Autophagy as a Vital Therapy Target for Renal Cell Carcinoma**. *Frontiers in pharmacology* 2020, **11**:518225.
94. Rangwala R, Chang YC, Hu J, Algazy KM, Evans TL, Fecher LA, Schuchter LM, Torigian DA, Panosian JT, Troxel AB *et al*: **Combined MTOR and autophagy inhibition: phase I trial of hydroxychloroquine and temsirolimus in patients with advanced solid tumors and melanoma**. *Autophagy* 2014, **10**(8):1391-1402.
95. Barnard RA, Wittenburg LA, Amaravadi RK, Gustafson DL, Thorburn A, Thamm DH: **Phase I clinical trial and pharmacodynamic evaluation of combination hydroxychloroquine and doxorubicin treatment in pet dogs treated for spontaneously occurring lymphoma**. *Autophagy* 2014, **10**(8):1415-1425.
96. Zhang Y, Chen M, Liu M, Xu Y, Wu G: **Glycolysis-Related Genes Serve as Potential Prognostic Biomarkers in Clear Cell Renal Cell Carcinoma**. *Oxidative medicine and cellular longevity* 2021, **2021**:6699808.
97. Metallo CM, Gameiro PA, Bell EL, Mattaini KR, Yang J, Hiller K, Jewell CM, Johnson ZR, Irvine DJ, Guarente L *et al*: **Reductive glutamine metabolism by IDH1 mediates lipogenesis under hypoxia**. *Nature* 2011, **481**(7381):380-384.
98. Wettersten HI, Aboud OA, Lara PN, Jr., Weiss RH: **Metabolic reprogramming in clear cell renal cell carcinoma**. *Nature reviews Nephrology* 2017, **13**(7):410-419.

99. Hakimi AA, Reznik E, Lee CH, Creighton CJ, Brannon AR, Luna A, Aksoy BA, Liu EM, Shen R, Lee W *et al*: **An Integrated Metabolic Atlas of Clear Cell Renal Cell Carcinoma**. *Cancer cell* 2016, **29**(1):104-116.
100. Teng R, Liu Z, Tang H, Zhang W, Chen Y, Xu R, Chen L, Song J, Liu X, Deng H: **HSP60 silencing promotes Warburg-like phenotypes and switches the mitochondrial function from ATP production to biosynthesis in ccRCC cells**. *Redox biology* 2019, **24**:101218.
101. Clark PE: **The role of VHL in clear-cell renal cell carcinoma and its relation to targeted therapy**. *Kidney international* 2009, **76**(9):939-945.
102. Ambrosetti D, Dufies M, Dadone B, Durand M, Borchiellini D, Amiel J, Pouyssegur J, Rioux-Leclercq N, Pages G, Burel-Vandenbos F *et al*: **The two glycolytic markers GLUT1 and MCT1 correlate with tumor grade and survival in clear-cell renal cell carcinoma**. *PloS one* 2018, **13**(2):e0193477.
103. Li B, Qiu B, Lee DS, Walton ZE, Ochocki JD, Mathew LK, Mancuso A, Gade TP, Keith B, Nissim I *et al*: **Fructose-1,6-bisphosphatase opposes renal carcinoma progression**. *Nature* 2014, **513**(7517):251-255.
104. Duvel K, Yecies JL, Menon S, Raman P, Lipovsky AI, Souza AL, Triantafellow E, Ma Q, Gorski R, Cleaver S *et al*: **Activation of a metabolic gene regulatory network downstream of mTOR complex 1**. *Molecular cell* 2010, **39**(2):171-183.
105. Hu CJ, Wang LY, Chodosh LA, Keith B, Simon MC: **Differential roles of hypoxia-inducible factor 1alpha (HIF-1alpha) and HIF-2alpha in hypoxic gene regulation**. *Molecular and cellular biology* 2003, **23**(24):9361-9374.
106. Kim JW, Tchernyshyov I, Semenza GL, Dang CV: **HIF-1-mediated expression of pyruvate dehydrogenase kinase: a metabolic switch required for cellular adaptation to hypoxia**. *Cell metabolism* 2006, **3**(3):177-185.
107. Kim JW, Zeller KI, Wang Y, Jegga AG, Aronow BJ, O'Donnell KA, Dang CV: **Evaluation of myc E-box phylogenetic footprints in glycolytic genes by chromatin immunoprecipitation assays**. *Molecular and cellular biology* 2004, **24**(13):5923-5936.
108. Iyer NV, Kotch LE, Agani F, Leung SW, Laughner E, Wenger RH, Gassmann M, Gearhart JD, Lawler AM, Yu AY *et al*: **Cellular and developmental control of O2 homeostasis by hypoxia-inducible factor 1 alpha**. *Genes & development* 1998, **12**(2):149-162.
109. Langbein S, Frederiks WM, zur Hausen A, Popa J, Lehmann J, Weiss C, Alken P, Coy JF: **Metastasis is promoted by a bioenergetic switch: new targets for progressive renal cell cancer**. *International journal of cancer* 2008, **122**(11):2422-2428.
110. Zhang Q, Yang Z, Han Q, Bai H, Wang Y, Yi X, Yi Z, Yang L, Jiang L, Song X *et al*: **G6PD promotes renal cell carcinoma proliferation through positive feedback regulation of p-STAT3**. *Oncotarget* 2017, **8**(65):109043-109060.
111. Fang Z, Sun Q, Yang H, Zheng J: **SDHB Suppresses the Tumorigenesis and Development of ccRCC by Inhibiting Glycolysis**. *Frontiers in oncology* 2021, **11**:639408.
112. Sudarshan S, Shanmugasundaram K, Naylor SL, Lin S, Livi CB, O'Neill CF, Parekh DJ, Yeh IT, Sun LZ, Block K: **Reduced expression of fumarate hydratase in clear cell renal cancer mediates HIF-2alpha accumulation and promotes migration and invasion**. *PloS one* 2011, **6**(6):e21037.
113. Shim EH, Livi CB, Rakheja D, Tan J, Benson D, Parekh V, Kho EY, Ghosh AP, Kirkman R, Velu S *et al*: **L-2-Hydroxyglutarate: an epigenetic modifier and putative oncometabolite in renal cancer**. *Cancer discovery* 2014, **4**(11):1290-1298.
114. Du W, Zhang L, Brett-Morris A, Aguila B, Kerner J, Hoppel CL, Puchowicz M, Serra D, Herrero L, Rini BI *et al*: **HIF drives lipid deposition and cancer in ccRCC via repression of fatty acid metabolism**. *Nature communications* 2017, **8**(1):1769.

115. Xu W, Hu X, Anwaier A, Wang J, Liu W, Tian X, Zhu W, Ma C, Wan F, Shi G *et al*: **Fatty Acid Synthase Correlates With Prognosis-Related Abdominal Adipose Distribution and Metabolic Disorders of Clear Cell Renal Cell Carcinoma**. *Frontiers in molecular biosciences* 2020, **7**:610229.
116. Bianchi C, Meregalli C, Bombelli S, Di Stefano V, Salerno F, Torsello B, De Marco S, Bovo G, Cifola I, Mangano E *et al*: **The glucose and lipid metabolism reprogramming is grade-dependent in clear cell renal cell carcinoma primary cultures and is targetable to modulate cell viability and proliferation**. *Oncotarget* 2017, **8**(69):113502-113515.
117. Drabkin HA, Gemmill RM: **Cholesterol and the development of clear-cell renal carcinoma**. *Current opinion in pharmacology* 2012, **12**(6):742-750.
118. Teng L, Chen Y, Cao Y, Wang W, Xu Y, Wang Y, Lv J, Li C, Su Y: **Overexpression of ATP citrate lyase in renal cell carcinoma tissues and its effect on the human renal carcinoma cells in vitro**. *Oncology letters* 2018, **15**(5):6967-6974.
119. Sreedhar A, Zhao Y: **Dysregulated metabolic enzymes and metabolic reprogramming in cancer cells**. *Biomedical reports* 2018, **8**(1):3-10.
120. Kim J, Thompson B, Han S, Lotan Y, McDonald JG, Ye J: **Uptake of HDL-cholesterol contributes to lipid accumulation in clear cell renal cell carcinoma**. *Biochimica et biophysica acta Molecular and cell biology of lipids* 2019, **1864**(12):158525.
121. Murphy S, Martin S, Parton RG: **Lipid droplet-organelle interactions; sharing the fats**. *Biochimica et biophysica acta* 2009, **1791**(6):441-447.
122. Cui L, Liu P: **Two Types of Contact Between Lipid Droplets and Mitochondria**. *Frontiers in cell and developmental biology* 2020, **8**:618322.
123. Guo Y, Cordes KR, Farese RV, Jr., Walther TC: **Lipid droplets at a glance**. *Journal of cell science* 2009, **122**(Pt 6):749-752.
124. Klecker T, Braun RJ, Westermann B: **Lipid Droplets Guard Mitochondria during Autophagy**. *Developmental cell* 2017, **42**(1):1-2.
125. Koizume S, Miyagi Y: **Lipid Droplets: A Key Cellular Organelle Associated with Cancer Cell Survival under Normoxia and Hypoxia**. *International journal of molecular sciences* 2016, **17**(9).
126. Gebhard RL, Clayman RV, Prigge WF, Figenshau R, Staley NA, Reesey C, Bear A: **Abnormal cholesterol metabolism in renal clear cell carcinoma**. *Journal of lipid research* 1987, **28**(10):1177-1184.
127. Sundelin JP, Stahlman M, Lundqvist A, Levin M, Parini P, Johansson ME, Boren J: **Increased expression of the very low-density lipoprotein receptor mediates lipid accumulation in clear-cell renal cell carcinoma**. *PloS one* 2012, **7**(11):e48694.
128. Zhang GM, Wang MY, Liu YN, Zhu Y, Wan FN, Wei QY, Ye DW: **Functional variants in the low-density lipoprotein receptor gene are associated with clear cell renal cell carcinoma susceptibility**. *Carcinogenesis* 2017, **38**(12):1241-1248.
129. Liu K, Czaja MJ: **Regulation of lipid stores and metabolism by lipophagy**. *Cell death and differentiation* 2013, **20**(1):3-11.
130. Xu G, Jiang Y, Xiao Y, Liu XD, Yue F, Li W, Li X, He Y, Jiang X, Huang H *et al*: **Fast clearance of lipid droplets through MAP1S-activated autophagy suppresses clear cell renal cell carcinomas and promotes patient survival**. *Oncotarget* 2016, **7**(5):6255-6265.
131. Hao J, Zhu L, Li F, Liu Q, Zhao X, Liu S, Xing L, Feng X, Duan H: **Phospho-mTOR: a novel target in regulation of renal lipid metabolism abnormality of diabetes**. *Experimental cell research* 2013, **319**(14):2296-2306.
132. Cheng M, Bhujwalla ZM, Glunde K: **Targeting Phospholipid Metabolism in Cancer**. *Frontiers in oncology* 2016, **6**:266.

133. Szachowicz-Petelska B, Dobrzynska I, Skrodzka M, Darewicz B, Figaszewski ZA, Kudelski J: **Phospholipid composition and electric charge in healthy and cancerous parts of human kidneys**. *The Journal of membrane biology* 2013, **246**(5):421-425.
134. Park F, Miller DD: **Role of lysophosphatidic acid and its receptors in the kidney**. *Physiological genomics* 2017, **49**(11):659-666.
135. Su SC, Hu X, Kenney PA, Merrill MM, Babaian KN, Zhang XY, Maity T, Yang SF, Lin X, Wood CG: **Autotaxin-lysophosphatidic acid signaling axis mediates tumorigenesis and development of acquired resistance to sunitinib in renal cell carcinoma**. *Clinical cancer research : an official journal of the American Association for Cancer Research* 2013, **19**(23):6461-6472.
136. Hashimoto S, Mikami S, Sugino H, Yoshikawa A, Hashimoto A, Onodera Y, Furukawa S, Handa H, Oikawa T, Okada Y *et al*: **Lysophosphatidic acid activates Arf6 to promote the mesenchymal malignancy of renal cancer**. *Nature communications* 2016, **7**:10656.
137. Fei W, Shui G, Zhang Y, Krahmer N, Ferguson C, Kapterian TS, Lin RC, Dawes IW, Brown AJ, Li P *et al*: **A role for phosphatidic acid in the formation of "supersized" lipid droplets**. *PLoS genetics* 2011, **7**(7):e1002201.
138. Jasen P: **From the "silent killer" to the "whispering disease": ovarian cancer and the uses of metaphor**. *Medical history* 2009, **53**(4):489-512.
139. Doubeni CA, Doubeni AR, Myers AE: **Diagnosis and Management of Ovarian Cancer**. *American family physician* 2016, **93**(11):937-944.
140. Slatnik CL, Duff E: **Ovarian cancer: Ensuring early diagnosis**. *The Nurse practitioner* 2015, **40**(9):47-54.
141. Minion LE, Dolinsky JS, Chase DM, Dunlop CL, Chao EC, Monk BJ: **Hereditary predisposition to ovarian cancer, looking beyond BRCA1/BRCA2**. *Gynecologic oncology* 2015, **137**(1):86-92.
142. Salehi F, Dunfield L, Phillips KP, Krewski D, Vanderhyden BC: **Risk factors for ovarian cancer: an overview with emphasis on hormonal factors**. *Journal of toxicology and environmental health Part B, Critical reviews* 2008, **11**(3-4):301-321.
143. Javadi S, Ganeshan DM, Qayyum A, Iyer RB, Bhosale P: **Ovarian Cancer, the Revised FIGO Staging System, and the Role of Imaging**. *AJR American journal of roentgenology* 2016, **206**(6):1351-1360.
144. Kurnit KC, Fleming GF, Lengyel E: **Updates and New Options in Advanced Epithelial Ovarian Cancer Treatment**. *Obstetrics and gynecology* 2021, **137**(1):108-121.
145. Winter-Roach BA, Kitchener HC, Lawrie TA: **Adjuvant (post-surgery) chemotherapy for early stage epithelial ovarian cancer**. *The Cochrane database of systematic reviews* 2012(3):CD004706.
146. Engel J, Eckel R, Schubert-Fritschle G, Kerr J, Kuhn W, Diebold J, Kimmig R, Rehbock J, Holzel D: **Moderate progress for ovarian cancer in the last 20 years: prolongation of survival, but no improvement in the cure rate**. *European journal of cancer* 2002, **38**(18):2435-2445.
147. Gonzalez Bosquet J, Newtson AM, Chung RK, Thiel KW, Ginader T, Goodheart MJ, Leslie KK, Smith BJ: **Prediction of chemo-response in serous ovarian cancer**. *Molecular cancer* 2016, **15**(1):66.
148. Devouassoux-Shisheboran M, Genestie C: **Pathobiology of ovarian carcinomas**. *Chinese journal of cancer* 2015, **34**(1):50-55.
149. Jayson GC, Kohn EC, Kitchener HC, Ledermann JA: **Ovarian cancer**. *Lancet* 2014, **384**(9951):1376-1388.
150. Prat J: **Ovarian carcinomas: five distinct diseases with different origins, genetic alterations, and clinicopathological features**. *Virchows Archiv : an international journal of pathology* 2012, **460**(3):237-249.

151. Lengyel E: **Ovarian cancer development and metastasis**. *The American journal of pathology* 2010, **177**(3):1053-1064.
152. Colvin EK, Howell VM: **Why the dual origins of high grade serous ovarian cancer matter**. *Nature communications* 2020, **11**(1):1200.
153. Fathalla MF: **Incessant ovulation--a factor in ovarian neoplasia?** *Lancet* 1971, **2**(7716):163.
154. Klotz DM, Wimberger P: **Cells of origin of ovarian cancer: ovarian surface epithelium or fallopian tube?** *Archives of gynecology and obstetrics* 2017, **296**(6):1055-1062.
155. Ness RB, Grisso JA, Klapper J, Schlesselman JJ, Silberzweig S, Vergona R, Morgan M, Wheeler JE: **Risk of ovarian cancer in relation to estrogen and progestin dose and use characteristics of oral contraceptives. SHARE Study Group. Steroid Hormones and Reproductions**. *American journal of epidemiology* 2000, **152**(3):233-241.
156. Gwinn ML, Lee NC, Rhodes PH, Layde PM, Rubin GL: **Pregnancy, breast feeding, and oral contraceptives and the risk of epithelial ovarian cancer**. *Journal of clinical epidemiology* 1990, **43**(6):559-568.
157. Banet N, Kurman RJ: **Two types of ovarian cortical inclusion cysts: proposed origin and possible role in ovarian serous carcinogenesis**. *International journal of gynecological pathology : official journal of the International Society of Gynecological Pathologists* 2015, **34**(1):3-8.
158. Kurman RJ, Shih Ie M: **Molecular pathogenesis and extraovarian origin of epithelial ovarian cancer--shifting the paradigm**. *Human pathology* 2011, **42**(7):918-931.
159. Hao D, Li J, Jia S, Meng Y, Zhang C, Wang L, Di LJ: **Integrated Analysis Reveals Tubal- and Ovarian-Originated Serous Ovarian Cancer and Predicts Differential Therapeutic Responses**. *Clinical cancer research : an official journal of the American Association for Cancer Research* 2017, **23**(23):7400-7411.
160. Piek JM, van Diest PJ, Zweemer RP, Jansen JW, Poort-Keesom RJ, Menko FH, Gille JJ, Jongsma AP, Pals G, Kenemans P *et al*: **Dysplastic changes in prophylactically removed Fallopian tubes of women predisposed to developing ovarian cancer**. *The Journal of pathology* 2001, **195**(4):451-456.
161. Hatano Y, Fukuda S, Makino H, Tomita H, Morishige KI, Hara A: **High-grade serous carcinoma with discordant p53 signature: report of a case with new insight regarding high-grade serous carcinogenesis**. *Diagnostic pathology* 2018, **13**(1):24.
162. Kuhn E, Meeker A, Wang TL, Sehdev AS, Kurman RJ, Shih Ie M: **Shortened telomeres in serous tubal intraepithelial carcinoma: an early event in ovarian high-grade serous carcinogenesis**. *The American journal of surgical pathology* 2010, **34**(6):829-836.
163. George SH, Shaw P: **BRCA and Early Events in the Development of Serous Ovarian Cancer**. *Frontiers in oncology* 2014, **4**:5.
164. Kindelberger DW, Lee Y, Miron A, Hirsch MS, Feltmate C, Medeiros F, Callahan MJ, Garner EO, Gordon RW, Birch C *et al*: **Intraepithelial carcinoma of the fimbria and pelvic serous carcinoma: Evidence for a causal relationship**. *The American journal of surgical pathology* 2007, **31**(2):161-169.
165. Gilks CB, Irving J, Kobel M, Lee C, Singh N, Wilkinson N, McCluggage WG: **Incidental nonuterine high-grade serous carcinomas arise in the fallopian tube in most cases: further evidence for the tubal origin of high-grade serous carcinomas**. *The American journal of surgical pathology* 2015, **39**(3):357-364.
166. Nakamura K, Nakayama K, Ishikawa N, Ishikawa M, Sultana R, Kiyono T, Kyo S: **Reconstitution of high-grade serous ovarian carcinoma from primary fallopian tube secretory epithelial cells**. *Oncotarget* 2018, **9**(16):12609-12619.

167. Yamamoto Y, Ning G, Howitt BE, Mehra K, Wu L, Wang X, Hong Y, Kern F, Wei TS, Zhang T *et al*: **In vitro and in vivo correlates of physiological and neoplastic human Fallopian tube stem cells**. *The Journal of pathology* 2016, **238**(4):519-530.
168. Perets R, Wyant GA, Muto KW, Bijron JG, Poole BB, Chin KT, Chen JY, Ohman AW, Stepule CD, Kwak S *et al*: **Transformation of the fallopian tube secretory epithelium leads to high-grade serous ovarian cancer in Brca;Tp53;Pten models**. *Cancer cell* 2013, **24**(6):751-765.
169. Lawrenson K, Fonseca MAS, Liu AY, Segato Dezem F, Lee JM, Lin X, Corona RI, Abbasi F, Vavra KC, Dinh HQ *et al*: **A Study of High-Grade Serous Ovarian Cancer Origins Implicates the SOX18 Transcription Factor in Tumor Development**. *Cell reports* 2019, **29**(11):3726-3735 e3724.
170. Zhang S, Dolgalev I, Zhang T, Ran H, Levine DA, Neel BG: **Both fallopian tube and ovarian surface epithelium are cells-of-origin for high-grade serous ovarian carcinoma**. *Nature communications* 2019, **10**(1):5367.
171. Torti SV, Torti FM: **Iron and cancer: more ore to be mined**. *Nature reviews Cancer* 2013, **13**(5):342-355.
172. Torti SV, Torti FM: **Iron: The cancer connection**. *Molecular aspects of medicine* 2020, **75**:100860.
173. Manz DH, Blanchette NL, Paul BT, Torti FM, Torti SV: **Iron and cancer: recent insights**. *Annals of the New York Academy of Sciences* 2016, **1368**(1):149-161.
174. Recalcati S, Gammella E, Cairo G: **Dysregulation of iron metabolism in cancer stem cells**. *Free radical biology & medicine* 2019, **133**:216-220.
175. Basuli D, Tesfay L, Deng Z, Paul B, Yamamoto Y, Ning G, Xian W, McKeon F, Lynch M, Crum CP *et al*: **Iron addiction: a novel therapeutic target in ovarian cancer**. *Oncogene* 2017, **36**(29):4089-4099.
176. Robertson DM: **Hemochromatosis and ovarian cancer**. *Women's health* 2011, **7**(5):525-527.
177. Gannon PO, Medelci S, Le Page C, Beaulieu M, Provencher DM, Mes-Masson AM, Santos MM: **Impact of hemochromatosis gene (HFE) mutations on epithelial ovarian cancer risk and prognosis**. *International journal of cancer* 2011, **128**(10):2326-2334.
178. Jung M, Mertens C, Tomat E, Brune B: **Iron as a Central Player and Promising Target in Cancer Progression**. *International journal of molecular sciences* 2019, **20**(2).
179. Brown RAM, Richardson KL, Kabir TD, Trinder D, Ganss R, Leedman PJ: **Altered Iron Metabolism and Impact in Cancer Biology, Metastasis, and Immunology**. *Frontiers in oncology* 2020, **10**:476.
180. Cragg L, Hebbel RP, Miller W, Solovey A, Selby S, Enright H: **The iron chelator L1 potentiates oxidative DNA damage in iron-loaded liver cells**. *Blood* 1998, **92**(2):632-638.
181. Greene CJ, Attwood K, Sharma NJ, Gross KW, Smith GJ, Xu B, Kauffman EC: **Transferrin receptor 1 upregulation in primary tumor and downregulation in benign kidney is associated with progression and mortality in renal cell carcinoma patients**. *Oncotarget* 2017, **8**(63):107052-107075.
182. Calzolari A, Deaglio S, Maldi E, Cassoni P, Malavasi F, Testa U: **TfR2 expression in human colon carcinomas**. *Blood cells, molecules & diseases* 2009, **43**(3):243-249.
183. Pinnix ZK, Miller LD, Wang W, D'Agostino R, Jr., Kute T, Willingham MC, Hatcher H, Tesfay L, Sui G, Di X *et al*: **Ferroportin and iron regulation in breast cancer progression and prognosis**. *Science translational medicine* 2010, **2**(43):43ra56.
184. Alkhateeb AA, Han B, Connor JR: **Ferritin stimulates breast cancer cells through an iron-independent mechanism and is localized within tumor-associated macrophages**. *Breast cancer research and treatment* 2013, **137**(3):733-744.

185. Sasu BJ, Li H, Rose MJ, Arvedson TL, Doellgast G, Molineux G: **Serum hepcidin but not prohepcidin may be an effective marker for anemia of inflammation (AI)**. *Blood cells, molecules & diseases* 2010, **45**(3):238-245.
186. Boult J, Roberts K, Brookes MJ, Hughes S, Bury JP, Cross SS, Anderson GJ, Spychal R, Iqbal T, Tselepis C: **Overexpression of cellular iron import proteins is associated with malignant progression of esophageal adenocarcinoma**. *Clinical cancer research : an official journal of the American Association for Cancer Research* 2008, **14**(2):379-387.
187. Yamada Y, Shigetomi H, Onogi A, Haruta S, Kawaguchi R, Yoshida S, Furukawa N, Nagai A, Tanase Y, Tsunemi T *et al*: **Redox-active iron-induced oxidative stress in the pathogenesis of clear cell carcinoma of the ovary**. *International journal of gynecological cancer : official journal of the International Gynecological Cancer Society* 2011, **21**(7):1200-1207.
188. Itamochi H, Kigawa J, Terakawa N: **Mechanisms of chemoresistance and poor prognosis in ovarian clear cell carcinoma**. *Cancer science* 2008, **99**(4):653-658.
189. Yamaguchi K, Mandai M, Toyokuni S, Hamanishi J, Higuchi T, Takakura K, Fujii S: **Contents of endometriotic cysts, especially the high concentration of free iron, are a possible cause of carcinogenesis in the cysts through the iron-induced persistent oxidative stress**. *Clinical cancer research : an official journal of the American Association for Cancer Research* 2008, **14**(1):32-40.
190. Defrere S, Lousse JC, Gonzalez-Ramos R, Colette S, Donnez J, Van Langendonckt A: **Potential involvement of iron in the pathogenesis of peritoneal endometriosis**. *Molecular human reproduction* 2008, **14**(7):377-385.
191. Singh AK, Chattopadhyay R, Chakravarty B, Chaudhury K: **Markers of oxidative stress in follicular fluid of women with endometriosis and tubal infertility undergoing IVF**. *Reproductive toxicology* 2013, **42**:116-124.
192. Macfarlane LA, Murphy PR: **MicroRNA: Biogenesis, Function and Role in Cancer**. *Current genomics* 2010, **11**(7):537-561.
193. Doench JG, Sharp PA: **Specificity of microRNA target selection in translational repression**. *Genes & development* 2004, **18**(5):504-511.
194. Loeb GB, Khan AA, Canner D, Hiatt JB, Shendure J, Darnell RB, Leslie CS, Rudensky AY: **Transcriptome-wide miR-155 binding map reveals widespread noncanonical microRNA targeting**. *Molecular cell* 2012, **48**(5):760-770.
195. Si W, Shen J, Zheng H, Fan W: **The role and mechanisms of action of microRNAs in cancer drug resistance**. *Clinical epigenetics* 2019, **11**(1):25.
196. Saini HK, Griffiths-Jones S, Enright AJ: **Genomic analysis of human microRNA transcripts**. *Proceedings of the National Academy of Sciences of the United States of America* 2007, **104**(45):17719-17724.
197. Rodriguez A, Griffiths-Jones S, Ashurst JL, Bradley A: **Identification of mammalian microRNA host genes and transcription units**. *Genome research* 2004, **14**(10A):1902-1910.
198. Ul Hussain M: **Micro-RNAs (miRNAs): genomic organisation, biogenesis and mode of action**. *Cell and tissue research* 2012, **349**(2):405-413.
199. Marco A, Ninova M, Ronshaugen M, Griffiths-Jones S: **Clusters of microRNAs emerge by new hairpins in existing transcripts**. *Nucleic acids research* 2013, **41**(16):7745-7752.
200. Friedman RC, Farh KK, Burge CB, Bartel DP: **Most mammalian mRNAs are conserved targets of microRNAs**. *Genome research* 2009, **19**(1):92-105.
201. Wang Y, Luo J, Zhang H, Lu J: **microRNAs in the Same Clusters Evolve to Coordinately Regulate Functionally Related Genes**. *Molecular biology and evolution* 2016, **33**(9):2232-2247.

202. Yuan X, Liu C, Yang P, He S, Liao Q, Kang S, Zhao Y: **Clustered microRNAs' coordination in regulating protein-protein interaction network**. *BMC systems biology* 2009, **3**:65.
203. Kabekkodu SP, Shukla V, Varghese VK, J DS, Chakrabarty S, Satyamoorthy K: **Clustered miRNAs and their role in biological functions and diseases**. *Biological reviews of the Cambridge Philosophical Society* 2018, **93**(4):1955-1986.
204. Seitz H, Royo H, Bortolin ML, Lin SP, Ferguson-Smith AC, Cavaille J: **A large imprinted microRNA gene cluster at the mouse Dlk1-Gtl2 domain**. *Genome research* 2004, **14**(9):1741-1748.
205. Barlow DP, Bartolomei MS: **Genomic imprinting in mammals**. *Cold Spring Harbor perspectives in biology* 2014, **6**(2).
206. Nadal E, Zhong J, Lin J, Reddy RM, Ramnath N, Orringer MB, Chang AC, Beer DG, Chen G: **A MicroRNA cluster at 14q32 drives aggressive lung adenocarcinoma**. *Clinical cancer research : an official journal of the American Association for Cancer Research* 2014, **20**(12):3107-3117.
207. Malnou EC, Umlauf D, Mouysset M, Cavaille J: **Imprinted MicroRNA Gene Clusters in the Evolution, Development, and Functions of Mammalian Placenta**. *Frontiers in genetics* 2018, **9**:706.
208. Martinez-Micaelo N, Beltran-Debon R, Aragones G, Faiges M, Alegret JM: **MicroRNAs Clustered within the 14q32 Locus Are Associated with Endothelial Damage and Microparticle Secretion in Bicuspid Aortic Valve Disease**. *Frontiers in physiology* 2017, **8**:648.
209. Okamoto K, Koda M, Okamoto T, Onoyama T, Miyoshi K, Kishina M, Kato J, Tokunaga S, Sugihara TA, Hara Y *et al*: **A Series of microRNA in the Chromosome 14q32.2 Maternally Imprinted Region Related to Progression of Non-Alcoholic Fatty Liver Disease in a Mouse Model**. *PloS one* 2016, **11**(5):e0154676.
210. Dimmeler S, Yla-Herttuala S: **14q32 miRNA cluster takes center stage in neovascularization**. *Circulation research* 2014, **115**(8):680-682.
211. Zhang B, Pan X, Cobb GP, Anderson TA: **microRNAs as oncogenes and tumor suppressors**. *Developmental biology* 2007, **302**(1):1-12.
212. Kent OA, Mendell JT: **A small piece in the cancer puzzle: microRNAs as tumor suppressors and oncogenes**. *Oncogene* 2006, **25**(46):6188-6196.
213. Martin-Guerrero I, Bilbao-Aldaiturriaga N, Gutierrez-Camino A, Santos-Zorrozua B, Dolzan V, Patino-Garcia A, Garcia-Orad A: **Variants in the 14q32 miRNA cluster are associated with osteosarcoma risk in the Spanish population**. *Scientific reports* 2018, **8**(1):15414.
214. Jishnu PV, Jayaram P, Shukla V, Varghese VK, Pandey D, Sharan K, Chakrabarty S, Satyamoorthy K, Kabekkodu SP: **Prognostic role of 14q32.31 miRNA cluster in various carcinomas: a systematic review and meta-analysis**. *Clinical & experimental metastasis* 2020, **37**(1):31-46.
215. Geraldo MV, Nakaya HI, Kimura ET: **Down-regulation of 14q32-encoded miRNAs and tumor suppressor role for miR-654-3p in papillary thyroid cancer**. *Oncotarget* 2017, **8**(6):9597-9607.
216. Honda S, Chatterjee A, Leichter AL, Miyagi H, Minato M, Fujiyoshi S, Ara M, Kitagawa N, Tanaka M, Tanaka Y *et al*: **A MicroRNA Cluster in the DLK1-DIO3 Imprinted Region on Chromosome 14q32.2 Is Dysregulated in Metastatic Hepatoblastomas**. *Frontiers in oncology* 2020, **10**:513601.
217. Aguda BD, Kim Y, Piper-Hunter MG, Friedman A, Marsh CB: **MicroRNA regulation of a cancer network: consequences of the feedback loops involving miR-17-92, E2F, and Myc**. *Proceedings of the National Academy of Sciences of the United States of America* 2008, **105**(50):19678-19683.

218. Mi S, Li Z, Chen P, He C, Cao D, Elkahloun A, Lu J, Pelloso LA, Wunderlich M, Huang H *et al*: **Aberrant overexpression and function of the miR-17-92 cluster in MLL-rearranged acute leukemia**. *Proceedings of the National Academy of Sciences of the United States of America* 2010, **107**(8):3710-3715.
219. Nojima M, Matsui T, Tamori A, Kubo S, Shirabe K, Kimura K, Shimada M, Utsunomiya T, Kondo Y, Iio E *et al*: **Global, cancer-specific microRNA cluster hypomethylation was functionally associated with the development of non-B non-C hepatocellular carcinoma**. *Molecular cancer* 2016, **15**(1):31.
220. Dai R, Lu R, Ahmed SA: **The Upregulation of Genomic Imprinted DLK1-Dio3 miRNAs in Murine Lupus Is Associated with Global DNA Hypomethylation**. *PloS one* 2016, **11**(4):e0153509.
221. Issa JP: **CpG island methylator phenotype in cancer**. *Nature reviews Cancer* 2004, **4**(12):988-993.
222. Beygo J, Kuchler A, Gillessen-Kaesbach G, Albrecht B, Eckle J, Eggermann T, Gellhaus A, Kanber D, Kordass U, Ludecke HJ *et al*: **New insights into the imprinted MEG8-DMR in 14q32 and clinical and molecular description of novel patients with Temple syndrome**. *European journal of human genetics : EJHG* 2017, **25**(8):935-945.
223. Gonzalez-Vallinas M, Rodriguez-Paredes M, Albrecht M, Sticht C, Stichel D, Gutekunst J, Pitea A, Sass S, Sanchez-Rivera FJ, Lorenzo-Bermejo J *et al*: **Epigenetically Regulated Chromosome 14q32 miRNA Cluster Induces Metastasis and Predicts Poor Prognosis in Lung Adenocarcinoma Patients**. *Molecular cancer research : MCR* 2018, **16**(3):390-402.
224. Zehavi L, Avraham R, Barzilai A, Bar-Ilan D, Navon R, Sidi Y, Avni D, Leibowitz-Amit R: **Silencing of a large microRNA cluster on human chromosome 14q32 in melanoma: biological effects of mir-376a and mir-376c on insulin growth factor 1 receptor**. *Molecular cancer* 2012, **11**:44.
225. Pogribny IP, Tryndyak VP, Pogribna M, Shpyleva S, Surratt G, Gamboa da Costa G, Beland FA: **Modulation of intracellular iron metabolism by iron chelation affects chromatin remodeling proteins and corresponding epigenetic modifications in breast cancer cells and increases their sensitivity to chemotherapeutic agents**. *International journal of oncology* 2013, **42**(5):1822-1832.
226. Song G, Wang L: **Transcriptional mechanism for the paired miR-433 and miR-127 genes by nuclear receptors SHP and ERRgamma**. *Nucleic acids research* 2008, **36**(18):5727-5735.
227. Yoshioka Y, Kosaka N, Ochiya T, Kato T: **Micromanaging Iron Homeostasis: hypoxia-inducible micro-RNA-210 suppresses iron homeostasis-related proteins**. *The Journal of biological chemistry* 2012, **287**(41):34110-34119.
228. Davis M, Clarke S: **Influence of microRNA on the maintenance of human iron metabolism**. *Nutrients* 2013, **5**(7):2611-2628.
229. Castoldi M, Muckenthaler MU: **Regulation of iron homeostasis by microRNAs**. *Cellular and molecular life sciences : CMLS* 2012, **69**(23):3945-3952.
230. Wallace DF, Crawford DH, Subramaniam VN: **The control of iron homeostasis: microRNAS join the party**. *Gastroenterology* 2011, **141**(4):1520-1522.
231. Pogue AI, Percy ME, Cui JG, Li YY, Bhattacharjee S, Hill JM, Kruck TP, Zhao Y, Lukiw WJ: **Up-regulation of NF-kB-sensitive miRNA-125b and miRNA-146a in metal sulfate-stressed human astroglial (HAG) primary cell cultures**. *Journal of inorganic biochemistry* 2011, **105**(11):1434-1437.
232. Faller M, Matsunaga M, Yin S, Loo JA, Guo F: **Heme is involved in microRNA processing**. *Nature structural & molecular biology* 2007, **14**(1):23-29.

233. Li Y, Lin L, Li Z, Ye X, Xiong K, Aryal B, Xu Z, Paroo Z, Liu Q, He C *et al*: **Iron homeostasis regulates the activity of the microRNA pathway through poly(C)-binding protein 2**. *Cell metabolism* 2012, **15**(6):895-904.
234. Smith DM, Patel S, Raffoul F, Haller E, Mills GB, Nanjundan M: **Arsenic trioxide induces a beclin-1-independent autophagic pathway via modulation of SnoN/SkiL expression in ovarian carcinoma cells**. *Cell death and differentiation* 2010, **17**(12):1867-1881.
235. Torres A, Torres K, Wdowiak P, Paszkowski T, Maciejewski R: **Selection and validation of endogenous controls for microRNA expression studies in endometrioid endometrial cancer tissues**. *Gynecologic oncology* 2013, **130**(3):588-594.
236. Gee HE, Buffa FM, Camps C, Ramachandran A, Leek R, Taylor M, Patil M, Sheldon H, Betts G, Homer J *et al*: **The small-nucleolar RNAs commonly used for microRNA normalisation correlate with tumour pathology and prognosis**. *British journal of cancer* 2011, **104**(7):1168-1177.
237. Dutta P, Haller E, Sharp A, Nanjundan M: **MIR494 reduces renal cancer cell survival coinciding with increased lipid droplets and mitochondrial changes**. *BMC cancer* 2016, **16**:33.
238. Rockfield S, Flores I, Nanjundan M: **Expression and function of nuclear receptor coactivator 4 isoforms in transformed endometriotic and malignant ovarian cells**. *Oncotarget* 2018, **9**(4):5344-5367.
239. Bauckman KA, Haller E, Flores I, Nanjundan M: **Iron modulates cell survival in a Ras- and MAPK-dependent manner in ovarian cells**. *Cell death & disease* 2013, **4**:e592.
240. Motzer RJ, Jonasch E, Agarwal N, Bhayani S, Bro WP, Chang SS, Choueiri TK, Costello BA, Derweesh IH, Fishman M *et al*: **Kidney Cancer, Version 2.2017, NCCN Clinical Practice Guidelines in Oncology**. *Journal of the National Comprehensive Cancer Network : JNCCN* 2017, **15**(6):804-834.
241. Hakimi AA, Pham CG, Hsieh JJ: **A clear picture of renal cell carcinoma**. *Nature genetics* 2013, **45**(8):849-850.
242. Voss MH, Molina AM, Motzer RJ: **mTOR inhibitors in advanced renal cell carcinoma**. *Hematology/oncology clinics of North America* 2011, **25**(4):835-852.
243. Soliman GA, Acosta-Jaquez HA, Fingar DC: **mTORC1 inhibition via rapamycin promotes triacylglycerol lipolysis and release of free fatty acids in 3T3-L1 adipocytes**. *Lipids* 2010, **45**(12):1089-1100.
244. Rambold AS, Cohen S, Lippincott-Schwartz J: **Fatty acid trafficking in starved cells: regulation by lipid droplet lipolysis, autophagy, and mitochondrial fusion dynamics**. *Developmental cell* 2015, **32**(6):678-692.
245. Li J, Kim SG, Blenis J: **Rapamycin: one drug, many effects**. *Cell metabolism* 2014, **19**(3):373-379.
246. Eskelinen EL: **Autophagy: Supporting cellular and organismal homeostasis by self-eating**. *The international journal of biochemistry & cell biology* 2019, **111**:1-10.
247. Poklepovic A, Gewirtz DA: **Outcome of early clinical trials of the combination of hydroxychloroquine with chemotherapy in cancer**. *Autophagy* 2014, **10**(8):1478-1480.
248. Riaz A, Huang Y, Johansson S: **G-Protein-Coupled Lysophosphatidic Acid Receptors and Their Regulation of AKT Signaling**. *International journal of molecular sciences* 2016, **17**(2):215.
249. Valdes-Rives SA, Gonzalez-Arenas A: **Autotaxin-Lysophosphatidic Acid: From Inflammation to Cancer Development**. *Mediators of inflammation* 2017, **2017**:9173090.
250. Umezu-Goto M, Tanyi J, Lahad J, Liu S, Yu S, Lapushin R, Hasegawa Y, Lu Y, Trost R, Bevers T *et al*: **Lysophosphatidic acid production and action: validated targets in cancer?** *Journal of cellular biochemistry* 2004, **92**(6):1115-1140.

251. Xu A, Ahsanul Kabir Khan M, Chen F, Zhong Z, Chen HC, Song Y: **Overexpression of autotaxin is associated with human renal cell carcinoma and bladder carcinoma and their progression**. *Med Oncol* 2016, **33**(11):131.
252. Ryan MJ, Johnson G, Kirk J, Fuerstenberg SM, Zager RA, Torok-Storb B: **HK-2: an immortalized proximal tubule epithelial cell line from normal adult human kidney**. *Kidney international* 1994, **45**(1):48-57.
253. Chakravarthi BV, Nepal S, Varambally S: **Genomic and Epigenomic Alterations in Cancer**. *The American journal of pathology* 2016, **186**(7):1724-1735.
254. Ricketts CJ, De Cubas AA, Fan H, Smith CC, Lang M, Reznik E, Bowlby R, Gibb EA, Akbani R, Beroukhim R *et al*: **The Cancer Genome Atlas Comprehensive Molecular Characterization of Renal Cell Carcinoma**. *Cell reports* 2018, **23**(12):3698.
255. Rathmell WK, Chen S: **VHL inactivation in renal cell carcinoma: implications for diagnosis, prognosis and treatment**. *Expert review of anticancer therapy* 2008, **8**(1):63-73.
256. Monzon FA, Alvarez K, Peterson L, Truong L, Amato RJ, Hernandez-McClain J, Tannir N, Parwani AV, Jonasch E: **Chromosome 14q loss defines a molecular subtype of clear-cell renal cell carcinoma associated with poor prognosis**. *Modern pathology : an official journal of the United States and Canadian Academy of Pathology, Inc* 2011, **24**(11):1470-1479.
257. Cerami E, Gao J, Dogrusoz U, Gross BE, Sumer SO, Aksoy BA, Jacobsen A, Byrne CJ, Heuer ML, Larsson E *et al*: **The cBio cancer genomics portal: an open platform for exploring multidimensional cancer genomics data**. *Cancer discovery* 2012, **2**(5):401-404.
258. Gao J, Aksoy BA, Dogrusoz U, Dresdner G, Gross B, Sumer SO, Sun Y, Jacobsen A, Sinha R, Larsson E *et al*: **Integrative analysis of complex cancer genomics and clinical profiles using the cBioPortal**. *Science signaling* 2013, **6**(269):pl1.
259. Haas NB, Appleman LJ, Stein M, Redlinger M, Wilks M, Xu X, Onorati A, Kalavacharla A, Kim T, Zhen CJ *et al*: **Autophagy Inhibition to Augment mTOR Inhibition: a Phase I/II Trial of Everolimus and Hydroxychloroquine in Patients with Previously Treated Renal Cell Carcinoma**. *Clinical cancer research : an official journal of the American Association for Cancer Research* 2019, **25**(7):2080-2087.
260. Lotze MT, Maranchie J, Appleman L: **Inhibiting autophagy: a novel approach for the treatment of renal cell carcinoma**. *Cancer J* 2013, **19**(4):341-347.
261. Saito K, Arai E, Maekawa K, Ishikawa M, Fujimoto H, Taguchi R, Matsumoto K, Kanai Y, Saito Y: **Lipidomic Signatures and Associated Transcriptomic Profiles of Clear Cell Renal Cell Carcinoma**. *Scientific reports* 2016, **6**:28932.
262. Mooberry LK, Sabnis NA, Panchoo M, Nagarajan B, Lacko AG: **Targeting the SR-B1 Receptor as a Gateway for Cancer Therapy and Imaging**. *Frontiers in pharmacology* 2016, **7**:466.
263. Rapaport D: **Finding the right organelle. Targeting signals in mitochondrial outer-membrane proteins**. *EMBO reports* 2003, **4**(10):948-952.
264. Beloribi-Djefaflia S, Vasseur S, Guillaumond F: **Lipid metabolic reprogramming in cancer cells**. *Oncogenesis* 2016, **5**:e189.
265. Rohwedder A, Zhang Q, Rudge SA, Wakelam MJ: **Lipid droplet formation in response to oleic acid in Huh-7 cells is mediated by the fatty acid receptor FFAR4**. *Journal of cell science* 2014, **127**(Pt 14):3104-3115.
266. Jiang L, Wang W, He Q, Wu Y, Lu Z, Sun J, Liu Z, Shao Y, Wang A: **Oleic acid induces apoptosis and autophagy in the treatment of Tongue Squamous cell carcinomas**. *Scientific reports* 2017, **7**(1):11277.
267. Liotti A, Cosimato V, Mirra P, Cali G, Conza D, Secondo A, Luongo G, Terracciano D, Formisano P, Beguinot F *et al*: **Oleic acid promotes prostate cancer malignant**

phenotype via the G protein-coupled receptor FFA1/GPR40. *Journal of cellular physiology* 2018, **233**(9):7367-7378.
268. Navarro-Tito N, Soto-Guzman A, Castro-Sanchez L, Martinez-Orozco R, Salazar EP: **Oleic acid promotes migration on MDA-MB-231 breast cancer cells through an arachidonic acid-dependent pathway**. *The international journal of biochemistry & cell biology* 2010, **42**(2):306-317.
269. Yu S, Murph MM, Lu Y, Liu S, Hall HS, Liu J, Stephens C, Fang X, Mills GB: **Lysophosphatidic acid receptors determine tumorigenicity and aggressiveness of ovarian cancer cells**. *Journal of the National Cancer Institute* 2008, **100**(22):1630-1642.
270. Maycotte P, Marin-Hernandez A, Goyri-Aguirre M, Anaya-Ruiz M, Reyes-Leyva J, Cortes-Hernandez P: **Mitochondrial dynamics and cancer**. *Tumour biology : the journal of the International Society for Oncodevelopmental Biology and Medicine* 2017, **39**(5):1010428317698391.
271. Aon MA, Bhatt N, Cortassa SC: **Mitochondrial and cellular mechanisms for managing lipid excess**. *Frontiers in physiology* 2014, **5**:282.
272. Morita M, Prudent J, Basu K, Goyon V, Katsumura S, Hulea L, Pearl D, Siddiqui N, Strack S, McGuirk S *et al*: **mTOR Controls Mitochondrial Dynamics and Cell Survival via MTFP1**. *Molecular cell* 2017, **67**(6):922-935 e925.
273. Yan C, Wei H, Minjuan Z, Yan X, Jingyue Y, Wenchao L, Sheng H: **The mTOR inhibitor rapamycin synergizes with a fatty acid synthase inhibitor to induce cytotoxicity in ER/HER2-positive breast cancer cells**. *PloS one* 2014, **9**(5):e97697.
274. Ramesh J, Ronsard L, Gao A, Venugopal B: **Autophagy Intertwines with Different Diseases-Recent Strategies for Therapeutic Approaches**. *Diseases* 2019, **7**(1).
275. Rodrik-Outmezguine VS, Chandarlapaty S, Pagano NC, Poulikakos PI, Scaltriti M, Moskatel E, Baselga J, Guichard S, Rosen N: **mTOR kinase inhibition causes feedback-dependent biphasic regulation of AKT signaling**. *Cancer discovery* 2011, **1**(3):248-259.
276. Sathe A, Chalaud G, Oppolzer I, Wong KY, von Busch M, Schmid SC, Tong Z, Retz M, Gschwend JE, Schulz WA *et al*: **Parallel PI3K, AKT and mTOR inhibition is required to control feedback loops that limit tumor therapy**. *PloS one* 2018, **13**(1):e0190854.
277. Yang J, Xu J, Han X, Wang H, Zhang Y, Dong J, Deng Y, Wang J: **Lysophosphatidic Acid Is Associated With Cardiac Dysfunction and Hypertrophy by Suppressing Autophagy via the LPA3/AKT/mTOR Pathway**. *Frontiers in physiology* 2018, **9**:1315.
278. Genc GE, Hipolito VEB, Botelho RJ, Gumuslu S: **Lysophosphatidic acid represses autophagy in prostate carcinoma cells**. *Biochemistry and cell biology = Biochimie et biologie cellulaire* 2019, **97**(4):387-396.
279. Tang W, Yuan J, Chen X, Gu X, Luo K, Li J, Wan B, Wang Y, Yu L: **Identification of a novel human lysophosphatidic acid acyltransferase, LPAAT-theta, which activates mTOR pathway**. *Journal of biochemistry and molecular biology* 2006, **39**(5):626-635.
280. Xu M, Liu Z, Wang C, Yao B, Zheng X: **EDG2 enhanced the progression of hepatocellular carcinoma by LPA/PI3K/AKT/ mTOR signaling**. *Oncotarget* 2017, **8**(39):66154-66168.
281. Benesch MG, Zhao YY, Curtis JM, McMullen TP, Brindley DN: **Regulation of autotaxin expression and secretion by lysophosphatidate and sphingosine 1-phosphate**. *Journal of lipid research* 2015, **56**(6):1134-1144.
282. Pal MK, Jaiswar SP, Dwivedi VN, Tripathi AK, Dwivedi A, Sankhwar P: **MicroRNA: a new and promising potential biomarker for diagnosis and prognosis of ovarian cancer**. *Cancer biology & medicine* 2015, **12**(4):328-341.
283. Gozzelino R, Arosio P: **Iron Homeostasis in Health and Disease**. *International journal of molecular sciences* 2016, **17**(1).

284. Rockfield S, Chhabra R, Robertson M, Rehman N, Bisht R, Nanjundan M: **Links Between Iron and Lipids: Implications in Some Major Human Diseases**. *Pharmaceuticals* 2018, **11**(4).
285. Yang WS, Stockwell BR: **Ferroptosis: Death by Lipid Peroxidation**. *Trends in cell biology* 2016, **26**(3):165-176.
286. Skouta R, Dixon SJ, Wang J, Dunn DE, Orman M, Shimada K, Rosenberg PA, Lo DC, Weinberg JM, Linkermann A *et al*: **Ferrostatins inhibit oxidative lipid damage and cell death in diverse disease models**. *Journal of the American Chemical Society* 2014, **136**(12):4551-4556.
287. Steegmann-Olmedillas JL: **The role of iron in tumour cell proliferation**. *Clinical & translational oncology : official publication of the Federation of Spanish Oncology Societies and of the National Cancer Institute of Mexico* 2011, **13**(2):71-76.
288. Rockfield S, Guergues J, Rehman N, Smith A, Bauckman KA, Stevens SM, Jr., Nanjundan M: **Proteomic Profiling of Iron-Treated Ovarian Cells Identifies AKT Activation that Modulates the CLEAR Network**. *Proteomics* 2018, **18**(23):e1800244.
289. Labidi-Galy SI, Papp E, Hallberg D, Niknafs N, Adleff V, Noe M, Bhattacharya R, Novak M, Jones S, Phallen J *et al*: **High grade serous ovarian carcinomas originate in the fallopian tube**. *Nature communications* 2017, **8**(1):1093.
290. Formosa A, Markert EK, Lena AM, Italiano D, Finazzi-Agro E, Levine AJ, Bernardini S, Garabadgiu AV, Melino G, Candi E: **MicroRNAs, miR-154, miR-299-5p, miR-376a, miR-376c, miR-377, miR-381, miR-487b, miR-485-3p, miR-495 and miR-654-3p, mapped to the 14q32.31 locus, regulate proliferation, apoptosis, migration and invasion in metastatic prostate cancer cells**. *Oncogene* 2014, **33**(44):5173-5182.
291. Uppal A, Wightman SC, Mallon S, Oshima G, Pitroda SP, Zhang Q, Huang X, Darga TE, Huang L, Andrade J *et al*: **14q32-encoded microRNAs mediate an oligometastatic phenotype**. *Oncotarget* 2015, **6**(6):3540-3552.
292. Lin SP, Youngson N, Takada S, Seitz H, Reik W, Paulsen M, Cavaille J, Ferguson-Smith AC: **Asymmetric regulation of imprinting on the maternal and paternal chromosomes at the Dlk1-Gtl2 imprinted cluster on mouse chromosome 12**. *Nature genetics* 2003, **35**(1):97-102.
293. Wylie AA, Murphy SK, Orton TC, Jirtle RL: **Novel imprinted DLK1/GTL2 domain on human chromosome 14 contains motifs that mimic those implicated in IGF2/H19 regulation**. *Genome research* 2000, **10**(11):1711-1718.
294. Kagami M, Sekita Y, Nishimura G, Irie M, Kato F, Okada M, Yamamori S, Kishimoto H, Nakayama M, Tanaka Y *et al*: **Deletions and epimutations affecting the human 14q32.2 imprinted region in individuals with paternal and maternal upd(14)-like phenotypes**. *Nature genetics* 2008, **40**(2):237-242.
295. Goossens EAC, de Vries MR, Simons KH, Putter H, Quax PHA, Nossent AY: **miRMap: Profiling 14q32 microRNA Expression and DNA Methylation Throughout the Human Vasculature**. *Frontiers in cardiovascular medicine* 2019, **6**:113.
296. Karst AM, Drapkin R: **Primary culture and immortalization of human fallopian tube secretory epithelial cells**. *Nature protocols* 2012, **7**(9):1755-1764.
297. Lattuada D, Uberti F, Colciaghi B, Morsanuto V, Maldi E, Squarzanti DF, Molinari C, Boldorini R, Bulfoni A, Colombo P *et al*: **Fimbrial cells exposure to catalytic iron mimics carcinogenic changes**. *International journal of gynecological cancer : official journal of the International Gynecological Cancer Society* 2015, **25**(3):389-398.
298. Guergues J, Wohlfahrt J, Zhang P, Liu B, Stevens SM, Jr.: **Deep proteome profiling reveals novel pathways associated with pro-inflammatory and alcohol-induced microglial activation phenotypes**. *Journal of proteomics* 2020, **220**:103753.
299. Guergues J, Zhang P, Liu B, Stevens SM, Jr.: **Improved Methodology for Sensitive and Rapid Quantitative Proteomic Analysis of Adult-Derived Mouse Microglia:**

Application to a Novel In Vitro Mouse Microglial Cell Model. *Proteomics* 2019, **19**(11):e1800469.
300. Ramus C, Hovasse A, Marcellin M, Hesse AM, Mouton-Barbosa E, Bouyssie D, Vaca S, Carapito C, Chaoui K, Bruley C *et al*: **Benchmarking quantitative label-free LC-MS data processing workflows using a complex spiked proteomic standard dataset**. *Journal of proteomics* 2016, **132**:51-62.
301. Lee EM, Shin S, Cha HJ, Yoon Y, Bae S, Jung JH, Lee SM, Lee SJ, Park IC, Jin YW *et al*: **Suberoylanilide hydroxamic acid (SAHA) changes microRNA expression profiles in A549 human non-small cell lung cancer cells**. *International journal of molecular medicine* 2009, **24**(1):45-50.
302. Nalls D, Tang SN, Rodova M, Srivastava RK, Shankar S: **Targeting epigenetic regulation of miR-34a for treatment of pancreatic cancer by inhibition of pancreatic cancer stem cells**. *PloS one* 2011, **6**(8):e24099.
303. Qiu X, Hother C, Ralfkiaer UM, Sogaard A, Lu Q, Workman CT, Liang G, Jones PA, Gronbaek K: **Equitoxic doses of 5-azacytidine and 5-aza-2'deoxycytidine induce diverse immediate and overlapping heritable changes in the transcriptome**. *PloS one* 2010, **5**(9).
304. Perez-Riverol Y, Csordas A, Bai J, Bernal-Llinares M, Hewapathirana S, Kundu DJ, Inuganti A, Griss J, Mayer G, Eisenacher M *et al*: **The PRIDE database and related tools and resources in 2019: improving support for quantification data**. *Nucleic acids research* 2019, **47**(D1):D442-D450.
305. Dutta P, Bui T, Bauckman KA, Keyomarsi K, Mills GB, Nanjundan M: **EVI1 splice variants modulate functional responses in ovarian cancer cells**. *Molecular oncology* 2013, **7**(3):647-668.
306. Park J, Zhang X, Lee SK, Song NY, Son SH, Kim KR, Shim JH, Park KK, Chung WY: **CCL28-induced RARbeta expression inhibits oral squamous cell carcinoma bone invasion**. *The Journal of clinical investigation* 2019, **129**(12):5381-5399.
307. Rossaert E, Pollari E, Jaspers T, Van Helleputte L, Jarpe M, Van Damme P, De Bock K, Moisse M, Van Den Bosch L: **Restoration of histone acetylation ameliorates disease and metabolic abnormalities in a FUS mouse model**. *Acta neuropathologica communications* 2019, **7**(1):107.
308. Rodgers LH, E Oh, Young AN, Burdette JE: **Loss of PAX8 in high-grade serous ovarian cancer reduces cell survival despite unique modes of action in the fallopian tube and ovarian surface epithelium**. *Oncotarget* 2016, **7**(22):32785-32795.
309. Jazaeri AA, Ferriss JS, Bryant JL, Dalton MS, Dutta A: **Evaluation of EVI1 and EVI1s (Delta324) as potential therapeutic targets in ovarian cancer**. *Gynecologic oncology* 2010, **118**(2):189-195.
310. Perkins AS, Fishel R, Jenkins NA, Copeland NG: **Evi-1, a murine zinc finger proto-oncogene, encodes a sequence-specific DNA-binding protein**. *Molecular and cellular biology* 1991, **11**(5):2665-2674.
311. Delwel R, Funabiki T, Kreider BL, Morishita K, Ihle JN: **Four of the seven zinc fingers of the Evi-1 myeloid-transforming gene are required for sequence-specific binding to GA(C/T)AAGA(T/C)AAGATAA**. *Molecular and cellular biology* 1993, **13**(7):4291-4300.
312. Funabiki T, Kreider BL, Ihle JN: **The carboxyl domain of zinc fingers of the Evi-1 myeloid transforming gene binds a consensus sequence of GAAGATGAG**. *Oncogene* 1994, **9**(6):1575-1581.
313. Yatsula B, Lin S, Read AJ, Poholek A, Yates K, Yue D, Hui P, Perkins AS: **Identification of binding sites of EVI1 in mammalian cells**. *The Journal of biological chemistry* 2005, **280**(35):30712-30722.
314. Tan W, Liu B, Qu S, Liang G, Luo W, Gong C: **MicroRNAs and cancer: Key paradigms in molecular therapy**. *Oncology letters* 2018, **15**(3):2735-2742.

315. Durkin SG, Glover TW: **Chromosome fragile sites**. *Annual review of genetics* 2007, **41**:169-192.
316. Bandera CA, Takahashi H, Behbakht K, Liu PC, LiVolsi VA, Benjamin I, Morgan MA, King SA, Rubin SC, Boyd J: **Deletion mapping of two potential chromosome 14 tumor suppressor gene loci in ovarian carcinoma**. *Cancer research* 1997, **57**(3):513-515.
317. Hoshi M, Otagiri N, Shiwaku HO, Asakawa S, Shimizu N, Kaneko Y, Ohi R, Hayashi Y, Horii A: **Detailed deletion mapping of chromosome band 14q32 in human neuroblastoma defines a 1.1-Mb region of common allelic loss**. *British journal of cancer* 2000, **82**(11):1801-1807.
318. Niu CS, Yang Y, Cheng CD: **MiR-134 regulates the proliferation and invasion of glioblastoma cells by reducing Nanog expression**. *International journal of oncology* 2013, **42**(5):1533-1540.
319. Anaya-Ruiz M, Bandala C, Perez-Santos JL: **miR-485 acts as a tumor suppressor by inhibiting cell growth and migration in breast carcinoma T47D cells**. *Asian Pacific journal of cancer prevention : APJCP* 2013, **14**(6):3757-3760.
320. Lim L, Balakrishnan A, Huskey N, Jones KD, Jodari M, Ng R, Song G, Riordan J, Anderton B, Cheung ST *et al*: **MicroRNA-494 within an oncogenic microRNA megacluster regulates G1/S transition in liver tumorigenesis through suppression of mutated in colorectal cancer**. *Hepatology* 2014, **59**(1):202-215.
321. Yu C, Wang M, Li Z, Xiao J, Peng F, Guo X, Deng Y, Jiang J, Sun C: **MicroRNA-138-5p regulates pancreatic cancer cell growth through targeting FOXC1**. *Cellular oncology* 2015, **38**(3):173-181.
322. Jiang B, Mu W, Wang J, Lu J, Jiang S, Li L, Xu H, Tian H: **MicroRNA-138 functions as a tumor suppressor in osteosarcoma by targeting differentiated embryonic chondrocyte gene 2**. *Journal of experimental & clinical cancer research : CR* 2016, **35**:69.
323. Qu M, Zhu Y, Jin M: **MicroRNA-138 inhibits SOX12 expression and the proliferation, invasion and migration of ovarian cancer cells**. *Experimental and therapeutic medicine* 2018, **16**(3):1629-1638.
324. Qiu H, Chen F, Chen M: **MicroRNA-138 negatively regulates the hypoxia-inducible factor 1alpha to suppress melanoma growth and metastasis**. *Biology open* 2019, **8**(8).
325. Zhang J, Liu J, Wu J, Li W, Chen Z, Yang L: **Progression of the role of CRYAB in signaling pathways and cancers**. *OncoTargets and therapy* 2019, **12**:4129-4139.
326. Adorno-Cruz V, Liu H: **Regulation and functions of integrin alpha2 in cell adhesion and disease**. *Genes & diseases* 2019, **6**(1):16-24.
327. Lehmann U, Wingen LU, Brakensiek K, Wedemeyer H, Becker T, Heim A, Metzig K, Hasemeier B, Kreipe H, Flemming P: **Epigenetic defects of hepatocellular carcinoma are already found in non-neoplastic liver cells from patients with hereditary haemochromatosis**. *Human molecular genetics* 2007, **16**(11):1335-1342.
328. Ye Q, Trivedi M, Zhang Y, Bohlke M, Alsulimani H, Chang J, Maher T, Deth R, Kim J: **Brain iron loading impairs DNA methylation and alters GABAergic function in mice**. *FASEB journal : official publication of the Federation of American Societies for Experimental Biology* 2019, **33**(2):2460-2471.
329. Adler EK, Corona RI, Lee JM, Rodriguez-Malave N, Mhawech-Fauceglia P, Sowter H, Hazelett DJ, Lawrenson K, Gayther SA: **The PAX8 cistrome in epithelial ovarian cancer**. *Oncotarget* 2017, **8**(65):108316-108332.
330. Zhang J, Shi J, Zhang G, Zhang X, Yang X, Yang S, Wang J, Hu K, Ke X, Fu L: **MicroRNA-425 upregulation indicates better prognosis in younger acute myeloid leukemia patients undergoing chemotherapy**. *Oncology letters* 2019, **17**(6):5793-5802.

331. Saito Y, Saito H, Liang G, Friedman JM: **Epigenetic alterations and microRNA misexpression in cancer and autoimmune diseases: a critical review**. *Clinical reviews in allergy & immunology* 2014, **47**(2):128-135.
332. Bianchi M, Renzini A, Adamo S, Moresi V: **Coordinated Actions of MicroRNAs with other Epigenetic Factors Regulate Skeletal Muscle Development and Adaptation**. *International journal of molecular sciences* 2017, **18**(4).
333. Ramassone A, Pagotto S, Veronese A, Visone R: **Epigenetics and MicroRNAs in Cancer**. *International journal of molecular sciences* 2018, **19**(2).
334. Edwards CA, Mungall AJ, Matthews L, Ryder E, Gray DJ, Pask AJ, Shaw G, Graves JA, Rogers J, consortium S *et al*: **The evolution of the DLK1-DIO3 imprinted domain in mammals**. *PLoS biology* 2008, **6**(6):e135.
335. Zeng TB, He HJ, Han ZB, Zhang FW, Huang ZJ, Liu Q, Cui W, Wu Q: **DNA methylation dynamics of a maternally methylated DMR in the mouse Dlk1-Dio3 domain**. *FEBS letters* 2014, **588**(24):4665-4671.
336. Carr MS, Yevtodiyenko A, Schmidt CL, Schmidt JV: **Allele-specific histone modifications regulate expression of the Dlk1-Gtl2 imprinted domain**. *Genomics* 2007, **89**(2):280-290.
337. Kisliouk T, Yosefi S, Meiri N: **MiR-138 inhibits EZH2 methyltransferase expression and methylation of histone H3 at lysine 27, and affects thermotolerance acquisition**. *The European journal of neuroscience* 2011, **33**(2):224-235.
338. Shao L, Hou C: **miR-138 activates NF-kappaB signaling and PGRN to promote rheumatoid arthritis via regulating HDAC4**. *Biochemical and biophysical research communications* 2019, **519**(1):166-171.
339. Sarkar S, Abujamra AL, Loew JE, Forman LW, Perrine SP, Faller DV: **Histone deacetylase inhibitors reverse CpG methylation by regulating DNMT1 through ERK signaling**. *Anticancer research* 2011, **31**(9):2723-2732.
340. Zhou Q, Agoston AT, Atadja P, Nelson WG, Davidson NE: **Inhibition of histone deacetylases promotes ubiquitin-dependent proteasomal degradation of DNA methyltransferase 1 in human breast cancer cells**. *Molecular cancer research : MCR* 2008, **6**(5):873-883.
341. Stresemann C, Lyko F: **Modes of action of the DNA methyltransferase inhibitors azacytidine and decitabine**. *International journal of cancer* 2008, **123**(1):8-13.
342. Mitomo S, Maesawa C, Ogasawara S, Iwaya T, Shibazaki M, Yashima-Abo A, Kotani K, Oikawa H, Sakurai E, Izutsu N *et al*: **Downregulation of miR-138 is associated with overexpression of human telomerase reverse transcriptase protein in human anaplastic thyroid carcinoma cell lines**. *Cancer science* 2008, **99**(2):280-286.
343. Zhang XL, Xu LL, Wang F: **Hsa_circ_0020397 regulates colorectal cancer cell viability, apoptosis and invasion by promoting the expression of the miR-138 targets TERT and PD-L1**. *Cell biology international* 2017, **41**(9):1056-1064.
344. Zhou N, Fei D, Zong S, Zhang M, Yue Y: **MicroRNA-138 inhibits proliferation, migration and invasion through targeting hTERT in cervical cancer**. *Oncology letters* 2016, **12**(5):3633-3639.
345. Qureshi-Baig K, Ullmann P, Haan S, Letellier E: **Tumor-Initiating Cells: a criTICal review of isolation approaches and new challenges in targeting strategies**. *Molecular cancer* 2017, **16**(1):40.
346. Zhu P, Fan Z: **Cancer stem cells and tumorigenesis**. *Biophysics reports* 2018, **4**(4):178-188.
347. Chanvorachote P, Luanpitpong S: **Iron induces cancer stem cells and aggressive phenotypes in human lung cancer cells**. *American journal of physiology Cell physiology* 2016, **310**(9):C728-739.

348. Marcato P, Dean CA, Giacomantonio CA, Lee PW: **Aldehyde dehydrogenase: its role as a cancer stem cell marker comes down to the specific isoform**. *Cell cycle* 2011, **10**(9):1378-1384.
349. Clark DW, Palle K: **Aldehyde dehydrogenases in cancer stem cells: potential as therapeutic targets**. *Annals of translational medicine* 2016, **4**(24):518.
350. Ono Y, Fukuhara N, Yoshie O: **TAL1 and LIM-only proteins synergistically induce retinaldehyde dehydrogenase 2 expression in T-cell acute lymphoblastic leukemia by acting as cofactors for GATA3**. *Molecular and cellular biology* 1998, **18**(12):6939-6950.
351. Auersperg N: **The stem-cell profile of ovarian surface epithelium is reproduced in the oviductal fimbriae, with increased stem-cell marker density in distal parts of the fimbriae**. *International journal of gynecological pathology : official journal of the International Society of Gynecological Pathologists* 2013, **32**(5):444-453.
352. Wang Y, Shao F, Chen L: **ALDH1A2 suppresses epithelial ovarian cancer cell proliferation and migration by downregulating STAT3**. *OncoTargets and therapy* 2018, **11**:599-608.
353. Morton SU, Scherz PJ, Cordes KR, Ivey KN, Stainier DY, Srivastava D: **microRNA-138 modulates cardiac patterning during embryonic development**. *Proceedings of the National Academy of Sciences of the United States of America* 2008, **105**(46):17830-17835.
354. Wu TS, Yang JJ, Yu FY, Liu BH: **Cardiotoxicity of mycotoxin citrinin and involvement of microRNA-138 in zebrafish embryos**. *Toxicological sciences : an official journal of the Society of Toxicology* 2013, **136**(2):402-412.
355. Hannen R, Bartsch JW: **Essential roles of telomerase reverse transcriptase hTERT in cancer stemness and metastasis**. *FEBS letters* 2018, **592**(12):2023-2031.
356. Tsai CC, Chen CL, Liu HC, Lee YT, Wang HW, Hou LT, Hung SC: **Overexpression of hTERT increases stem-like properties and decreases spontaneous differentiation in human mesenchymal stem cell lines**. *Journal of biomedical science* 2010, **17**:64.
357. Wang X, Zhao Y, Cao W, Wang C, Sun B, Chen J, Li S, Chen J, Cui M, Zhang B *et al*: **miR-138-5p acts as a tumor suppressor by targeting hTERT in human colorectal cancer**. *International journal of clinical and experimental pathology* 2017, **10**(12):11516-11525.
358. Tong GX, Devaraj K, Hamele-Bena D, Yu WM, Turk A, Chen X, Wright JD, Greenebaum E: **Pax8: a marker for carcinoma of Mullerian origin in serous effusions**. *Diagnostic cytopathology* 2011, **39**(8):567-574.
359. Ozcan A, Shen SS, Hamilton C, Anjana K, Coffey D, Krishnan B, Truong LD: **PAX 8 expression in non-neoplastic tissues, primary tumors, and metastatic tumors: a comprehensive immunohistochemical study**. *Modern pathology : an official journal of the United States and Canadian Academy of Pathology, Inc* 2011, **24**(6):751-764.
360. Cancer Genome Atlas Research N: **Integrated genomic analyses of ovarian carcinoma**. *Nature* 2011, **474**(7353):609-615.
361. Ordonez NG: **Value of PAX8, PAX2, claudin-4, and h-caldesmon immunostaining in distinguishing peritoneal epithelioid mesotheliomas from serous carcinomas**. *Modern pathology : an official journal of the United States and Canadian Academy of Pathology, Inc* 2013, **26**(4):553-562.
362. Wang Y, Wang Y, Li J, Yuan Z, Yuan B, Zhang T, Cragun JM, Kong B, Zheng W: **PAX8: a sensitive and specific marker to identify cancer cells of ovarian origin for patients prior to neoadjuvant chemotherapy**. *Journal of hematology & oncology* 2013, **6**:60.
363. Chai HJ, Ren Q, Fan Q, Ye L, Du GY, Du HW, Xu W, Li Y, Zhang L, Cheng ZP: **PAX8 is a potential marker for the diagnosis of primary epithelial ovarian cancer**. *Oncology letters* 2017, **14**(5):5871-5875.

364. Bi L, Yang Q, Yuan J, Miao Q, Duan L, Li F, Wang S: **MicroRNA-127-3p acts as a tumor suppressor in epithelial ovarian cancer by regulating the BAG5 gene**. *Oncology reports* 2016, **36**(5):2563-2570.
365. Chen L, Kong G, Zhang C, Dong H, Yang C, Song G, Guo C, Wang L, Yu H: **MicroRNA-432 functions as a tumor suppressor gene through targeting E2F3 and AXL in lung adenocarcinoma**. *Oncotarget* 2016, **7**(15):20041-20053.
366. Zhou Z, Li Z, Shen Y, Chen T: **MicroRNA-138 directly targets TNFAIP8 and acts as a tumor suppressor in osteosarcoma**. *Experimental and therapeutic medicine* 2017, **14**(4):3665-3673.
367. Akatsuka S, Yamashita Y, Ohara H, Liu YT, Izumiya M, Abe K, Ochiai M, Jiang L, Nagai H, Okazaki Y *et al*: **Fenton reaction induced cancer in wild type rats recapitulates genomic alterations observed in human cancer**. *PloS one* 2012, **7**(8):e43403.
368. Kowdley KV: **Iron, hemochromatosis, and hepatocellular carcinoma**. *Gastroenterology* 2004, **127**(5 Suppl 1):S79-86.
369. Radulescu S, Brookes MJ, Salgueiro P, Ridgway RA, McGhee E, Anderson K, Ford SJ, Stones DH, Iqbal TH, Tselepis C *et al*: **Luminal iron levels govern intestinal tumorigenesis after Apc loss in vivo**. *Cell reports* 2012, **2**(2):270-282.
370. Bhutia YD, Ogura J, Grippo PJ, Torres C, Sato T, Wachtel M, Ramachandran S, Babu E, Sivaprakasam S, Rajasekaran D *et al*: **Chronic exposure to excess iron promotes EMT and cancer via p53 loss in pancreatic cancer**. *Asian journal of pharmaceutical sciences* 2020, **15**(2):237-251.
371. Rockfield S, Raffel J, Mehta R, Rehman N, Nanjundan M: **Iron overload and altered iron metabolism in ovarian cancer**. *Biological chemistry* 2017, **398**(9):995-1007.
372. Defrere S, Van Langendonckt A, Vaesen S, Jouret M, Gonzalez Ramos R, Gonzalez D, Donnez J: **Iron overload enhances epithelial cell proliferation in endometriotic lesions induced in a murine model**. *Human reproduction* 2006, **21**(11):2810-2816.
373. Emori MM, Drapkin R: **The hormonal composition of follicular fluid and its implications for ovarian cancer pathogenesis**. *Reproductive biology and endocrinology : RB&E* 2014, **12**:60.
374. Van Langendonckt A, Casanas-Roux F, Donnez J: **Iron overload in the peritoneal cavity of women with pelvic endometriosis**. *Fertility and sterility* 2002, **78**(4):712-718.
375. Shah PP, Hutchinson LE, Kakar SS: **Emerging role of microRNAs in diagnosis and treatment of various diseases including ovarian cancer**. *Journal of ovarian research* 2009, **2**(1):11.
376. Seven M, Karatas OF, Duz MB, Ozen M: **The role of miRNAs in cancer: from pathogenesis to therapeutic implications**. *Future oncology* 2014, **10**(6):1027-1048.
377. Stransky B, de Souza SJ: **Modeling tumor evolutionary dynamics**. *Frontiers in physiology* 2012, **3**:480.
378. Katt ME, Placone AL, Wong AD, Xu ZS, Searson PC: **In Vitro Tumor Models: Advantages, Disadvantages, Variables, and Selecting the Right Platform**. *Frontiers in bioengineering and biotechnology* 2016, **4**:12.
379. Kim O, Park EY, Klinkebiel DL, Pack SD, Shin YH, Abdullaev Z, Emerson RE, Coffey DM, Kwon SY, Creighton CJ *et al*: **In vivo modeling of metastatic human high-grade serous ovarian cancer in mice**. *PLoS genetics* 2020, **16**(6):e1008808.
380. Tudrej P, Kujawa KA, Cortez AJ, Lisowska KM: **Characteristics of in Vivo Model Systems for Ovarian Cancer Studies**. *Diagnostics* 2019, **9**(3).
381. White EA, Kenny HA, Lengyel E: **Three-dimensional modeling of ovarian cancer**. *Advanced drug delivery reviews* 2014, **79-80**:184-192.
382. Hoarau-Vechot J, Rafii A, Touboul C, Pasquier J: **Halfway between 2D and Animal Models: Are 3D Cultures the Ideal Tool to Study Cancer-Microenvironment Interactions?** *International journal of molecular sciences* 2018, **19**(1).

383. Rensvold JW, Krautkramer KA, Dowell JA, Denu JM, Pagliarini DJ: **Iron Deprivation Induces Transcriptional Regulation of Mitochondrial Biogenesis**. *The Journal of biological chemistry* 2016, **291**(40):20827-20837.
384. Pang L, Li B, Zheng B, Niu L, Ge L: **miR-138 inhibits gastric cancer growth by suppressing SOX4**. *Oncology reports* 2017, **38**(2):1295-1302.
385. Luo J, Chen P, Xie W, Wu F: **MicroRNA-138 inhibits cell proliferation in hepatocellular carcinoma by targeting Sirt1**. *Oncology reports* 2017, **38**(2):1067-1074.
386. Yeh M, Oh CS, Yoo JY, Kaur B, Lee TJ: **Pivotal role of microRNA-138 in human cancers**. *American journal of cancer research* 2019, **9**(6):1118-1126.
387. Hesson LB, Cooper WN, Latif F: **Evaluation of the 3p21.3 tumour-suppressor gene cluster**. *Oncogene* 2007, **26**(52):7283-7301.
388. da Costa Prando E, Cavalli LR, Rainho CA: **Evidence of epigenetic regulation of the tumor suppressor gene cluster flanking RASSF1 in breast cancer cell lines**. *Epigenetics* 2011, **6**(12):1413-1424.
389. Jin C, Rajabi H, Kufe D: **miR-1226 targets expression of the mucin 1 oncoprotein and induces cell death**. *International journal of oncology* 2010, **37**(1):61-69.
390. Hu H, Zhao X, Jin Z, Hou M: **Hsa-let-7g miRNA regulates the anti-tumor effects of gastric cancer cells under oxidative stress through the expression of DDR genes**. *The Journal of toxicological sciences* 2015, **40**(3):329-338.
391. Jiang C, Shen F, Du J, Hu Z, Li X, Su J, Wang X, Huang X: **MicroRNA-564 is downregulated in glioblastoma and inhibited proliferation and invasion of glioblastoma cells by targeting TGF-beta1**. *Oncotarget* 2016, **7**(35):56200-56208.
392. Ahmad A, Zhang W, Wu M, Tan S, Zhu T: **Tumor-suppressive miRNA-135a inhibits breast cancer cell proliferation by targeting ELK1 and ELK3 oncogenes**. *Genes & genomics* 2018, **40**(3):243-251.
393. Song Z, Yang H, Wu X, Kong C, Xu C: **microRNA-564 inhibits the aggressive phenotypes of papillary thyroid cancer by directly targeting astrocyte-elevated gene-1**. *OncoTargets and therapy* 2019, **12**:4869-4881.
394. Zhang EL, Gu J, Zhang ZY, Dong KS, Liang BY, Huang ZY: **MicroRNA expression profiling in patients with hepatocellular carcinoma of familial aggregation and hepatitis B virus infection**. *Oncology letters* 2017, **14**(1):971-976.
395. Nagpal N, Ahmad HM, Chameettachal S, Sundar D, Ghosh S, Kulshreshtha R: **HIF-inducible miR-191 promotes migration in breast cancer through complex regulation of TGFbeta-signaling in hypoxic microenvironment**. *Scientific reports* 2015, **5**:9650.
396. Liu JB, Yan YJ, Shi J, Wu YB, Li YF, Dai LF, Ma XT: **Upregulation of microRNA-191 can serve as an independent prognostic marker for poor survival in prostate cancer**. *Medicine* 2019, **98**(29):e16193.
397. Yang C, Ota-Kurogi N, Ikeda K, Okumura T, Horie-Inoue K, Takeda S, Inoue S: **microRNA-191 regulates endometrial cancer cell growth via TET1-mediated epigenetic modulation of APC**. *Journal of biochemistry* 2020.
398. Ma J, Liu J, Wang Z, Gu X, Fan Y, Zhang W, Xu L, Zhang J, Cai D: **NF-kappaB-dependent microRNA-425 upregulation promotes gastric cancer cell growth by targeting PTEN upon IL-1beta induction**. *Molecular cancer* 2014, **13**:40.
399. Angius A, Pira G, Scanu AM, Uva P, Sotgiu G, Saderi L, Manca A, Serra C, Uleri E, Piu C *et al*: **MicroRNA-425-5p Expression Affects BRAF/RAS/MAPK Pathways In Colorectal Cancers**. *International journal of medical sciences* 2019, **16**(11):1480-1491.
400. Sokilde R, Persson H, Ehinger A, Pirona AC, Ferno M, Hegardt C, Larsson C, Loman N, Malmberg M, Ryden L *et al*: **Refinement of breast cancer molecular classification by miRNA expression profiles**. *BMC genomics* 2019, **20**(1):503.

401. Chen X, Zhong SL, Lu P, Wang DD, Zhou SY, Yang SJ, Shen HY, Zhang L, Zhang XH, Zhao JH *et al*: **miR-4443 Participates in the Malignancy of Breast Cancer**. *PloS one* 2016, **11**(8):e0160780.
402. Doridot L, Houry D, Gaillard H, Chelbi ST, Barbaux S, Vaiman D: **miR-34a expression, epigenetic regulation, and function in human placental diseases**. *Epigenetics* 2014, **9**(1):142-151.
403. Harada K, Baba Y, Ishimoto T, Kosumi K, Tokunaga R, Izumi D, Ohuchi M, Nakamura K, Kiyozumi Y, Kurashige J *et al*: **Suppressor microRNA-145 Is Epigenetically Regulated by Promoter Hypermethylation in Esophageal Squamous Cell Carcinoma**. *Anticancer research* 2015, **35**(9):4617-4624.
404. Liu S, Howell PM, Riker AI: **Up-regulation of miR-182 expression after epigenetic modulation of human melanoma cells**. *Annals of surgical oncology* 2013, **20**(5):1745-1752.
405. Liu X, Chen X, Yu X, Tao Y, Bode AM, Dong Z, Cao Y: **Regulation of microRNAs by epigenetics and their interplay involved in cancer**. *Journal of experimental & clinical cancer research : CR* 2013, **32**:96.
406. Sun SN, Hu S, Shang YP, Li LY, Zhou H, Chen JS, Yang JF, Li J, Huang Q, Shen CP *et al*: **Relevance function of microRNA-708 in the pathogenesis of cancer**. *Cellular signalling* 2019, **63**:109390.
407. Piletic K, Kunej T: **MicroRNA epigenetic signatures in human disease**. *Archives of toxicology* 2016, **90**(10):2405-2419.
408. Zhang J, Qu P, Zhou C, Liu X, Ma X, Wang M, Wang Y, Su J, Liu J, Zhang Y: **MicroRNA-125b is a key epigenetic regulatory factor that promotes nuclear transfer reprogramming**. *The Journal of biological chemistry* 2017, **292**(38):15916-15926.
409. Chen Z, Wang X, Liu R, Chen L, Yi J, Qi B, Shuang Z, Liu M, Li X, Li S *et al*: **KDM4B-mediated epigenetic silencing of miRNA-615-5p augments RAB24 to facilitate malignancy of hepatoma cells**. *Oncotarget* 2017, **8**(11):17712-17725.
410. Dakhlallah D, Batte K, Wang Y, Cantemir-Stone CZ, Yan P, Nuovo G, Mikhail A, Hitchcock CL, Wright VP, Nana-Sinkam SP *et al*: **Epigenetic regulation of miR-17~92 contributes to the pathogenesis of pulmonary fibrosis**. *American journal of respiratory and critical care medicine* 2013, **187**(4):397-405.
411. Tsai KW, Kao HW, Chen HC, Chen SJ, Lin WC: **Epigenetic control of the expression of a primate-specific microRNA cluster in human cancer cells**. *Epigenetics* 2009, **4**(8):587-592.
412. Rui T, Xu S, Zhang X, Huang H, Feng S, Zhan S, Xie H, Zhou L, Ling Q, Zheng S: **The chromosome 19 microRNA cluster, regulated by promoter hypomethylation, is associated with tumour burden and poor prognosis in patients with hepatocellular carcinoma**. *Journal of cellular physiology* 2020.
413. Burger PE, Gupta R, Xiong X, Ontiveros CS, Salm SN, Moscatelli D, Wilson EL: **High aldehyde dehydrogenase activity: a novel functional marker of murine prostate stem/progenitor cells**. *Stem cells* 2009, **27**(9):2220-2228.
414. Hartomo TB, Van Huyen Pham T, Yamamoto N, Hirase S, Hasegawa D, Kosaka Y, Matsuo M, Hayakawa A, Takeshima Y, Iijima K *et al*: **Involvement of aldehyde dehydrogenase 1A2 in the regulation of cancer stem cell properties in neuroblastoma**. *International journal of oncology* 2015, **46**(3):1089-1098.
415. Du W, Elemento O: **Cancer systems biology: embracing complexity to develop better anticancer therapeutic strategies**. *Oncogene* 2015, **34**(25):3215-3225.
416. Fan D, Liu Q, Wu F, Liu N, Qu H, Yuan Y, Li Y, Gao H, Ge J, Xu Y *et al*: **Prognostic significance of PI3K/AKT/ mTOR signaling pathway members in clear cell renal cell carcinoma**. *PeerJ* 2020, **8**:e9261.

417. Chhabra R, Nanjundan M: **Lysophosphatidic acid reverses Temsirolimus-induced changes in lipid droplets and mitochondrial networks in renal cancer cells**. *PloS one* 2020, **15**(6):e0233887.
418. Chen M, Ye Y, Yang H, Tamboli P, Matin S, Tannir NM, Wood CG, Gu J, Wu X: **Genome-wide profiling of chromosomal alterations in renal cell carcinoma using high-density single nucleotide polymorphism arrays**. *International journal of cancer* 2009, **125**(10):2342-2348.
419. Greife A, Knievel J, Ribarska T, Niegisch G, Schulz WA: **Concomitant downregulation of the imprinted genes DLK1 and MEG3 at 14q32.2 by epigenetic mechanisms in urothelial carcinoma**. *Clinical epigenetics* 2014, **6**(1):29.
420. Zhang L, Volinia S, Bonome T, Calin GA, Greshock J, Yang N, Liu CG, Giannakakis A, Alexiou P, Hasegawa K *et al*: **Genomic and epigenetic alterations deregulate microRNA expression in human epithelial ovarian cancer**. *Proceedings of the National Academy of Sciences of the United States of America* 2008, **105**(19):7004-7009.
421. Chhabra R, Rockfield S, Guergues J, Nadeau OW, Hill R, Stevens SM, Jr., Nanjundan M: **Global miRNA/proteomic analyses identify miRNAs at 14q32 and 3p21, which contribute to features of chronic iron-exposed fallopian tube epithelial cells**. *Scientific reports* 2021, **11**(1):6270.
422. Maliszewska-Olejniczak K, Brodaczewska KK, Bielecka ZF, Solarek W, Kornakiewicz A, Szczylik C, Porta C, Czarnecka AM: **Development of extracellular matrix supported 3D culture of renal cancer cells and renal cancer stem cells**. *Cytotechnology* 2019, **71**(1):149-163.
423. Pinzon N, Li B, Martinez L, Sergeeva A, Presumey J, Apparailly F, Seitz H: **microRNA target prediction programs predict many false positives**. *Genome research* 2017, **27**(2):234-245.
424. Cargile BJ, Bundy JL, Stephenson JL, Jr.: **Potential for false positive identifications from large databases through tandem mass spectrometry**. *Journal of proteome research* 2004, **3**(5):1082-1085.
425. Chandramouli K, Qian PY: **Proteomics: challenges, techniques and possibilities to overcome biological sample complexity**. *Human genomics and proteomics : HGP* 2009, **2009**.
426. Cavaille J, Seitz H, Paulsen M, Ferguson-Smith AC, Bachellerie JP: **Identification of tandemly-repeated C/D snoRNA genes at the imprinted human 14q32 domain reminiscent of those at the Prader-Willi/Angelman syndrome region**. *Human molecular genetics* 2002, **11**(13):1527-1538.
427. Benetatos L, Vartholomatos G, Hatzimichael E: **MEG3 imprinted gene contribution in tumorigenesis**. *International journal of cancer* 2011, **129**(4):773-779.
428. Abdallah BM, Jensen CH, Gutierrez G, Leslie RG, Jensen TG, Kassem M: **Regulation of human skeletal stem cells differentiation by Dlk1/Pref-1**. *Journal of bone and mineral research : the official journal of the American Society for Bone and Mineral Research* 2004, **19**(5):841-852.
429. Sekita Y, Wagatsuma H, Nakamura K, Ono R, Kagami M, Wakisaka N, Hino T, Suzuki-Migishima R, Kohda T, Ogura A *et al*: **Role of retrotransposon-derived imprinted gene, Rtl1, in the feto-maternal interface of mouse placenta**. *Nature genetics* 2008, **40**(2):243-248.
430. Wang Y, Sul HS: **Pref-1 regulates mesenchymal cell commitment and differentiation through Sox9**. *Cell metabolism* 2009, **9**(3):287-302.
431. Laddha SV, Nayak S, Paul D, Reddy R, Sharma C, Jha P, Hariharan M, Agrawal A, Chowdhury S, Sarkar C *et al*: **Genome-wide analysis reveals downregulation of miR-379/miR-656 cluster in human cancers**. *Biology direct* 2013, **8**:10.

432. Sarver AL, Thayanithy V, Scott MC, Cleton-Jansen AM, Hogendoorn PC, Modiano JF, Subramanian S: **MicroRNAs at the human 14q32 locus have prognostic significance in osteosarcoma**. *Orphanet journal of rare diseases* 2013, **8**:7.
433. Arai E, Ushijima S, Tsuda H, Fujimoto H, Hosoda F, Shibata T, Kondo T, Imoto I, Inazawa J, Hirohashi S *et al*: **Genetic clustering of clear cell renal cell carcinoma based on array-comparative genomic hybridization: its association with DNA methylation alteration and patient outcome**. *Clinical cancer research : an official journal of the American Association for Cancer Research* 2008, **14**(17):5531-5539.
434. Han X, Wang X, Li H, Zhang H: **Mechanism of microRNA-431-5p-EPB41L1 interaction in glioblastoma multiforme cells**. *Archives of medical science : AMS* 2019, **15**(6):1555-1564.
435. Kong Q, Han J, Deng H, Wu F, Guo S, Ye Z: **miR-431-5p alters the epithelial-to-mesenchymal transition markers by targeting UROC28 in hepatoma cells**. *OncoTargets and therapy* 2018, **11**:6489-6503.
436. Huang W, Zeng C, Hu S, Wang L, Liu J: **ATG3, a Target of miR-431-5p, Promotes Proliferation and Invasion of Colon Cancer via Promoting Autophagy**. *Cancer management and research* 2019, **11**:10275-10285.
437. Jiang Q, Cheng L, Ma D, Zhao Y: **FBXL19-AS1 exerts oncogenic function by sponging miR-431-5p to regulate RAF1 expression in lung cancer**. *Bioscience reports* 2019, **39**(1).
438. Yang J, Zhu H, Jin Y, Song Y: **MiR-431 inhibits cell proliferation and induces cell apoptosis by targeting CDK14 in pancreatic cancer**. *European review for medical and pharmacological sciences* 2018, **22**(14):4493-4499.
439. Tanaka T, Arai M, Jiang X, Sugaya S, Kanda T, Fujii K, Kita K, Sugita K, Imazeki F, Miyashita T *et al*: **Downregulation of microRNA-431 by human interferon-beta inhibits viability of medulloblastoma and glioblastoma cells via upregulation of SOCS6**. *International journal of oncology* 2014, **44**(5):1685-1690.
440. Tanaka T, Sugaya S, Kita K, Arai M, Kanda T, Fujii K, Imazeki F, Sugita K, Yokosuka O, Suzuki N: **Inhibition of cell viability by human IFN-beta is mediated by microRNA-431**. *International journal of oncology* 2012, **40**(5):1470-1476.
441. Liu R, Ma X, Xu L, Wang D, Jiang X, Zhu W, Cui B, Ning G, Lin D, Wang S: **Differential microRNA expression in peripheral blood mononuclear cells from Graves' disease patients**. *The Journal of clinical endocrinology and metabolism* 2012, **97**(6):E968-972.
442. Kaudewitz D, Skroblin P, Bender LH, Barwari T, Willeit P, Pechlaner R, Sunderland NP, Willeit K, Morton AC, Armstrong PC *et al*: **Association of MicroRNAs and YRNAs With Platelet Function**. *Circulation research* 2016, **118**(3):420-432.
443. Ross SP, Baker KE, Fisher A, Hoff L, Pak ES, Murashov AK: **miRNA-431 Prevents Amyloid-beta-Induced Synapse Loss in Neuronal Cell Culture Model of Alzheimer's Disease by Silencing Kremen1**. *Frontiers in cellular neuroscience* 2018, **12**:87.
444. Lee KP, Shin YJ, Panda AC, Abdelmohsen K, Kim JY, Lee SM, Bahn YJ, Choi JY, Kwon ES, Baek SJ *et al*: **miR-431 promotes differentiation and regeneration of old skeletal muscle by targeting Smad4**. *Genes & development* 2015, **29**(15):1605-1617.
445. Wertz MH, Winden K, Neveu P, Ng SY, Ercan E, Sahin M: **Cell-type-specific miR-431 dysregulation in a motor neuron model of spinal muscular atrophy**. *Human molecular genetics* 2016, **25**(11):2168-2181.
446. Wu R, Li H, Li T, Zhang Y, Zhu D: **Myostatin regulates miR-431 expression via the Ras-Mek-Erk signaling pathway**. *Biochemical and biophysical research communications* 2015, **461**(2):224-229.
447. Zhang X, Zhang M, Cheng J, Lv Z, Wang F, Cai Z: **MiR-411 functions as a tumor suppressor in renal cell cancer**. *The International journal of biological markers* 2017, **32**(4):e454-e460.

448. Liu Y, Liu T, Jin H, Yin L, Yu H, Bi J: **MiR-411 suppresses the development of bladder cancer by regulating ZnT1**. *OncoTargets and therapy* 2018, **11**:8695-8704.
449. Guo L, Yuan J, Xie N, Wu H, Chen W, Song S, Wang X: **miRNA-411 acts as a potential tumor suppressor miRNA via the downregulation of specificity protein 1 in breast cancer**. *Molecular medicine reports* 2016, **14**(4):2975-2982.
450. Zhang C, Wang H, Deng M, He L, Ping F, He Y, Fan Z, Cheng B, Xia J: **Upregulated miR4115p levels promote lymph node metastasis by targeting RYBP in head and neck squamous cell carcinoma**. *International journal of molecular medicine* 2021, **47**(4).
451. Jin H, Sun W, Zhang Y, Yan H, Liufu H, Wang S, Chen C, Gu J, Hua X, Zhou L *et al*: **MicroRNA-411 Downregulation Enhances Tumor Growth by Upregulating MLLT11 Expression in Human Bladder Cancer**. *Molecular therapy Nucleic acids* 2018, **11**:312-322.
452. Kulkarni SR, Armstrong LE, Slitt AL: **Caloric restriction-mediated induction of lipid metabolism gene expression in liver is enhanced by Keap1-knockdown**. *Pharmaceutical research* 2013, **30**(9):2221-2231.
453. Huan T, Rong J, Liu C, Zhang X, Tanriverdi K, Joehanes R, Chen BH, Murabito JM, Yao C, Courchesne P *et al*: **Genome-wide identification of microRNA expression quantitative trait loci**. *Nature communications* 2015, **6**:6601.
454. Liang C, Ding J, Yang Y, Deng L, Li X: **MicroRNA-433 inhibits cervical cancer progression by directly targeting metadherin to regulate the AKT and beta-catenin signalling pathways**. *Oncology reports* 2017, **38**(6):3639-3649.
455. Zhang T, Jiang K, Zhu X, Zhao G, Wu H, Deng G, Qiu C: **miR-433 inhibits breast cancer cell growth via the MAPK signaling pathway by targeting Rap1a**. *International journal of biological sciences* 2018, **14**(6):622-632.
456. Tang X, Lin J, Wang G, Lu J: **MicroRNA-433-3p promotes osteoblast differentiation through targeting DKK1 expression**. *PloS one* 2017, **12**(6):e0179860.
457. Hourigan ST, Solly EL, Nankivell VA, Ridiandries A, Weimann BM, Henriquez R, Tepper ER, Zhang JQJ, Tsatralis T, Clayton ZE *et al*: **The regulation of miRNAs by reconstituted high-density lipoproteins in diabetes-impaired angiogenesis**. *Scientific reports* 2018, **8**(1):13596.
458. Lv W, Fan F, Wang Y, Gonzalez-Fernandez E, Wang C, Yang L, Booz GW, Roman RJ: **Therapeutic potential of microRNAs for the treatment of renal fibrosis and CKD**. *Physiological genomics* 2018, **50**(1):20-34.
459. Yin H, Qiu X, Shan Y, You B, Xie L, Zhang P, Zhao J, You Y: **HIF-1alpha downregulation of miR-433-3p in adipocyte-derived exosomes contributes to NPC progression via targeting SCD1**. *Cancer science* 2021, **112**(4):1457-1470.
460. Sun S, Wang X, Xu X, Di H, Du J, Xu B, Wang Q, Wang J: **MiR-433-3p suppresses cell growth and enhances chemosensitivity by targeting CREB in human glioma**. *Oncotarget* 2017, **8**(3):5057-5068.
461. Guo LH, Li H, Wang F, Yu J, He JS: **The Tumor Suppressor Roles of miR-433 and miR-127 in Gastric Cancer**. *International journal of molecular sciences* 2013, **14**(7):14171-14184.
462. Shi Q, Wang Y, Mu Y, Wang X, Fan Q: **MiR-433-3p Inhibits Proliferation and Invasion of Esophageal Squamous Cell Carcinoma by Targeting GRB2**. *Cellular physiology and biochemistry : international journal of experimental cellular physiology, biochemistry, and pharmacology* 2018, **46**(5):2187-2196.
463. Fellenberg J, Lehner B, Saehr H, Schenker A, Kunz P: **Tumor Suppressor Function of miR-127-3p and miR-376a-3p in Osteosarcoma Cells**. *Cancers* 2019, **11**(12).
464. Yang Z, Zhang Y, Wang L: **A feedback inhibition between miRNA-127 and TGFbeta/c-Jun cascade in HCC cell migration via MMP13**. *PloS one* 2013, **8**(6):e65256.

465. Zhang L, Zhang Y, Zhang X, Zhang Y, Jiang Y, Xiao X, Tan J, Yuan W, Liu Y: **MicroRNA-433 Inhibits the Proliferation and Migration of HUVECs and Neurons by Targeting Hypoxia-Inducible Factor 1 Alpha**. *Journal of molecular neuroscience : MN* 2017, **61**(2):135-143.
466. Estep M, Armistead D, Hossain N, Elarainy H, Goodman Z, Baranova A, Chandhoke V, Younossi ZM: **Differential expression of miRNAs in the visceral adipose tissue of patients with non-alcoholic fatty liver disease**. *Alimentary pharmacology & therapeutics* 2010, **32**(3):487-497.
467. Chen J, Wang M, Guo M, Xie Y, Cong YS: **miR-127 regulates cell proliferation and senescence by targeting BCL6**. *PloS one* 2013, **8**(11):e80266.
468. Wang L, Wang X, Jiang X: **miR-127 suppresses gastric cancer cell migration and invasion via targeting Wnt7a**. *Oncology letters* 2019, **17**(3):3219-3226.
469. Wan N, Yang W, Cheng H, Wang J: **FOXD3-AS1 Contributes to the Progression of Melanoma Via miR-127-3p/FJX1 Axis**. *Cancer biotherapy & radiopharmaceuticals* 2020, **35**(8):596-604.
470. Yu Y, Liu L, Ma R, Gong H, Xu P, Wang C: **MicroRNA-127 is aberrantly downregulated and acted as a functional tumor suppressor in human pancreatic cancer**. *Tumour biology : the journal of the International Society for Oncodevelopmental Biology and Medicine* 2016, **37**(10):14249-14257.
471. Gao X, Wang X, Cai K, Wang W, Ju Q, Yang X, Wang H, Wu H: **MicroRNA-127 is a tumor suppressor in human esophageal squamous cell carcinoma through the regulation of oncogene FMNL3**. *European journal of pharmacology* 2016, **791**:603-610.
472. Zhang S, Zhang X, Fu X, Li W, Xing S, Yang Y: **Identification of common differentially-expressed miRNAs in ovarian cancer cells and their exosomes compared with normal ovarian surface epithelial cell cells**. *Oncology letters* 2018, **16**(2):2391-2401.
473. Yang Z, Cappello T, Wang L: **Emerging role of microRNAs in lipid metabolism**. *Acta pharmaceutica Sinica B* 2015, **5**(2):145-150.
474. Liu Y, Lu C, Zhou Y, Zhang Z, Sun L: **Circular RNA hsa_circ_0008039 promotes breast cancer cell proliferation and migration by regulating miR-432-5p/E2F3 axis**. *Biochemical and biophysical research communications* 2018, **502**(3):358-363.
475. Liu H, Xue L, Song C, Liu F, Jiang T, Yang X: **Overexpression of circular RNA circ_001569 indicates poor prognosis in hepatocellular carcinoma and promotes cell growth and metastasis by sponging miR-411-5p and miR-432-5p**. *Biochemical and biophysical research communications* 2018, **503**(4):2659-2665.
476. Yang G, Han B, Feng T: **ZFAS1 knockdown inhibits viability and enhances cisplatin cytotoxicity by up-regulating miR-432-5p in glioma cells**. *Basic & clinical pharmacology & toxicology* 2019, **125**(6):518-526.
477. Zhang J, Xu C, Gao Y, Wang Y, Ding Z, Zhang Y, Shen W, Zheng Y, Wan Y: **A Novel Long Non-coding RNA, MSTRG.51053.2 Regulates Cisplatin Resistance by Sponging the miR-432-5p in Non-small Cell Lung Cancer Cells**. *Frontiers in oncology* 2020, **10**:215.
478. Luo M, Hu Z, Kong Y, Li L: **MicroRNA-432-5p inhibits cell migration and invasion by targeting CXCL5 in colorectal cancer**. *Experimental and therapeutic medicine* 2021, **21**(4):301.
479. Chen H, Chi Y, Chen M, Zhao L: **Long Intergenic Non-Coding RNA LINC00885 Promotes Tumorigenesis of Cervical Cancer by Upregulating MACC1 Expression Through Serving as a Competitive Endogenous RNA for microRNA-432-5p**. *Cancer management and research* 2021, **13**:1435-1447.
480. Sun J, Zhang B, Lan X, Zhang C, Lei C, Chen H: **Comparative transcriptome analysis reveals significant differences in MicroRNA expression and their target genes between adipose and muscular tissues in cattle**. *PloS one* 2014, **9**(7):e102142.

481. Ma M, Wang X, Chen X, Cai R, Chen F, Dong W, Yang G, Pang W: **MicroRNA-432 targeting E2F3 and P55PIK inhibits myogenesis through PI3K/AKT/mTOR signaling pathway**. *RNA biology* 2017, **14**(3):347-360.
482. Sobczuk P, Brodziak A, Khan MI, Chhabra S, Fiedorowicz M, Welniak-Kaminska M, Synoradzki K, Bartnik E, Cudnoch-Jedrzejewska A, Czarnecka AM: **Choosing The Right Animal Model for Renal Cancer Research**. *Translational oncology* 2020, **13**(3):100745.
483. Court F, Tayama C, Romanelli V, Martin-Trujillo A, Iglesias-Platas I, Okamura K, Sugahara N, Simon C, Moore H, Harness JV *et al*: **Genome-wide parent-of-origin DNA methylation analysis reveals the intricacies of human imprinting and suggests a germline methylation-independent mechanism of establishment**. *Genome research* 2014, **24**(4):554-569.
484. Gagne A, Hochman A, Qureshi M, Tong C, Arbon J, McDaniel K, Davis TL: **Analysis of DNA methylation acquisition at the imprinted Dlk1 locus reveals asymmetry at CpG dyads**. *Epigenetics & chromatin* 2014, **7**:9.
485. Geuns E, De Temmerman N, Hilven P, Van Steirteghem A, Liebaers I, De Rycke M: **Methylation analysis of the intergenic differentially methylated region of DLK1-GTL2 in human**. *European journal of human genetics : EJHG* 2007, **15**(3):352-361.
486. Beygo J, Elbracht M, de Groot K, Begemann M, Kanber D, Platzer K, Gillessen-Kaesbach G, Vierzig A, Green A, Heller R *et al*: **Novel deletions affecting the MEG3-DMR provide further evidence for a hierarchical regulation of imprinting in 14q32**. *European journal of human genetics : EJHG* 2015, **23**(2):180-188.
487. Bens S, Kolarova J, Gillessen-Kaesbach G, Buiting K, Beygo J, Caliebe A, Ammerpohl O, Siebert R: **The differentially methylated region of MEG8 is hypermethylated in patients with Temple syndrome**. *Epigenomics* 2015, **7**(7):1089-1097.
488. Lehner B, Kunz P, Saehr H, Fellenberg J: **Epigenetic silencing of genes and microRNAs within the imprinted Dlk1-Dio3 region at human chromosome 14.32 in giant cell tumor of bone**. *BMC cancer* 2014, **14**:495.
489. Li JL, Okada S, Hamazaki S, Ebina Y, Midorikawa O: **Subacute nephrotoxicity and induction of renal cell carcinoma in mice treated with ferric nitrilotriacetate**. *Cancer research* 1987, **47**(7):1867-1869.
490. Zhong Y, Onuki J, Yamasaki T, Ogawa O, Akatsuka S, Toyokuni S: **Genome-wide analysis identifies a tumor suppressor role for aminoacylase 1 in iron-induced rat renal cell carcinoma**. *Carcinogenesis* 2009, **30**(1):158-164.
491. Alberghini A, Recalcati S, Tacchini L, Santambrogio P, Campanella A, Cairo G: **Loss of the von Hippel Lindau tumor suppressor disrupts iron homeostasis in renal carcinoma cells**. *The Journal of biological chemistry* 2005, **280**(34):30120-30128.
492. Greene CJ, Sharma NJ, Fiorica PN, Forrester E, Smith GJ, Gross KW, Kauffman EC: **Suppressive effects of iron chelation in clear cell renal cell carcinoma and their dependency on VHL inactivation**. *Free radical biology & medicine* 2019, **133**:295-309.
493. Camarena V, Huff TC, Wang G: **Epigenomic regulation by labile iron**. *Free radical biology & medicine* 2021, **170**:44-49.
494. Gu X, Sun J, Li S, Wu X, Li L: **Oxidative stress induces DNA demethylation and histone acetylation in SH-SY5Y cells: potential epigenetic mechanisms in gene transcription in Abeta production**. *Neurobiology of aging* 2013, **34**(4):1069-1079.
495. Mahalingaiah PK, Ponnusamy L, Singh KP: **Oxidative stress-induced epigenetic changes associated with malignant transformation of human kidney epithelial cells**. *Oncotarget* 2017, **8**(7):11127-11143.
496. Cao LL, Liu H, Yue Z, Liu L, Pei L, Gu J, Wang H, Jia M: **Iron chelation inhibits cancer cell growth and modulates global histone methylation status in colorectal cancer**. *Biometals : an international journal on the role of metal ions in biology, biochemistry, and medicine* 2018, **31**(5):797-805.

497. Khodaverdian V, Tapadar S, MacDonald IA, Xu Y, Ho PY, Bridges A, Rajpurohit P, Sanghani BA, Fan Y, Thangaraju M *et al*: **Deferiprone: Pan-selective Histone Lysine Demethylase Inhibition Activity and Structure Activity Relationship Study**. *Scientific reports* 2019, **9**(1):4802.
498. Qi Y, Wang L, Wang K, Peng Z, Ma Y, Zheng Z, Shang D, Xu W, Zheng J: **New mechanistic insights of clear cell renal cell carcinoma from integrated miRNA and mRNA expression profiling studies**. *Biomedicine & pharmacotherapy = Biomedecine & pharmacotherapie* 2019, **111**:821-834.
499. Aguiari G: **MicroRNAs in clear cell renal cell carcinoma: biological functions and applications**. *Journal of kidney cancer and VHL* 2015, **2**(4):140-152.

Appendices

Appendix A:

Copyright Permissions

Chapter 1

Re: Requesting permission to use published content in doctoral dissertation

Publisher MDPI <publisher@mdpi.com>
Tue 7/27/2021 9:41 PM

To: Ravneet Kaur Chhabra <chhabra@usf.edu>; undefined <owen.shu@mdpi.com>
Cc: oliver.hill@mdpi.com <oliver.hill@mdpi.com>; support@mdpi.com <support@mdpi.com>

Dear Ravneet Chhabra,

Thank you very much for your interest in said material.

All MDPI journals are Open Access and subject to the Creative Commons Attribution License (CC BY). The CC BY permits unrestricted use, distribution, and reproduction of the material in any medium, even commercially, ***provided the original work is properly cited***. You do not have to pay anything for permission.

For more information on the CC BY License, please see here:
https://creativecommons.org/licenses/by/4.0/legalcode

Best regards,
Tim Gasser

Am 24/07/2021 um 15:49 schrieb Ravneet Kaur Chhabra:

> Dear Editor,
>
> I am a doctoral candidate from the University of South Florida, Tampa FL. USA. I am currently writing my doctoral dissertation and this email is to humbly request for your permission to include the article (either the entire manuscript as published or a rewrite of the manuscript with the data and content) "Iron Pathways and Iron Chelation Approaches in Viral, Microbial, and Fungal Infections". This review article was published in "MDPI: Pharmaceuticals" on September 25, 2020; the doi is 10.3390/ph13100275. I am the primary author on this article.
>
> In case this is not the correct email address to reach out with this request, please re-direct me to the correct one.
> I would greatly appreciate your help and thank you in advance for your valuable time.
>
> Sincerely,
>
> Ravneet Chhabra
> Doctoral candidate, CMMB Department,
> University of South Florida, Tampa. FL. USA

--
Tim Gasser
Communications & Marketing Assistant, MDPI
St. Alban-Anlage 66, 4052 Basel, Switzerland
www.mdpi.com

Chapter 3

Re: Requesting permission to use published content in doctoral dissertation

noreply@salesforce.com <noreply@salesforce.com>
on behalf of
plosone <plosone@plos.org>
Tue 3/30/2021 10:19 AM
To: Chhabra, Ravneet Kaur <chhabra@usf.edu>

Dear Dr. Chhabra,

Thank you for your message. PLOS ONE publishes all of the content in the articles under an open access license called "CC-BY." This license allows you to download, reuse, reprint, modify, distribute, and/or copy articles or images in PLOS journals, so long as the original creators are credited (e.g., including the article's citation and/or the image credit). Additional permissions are not required. You can read about our open access license here: http://journals.plos.org/plosone/s/licenses-and-copyright

There are many ways to access our content, including HTML, XML, and PDF versions of each article. Higher resolution versions of figures can be downloaded directly from the article.

Thank you for your interest in PLOS ONE and for your continued support of the Open Access model. Please do not hesitate to be in touch with any additional questions.

Kind regards,

Rachel Saunders-Singer
Editorial Office

PLOS | plos.org

Empowering researchers to transform science

1160 Battery Street, Suite 225, San Francisco, CA 94111

Case Number: 07078838
ref:_00DU0lfis._5004P1SeXvE:ref

---------- Original Message ----------
From: Chhabra, Ravneet Kaur [chhabra@usf.edu]
Sent: 3/29/2021 4:28 PM
To: plosone@plos.org
Subject: Requesting permission to use published content in doctoral dissertation

Dear Editor,

I am a doctoral candidate from the University of South Florida, Tampa FL. USA. I am currently writing my doctoral dissertation and would like to include the article (either the entire manuscript as published or a rewrite of the manuscript with the data and content) "Lysophosphatidic acid reverses Temsirolimus-induced changes in lipid droplets and mitochondrial networks in renal cancer cells". I am the primary author on the article, and it was published in PLOS One on June 3, 2020. The doi is 10.1371/journal.pone.0233887.

I would greatly appreciate your help and thank you in advance for your valuable time.

Sincerely,
Ravneet Chhabra

Doctoral candidate, Department of CMMB,
University of South Florida, Tampa. FL. USA

Chapter 4

RE: Requesting permission to use published content in doctoral dissertation

Journalpermissions <journalpermissions@springernature.com>

Mon 4/19/2021 9:46 AM

To: Chhabra, Ravneet Kaur <chhabra@usf.edu>

Dear Ravneet,

Thank you for your email. This work is licensed under a Creative Commons Attribution 4.0 International License, which permits unrestricted use, distribution, and reproduction in any medium, provided you give appropriate credit to the original author(s) and the source, provide a link to the Creative Commons license, and indicate if changes were made. You are not required to obtain permission to reuse this article. The images or other third party material in this article are included in the article's Creative Commons license, unless indicated otherwise in the credit line; if the material is not included under the Creative Commons license, users will need to obtain permission from the license holder to reproduce the material. To view a copy of this license, visit http://creativecommons.org/licenses/by/4.0/.

Concerning step 2, please include a normal citation with this link:

http://creativecommons.org/licenses/by/4.0/

Best wishes,
Paloma

Paloma Hammond
Rights Executive

SpringerNature
The Campus, 4 Crinan Street, London N1 9XW, United Kingdom

E paloma.hammond@springernature.com

https://www.macmillanihe.com/
http://www.nature.com
http://www.springer.com
https://www.palgrave.com/gp/

On Mon, 29 Mar at 4:19 PM , Chhabra, Ravneet Kaur <chhabra@usf.edu> wrote:

[External - Use Caution]

Dear Editor,

I am a doctoral candidate from the University of South Florida, Tampa FL. USA. I am currently writing my doctoral dissertation and would like to include the article (either the entire manuscript as published or a rewrite of the manuscript with the data and content) "Global miRNA/proteomic analyses identify miRNAs at 14q32 and 3p21, which contribute to features of chronic iron-exposed fallopian tube epithelial cells.", which was published in Scientific Reports on March 18, 2021. The doi is 10.1038/s41598-021-85342-y.

I would greatly appreciate your help and thank you in advance for your valuable time.

Sincerely,
Ravneet Chhabra

Appendix B:

Additional Methods and Protocols used for current and future projects

RPTEC cell Immortalization

The primary renal proximal tubule cells were immortalized using different plasmids simultaneously to determine which (if any) methods can lead to reduction in 14q32 miRNA levels. For RPTEC immortalization, the retroviral plasmids (pBabe-puro, pVSVG, pCGP, hTERT, LTAg, c-Myc and H-Ras) were transfected in various permutations into HEK293T cells. First, HEK293T cells were seeded in 6-well plates at 1,500,000 cells/well. Post-cell adherence, the complete media was exchanged to pre-warmed serum free media. Transfection reactions were next prepared in cryovials by adding 100 µl serum free media, 1 µg plasmid DNA and 3 µl Fugene HD. After 6 hours of transfection, cells were overlaid with 2 ml of pre-warmed complete media. The concentrations for all plasmids used are mentioned in the table below:

Table A1: Details of the plasmids used for RPTEC Immortalization.

Plasmid	***Catalog Number (Addgene)***	***Concentration***
pBabe-puro	#1764	2282.03 ng/ µl
hTERT-HA	#1772	2761.44 ng/ µl
SV40 LTAg	#14088	1670.14 ng/ µl
H-Ras ^{V12A}	#9051	1082.86 ng/ µl
psPAX2	#12260	2038.3 ng/ µl
pVSVG	#12259	2805.8 ng/ µl
c-Myc ^{T58A}	#20076	2170.51 ng/ µl

Twenty-four hours post-transfection, the cells were recovered by replacing the media in 6-well plates with 2 ml of pre-warmed complete media. Forty-eight hours post-transfection, the retrovirus (1X RV) was collected from the supernatant media of the HEK293T cells and filter sterilized using a 0.45-micron filter. The cells were then replenished with fresh complete media in the 6-well plates and allowed to incubate for a further 24-hour period to collect the 2X RV retrovirus supernatant media. The retrovirus solutions were stored at -80°C freezer until ready to use.

Simultaneously, RPTEC cells were seeded into T25 flasks for retroviral infection to initiate the immortalization process. These cells were seeded at 125,000 cells per T25 flask to generate the following cultures in 7 independent flasks:

hTERT only

LTAg only

hTERT+LTAg

LTAg+hTERT+c-Myc+H-Ras

hTERT+Control shRNA

hTERT+ VHL shRNA.

Once ready, these cells were infected with appropriate retrovirus which was thawed at 37C. The infection media was prepared by adding 2ml of 1X retrovirus to 2ml complete media with 8 µg/ml polybrene. The cultures were placed into the BSL-II incubator and monitored daily for viral toxicity. The following day, the media was exchanged in all flasks with fresh appropriate basal media and the media replenished once a week for maintenance and expansion of the cultures.

CRISPR-Cas9 mediated 14q32 miRNA cluster activation

HEK293T and FAC-FTSEC cells (in progress): The 54 miRNAs present at 14q32 locus are sub-divided into two sub-clusters, as represented in the figure below. For explanation purpose, I will refer to the first sub-cluster as miRNA sub-cluster A and second one as miRNA sub-cluster B (as shown in figure 31).

sgRNA Design

The first step to CRISPR-Cas9 mediated activation was obtaining appropriate sgRNAs for specific 14q32 miRNA loci. The oligonucleotide sequences for sgRNAs targeting miR-381 loci in sub-cluster B were derived from a prior published study [223], which have been called as sgRNAs A and B in our studies, the sequences of which are included below:

sgRNA A: CGCACCAGGTGCGTGCATG

sgRNA B: CAGTCGGGGTGTAAAAAGC

For sub-cluster A, miR-493 locus was targeted and sgRNAs were designed using different CRSIPR activation tools, as follows:

1. CRISPR-ERA (http://crispr-era.stanford.edu/finish.jsp#s3) was used first to select gene activation and added the gene MIR493 (first gene to be targeted for activation). Then, selected U6 promoter (based on the vector pLKO-U6sgRNA_improved-EF1s-GFP-P2A-Blasticidin). The table derived for sgRNAs list was downloaded (obtained in form of .txt file) and copied this into excel file. Now, to narrow down the sgRNA sequences, deleted sgRNAs with transcription start site (TSS) distance of more than 200 bp; selected the ones targeting negative strand and Efficacy+Specificity score of less than 10. Further, narrowed down the sgRNAs by selecting the ones with less than 100 bp TSS distance, considering the promoter region will be present upstream of the target miRNA.

2. Another tool used for sgRNA design was from Broad institute specific for “CRISPRa”: Added the NCBI gene ID for MIR493 (i.e. 574450), and searched for sgRNAs. The results obtained were downloaded as .txt file and saved as excel file.

Once both lists were generated, I compared the gRNAs from the two websites and selected the two common sgRNAs obtained from both the tools. To double check these sgRNAs, I used CAS OFFINDER (http://www.rgenome.net/cas-offinder/), which showed the same specific target positions on chr14 as desired, and 0 mismatches.

The two sgRNAs (C and D) designed targeting site upstream of miR-493 were:

sgRNA C: AGCCGTGATGATGGAGTCCA

sgRNA D: AGAGATGAGATGCTGTGCCC

The locus of each miRNA is included in the table below:

Table A2: MicroRNA loci at chromosome 14q32 derived from UCSC genome browser.

miRNA	Position
2392	chr14:100,814,491-100,814,574
770	chr14:100,852,390-100,852,487
493	chr14:100,869,060-100,869,148
337	chr14:100,874,493-100,874,585
665	chr14:100,875,033-100,875,104
431	chr14:100,881,007-100,881,120
433	chr14:100,881,886-100,881,978
127	chr14:100,882,979-100,883,075
432	chr14:100,884,483-100,884,576

Table A2 (Continued)

136	chr14:100,884,702-100,884,783
370	chr14:100,911,139-100,911,213
379	chr14:101,022,066-101,022,132
411	chr14:101,023,325-101,023,420
299	chr14:101,023,325-101,023,420
380	chr14:101,025,017-101,025,077
1197	chr14:101,025,564-101,025,651
323a	chr14:101,025,732-101,025,817
758	chr14:101,026,020-101,026,107
329-1	chr14:101,026,785-101,026,864
329-2	chr14:101,027,100-101,027,183
494	chr14:101,029,634-101,029,714
1193	chr14:101,030,052-101,030,129
543	chr14:101,031,987-101,032,064
495	chr14:101,033,755-101,033,836
376c	chr14:101,039,690-101,039,755
376a2	chr14:101,040,069-101,040,148
654	chr14:101,040,219-101,040,299
376b	chr14:101,040,436-101,040,535
376a1	chr14:101,040,782-101,040,849
300	chr14:101,041,363-101,041,445
1185-1	chr14:101,042,977-101,043,062
1185-2	chr14:101,044,198-101,044,283
381	chr14:101,045,920-101,045,994
487b	chr14:101,046,455-101,046,538
539	chr14:101,047,321-101,047,398

Table A2 (Continued)

889	chr14:101,047,901-101,047,979
544a	chr14:101,048,658-101,048,748
655	chr14:101,049,550-101,049,646
487a	chr14:101,052,446-101,052,525
382	chr14:101,054,306-101,054,381
134	chr14:101,054,687-101,054,759
668	chr14:101,055,258-101,055,323
485	chr14:101,055,419-101,055,491
323b	chr14:101,056,219-101,056,300
154	chr14:101,059,755-101,059,838
496	chr14:101,060,573-101,060,674
377	chr14:101,062,050-101,062,118
541	chr14:101,064,495-101,064,578
409	chr14:101,065,300-101,065,378
412	chr14:101,065,447-101,065,537
369	chr14:101,065,598-101,065,667
410	chr14:101,065,912-101,065,991
656	chr14:101,066,724-101,066,801
1247	chr14:101,560,287-101,560,422

Cloning and sequencing*:*

The plasmids used for this experiment were “Lenti-EFS-dCas9-VPR-PGK-Puro” and “pLKO-U6sgRNA_improved-EF1s-GFP-P2A-Blasticidin”, the maps of which are included below:

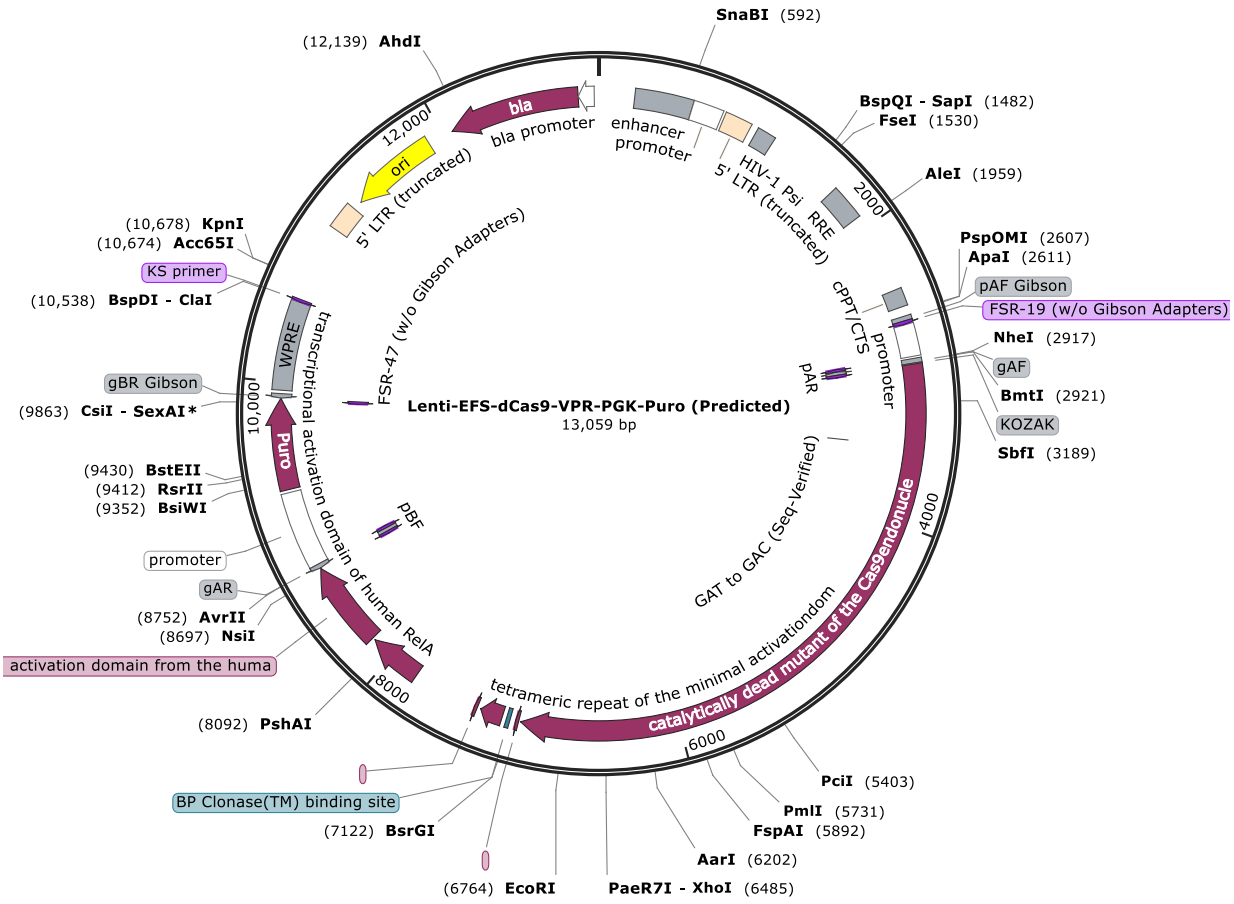

Figure A1: Plasmid Map for Lenti-EFS-dCas9-VPR-PGK-Puro used for Cas9 expressing cell line generation

The figure above shows the plasmid map of Lenti-EFS-dCas9-VPR-PGK-Puro plasmid which was used for stable cell line generation.

The sgRNAs were derived as Top and bottom sequence oligos. Prepared 100uM oligos in molecular grade water by pulse spinning the oligo tubes at 1000 rpm for 10 seconds and adding water directly to the tube (putting the tubes upright in ice bucket).

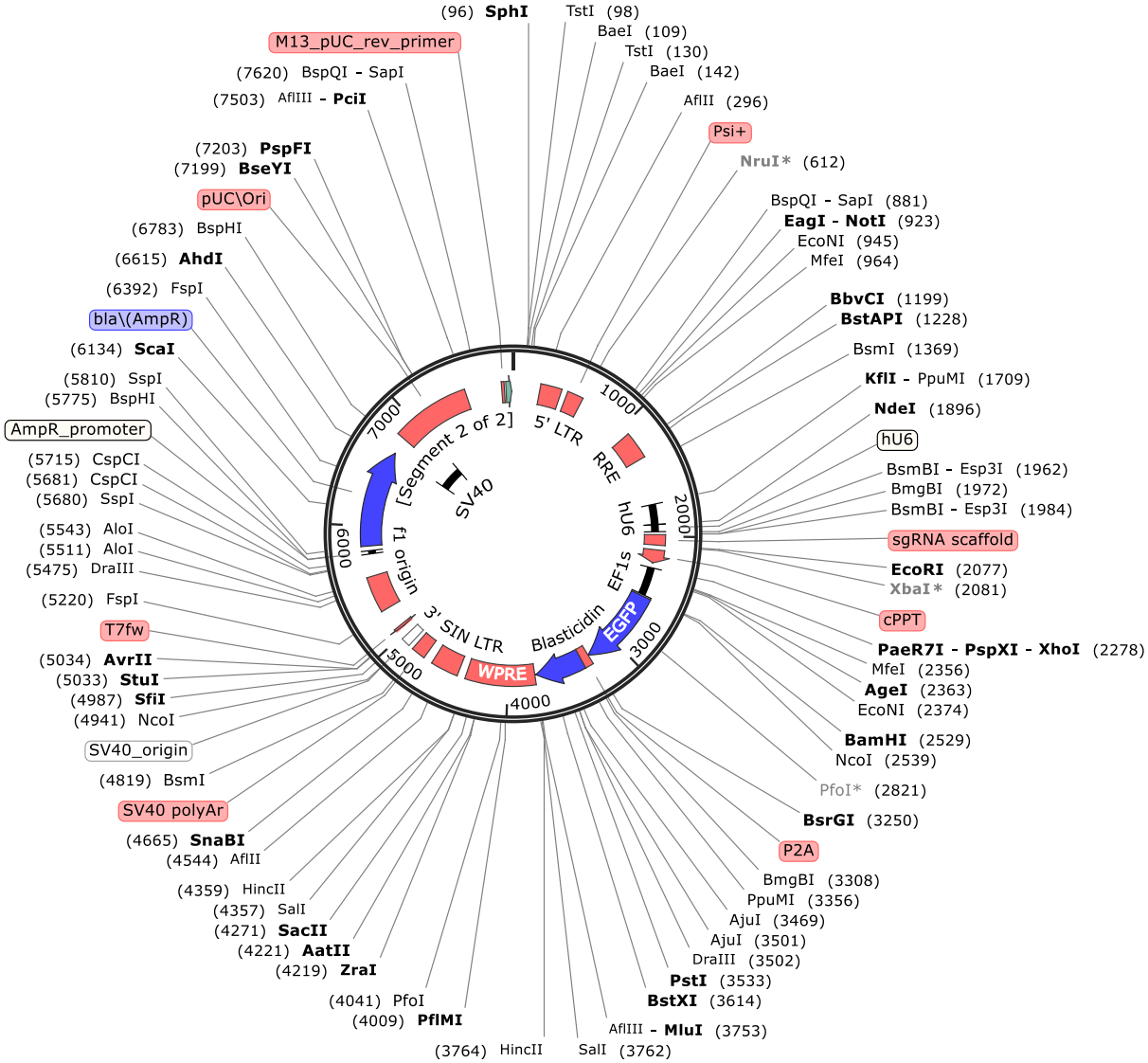

pLKO-U6sgRNA_improved-EF1s-GFP-P2A-Blasticidin (BsrGI, MluI from Ebert) (1)
7910 bp

Figure A2: Plasmid Map for pLKO-U6sgRNA_improved-EF1s-GFP-P2A-Blasticidin used for double stable cell line generation for CRISPR activation

The figure above shows the plasmid map of pLKO-U6sgRNA_improved-EF1s-GFP-P2A-Blasticidin which was used for stable cell line generation.

For example: Oligo C [29]: 26.4 nmoles. Added 264 µl water to the tube directly at the bottom.

Oligo C (Bottom): 23.5 nmoles. Added 235ul water to the tube directly at the bottom.

Once added, these tubes were allowed to sit on ice for 10 minutes and vortexed briefly to mix thoroughly. Rolled the tubes on side as well properly making sure that it is mixed well.

Next step was phosphorylation and annealing each pair of oligos: prepared the reactions in PCR tubes. Added the following reagents directly to the bottom of the tubes and pulse spin if required:

Oligo (Top) 100uM -	1ul
Oligo (bottom) 100uM -	1ul
10X T4 ligation buffer -	1ul
dd H2O -	6.5ul
T4 PNK (NEB M0201S) -	0.5ul
Total -	10ul

Run these reactions in the thermocycler with the set CRISPR-1 program at 37°C for 30 minutes: 95°C for 5minutes; 25°C at 5°C/1 min and 4°C forever.

Next, diluted the annealed oligos from this step at a 1:200 dilution in molecular grade water (1ul in 199 µl water) in eppendorf tubes. Now the ligation reaction was set up in eppendorf tubes for control and individual oligos at room temperature as follows:

Control:

Digested pLKO -50ng -	0.6ul
Molecular grade water -	4.4ul
2X Quik ligase buffer -	5ul
DNA Quick ligase -	1ul
Total -	11ul

Oligo sample:

Digested pLKO- 50ng -	0.6ul
Oligo annealed -	1ul
2X Quik ligase buffer -	5ul
DNA Quick ligase -	1ul
Molecular grade water -	3.4ul
Total -	11ul

Incubated this reaction at room temperature for 10 minutes.

Once ligation was completed, 4 µl of ligation reaction was added into Top10 F' *E. coli* competent cell tubes (already thawed on ice) and incubated for 30 minutes on ice. Then, this was heat shocked for 30 seconds at 42°C in thermomixer. After Placing on ice immediately for 2 minutes, 250µl of SOC media was added (already at room temperature) directly in the tubes. This was Incubated for 1 hour at 37°C in the thermomixer with shaking on. bacteria were spun at 14,000rpm for 3 minutes to pellet the bacteria. supernatant was discarded and pellet was resuspended into 20µl of SOC media. This mixture was then plated onto the appropriate three pre-prepared pre-warmed LB-AMP plates. Incubated overnight at 37°C in incubator.

Next day, post observation, 5 colonies were selected for each sgRNA. Colonies were picked with a pipette tip, one for each, and were added in 2ml LB media/2µl Amp in the white capped tubes. These tubes were placed on the shaker overnight at 37°C.

Next day, 16-18 hours post inoculation, mini plasmid prep procedure was performed as follows:1ml of bacterial suspension was transferred into an Eppendorf tube and centrifuged for 2 minutes at 15,000 rpm. The supernatant was discarded in a 50ml tube containing bleach, retaining pellet, which was resuspended in 250µl of Buffer P1 (stored in fridge). 250µl of Buffer P2 was

added and the tubes were inverted 5 times. These were incubated for 5 minutes and 350µl of Buffer N3 was added. all the tubes were inverted 5 times and centrifuged at 13,000 rpm for 10 minutes. supernatant was added to QIAprep spin column and pellet was discarded. Thus, was centrifuged for 1 minute at 13,000 rpm and flow-through was discarded. Buffer PB (500µl) was added to spin column. This was centrifuged for 1 minute at 13,000 rpm and discarded flow-through. Buffer PE (700µl) was added, and this was centrifuged for 1 minute at 13,000 rpm and flow-through was discarded. This was centrifuged for an additional 1 minute at 13,000 rpm. Spin column was placed into a clean, labeled eppendorf. Collecting tube was discarded. Then, 50µl of Buffer EB to was added to the This was added directly to the center of the filter at the bottom of the column. This was allowed to stand for 1 minute and then centrifuged for 1 minute at 13,000 rpm. Removed and discarded column. The plasmids were quantified using nanodrop.

Next step was to set up double digest to check the presence of insert, using Cut Smart buffer:

*BamHI- HF (2529 bp) and Esp31/BsmBI (1962 bp)

Restriction digest was set up as follows:

Miniprep DNA: 8ul

10X Cutsmart buffer: 1ul

BamHI-HF: 1ul

Total Volume- 10ul

Pulse spun and kept this at 37°C overnight.

Next day, digested the BamHI-digested product with BsmBI as follows:

BamHI-digested product: 10 µl

10X fast digest buffer: 5 µl

Fast digest BsmBI/Esp3I: 1 µl

Water: 34 µl

Total- 50 µl

Kept at 37°C for 30 minutes on thermomixer.

Agarose gel was run and one specific band of 7000bp was observed suggesting the presence of insert (Include agarose gel results below). These samples were then sent for sequencing analysis to further validate the presence of sgRNAs within the plasmid. Sequencing results showed all clones to be positive, meaning that all sgRNAs were successfully cloned within the “pLKO-U6sgRNA_improved-EF1s-GFP-P2A-Blasticidin” plasmid. Based on the results, the specific clones selected for double stable cell line generation were sgRNAs A5, B2, C2 and D1. Large plasmid prep procedure was completed for these sgRNAs to extract the plasmid DNA at higher concentration in larger volume. The volume of tissue culture grade water used for re-suspension of large plasmid prep pellets were 50 µl for sgRNAs A5 and B2, 150 µl for sgRNA C2 and 30 µl for sgRNA D1.

Cell culture details for double stable cell line generation

HEK293T and FAC-FT194 cells were first transfected with “Lenti-EFS-dCas9-VPR-PGK-Puro” plasmid and selected with an appropriate dose of puromycin (see Table 12) to generate Cas9-expressing stable cell lines. The transfection was set up using 100 µl serum free media, 1 µg plasmid DNA and 3 µl Fugene HD for each sample. Cells were overlaid with complete media 6 hours post-transfection. Twenty-four hours post-transfection, cells were replenished with pre-warmed complete media and 48 hours post-transfection media was replaced to add cell-specific appropriate dose of puromycin. These cells were maintained for long-term with replenishment of media every few days with puromycin containing media. Once ready, cells were seeded for western blotting analysis using Cas9 antibody and frozen at different passages with continued selection with puromycin for multiple passages.

After generation of Cas9 expressing stable cell lines, sgRNAs A5, B2, C2, D1 and control (empty pLKO plasmid) were transfected in these cells using 100µl serum free media, 1 µg plasmid DNA and 3 µl Fugene HD for each sample. Cells were then overlaid with complete media after 6 hours.

Twenty-four hours post-transfection, cells were replenished with pre-warmed complete media and 48 hours post-transfection media was replaced to add cell-specific appropriate dose of puromycin and blasticidin. The media was replenished every few days for double stable cell line generation. To validate the expression of pLKO plasmid in these cells, GFP expression was analyzed via western blotting analysis from the total cell lysates. The detailed steps for double stable cell line generation are summarized in the excel file saved on the USF Cloud storage Box drive in Ravneet's Experimental Planning folder: "HEK293T-Cas9_sgRNA steps" and "FT194-Cas9-sgRNA cell line generation".